REGULATION OF MICROTUBULE NUCLEATION IN *SCHIZOSACCHAROMYCES POMBE*: RECRUITMENT OF MTO1 TO THE SITE OF THE PROSPECTIVE eMTOC

Victoria Jane Miller

Doctor of Philosophy
The University of Edinburgh
2009

Acknowledgements

First, I would like to thank my supervisor Ken Sawin for his guidance, patience and enthusiasm, for constantly challenging and inspiring me to become a better scientist and giving me an appreciation of the importance of details. I could not have done this without him.

That I have enjoyed my time in Edinburgh so much is due in no small part to the people with whom I have worked in the lab. My thanks go to Andy Anders, Claudia Bicho, Lynda Groocock, Itaru Samejima and Hilary Snaith for always being available to offer advice and a friendly ear. Thanks also to Kevin Hardwick for acting as my second supervisor.

Within the Wellcome Trust Centre for Cell Biology, I would like to thank Flavia de Lima Alves and Juri Rappsilber for performing mass spectrometry; David Kelly for providing technical support for the confocal microscope; staff in the media kitchen and stores for background support and also to the Centre Managers David Brown and Greg Anderson for keeping the equipment in working order. My work could not have been done without the numerous people in the centre who generously shared not only reagents, plasmids, strains and equipment, but also their advice and experiences. Particular thanks go to the Allshire, Beggs, Hardwick and Ohkura labs.

Similar thanks go to people in the wider scientific community: Mohan Balasubramanian, Stefania Castagnetti, Fred Chang, Peter Fantes, Colin Gordon,

Kentaro Nakano, Snezhana Oliferenko, Viesturs Simanis, Jian-Qiu Wu and Hiro Yamano all provided strains, plasmids and/or advice. A special mention goes to Tom Pollard for sending me a large number of YFP-fusion proteins.

I am grateful to the BBSRC for funding this project.

I wish to thank my family and friends for all their help. Finally, I would like to thank my partner Michael Webb for his boundless support and encouragement.

Declaration

This thesis is a presentation of my original research work. Where the contributions of other have been referred to, this has been acknowledged in the text.

V Miller

Abstract

Mto1 recruits γ-tubulin to the sites of cytoplasmic microtubule nucleation in the fission yeast *Schizosaccharomyces pombe*. The regulation of Mto1 localisation is central to re-modelling of the microtubule cytoskeleton during the cell cycle. This thesis describes how Mto1 is recruited to the cell equator during mitosis, thereby establishing the equatorial microtubule nucleation centre (eMTOC).

F-actin is found to be required for Mto1 localisation to the cell equator and Mto1 is shown to co-localise with the cytokinetic actin ring (CAR). Yeast 2-hybrid screening and tandem-affinity purification were used to screen for additional proteins required for Mto1 localisation to the equator. Further candidate screening identified Myp2, a type II myosin present in the CAR, as being required for Mto1 localisation to the cell equator. Myp2 is shown to physically interact with Mto1 and to be required for formation of the post-anaphase microtubule array.

The regulation of Mto1 localisation to the cell equator was also studied. Time-lapse microscopy reveals that Mto1 localisation to the equator does not require either the anaphase-promoting complex or the septation initiation network, both of which have been previously shown to be necessary for the recruitment of γ-tubulin to the eMTOC.

Maintenance of the equatorial CAR has previously been attributed to the post-anaphase array. The position of the CAR in the *mto1-427* mutant strain, which fails

to nucleate a PAA, is shown to be unaltered from wild-type strain during exponential growth, suggesting that the PAA does not centre the CAR during normal growth.

Table of Contents

List of Abbreviations

3-AT	3’aminotriazole
aa	Amino acid
APC	Anaphase-promoting complex
bp	base pair
C	Celsius
CAR	Cytokinetic actin ring
CHD	Calponin homology domain
CM1	Centrosomin motif
DAPI	4,6-diamino-2-phenylindole
eMTOC	Equatorial microtubule organising centre
GFP	Green fluorescent protein
KS	Sawin laboratory yeast strain
Lat B	Latrunculin B
iMTOC	Interphase microtubule organising centre
MS	Mass spectrometry
MTOC	Microtubule organising centre
nmt	No message in thiamine
OKS	Sawin laboratory oligonucleotide
PAA	Post-anaphase array
PAGE	Poly acrylamide gel electrophoresis
PCR	Polymerase chain reaction

pKS	Sawin laboratory plasmid
psi	Pound per square inch
RFP	Red fluorescent protein
rpm	Revolutions per minute
SDS	Sodium dodecyl sulfate
SIN	Septation initiation network
SPB	Spindle pole body
tdT	Tandem dimer tomato red fluorescent protein
TAP	Tandem affinity purification
TBS	Tris buffered saline
YE	Yeast extract
YFP	Yellow fluorescent protein
γ-TuC	Gamma tubulin complex
γ-TuSC	Gamma tubulin small complex
γ-TuRC	Gamma tubulin ring complex

List of Figures

List of Tables

List of Movies

PAA formation in *myp2*Δ cells

Movie 1 Deconvolved time-lapse wide-field microscopy sequence of *nmt81:GFP-atb2* cells. Arrows indicates appearance of PAA from the equator. Images acquired every 30 seconds; total time compression 300×.

Movie 2 Deconvolved time-lapse wide-field microscopy of live *myp2*Δ*:kanMx nmt81:GFP-atb2* cells. Arrow indicates the cell equator after mitotic spindle breakdown; the PAA is not seen. Images acquired every 30 seconds; total time compression 300×.

Mto1 localisation in APC mutant strains

Movie 3 Time-lapse confocal microscopy of wild-type *nmt41:GFP-mto1 rlc1-mCherry uch2-mCherry* cells; single cell montage. Left to right: colour combine; red channel: Rlc1-mCherry (CAR marker) and Uch2-mCherry (nuclear marker); green channel: *nmt41*:GFP-Mto1. Mto1 localises to the equator following nuclear division, co-localising with the CAR. Mto1 continues to co-localise with the CAR during CAR contraction. Images acquired every 60 seconds from 2 hr 06 min at 36 °C; duration: 36 min. Total time compression 600×.

Movie 4 Time-lapse confocal microscopy of wild-type *nmt41:GFP-mto1 rlc1-mCherry uch2-mCherry* cells; full field. Colour combine: red channel showing Rlc1-mCherry (CAR marker) and Uch2-mCherry (nuclear marker); green channel showing *nmt41*:GFP-Mto1. Images acquired every 60 seconds from 2 hr 06 min at 36 °C; duration: 36 min. Total time compression 600×.

Movie 5 Time-lapse confocal microscopy of *cut4.533 nmt41:GFP-mto1 rlc1-mCherry uch2-mCherry* cells; single cell montage. Left to right: colour combine; red channel: Rlc1-mCherry (CAR marker) and Uch2-mCherry (nuclear marker); green channel: *nmt41*:GFP-Mto1. Mto1 localises to the equator in the mononucleate cell, co-localising with the CAR. Mto1 continues to co-localise with the CAR as the CAR contracts, cutting the nucleus. Images acquired every 60 seconds from 2 hrs at 36 °C; duration: 35 min. Total time compression 600×.

Movie 6 Time-lapse confocal microscopy of *cut4.533 nmt41:GFP-mto1 rlc1-mCherry uch2-mCherry* cells; full field. Colour combine: red channel showing Rlc1-mCherry (CAR marker) and Uch2-mCherry (nuclear marker); green channel showing *nmt41*:GFP-Mto1. Images acquired every 60 seconds from 2 hrs at 36 °C; duration: 35 min. Total time compression 600×.

Movie 7 Time-lapse confocal microscopy of wild-type *nmt41:GFP-mto1 rlc1-mCherry uch2-mCherry*; single cell montage. Left to right: colour combine; red channel: Rlc1-mCherry (CAR marker) and Uch2-mCherry (nuclear marker); green channel: *nmt41*:GFP-Mto1. Mto1 localises to the equator following nuclear division,

co-localising with the CAR. Mto1 continues to co-localise with the CAR during CAR contraction. Images acquired every 60 seconds from 3 hr 20 min at 36 °C; duration: 63 min. Total time compression 600×.

Movie 8 Time-lapse confocal microscopy of wild-type *nmt41:GFP-mto1 rlc1-mCherry uch2-mCherry*; full field. Colour combine: red channel showing Rlc1-mCherry (CAR marker) and Uch2-mCherry (nuclear marker); green channel showing *nmt41*:GFP-Mto1. Images acquired every 60 seconds from 3 hr 20 min at 36 °C; duration: 63 min. Total time compression 600×.

Movie 9 Time-lapse confocal microscopy of *cut4.533 nmt41:GFP-mto1 rlc1-mCherry uch2-mCherry*; single cell montage. Left to right: colour combine; red channel: Rlc1-mCherry (CAR marker) and Uch2-mCherry (nuclear marker); green channel: *nmt41*:GFP-Mto1. Mto1 localises to the equator in the mononucleate cell, co-localising with the CAR. Mto1 continues to co-localise with the CAR as the CAR contracts, producing one mononucleate and one anucleate cell. Images acquired every 60 seconds from 3 hr 08 min at 36 °C; duration: 40 min. Total time compression 600×.

Movie 10 Time-lapse confocal microscopy of *cut4.533 nmt41:GFP-mto1 rlc1-mCherry uch2-mCherry*; full field. Colour combine: red channel showing Rlc1-mCherry (CAR marker) and Uch2-mCherry (nuclear marker); green channel showing *nmt41*:GFP-Mto1. Images acquired every 60 seconds from 3 hr 08 min at 36 °C; duration: 52 min. Total time compression 600×.

Movie 11 Time-lapse confocal microscopy of *cut8.563 nmt41:GFP-mto1 rlc1-mCherry uch2-mCherry*; single cell montage. Left to right: colour combine; red channel: Rlc1-mCherry (CAR marker) and Uch2-mCherry (nuclear marker); green channel: *nmt41*:GFP-Mto1. Mto1 localises to the equator in the mononucleate cell, co-localising with the CAR. Mto1 continues to co-localise with the CAR as the CAR contracts, cutting the cell. Images acquired every 60 seconds from 3 hr 12 min at 36 °C; duration: 40 min. Total time compression 600×.

Movie 12 Time-lapse confocal microscopy of *cut8.563 nmt41:GFP-mto1 rlc1-mCherry uch2-mCherry*; full field. Colour combine: red channel showing Rlc1-mCherry (CAR marker) and Uch2-mCherry (nuclear marker); green channel showing *nmt41*:GFP-Mto1. Images acquired every 60 seconds from 3 hr 12 min at 36 °C; duration: 70 min. Total time compression 600×.

Movie 13 Time-lapse confocal microscopy of *cut9.665 nmt41:GFP-mto1 rlc1-mCherry uch2-mCherry*; single cell montage. Left to right: colour combine; red channel: Rlc1-mCherry (CAR marker) and Uch2-mCherry (nuclear marker); green channel: *nmt41*:GFP-Mto1. Mto1 localises to the equator in the mononucleate cell, co-localising with the CAR. Mto1 continues to co-localise with the CAR as the CAR contracts, cutting the cell. Images acquired every 60 seconds from 3 hr 19 min at 36 °C; duration: 50 min. Total time compression 600×.

Movie 14 Time-lapse confocal microscopy of *cut9.665 nmt41:GFP-mto1 rlc1-mCherry uch2-mCherry*; full field. Colour combine: red channel showing Rlc1-mCherry (CAR marker) and Uch2-mCherry (nuclear marker); green channel showing *nmt41*:GFP-Mto1. Images acquired every 60 seconds from 3 hr 19 min at 36 °C; duration: 53 min. Total time compression 600×.

PAA formation in APC mutant strains

Movie 15 Time-lapse confocal microscopy of *cut4.533 rlc1-mCherry uch2-mCherry SV40:GFP-atb2*; single cell montage. Left to right: colour combine; red channel: Rlc1-mCherry (CAR marker) and Uch2-mCherry (nuclear marker); green channel: *SV40*:GFP-Mto1. The cell is mononucleate when the CAR contracts, but the mitotic spindle then elongates. Faint microtubules appear that span the horizontal axis of the cell. Images acquired every 30 seconds onwards from 3hr 10 min incubation at 36 °C; duration: 37 min. Total time compression 300×.

Movie 16 Time-lapse confocal microscopy of *cut4.533 rlc1-mCherry uch2-mCherry SV40:GFP-atb2*; full field. Colour combine: red channel showing Rlc1-mCherry (CAR marker) and Uch2-mCherry (nuclear marker); green channel: *SV40*:GFP-Mto1. Images acquired every 30 seconds onwards from 3hr 10 min incubation at 36 °C; duration: 37 min. Total time compression 300×.

Movie 17 Time-lapse confocal microscopy of *cut8.563 rlc1-mCherry uch2-mCherry SV40:GFP-atb2*; single cell montage. Left to right: colour combine; red channel: Rlc1-mCherry (CAR marker) and Uch2-mCherry (nuclear marker); green channel:

SV40:GFP-Mto1. The mitotic spindle elongates and the nucleus divides as the CAR contracts. Images acquired every 30 seconds onwards from 3hr 09 min incubation at 36 °C; duration: 15 min. Total time compression 300×.

Movie 18 Time-lapse confocal microscopy of *cut8.563 rlc1-mCherry uch2-mCherry SV40:GFP-atb2*; full field. Colour combine: red channel showing Rlc1-mCherry (CAR marker) and Uch2-mCherry (nuclear marker); green channel: *SV40*:GFP-Mto1. Images acquired every 30 seconds onwards from 3hr 09 min incubation at 36 °C; duration: 15 min. Total time compression 300×.

Movie 19 Time-lapse confocal microscopy of *cut9.665 rlc1-mCherry uch2-mCherry SV40:GFP-atb2*; single cell montage. Left to right: colour combine; red channel: Rlc1-mCherry (CAR marker) and Uch2-mCherry (nuclear marker); green channel: *SV40*:GFP-Mto1. After an extended metaphase, the mitotic spindle elongates as the CAR contracts, cutting the nucleus. Microtubule nucleation is seen from the CAR. Images acquired every 30 seconds onwards from 3 hr 15 min incubation at 36 °C; duration: 40 min. Total time compression 300×.

Movie 20 Time-lapse confocal microscopy of *cut9.665 rlc1-mCherry uch2-mCherry SV40:GFP-atb2*; full field. Colour combine: red channel showing Rlc1-mCherry (CAR marker) and Uch2-mCherry (nuclear marker); green channel: *SV40*:GFP-Mto1. Images acquired every 30 seconds onwards from 3 hrs 15 min incubation at 36 °C; duration: 40 min. Total time compression 300×.

Movie 21 Time-lapse confocal microscopy of *rlc1-mCherry uch2-mCherry SV40:GFP-atb2*; single cell montage. Left to right: colour combine; red channel: Rlc1-mCherry (CAR marker) and Uch2-mCherry (nuclear marker); green channel: *SV40*:GFP-Mto1. The mitotic spindle elongates, the nucleus divides and the nuclei segregate to the cell ends. The left nucleus then moves back towards the CAR. Images acquired every 30 seconds onwards from 3hrs 13 min incubation at 36 °C; duration: 30 min. Total time compression 300×.

Movie 22 Time-lapse confocal microscopy of *rlc1-mCherry uch2-mCherry SV40:GFP-atb2*; single cell montage. Left to right: colour combine; red channel: Rlc1-mCherry (CAR marker) and Uch2-mCherry (nuclear marker); green channel: *SV40*:GFP-Mto1. The right nucleus passes through the CAR (arrow). Images acquired every 30 seconds onwards from 3hrs 13 min incubation at 36 °C; duration: 30 min. Total time compression 300×.

Movie 23 Time-lapse confocal microscopy of *rlc1-mCherry uch2-mCherry SV40:GFP-atb2*; full field. Colour combine: red channel showing Rlc1-mCherry (CAR marker) and Uch2-mCherry (nuclear marker); green channel: *SV40*:GFP-Mto1. Images acquired every 30 seconds onwards from 3hrs 13 min incubation at 36 °C; duration: 30 min. Total time compression 300×.

PAA formation in SIN mutant strains

Movie 24 Time-lapse confocal microscopy of *sid4-SA1 nmt81:GFP-atb2* at the permissive temperature; single cell. PAA nucleation begins immediately before

mitotic spindle breakdown and continues as the cell divides. Images acquired every 30 seconds at 25°C; duration: 38 min. Total time compression 300×.

Movie 25 Time-lapse confocal microscopy of *sid4-SA1 nmt81:GFP-atb2* at the permissive temperature; full field. Images acquired every 30 seconds at 25°C; duration: 38 min. Total time compression 300×.

Movie 26 Time-lapse confocal microscopy of *cdc11-123 nmt81:GFP-atb2* at the permissive temperature; single cell. PAA nucleation begins prior to mitotic spindle breakdown and continues as the cell divides. Images acquired every 30 seconds at 25°C; duration: 63 min. Total time compression 300×.

Movie 27 Time-lapse confocal microscopy of *cdc11-123 nmt81:GFP-atb2* at the permissive temperature; full field. Images acquired every 30 seconds at 25°C; duration: 63 min. Total time compression 300×.

Movie 28 Time-lapse confocal microscopy of *cdc7-24 nmt81:GFP-atb2* at the permissive temperature; single cell. PAA nucleation begins immediately before mitotic spindle breakdown and continues as the cell divides. Images acquired every 30 seconds at 25°C; duration: 63 min. Total time compression 300×.

Movie 29 Time-lapse confocal microscopy of *cdc7-24 nmt81:GFP-atb2* at the permissive temperature; full field. Images acquired every 30 seconds at 25°C; duration: 63 min. Total time compression 300×.

Movie 30 Time-lapse confocal microscopy of *nmt81:GFP-atb2* at the restrictive temperature; single cell. The PAA is present but nucleation is delayed until septum formation. Images acquired every 30 seconds from 2 hr 55 min at 36.5 °C; duration: 49.5 min. Total time compression 300×.

Movie 31 Time-lapse confocal microscopy of *nmt81:GFP-atb2* at the restrictive temperature; full field. Images acquired every 30 seconds from 2 hr 55 min at 36.5 °C; duration: 49.5 min. Total time compression 300×.

Movie 32 Time-lapse confocal microscopy of *sid4-SA1 nmt81:GFP-atb2* at the restrictive temperature; single cell. The cell does not divide following mitotic spindle disassembly and the nuclei return to the cell centre. The PAA does not form. Images acquired every 30 seconds from 2 hr 17 min at 36.5 °C; duration: 74.5 min. Total time compression 300×.

Movie 33 Time-lapse confocal microscopy of *sid4-SA1 nmt81:GFP-atb2* at the restrictive temperature; full field. Images acquired every 30 seconds from 2hr 17 min at 36.5 °C; duration: 74.5 min. Total time compression 300×.

Movie 34 Time-lapse confocal microscopy of *cdc11-123 nmt81:GFP-atb2* at the restrictive temperature; single cell. The cell does not divide following mitotic spindle disassembly. The PAA does not form. Images acquired every 30 seconds from 2 hr 35 min at 36.5 °C; duration: 45.5 min. Total time compression 300×.

Movie 35 Time-lapse confocal microscopy of *cdc11-123 nmt81:GFP-atb2* at the restrictive temperature; full field. Images acquired every 30 seconds from 2 hr 35 min at 36.5 °C; duration: 45.5 min. Total time compression 300×.

Movie 36 Time-lapse confocal microscopy of *cdc7-24 nmt81:GFP-atb2* at the restrictive temperature; single cell. The cell does not divide following mitotic spindle disassembly and the nuclei return to the cell centre. The PAA does not form. Images acquired every 30 seconds from 2 hr 17 at 36.5 °C; duration: 72.5 min. Total time compression 300×.

Movie 37 Time-lapse confocal microscopy of *cdc7-24 nmt81:GFP-atb2* at the restrictive temperature; full field. Images acquired every 30 seconds from 2 hr 17 at 36.5 °C; duration: 72.5 min. Total time compression 300×.

Mto1 localisation in SIN mutant strains

Movie 38 Time-lapse confocal microscopy of *nmt41:GFP-mto1 rlc1-mCherry uch2-mCherry* at the restrictive temperature; single cell montage. Left to right: colour combine; red channel: Rlc1-mCherry (CAR marker) and Uch2-mCherry (nuclear marker); green channel: *nmt41*:GFP-Mto1. Mto1 localises to the equator in the mononucleate cell, co-localising with the CAR. Mto1 continues to co-localise with the CAR as the CAR contracts. Images acquired every 60 seconds from 2 hr 08 min at 36.5 °C; duration: 71 min. Total time compression 600×.

Movie 39 Time-lapse confocal microscopy of wild-type *nmt41:GFP-mto1 rlc1-mCherry uch2-mCherry*; full field. Colour combine: red channel showing Rlc1-mCherry (CAR marker) and Uch2-mCherry (nuclear marker); green channel showing *nmt41*:GFP-Mto1. Images acquired every 60 seconds from 2 hr 08 min at 36.5 °C; duration: 71 min. Total time compression 600×.

Movie 40 Time-lapse confocal microscopy of *sid4-SA1 nmt41:GFP-mto1 rlc1-mCherry uch2-mCherry* at the restrictive temperature; single cell montage. Left to right: colour combine; red channel: Rlc1-mCherry (CAR marker) and Uch2-mCherry (nuclear marker); green channel showing *nmt41*:GFP-Mto1. Mto1 is present at the CAR. The CAR then breaks down, leaving a binucleate cell. Images acquired every 60 seconds from 2 hr 01 min at 36 °C; duration: 31 min. Total time compression 600×.

Movie 41 Time-lapse confocal microscopy of *sid4-SA1 nmt41:GFP-mto1 rlc1-mCherry uch2-mCherry*; full field. Colour combine: red channel showing Rlc1-mCherry (CAR marker) and Uch2-mCherry (nuclear marker); green channel showing *nmt41*:GFP-Mto1. Images acquired every 60 seconds from 2 hr 01 min at 36 °C; duration: 31 min. Total time compression 600×.

Chapter I - Introduction

Microtubules

Microtubules are hollow polymer tubes found in eukaryotic cells. They are constructed from dimers of α- and β-tubulin. α-β-tubulin heterodimers interact to form protofilaments within microtubules, with each individual microtubule typically consisting of 13 protofilaments arranged as a helical structure. Microtubules are intrinsically polarised due to the head-to-tail alignment of the heterodimers, having a distinct plus end (where β-tubulin is exposed) and minus end (where α-tubulin is exposed). Individual microtubules are highly dynamic, undergoing cycles of growth and shrinkage as they explore the cellular environment (Mitchison and Kirschner, 1984; Desai and Mitchison, 1997). Within the cell most microtubules preferentially grow from the plus end and are stabilised at the minus end by nucleation sites (Dammermann et al., 2003).

Microtubules are an essential part of the eukaryotic cytoskeleton, being involved in both small-scale activities, such as the transport of proteins and organelles by molecular motors travelling along microtubules, and in large-scale phenomena such as the establishment of cell polarity, cellular movement (through cilia and flagella) and cell division (Raynaud-Messina and Merdes, 2007). Microtubules can interact to form distinct higher order structures, most notably the mitotic spindle. These higher-order arrays of microtubules are also dynamic, undergoing dramatic morphological changes during the cell cycle.

Microtubule nucleation

Microtubule nucleation is generally restricted to specific sites within cells, called microtubule organising centres (MTOCs). MTOCs control the number, distribution and polarity of microtubules within cells (Luders and Stearns, 2007). The predominant MTOC in higher eukaryotic cells is the centrosome. Electron micrographs show the centrosome to consist of two cylindrical centrioles in perpendicular alignment, each with nine triplets of microtubules arranged as blades around the perimeter of the cylinder (Rieder et al., 2001). The peri-centriolar matrix surrounding the centrioles is an amorphous material containing proteins such as pericentrin and ninein, involved in the nucleation and anchoring of microtubules (Doxsey *et al.*, 1994; Bouckson-Castaing *et al.*, 1996). During interphase the centrosome nucleates an array of microtubules that extends to the cell periphery; later in the cell cycle the centrosome, together with chromatin, (see below) nucleates the mitotic spindle. In yeast the spindle pole body (SPB) is functionally similar but structurally distinct to the centrosome. The SPB is a multilayered structure consisting of a series of plaques that is able to nucleate microtubules from both the nucleoplasmic and cytoplasmic face (Jaspersen and Winey, 2004).

Some cell types have microtubules that are not associated with the centrosome: neuronal cells contain a core of over-lapping microtubules that span the axon length, while kidney epithelial cells have microtubules that extend through the cell from the apical to the basal membrane (Keating and Borisy, 1999). Non-centrosomal microtubules allow for a wider range of microtubule arrays to be formed. Studies of cells in which the centrosome has been ablated (Khodjakov et al., 2000) reveal that

nucleation is not solely dependent on the centrosome, even in cells lacking extra-centrosomal arrays, as cells form microtubules in the absence of a functional centrosome. These microtubules then independently organise into functional spindles during mitosis, but cells lacking centrosomes have a high failure rate in cytokinesis (related to mitotic spindle mis-positioning), pointing to the role of the centrosome in establishing robust cell division (Khodjakov and Rieder, 2001).

The generation of non-centrosomal microtubules is not well understood. Some are thought to derive from the centrosome, either being released after nucleation or severed from pre-existing microtubules (Keating and Borisy, 1999). Other microtubules are nucleated in association with chromatin, including the meiotic spindle in many organisms (McKim and Hawley, 1995; Waters and Salmon, 1997). Microtubules are also nucleated by non-centrosomal MTOCs. Fruit fly wing epithelial cells contain non-centrosomal MTOCs. These nucleate microtubules with 15 protofilaments, in contrast to those nucleated by the centrosome in the same cells (which have the conventional 13), corroborating the separate origins of these microtubules (Mogensen and Tucker, 1987). Plant cells form an organised cortical microtubule array, nucleated from MTOCs on pre-existing microtubules (Murata et al., 2005). The fission yeast *Schizosaccharomyces pombe* contains a number of distinct MTOCs that nucleate distinct microtubule arrays at different times in the cell cycle (Hagan, 1998; Sawin and Tran, 2006); these are described in more detail below.

γ-tubulin promotes microtubule nucleation

MTOCs contain γ-tubulin, a member of the tubulin family, which promotes nucleation of microtubules. γ-tubulin was originally identified as a suppressor of a β-tubulin mutation in *Aspergillus nidulans* and has ~30% homology to α- and β-tubulin (Oakley and Oakley, 1989). Nucleation is the rate-limiting step of microtubule formation as initial nucleation intermediates are unstable in the absence of γ-tubulin, creating a kinetic barrier to nucleation (Job et al., 2003).

In vivo, γ-tubulin associates with additional proteins to form the γ-tubulin complex (γ-TuC). Two forms of this complex are commonly found: the γ-tubulin small complex (γ-TuSC), containing two copies of γ-tubulin (GCP1) plus one copy each of the accessory factors GCP2 and GCP3 (Murphy et al., 1998; Oegema et al., 1999), and the larger γ-tubulin ring complex (γ-TuRC), which contains multiple copies of the γ-TuSC, as well as GCP4, 5, 6 and GCP-WD (Martin *et al.*, 1998; Fava *et al.*, 1999; Oegema *et al.*, 1999; Gunawardane *et al.*, 2000; Zhang *et al.*, 2000; Murphy *et al.*, 2001; Gunawardane *et al.*, 2003; Haren *et al.*, 2006; Luders *et al.*, 2006; Verollet *et al.*, 2006). The γ-TuRC has been named because of its ring-like structure, as observed by electron microscopy. The accessory proteins GCP2-6 (named GCP for γ-complex protein) all contain a conserved 'grip' motif, the function of which is unknown (Gunawardane et al., 2000; Murphy et al., 2001). The *S. pombe* homologues of the core components are Gtb1/Tug1 (GCP1), Alp4 (GCP2) and Alp6 (GCP3) (Horio et al., 1991; Stearns et al., 1991; Vardy and Toda, 2000). Gfh1 (GCP4), Mod21 (GCP5) and Alp16 (GCP6) are homologues of the non-core components (Fujita *et al.*, 2002; Venkatram *et al.*, 2004; Anders *et al.*, 2006). The

non-core components are less well conserved than the core components. Figure 1 shows a diagram of the γ-TuRC in *S. pombe*.

The precise mechanism of microtubule nucleation is unknown. Two models of nucleation have been put forward: the 'template' model, where the γ-TuC acts as a direct template for nucleation (Zheng et al., 1995), and the 'protofilament' model where the γ-TuC forms a protofilament with which other protofilaments interact by lateral contacts to form a microtubule (Erickson and Stoffler, 1996). The template model is inspired by the ring structure of the γ-TuRC, and is the more widely accepted of the two models. This ring has a diameter of 25nm, the same diameter as a single microtubule, and can be seen to cap the minus ends of microtubules (Moritz *et al.*, 1995; Zheng *et al.*, 1995; Keating and Borisy, 2000; Moritz *et al.*, 2000; Wiese and Zheng, 2000).

While the γ-TuRC is considered to be the active form of the γ-TuC *in vivo* and is significantly better at promoting nucleation than the γ-TuSC (~150 times more active per mole of complex) (Oegema et al., 1999), the precise roles of the γ-TuRC and γ-TuSC are not clear. *S. cerevisiae* nucleates microtubules, despite lacking homologues of GCP4, 5 and 6 (Wiese and Zheng, 2006) and the γ-TuSC has been shown to promote some minimal microtubule nucleation *in vitro,* although this work took place at high concentrations of γ-TuSC (Oegema et al., 1999). It is theoretically possible that the γ-TuSC could self-associate to form larger complexes similar to the γ-TuRC even in the absence of these proteins (Vinh *et al.*, 2002; Kollman *et al.*, 2008). In addition, while *S. pombe* does contain the γ-TuRC form of the γ-TuC,

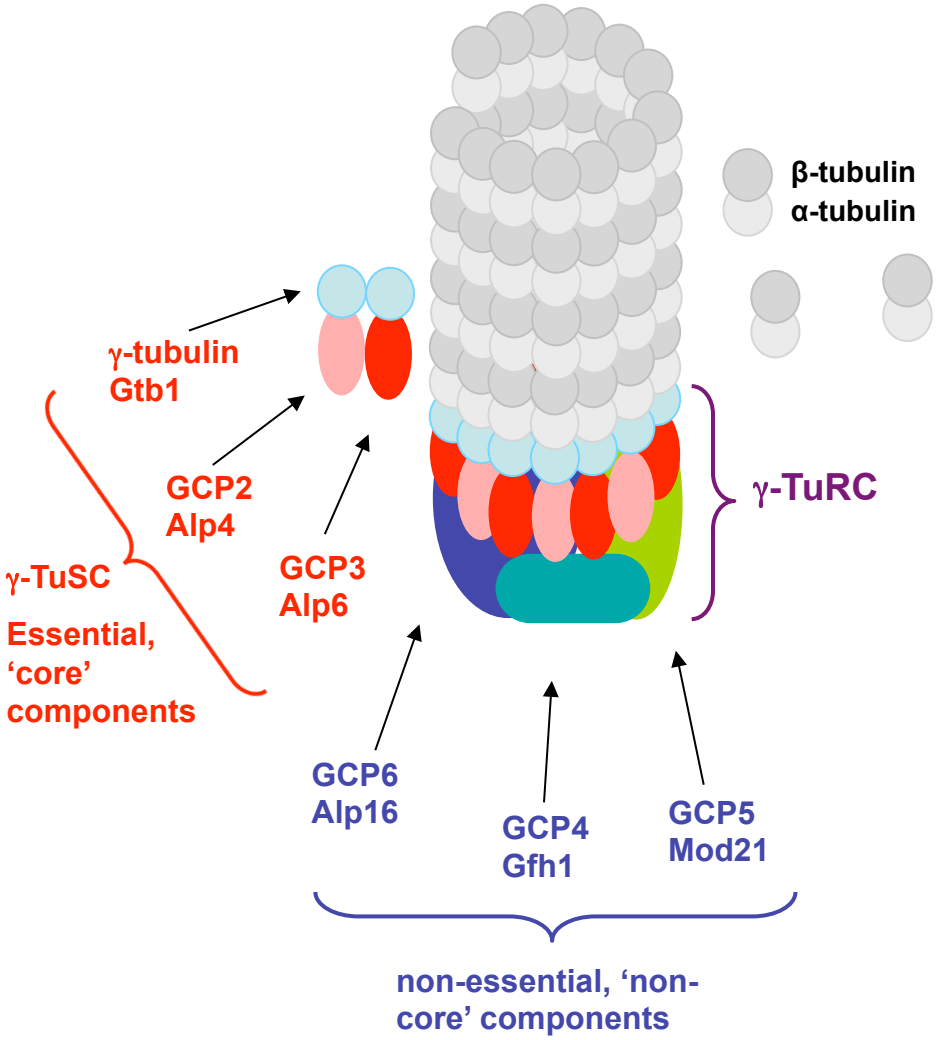

Figure 1 The γ-TuRC nucleates microtubule formation

In *S. pombe* the γ-TuRC consists of multiple copies of the γ-TuSC (Gtb1, Alp4 and Alp6) that interact with the non-core accessory proteins Alp16, Gfh1 and Mod21 to form a ring-like structure. The γ-TuRC is thought to nucleate microtubule by acting as a direct template for α-β tubulin dimer assembly as shown.

sucrose gradient separation has shown that the majority of γ-tubulin in *S. pombe* exists in the γ-TuSC form (Anders et al., 2006). Strains lacking the γ-TuRC specific components (including the triple *gfh1Δ mod21Δ alp16Δ* knockout) are viable and have qualitatively normal microtubule nucleation, although the number of microtubules nucleated from iMTOCs is reduced (Anders et al., 2006).

While the structural evidence rules out the 'protofilament' model as it was first conceived, a modified model has been proposed, where lateral bonds between β-tubulin and γ-tubulin are important and the γ-tubulin protofilament need not extend so far into the microtubule (Erickson, 2000). The contribution of each form of the γ-TuC to nucleation *in vivo* requires further investigation and this may aid the development of a unifying model of microtubule nucleation. In this work, γ-TuC is used where it is not possible to distinguish between the γ-TuSC and the γ-TuRC.

γ-tubulin also appears to regulate the plus-end dynamics of microtubules, as cells with mutations in γ-TuC proteins frequently contain very long microtubules that in *S. pombe* often curve round cell tips (Paluh *et al.*, 2000; Vardy and Toda, 2000; Tange *et al.*, 2004; Zimmerman and Chang, 2005; Anders *et al.*, 2006; Masuda *et al.*, 2006). How this occurs is unclear, but may be related to loading of EB1 proteins at the minus end (Cuschieri et al., 2006). Alternatively, this curving may be an indirect effect due to the altered ratio of tubulin subunits to nucleation sites (Sawin *et al.*, 2004; Samejima *et al.*, 2005).

The microtubule network undergoes tremendous changes during the cell cycle. Restricting microtubule nucleation to MTOCs allows cells to control when and where microtubules are formed, and the type, position and nucleating capacity of MTOCs must change to produce the changes in microtubule organisation, whether through the construction of new microtubules or by a change in nucleating capacity of a pre-existing MTOC (Khodjakov and Rieder, 1999). This control is necessary for the proper function of the cell, with centrosome abnormalities potentially causing genetic instability and cancer (Basto et al., 2008). How MTOCs and the localisation of γ-tubulin are controlled within cells is a question that is critical for our understanding of cell biology.

Microtubules in S. pombe

This project has used the fission yeast *S. pombe* to study microtubule nucleation. A commonly used laboratory model, *S. pombe* is a rod shaped single celled organism, with haploid cells typically 7-14 μm in length and 3-4 μm in width. Widely divergent from the other commonly used yeast model *S. cerevisiae* (Forsburg, 1999; Sipiczki, 2000), *S. pombe* was first isolated in 1893 and emerged as a model organism in the 1950s with the work of Urs Leopold and Murdoch Mitchison, before being notably used for the cell cycle experiments that led to Paul Nurse being awarded the 2001 Nobel Prize in Physiology or Medicine. It has the convenient features of being easily cultured with a short generation time (2-4 hours depending on growth conditions), has a well-defined cell cycle and is readily genetically manipulated. The genome sequence was published in 2002 (Wood et al., 2002) and *S. pombe* experimental

techniques have made full use of rapid advances in molecular biology, including the live imaging of fluorescently tagged proteins *in vivo*.

S. pombe, while having comparatively few microtubules, displays three distinct microtubule arrays during vegetative growth, each appearing at a specific stage of the cell cycle (Figure 2). Each microtubule array has a specific associated microtubule organising centre (MTOC) (Hagan, 1998; Sawin and Tran, 2006); regulation of MTOCs underpins restructuring of the microtubule cytoskeleton as the cell passes through the cell cycle. The abundance of MTOCs makes *S. pombe* an excellent model organism to use to study the mechanism and control of microtubule nucleation, addressing important questions in our understanding of how MTOCs are regulated in time and space.

Interphase MTOCs (iMTOCs) nucleate the anti-parallel bundles of microtubules that span the cell prior to mitosis. 3-4 bundles of interphase microtubules are found per cell, with approximately 2-5 microtubules per bundle (Drummond and Cross, 2000; Tran *et al.*, 2001; Carazo-Salas *et al.*, 2005; Hoog *et al.*, 2007). What constitutes an iMTOC has proved to be difficult to define, mainly due to subtle experimental considerations. The SPB undoubtedly nucleates some proportion of interphase microtubules; nucleation has also been suggested to occur from γ-TuC satellites present on existing microtubules (Janson et al., 2005), from the overlap region of antiparallel MT bundles in the centre of the cell (Busch and Brunner, 2004) (although it is disputed whether this is true *de novo* nucleation) and from sites on the nuclear envelope (Mata and Nurse, 1997; Hagan, 1998). The existence of these

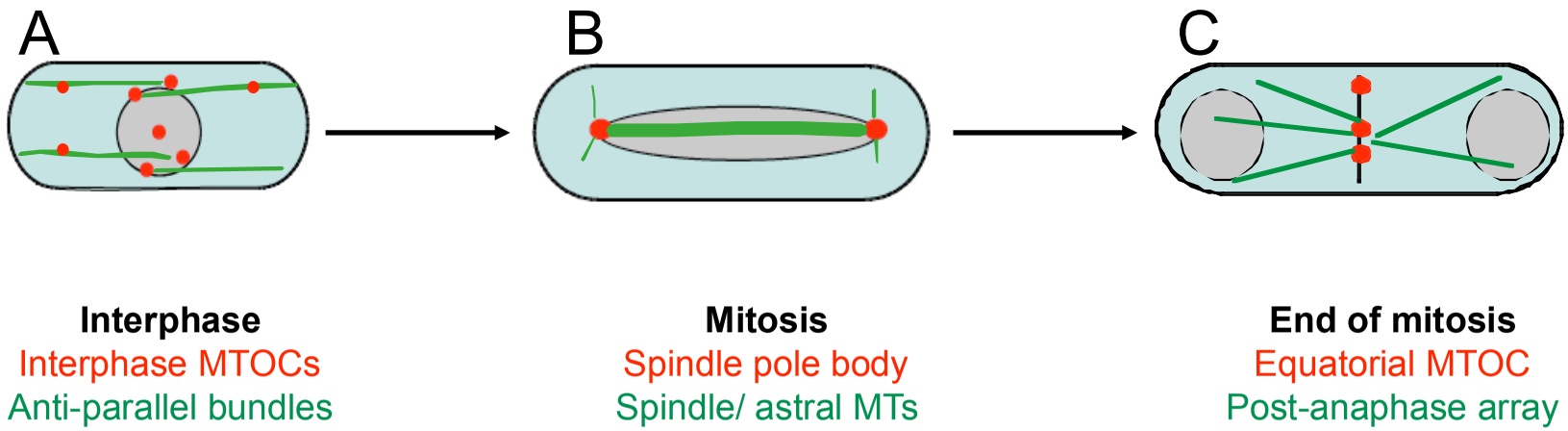

Figure 2 Microtubule organisation during the fission yeast cell cycle

Microtubule organisation is re-modelled at different stages of the cell cycle. (A) In interphase, microtubules are present as anti-parallel bundles. These are nucleated from the SPB and from iMTOCs. (B) In anaphase, astral microtubules are nucleated from the duplicated SPBs. (C) At the end of mitosis, the eMTOC forms at the cell equator and nucleates the PAA. When cell division is complete, the eMTOC disassembles and the new daughter cells enter interphase. MTOCs (containing γ-tubulin) are shown in red, microtubules in green. *S. pombe* undergoes a closed mitosis with no nuclear envelope breakdown.

nuclear iMTOCs was based on re-growth of microtubules after cold-shock treatment, which depolymerises microtubules; however the microtubule nucleation protein Mto1 is known to re-locate to the nuclear envelope after cold-shock (Sawin et al., 2004), making it difficult to judge the degree of microtubule nucleation from the nuclear envelope present under normal conditions.

Klp2 and Ase1 organise microtubules into overlapping antiparallel bundles during interphase. The kinesin motor protein Klp2 slides new microtubules along pre-existing microtubules, aligning the minus ends (Carazo-Salas et al., 2005), while Ase1 then bundles the collections of minus ends in an anti-parallel manner, forming a stable region of minus ends in the centre of the cell (Loiodice *et al.*, 2005; Yamashita *et al.*, 2005; Kapitein *et al.*, 2008). In doing so all microtubules present in the cell are incorporated into an anti-parallel array of bundled microtubules. Interphase microtubules then deliver polarity factors Tea1 and Tea4 to the cell tips (Mata and Nurse, 1997; Sawin and Nurse, 1998; Sawin and Snaith, 2004; Martin *et al.*, 2005). These proteins provide intracellular positional information (Hayles and Nurse, 2001) and are part of the machinery that determines cell polarity; if this positional information is absent or disrupted, cells display morphology defects such as curving or branching in response to stress (Sawin and Nurse, 1998; Niccoli *et al.*, 2003; Tatebe *et al.*, 2005). In addition, opposing forces generated as interphase bundles come into contact with the cell tips act to centre the nucleus within the cell (Tran *et al.*, 2001; Daga *et al.*, 2006). This also provides positional information within the cell; nuclear position prescribes the future division site through shuttling of the anillin-like protein Mid1 from the nucleus to the cell membrane, where it establishes the contractile actin ring (CAR) (Sohrmann *et al.*, 1996; Bahler *et al.*,

1998a; Motegi *et al.*, 2004). If the position of the nucleus is altered in early mitosis (by centrifugation or using optical tweezers), the division site is correspondingly changed (Daga and Chang, 2005; Tolic-Norrelykke et al., 2005).

The mitotic spindle is nucleated from the nuclear face of the SPB. The SPB embeds into the nuclear envelope at the start of mitosis, after it has duplicated (Ding et al., 1997). In common with other yeasts, *S. pombe* undergoes a closed mitosis, where the nuclear envelope does not breakdown. *S. pombe* has 3 chromosomes, to which the microtubules of the mitotic spindle attach via the kinetochores. The condensed chromosomes align in the centre of the cell (metaphase), separate and move apart (anaphase A) before the mitotic spindle elongates (anaphase B), segregating the duplicated chromosomes prior to cell division. The SPB also nucleates astral microtubules from the cytoplasmic face of the nucleus during mitosis, first appearing during anaphase. Astral microtubules have previously been implicated in a 'spindle-orientation' checkpoint (Oliferenko and Balasubramanian, 2002; Gachet *et al.*, 2004; Rajagopalan *et al.*, 2004; Tournier *et al.*, 2004); however the discovery that what were believed to be 'astral microtubules', present during metaphase, are in fact intra-nuclear (Zimmerman et al., 2004a), has substantially discredited the existence of the checkpoint (reviewed briefly in (Sawin and Tran, 2006)). What then is the purpose of astral microtubules? A number of experimental approaches have been used to show that spindle elongation does not depend on the presence of astral microtubules (Masuda *et al.*, 1990; Khodjakov *et al.*, 2004; Sawin *et al.*, 2004; Tolic-Norrelykke *et al.*, 2004; Venkatram *et al.*, 2004; Zimmerman and Chang, 2005). No function for astrals microtubule has yet been identified, and it is possible that astral microtubules

are simply evolutionary remnants with no function in *S. pombe*.

At the end of mitosis the equatorial MTOCs nucleate the post-anaphase array (PAA). The microtubules of the PAA radiate from the equatorial MTOC (eMTOC), a horseshoe-like structure present at the equator of the cell at the site of future septum formation (Heitz et al., 2001). The first signs of microtubule nucleation from the medial region take place immediately prior to spindle disassembly, and the PAA fully develops after mitotic spindle breakdown. The structure breaks down at cytokinesis, though some microtubules are thought to remain and contribute to the new interphase microtubule bundles that form. Growth of cells that lack the PAA, (*mto1Δ* mutant cells (Sawin et al., 2004; Venkatram et al., 2005) and cells where Rsp1, a protein involved in the disassembly of the eMTOC, is over-expressed (Zimmerman et al., 2004b)) demonstrate that the PAA is not essential for viability.

The precise function of the PAA is unknown. Cells lacking the PAA are viable but fail to maintain the CAR at the middle of the cell when cell division is delayed for 3 hrs (Pardo and Nurse, 2003; Venkatram et al., 2005). Correct positioning of the division plane is essential to avoid uneven distribution of nuclear material; in the absence of the PAA the CAR drifted from the centre when cells were arrested prior to cytokinesis. The microtubules of the PAA have also been suggested to have a role in separating duplicated nuclei, creating a safe distance between the nuclei and the division site (Hagan and Hyams, 1988; Hagan and Yanagida, 1997), although this is unlikely given that *mto1Δ* cells do not show defects in maintaining nuclear separation.

Do other fission yeasts have a PAA? The closely related yeast S*chizosaccharomyces japonicus* does not appear to have an eMTOC, as determined by γ-tubulin localisation (Horio et al., 2002). Extensive growth of astral microtubules is seen towards the end of anaphase, creating long microtubules that superficially resemble a PAA as they are first constricted and then severed by the contraction of the CAR and septum formation (Alfa and Hyams, 1990). Careful examination has revealed a small number of microtubules emerging from the cell equator that were previously over looked, possibly being nucleated from free floating cytoplasmic MTOCs rather than a tethered eMTOC (Horio et al., 2002). However, the majority of microtubules are thought to emerge from the SPB. This predicts that the minus ends of these microtubules will be localised at the cell tips, rather than being nucleated from the cell equator, with wide implications for PAA function. It should be kept in mind that all previous work has used fixed cells; live microscopy has the potential to reveal many hidden details of microtubule nucleation and should give a clearer picture of the extent of equatorial nucleation in *S. japonicus*.

The cytoskeleton of *S. octosporus,* the other member of the genus *Schizosaccharomyces*, has not yet been characterised. The genomes of both *S. japonicus* and *S. octosporus* have now been sequenced (available online at http://www.broad.mit.edu) and further studies of their cytoskeleton (especially using live microscopy to observe morphological changes across the cell cycle) may well provide new insights into the *S. pombe* cytoskeleton, and reveal how far the PAA has been conserved. It is possible that the PAA was present in a common ancestor of the fission yeasts, and had a distinct function, possibly in tethering the CAR, but that the

function has lost importance over the course of time. Nevertheless, *S. pombe* remains a uniquely suitable model for studying regulation of microtubule nucleation.

Mto1, a key regulator of microtubule nucleation, targets the γ-TuC to MTOCs

Mto1 (Microtubule organiser, initially known as Mod20 and Mbo1) recruits the γ-TuC to cytoplasmic MTOCs (Sawin et al., 2004; Venkatram et al., 2004). Deletion of Mto1 completely abolishes cytoplasmic microtubule nucleation. *Mto1Δ* cells lack astral microtubules and the PAA; the few interphase microtubules present in *mto1Δ* cells are derived from microtubules that have emerged from the nucleus (a phenomenon described in (Zimmerman et al., 2004a)). As with other mutants defective in microtubule nucleation, *mto1Δ* cells have elongated microtubules that abnormally curve around cell tips. Nucleation of the microtubules that build the mitotic spindle is thought to be mediated by Pcp1, a functional homologue of Mto1 that attaches the γ-TuC to the nuclear face of the SPB (Flory et al., 2002). Accordingly, *mto1Δ* cells have a normal mitotic spindle and the cells are viable. The defective microtubule nucleation seen in *mto1Δ* cells leads to mild morphology defects, with cells appearing as slightly curved. Visualisation of fluorescently labelled Mto1 shows that it localises to MTOCs. Mto1 is found at the SPB, forms a ring in the middle of the cell (the site of eMTOC) at the end of anaphase that later contracts, and is distributed along microtubules at sites that are thought to be iMTOCs. Mto1 co-immunoprecipitates the γ-TuC and is required to recruit the γ-TuC to the MTOCs at the various stages of the cell cycle. Mto1 localisation ultimately dictates γ-tubulin localisation and thus where microtubule nucleation will

occur. It follows that understanding how Mto1 localisation is regulated is essential for understanding how the localisation of the γ-tubulin to the different MTOCs is controlled at distinct times in the cell cycle. It is unclear whether Mto1 regulates cytoplasmic microtubule nucleation purely by controlling the localisation of the γ-TuC, or whether binding to Mto1 may somehow activate the γ-TuC.

Mto2, a second key regulator of cytoplasmic microtubule nucleation, also localises to MTOCSs and has been shown to physically interact with Mto1 (Samejima et al., 2005; Venkatram et al., 2005). *mto2Δ* cells have fewer interphase microtubules than wild-type cells, but do have astral microtubules and nucleate weak unfocused PAAs (Samejima et al., 2005; Venkatram et al., 2005). Mto2 and Mto1 bind the γ-tubulin complex co-operatively, with Mto1 being unable to co-purify γ -TuC in the absence of the Mto2 binding region (Samejima et al., 2008), although the increased number of microtubules present in the *mto2Δ* mutant compared to *mto1Δ* cells suggests that *in vivo* Mto1 may retain some ability to recruit the γ-TuC in the absence of Mto2. While soluble Mto1 may be unable to interact with γ-TuC in the absence of Mto2, small amounts of solid-phase Mto1 have been proposed to interact with γ-tubulin at SPBs and the eMTOC (Samejima et al., 2005), which would account for the microtubule nucleation that is observed. Mto1 localises to MTOCs in *mto2Δ* cells and so Mto1 localisation is independent of Mto2, while Mto2 localisation is dependent on the presence of Mto1 (Samejima et al., 2005; Venkatram et al., 2005). This indicates that localisation of the Mto1/Mto2/γ-TuC complex is regulated through Mto1.

Mto1 is a large protein of 1115 amino acids. Figure 3 shows key domains present in the Mto1 protein. Mto1 has a globular N-terminal domain of ~ 300 amino acids, with the remainder of the protein consisting primarily of extensive coiled coil regions. Coiled coil protein domains contain heptad repeats of hydrophobic and polar amino acids that form an amphipathic alpha helix; two or more coiled coils then interact to conceal the hydrophobic seam of the coil, exposing the hydrophilic region to the cytoplasm (Lupas and Gruber, 2005). Coiled-coil domains can thus promote protein-protein interaction including dimerisation. Mto1 has been shown to dimerise in vivo, with two differently tagged versions of Mto1 co-immunoprecipitating (L. Groocock, personal communication).

Mto1 is one of a number of proteins known to regulate the localisation of γ-tubulin. In *S.cerevisiae,* the protein SPC72 links the γ-TuSC to the cytoplasmic face of the SPB (Knop and Schiebel, 1998), and is therefore functionally similar to Mto1. Recently an RNAi screen led to the identification of several *D. melanogaster* genes that are required for γ-tubulin localisation to mitotic spindle microtubules, forming the augmin complex (Goshima et al., 2008; Meireles et al., 2009). This microtubule-based microtubule nucleation is similar to nucleation by iMTOCs found on interphase microtubules in *S. pombe*. Deletion of augmin complex subunits leads to the defects in cell division including a reduction in the number of spindle microtubules (Goshima et al., 2008) and to chromosomal misalignment during female meiosis (Meireles et al., 2009). Human homologues of the augmin proteins have been shown to interact with γ-tubulin (Lawo et al., 2009; Uehara et al., 2009). Another human protein, CDK5RAP2, is necessary for γ-TuRC attachment to the

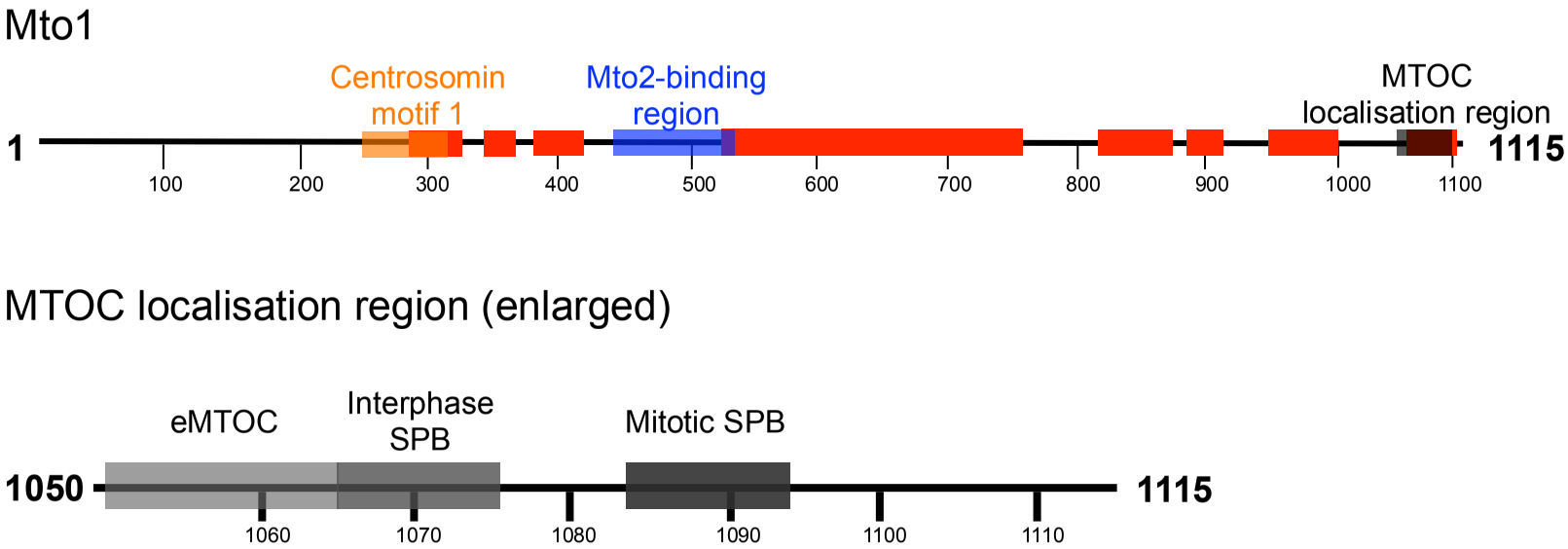

Figure 3 Mto1 protein structure

(*Adapted from Samejima et al., 2008*)

Mto1 contains extensive coiled-coil regions, shown in red (PAIRCOIL score >0.5, Berger et al., 1995). Mto1 interacts with γ−tubulin via the conserved centrosomin motif 1, shown in orange, and with Mto2 via the Mto2-binding region. At the extreme C-terminus there is an MTOC localisation region, shown in grey. The residues from 1051-1065 is necessary but not sufficient for Mto1 localisation to the eMTOC, from 1065-1075 for localisation to the interphase SPB and from 1085-1095 to localisation to the mitotic SPB.

centrosome (Fong et al., 2008). Mutations in *CDK5RAP2* and related centrosomal genes (*MCPH1, ASPM* and *CENPJ)* are linked to primary microcephaly, while mutations in the human pericentrin gene, known to interact with γ-tubulin (Dictenberg et al., 1998), can cause primordial dwarfism, a condition that also affects brain development (Rauch et al., 2008). Studies of these genes highlight the importance of γ-tubulin-interacting proteins in development. In higher eukaryotes the position of the spindle orientation affects the plane of cell division (Giansanti *et al.*, 2001; Fish *et al.*, 2006). Asymmetric cell division is an important mechanism for establishing cell differentiation; defects in microtubule nucleation can therefore have far-reaching effects on the growth and development of an organism.

Several proteins involved in microtubule nucleation contain the conserved centrosomin motif CM1, including *S. pombe* Mto1 and Pcp1, *S. cerevisiae* SPC110, *D. melanogaster* centrosomin and *H. sapiens* myomegalin and CDK5RAP2 (Sawin *et al.*, 2004; Zhang and Megraw, 2007; Fong *et al.*, 2008). This conserved motif is thought to mediate the interaction with γ-tubulin. The CM1 motif of *D. melanogaster* centrosomin is required for recruitment of γ-tubulin to the centrosome (Zhang and Megraw, 2007), and mutations in this region of Mto1 have been shown to disrupt the interaction between Mto1 and the γ-TuC, creating an *mto1*-null phenotype (Samejima et al., 2008). CM1-motif containing proteins are generally similar in structure, being large proteins (100-300 kDa), with several predicted coiled-coils, where the CM1 motif is positioned towards the amino terminus. However, the proteins have little sequence homology outside of the CM1 motif.

A short region of the carboxyl-terminus has been identified as necessary for correct Mto1 localisation (S. Rincon, Sawin Lab, personal communication). A truncated form of Mto1, with 64 nucleotides deleted at the carboxyl-terminal, Mto1(1-1051), is not present at the cell equator or the SPB; a slightly longer truncation, Mto1(1-1065) retains localisation to the cell equator but fails to localise to the SPB. From other truncations it has been deduced that residues 1065-1075 are required for localisation to the SPB during interphase and mitosis and 1085-1095 for localisation to the SPB only during mitosis. SPB localisation is not a pre-requisite for localisation of Mto1 to the eMTOC. The existence of these regions has led us to speculate that there may be a series of Mto1 interacting proteins that require these specific areas to interact with Mto1 and target them to the MTOCs at different times. A central aim of this project is to identify the protein that recruits Mto1 to the eMTOC.

Regulating the eMTOC

eMTOC formation is restricted to the end of anaphase. Detailed observation has established that Mto1 appears at the equator specifically when the SPBs are 8 μm apart, mid-way through anaphase B (Figure 4). What triggers the recruitment of Mto1 to the equator, leading to eMTOC formation? MTOC formation must be tightly regulated as part of the cell division cycle. Our current knowledge of eMTOC regulation suggests that multiple layers of control are present.

eMTOC formation is dependent on actin; in cells treated with latrunculin A to depolymerise F-actin, γ-tubulin is no longer present at the equator (Heitz et al., 2001) and PAAs are not seen (Pardo and Nurse, 2003). This indicates that the CAR or

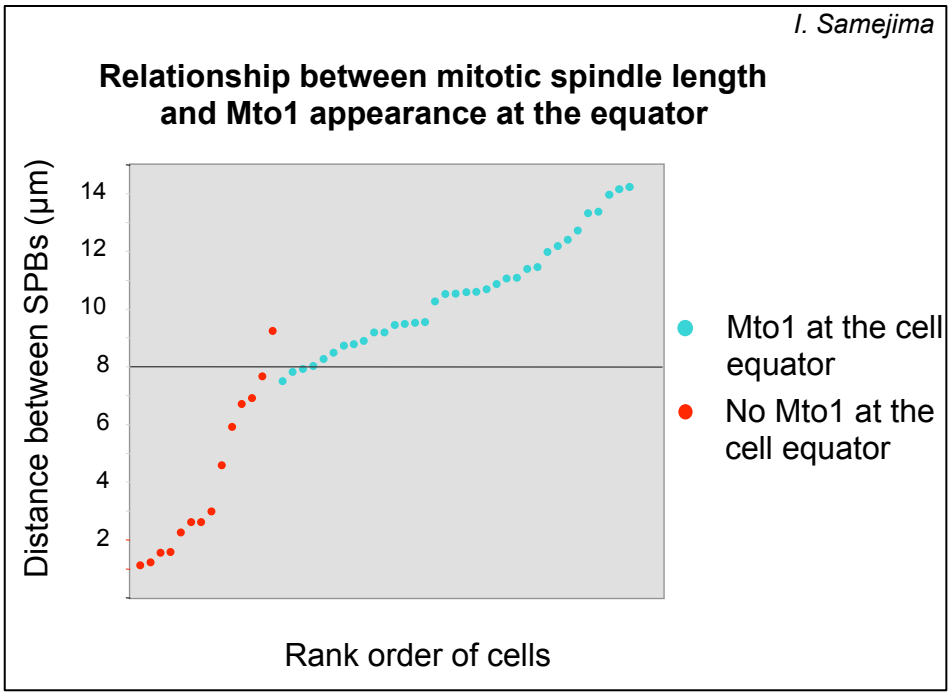

Figure 4 Timing of Mto1 appearance at the equator

Graph showing the mitotic spindle length, scored for the presence or absence of Mto1 at the equator and ranked according to increased length. Mto1 initially appears at the cell equator when the spindle measures ~8µm. At this time the cell is undergoing anaphase B. Data from I. Samejima, Sawin laboratory.

some other actin structure is required for eMTOC formation. The CAR forms at the cell division plane of animal cells and carries out cytokinesis. The CAR contains both actin and myosin and acts like a band of muscle, bisecting the cell when it contracts. The septum forms as the CAR contracts (Gould and Simanis, 1997); at the end of cytokinesis the septum is broken down, releasing two newly independent daughter cells. In *S. pombe* both the CAR and the eMTOC form in the centre of the cell. CAR assembly begins prior to SPB separation with the appearance of the type-II myosin heavy chain Myo2 plus the myosin light chains Rlc1 and Cdc4 at the cell equator (Kitayama et al., 1997; Le Goff et al., 2000; Motegi et al., 2004). Mid1 forms a wide band of small cortical nodes (Chang *et al.*, 1996; Sohrmann *et al.*, 1996; Bahler *et al.*, 1998a; Wu *et al.*, 2006). Polarity proteins at the cell tips also restrict Mid1 to the cell centre (Padte *et al.*, 2006; Huang *et al.*, 2007). In *mid1Δ* cells the CAR forms but is frequently mis-positioned (Chang et al., 1996; Sohrmann et al., 1996).

The components of the CAR appear in a defined sequence (Wu et al., 2003), a process that continues throughout mitosis. The nodes mature with the additional of three actin regulators: the IQGAP protein Rng2 (Eng et al., 1998), the formin Cdc12 (Chang et al., 1997) and the PCH protein Cdc15 (Fankhauser et al., 1995). Initially the CAR forms as a series of nodes that form a ring when Cdc12 nucleates actin filaments. In the node model of CAR formation these filaments are proposed to promote the coalescence of the network of nodes into a narrow band via a 'search, capture, pull and release mechanism' (Wu *et al.*, 2006; Vavylonis *et al.*, 2008). Evidence has also been found for an alternative 'aster' model (Arai and Mabuchi,

2002; Kamasaki et al., 2007), where F-actin is nucleated from a focus on one side of the cell (forming the 'aster'), rather than a network of short actin filaments. More work remains to be done to address outstanding issues and could lead to a new model of CAR formation that may incorporate aspects of both models. Following actin nucleation, the tropomyosin Cdc8 (Balasubramanian et al., 1992) then joins the ring, followed by the α-actinin Ain1 (Wu et al., 2001), and CAR construction concludes with the addition of a second type-II myosin, Myp2 (Bezanilla et al., 1997) shortly prior to CAR contraction.

The timing of cytokinesis must be precisely regulated so that it takes place only after chromosomes have been replicated and segregated. CAR contraction is controlled by the septation initiation network (SIN), the signalling pathway in *S. pombe* that directs the events occurring at the end of mitosis. The SIN has recently been shown to also be involved in CAR formation, being required for the hypophosphorylation and recruitment of Cdc15 to the CAR (Hachet and Simanis, 2008).The SIN is analogous to the mitotic exit network in *S. cerevisiae* and both pathways are GTPase signalling cascades that assemble at the SPBs (Simanis, 2003; Krapp *et al.*, 2004; Wolfe and Gould, 2005). Mutations in the SIN signalling pathway typically produce multi-nucleated cells that are unable to undergo cytokinesis (Balasubramanian et al., 1998); conversely, ectopic activation of the SIN can uncouple the cell division cycle from the nuclear division cycle, with cytokinesis taking place before genetic material has been segregated (Schmidt et al., 1997). The SIN pathway is necessary for eMTOC formation; γ-tubulin is not present at the cell equator in SIN mutant strains, despite the presence of a CAR (Heitz et al., 2001), and consistent with this, no PAA is

formed in SIN mutants (Pardo and Nurse, 2003). The SIN is negatively regulated by the spindle assembly checkpoint component Dma1 (Murone and Simanis, 1996; Guertin *et al.*, 2002), and γ-tubulin also does not localise to the cell equator when Dma1 is over-expressed (Heitz et al., 2001).

Figure 5 shows the proteins involved in the SIN. Sid4 and Cdc11 form a scaffold for signalling at the SPB (Krapp et al., 2001; Morrell et al., 2004), with Sid4 interacting with a structural component of the SPB, Ppc89. (Rosenberg et al., 2006). The SPBs are required for SIN signalling. Several of the SIN proteins show an asymmetric distribution, localising preferentially to the nascent SPB. The purpose of this is not clear and the 'mother' SBP can replace the 'daughter' if necessary (Magidson et al., 2006). The GTPase Spg1 then binds to Cdc11 (Morrell et al., 2004). Cdc11 is hyperphosphorylated during mitosis and this may be important for pathway activation (Krapp et al., 2001). Spg1 is regulated by Byr4 and Cdc16, which act together as a GTPase-activating protein (Furge et al., 1998). Byr4 contains binding sites for both Cdc16 and Spg1, and so mediates formation of the trimeric complex (Furge et al., 1999). No guanine nucleotide exchange factor has yet been identified for Spg1.

Once activated, Spg1 recruits Cdc7 to the SBP (Krapp et al., 2004). The kinase activity of Cdc7 is constant throughout the cell cycle (Sohrmann et al., 1998), indicating that the control of Cdc7 localisation may be important mechanism for channelling its activity. Then signal transduction continues first via the protein kinase Sid1 (in association with the regulatory subunit Cdc14) and then through

another kinase, Sid2 (in association with the regulatory subunit Mob1) (Guertin *et al.*, 2000; Krapp *et al.*, 2004). Sid2 relocates to the CAR from the SPB immediately prior to contraction (Sparks et al., 1999). The substrates of Sid2 have not been identified, and the ultimate trigger for CAR contraction is not currently known.

The SIN is integrated with other events in the cell cycle by the polo-like kinase, Plo1. Polo-like kinases have multiple functions during the cell cycle (Ohkura *et al.*, 1995; Donaldson *et al.*, 2001), but are primarily involved with promoting mitotic events, including mitotic exit. In *S. pombe* Plo1 is required for spindle formation and cytokinesis, including CAR formation (Ohkura et al., 1995) and localises to the mitotic SPB, mitotic spindle and to the CAR (Bahler *et al.*, 1998a; Mulvihill *et al.*, 1999; Mulvihill and Hyams, 2002). Plo1 lies upstream of the SIN, as over-expression of Plo1 induces CAR formation and septation in interphase cells (Ohkura *et al.*, 1995; Bahler *et al.*, 1998a); and Plo1 activity is independent of SIN activation (Tanaka et al., 2001). In agreement with this role for Plo1, Plo1 physically interacts with Sid4 (Morrell et al., 2004) and *plo1Δ* cells are unable to septate (Ohkura et al., 1995). Mutant alleles of a number of SIN genes are highly dependent on high-levels of expression of Plo1, suggesting that Plo1 and the SIN pathway functionally interact (Cullen et al., 2000). Plo1 over-expression is sufficient to drive eMTOC formation alongside CAR formation and septation, but only during the first round of multiple rounds of septation produced by the over-expression conditions (Heitz et al., 2001). As the SIN is necessary but not sufficient to drive eMTOC formation, this indicates that another pathway is additionally required to trigger eMTOC formation and suggests that Plo1 also activates this second regulatory pathway.

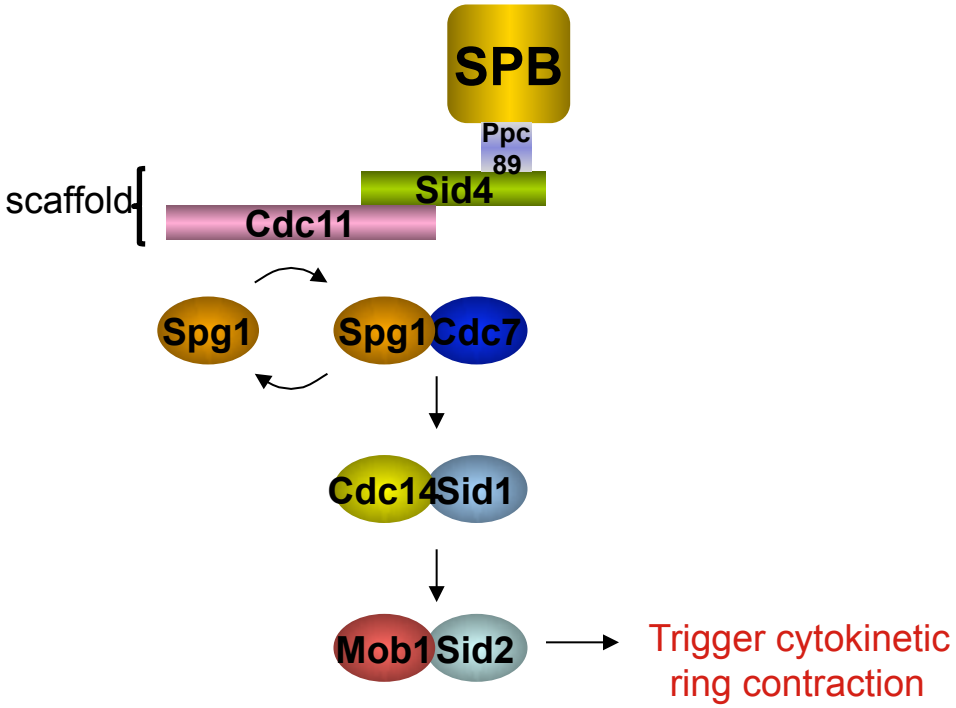

Figure 5 Outline of the SIN pathway

Sid4 and Cdc11 sit at the top of the SIN and form a scaffold for SIN pathway signaling at the SPB. Ppc89 links Sid4 to the SPB. The GTPase Spg1 is regulated by Byr4 and Cdc16 (not shown); once activated it binds the kinase Cdc7. The signal is transmitted through the additional kinases Sid1 and Sid2 (together with their regulatory subunits), triggering contraction of the CAR though an unknown mechanism.

It is also known that both γ-tubulin and Mto1 localise to the eMTOC independently of microtubules (Heitz et al., 2001; Sawin et al., 2004).

Polo is also known to activate the anaphase promoting complex (APC) (Charles et al., 1998; Descombes and Nigg, 1998; Nigg, 1998; Shirayama et al., 1998; van de Weerdt et al., 2005; van Leuken et al., 2009). The APC is an E3 ubiquitin ligase and initiates the events of anaphase by targeting key cell-cycle regulators for destruction by the proteasome (Zachariae and Nasmyth, 1999; Peters, 2006). In *S. pombe*, Plo1 has been found to physically interact with Cut23, a subunit of the APC, and over-expression of Plo1 can rescue a mutation in Cut23 that affects interaction with Plo1, causing metaphase arrest (May et al., 2002). The multiple subunits of the APC stably interact throughout the cell cycle, however the complex is transiently activated in mitosis and G1 by post-translational modification and association with APC activator proteins such as Slp1 and Ste9 (Peters, 2002). A number of *S. pombe* APC subunits have been identified (Yoon et al., 2002).

The action of the APC is blocked by the spindle assembly checkpoint until the mitotic spindle has correctly formed attachments to all chromosomes, in order to prevent aneuploidy. Once the kinetochore-microtubule attachments are established, inhibition of the APC is released (Reddy et al., 2007; Stegmeier et al., 2007), leading to sister chromatid separation. The mitotic spindle then elongates, segregating the chromosomes prior to cell division and the creation of new daughter cells. Recent work has identified a connection between the SIN and the APC: Nuc2p, a subunit of the APC, inhibits the SIN following cytokinesis (Chew and Balasubramanian, 2008).

Defects in the APC typically produce a 'cut' phenotype, where the single unreplicated nucleus is torn by the action of the contracting CAR in a cell that is unable to undergo anaphase (Hirano et al., 1986; Samejima et al., 1993; Yamada et al., 1997; Yanagida, 1998). Alternatively the cell division may generate one anucleate and one diploid cell. The APC is required for eMTOC formation, with γ-tubulin failing to localise to the equator in a number of 'cut' mutants, despite CAR formation and contraction (Heitz et al., 2001). It seems likely that the ability of Plo1 to drive eMTOC formation is due to its activation of both the APC and the SIN.

Controlled disassembly of MTOCs is also important when switching between different microtubule arrays. The J-domain protein Rsp1 is required for the disassembly of the eMTOC (Zimmerman et al., 2004b). Both *rsp1Δ* and the mutant *rsp1-1* strain (which contains a single amino acid substitution in the J-domain) have defects in interphase microtubule organisation and contain significantly fewer interphase bundles than wild-type cells. This leads to the random septum positioning that first led to the gene being identified. In *rsp1-1* cells, interphase microtubules radiate from a central aster that is the remains of the eMTOC from the previous round of cell division. Live imaging of alp4-GFP in *rsp1Δ* and *rsp1-1* cells shows that the eMTOC is not broken down after cytokinesis in these mutants. Rsp1 is reported to be necessary for the γ-tubulin complex to localise to satellite iMTOCs on microtubules based on alp4-GFP localisation in both *rsp1Δ* and *rsp1-1* cells. Rsp1 localises to these satellites and also to the SPBs and the eMTOC.

How Rsp1 contributes to eMTOC breakdown is not understood. Rsp1 has been shown to interact with Mto1 (Zimmerman and Chang, 2005); J-domain proteins interact with hsp70 proteins and the conformational change that accompanies this binding can disrupt other protein-protein interactions (for example the role of the J-domain protein auxilin in clathrin disassembly during endocytosis (Kelley, 1998). Therefore a Rsp1 mediated chaperone-based mechanism could disrupt the interaction between Mto1 and another component of the eMTOC (perhaps disrupting an interaction between Mto1 and the protein that recruits Mto1 to the eMTOC). Over-expression of Rsp1 inhibits eMTOC formation based on the localisation of Alp4-GFP; this inhibition requires an intact J-domain. It is interesting that the *rsp1-1* mutant should have a more severe phenotype than the *rsp1Δ* strain, although it is not clear what insight this provides into other functions of the Rsp1 protein.

In summary, eMTOC formation requires the CAR, the SIN regulatory pathway and the APC regulatory pathway. Once formed, the eMTOC nucleates the PAA and then breaks down at the end of cytokinesis, in a process that involves Rsp1. Localisation domains within Mto1 suggest that Mto1 may be recruited to the eMTOC by association with an unknown protein. The requirement for the CAR in eMTOC formation, plus the shared position of the eMTOC and the CAR at the cell equator suggest that this unknown protein could be a component of the CAR. Input from both the SIN and the APC regulatory pathways is required for γ-tubulin localisation to the eMTOC. This may take place through controlling Mto1, and so γ-TuC localisation. If so, the SIN and the APC will also be necessary for Mto1 localisation. Figure 6 outlines a hypothetical pathway for eMTOC formation.

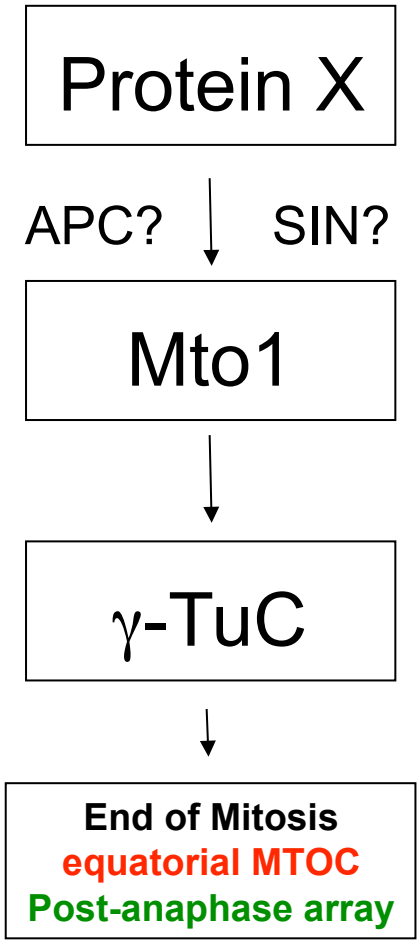

Figure 6 Schematic diagram showing hypothetical pathway of eMTOC formation

Mto1 recruits the γ-TuC to the site of the eMTOC. We propose that an additional protein, protein X, in turn interacts with Mto1 to recruit Mto1 to the eMTOC. In the absence of this protein Mto1 will not localise to the cell equator, no eMTOC will form and the PAA will not be nucleated. The SIN and the APC regulatory pathways are both required for eMTOC formation, but it is not known if they regulate the localisation of Mto1.

Project aims

To learn more about the regulation of microtubule nucleation in *S. pombe*, this work has focused on two objectives:

1. To identify the interacting protein(s) that recruit Mto1 to the site of the eMTOC
2. To investigate the regulation of Mto1 localisation to the eMTOC

Chapter III describes a yeast 2-hybrid screen performed to identify proteins that interact with Mto1. Chapter IV describes the identification of the type II myosin, Myp2, as being required for Mto1 localisation to the equator and further examines the interaction between Myp2 and Mto1, while Chapter V studies how Mto1 localisation to the site of eMTOC formation is regulated.

Chapter II - Materials and Methods

Strains, media and genetic methods.

Schizosaccharomyces pombe strains used in this work were grown in yeast extract (YE5S) medium or minimal medium with appropriate supplements (Moreno et al., 1991). Strain genotypes are listed in Table 1. *Saccharomyces cerevisiae* strains were grown in minimal medium with appropriate supplements (for 1 litre: 1.7 g yeast nitrogen base without amino acids (Bio 101 systems), 5 g ammonium sulphate, 1.47 g synthetic complete amino acid drop-out supplement lacking histidine, leucine, tryptophan (Kaiser mixture, Formedium), 20 g glucose, 2 pellets of sodium hydroxide.

The majority of stains made for this study were produced using genetic crosses. Freshly grown (1 day old) isolates of the strains to be crossed (one h+ and one h-) were streaked onto SPA plates. 10 μl of distilled water was added directly on top of the streaks and the strains mixed together using a sterile toothpick. Once dry the plates were left at 25-29°C for asci to form. These were then dissected to separate individual spores. A sterile inoculating loop was used to streak cells from 2-3 day old cross onto a plate of the relevant media (typically YE5S). The plate was then placed at 36°C for 1-4 hours to allow the ascus walls to break down. A Singer dissector was used to separate tetrads from a single cross and the plates placed at a suitable temperature to allow the spores to germinate (29°C; 25°C for temperature sensitive strains). Once colonies appeared, the donor plate was replicated onto selective media

to allow the identification of specific genotypes, coupled with visual inspection of fluorescent markers where appropriate. Temperature-sensitive strains were identified by replica plating in duplicate to media containing phloxin B, a dye that selectively stains dead cells, placing one plate at the restrictive temperature and one at the permissive temperature and comparing growth at the two different temperatures.

Random spore analysis was used in place of tetrad analysis for constructing strains where a large number of spores were to be analysed. 6 μl of Helicase (Helix pomatia juice, Life Technologies) was diluted in 600μl of sterile distilled water, a small amount of a three day old cross was added and the mixture incubated at 32°C for at least 6 hours to digest the ascus wall and vegetative cells. Spore number was counted using a haemocytometer and diluted appropriately in distilled water. The sample was then sonicated for 10 pulses at 50% power to separate spores and prevent the appearance of colonies with mixed genotypes. The sonicator tip being extensively cleaned with distilled water and finally ethanol between samples. Spores were plated at a density of 200-1000 spores per plate on appropriate media. If spores were plated to selective media, the same quantity of spores was also plated to YE5S to check the number of colonies emerging on the selective media relative to the total number of geminating spores.

Strains with *SV40:GFP-atb2* were created as follows. The original strain KS4956 *SV40:GFP-atb2* (kind gift of Fred Chang, Columbia University, USA) was crossed to KS4113 *cut4.533* to generate KS5062 *cut4.533 SV40:GFP-atb2* and also to KS4099 *cut9.665* to produce KS5106 *cut9.665 SV40:GFP-atb2*. KS4956 was also

crossed to the wild-type strain KS515 to change the mating type from h- to h+. KS5064 *h+ SV40:GFP-atb2* was then crossed to KS4111 *cut8.563* to generate KS5088 *cut8.563 SV40:GFP-atb2*. Rlc1-mCherry and Uch2-mCherry were later introduced to these strains by crossing KS5062 with KS4963 *cut4.533 myp2-YFP rlc1-mCherry uch2-mCherry* to create KS5177 *cut4.533 rlc1-mCherry uch2-mCherry SV40:GFP-atb2*, KS5106 *cut9.665 SV40-GFP-atb2* with KS5059 *cut9.665 alp4-GFP rlc1-mCherry uch2-mCherry* to create KS5179 *cut9.665 rlc1-mCherry uch2-mCherry SV40:GFP-atb2*. KS5088 was crossed with KS4843 *cut8.563 myp2-YFP rlc1-mCherry uch2-mCherry* to give KS5180 *cut8.563 uch2-mCherry SV40:GFP-atb2.* This in turn was crossed with KS4771 *nmt41:GFP-mto1 rlc1-mCherry uch2-mCherry* to give KS5203 *rlc1-mCherry uch2-mCherry SV40:GFP-atb2* and KS5205 *cut8.563 rlc1-mCherry uch2-mCherry SV40:GFP-atb2*.

Colony PCR was used to confirm gene deletion for KS4410 *myp2*Δ*::kanMx,* obtained from the *S. pombe* Deletion Mutant Library (Bioneer, http://pombe.bioneer.co.kr/). In the Bioneer deletion strains, the gene of interest has been replaced with a cassette containing a selectable kanamycine resistance marker via homologous recombination. DNA was prepared from freshly grown cells (1 day old). A pinhead amount of cells was added to 25 µl of 0.25% SDS/TE. The cells were boiled for 5 minutes, centrifuged to pellet cell debris and the supernatant retained. 25 µl PCR reactions were prepared as follows: distilled water to 25 µl, 1 µl DNA, 2.5 µl Buffer IV (10 × stock: 750 mM Tris-HCl pH 8.8, 200 mM $(NH_4)_2SO_4$, 0.1% Tween 20), 1.25 µl of 10 mM dNTPs, 3.5 µl of 25 mM $MgCl_2$, 2.5 µl of 10% Triton X-100, 0.25 µl each of OKS506/ OKS1856 (100 µM stock), 5 units Taq polymerase (Sawin laboratory) and 0.075 units of Pwo polymerase (Sawin

laboratory). The following PCR program was used: 1] 2 minutes at 94°C, 2] 30 seconds at 94°C, 3] 30 seconds at 50°C, 4] 3 minutes at 68°C, 5] Repeat steps 2-4 34 times, 6] 10 minutes at 68°C. This reaction generated an ~660 bp DNA fragment. No bands were seen for a control reaction carried out using template DNA from the wild-type strain KS516.

DNA sequencing was used to identify strains that contain *mto1-427* when constructing KS5067 *mto1-427 rlc1-mCherry uch2-mCherry*. Selective plating and visual screening was used to confirm the presence of both mCherry tagged proteins. Colony PCR was then used to amplify the *mto1* C-terminus. DNA was prepared from freshly grown cells (1 day old). A pinhead amount of cells was added to 25 µl of 0.25% SDS/TE. The cells were boiled for 5 minutes, centrifuged to pellet cell debris and the supernatant retained. 25 µl PCR reactions were prepared as follows: distilled water to 25 µl, 1 µl DNA, 2.5 µl Buffer IV (10 × stock: 750 mM Tris-HCl pH 8.8, 200 mM $(NH_4)_2SO_4$, 0.1% Tween 20), 1.25 µl of 10 mM dNTPs, 3.5 µl of 25 mM $MgCl_2$, 2.5 µl of 10% Triton X-100, 0.25 µl each of OKS1875/ OKS1138 (100 µM stock), 5 units Taq polymerase (Sawin laboratory). The following PCR program was used: 1] 2 minutes at 94°C, 2] 30 seconds at 94°C, 3] 30 seconds at 52°C, 4] 90 seconds at 72°C, 5] Repeat steps 2-4 34 times, 6] 3 minutes at 72°C. This reaction generated an ~500 bp DNA fragment. 5 µl of the PCR reaction was run on a 1% agarose gel to confirm the PCR reaction had worked. The remaining PCR was used for the sequencing reaction. To 6 µl of the remaining PCR product was added 1 µl Exonuclease I (NEB) and 1 µl Antarctic phosphatase (NEB). The reaction was incubated at 37°C for 15 minutes to degrade excess primer and to cleave 5' phosphates. The enzymes were then inactivated by heating at 80°C for 15 minutes. 2

μl of this mixture was added to 2 μl Big Dye 3.1 (Applied Biosciences), 5 μl distilled water and 1 μl of OKS1876 (6.7 μM stock) and the sequencing reaction was performed (96°C for 1 minute, then 25 cycles of: 96°C for 10 seconds, 50°C for 5 seconds, 60°C for 4 minutes) before samples were sent for sequencing to the University of Edinburgh sequencing service. The sequences were then examined to identify strains with the *mto1-427* substitutions: R1056A, E1059A and E1061A.

Colony PCR was used to distinguish between progeny containing *nmt41:GFP-mto1* and *mto1-GFP* during construction of SIN mutant strains. The oligonucleotides used to identify *nmt41:GFP-mto1* had homology to the kanamycin resistance marker associated with the respective promoter and to *mto1*. The second oligonucleotide pair recognised a region upstream of *mto1* and within the *mto1* coding region. DNA was prepared from freshly grown cells (1 day old). A pinhead amount of cells was added to 25 μl of 0.25% SDS/TE. The cells were boiled for 5 minutes, centrifuged to pellet cell debris and the supernatant retained. 25 μl PCR reactions were prepared as follows: distilled water to 25 μl, 1 μl DNA, 2.5 μl Buffer IV (10 × stock: 750 mM Tris-HCl pH 8.8, 200 mM $(NH_4)_2SO_4$, 0.1% Tween 20), 0.5 μl of 10 mM dNTPs, 1.5 μl of 25 mM $MgCl_2$, 1.25 μl of 20% Triton X-100, 0.125 μl each of OKS506/ OKS358 to identify *nmt41:GFP-mto1* or OKS506/ OKS503 to identify *mto1-GFP* (100 μM stock), 5 units Taq polymerase (Sawin laboratory), 0.075 units Pwo polymerase (Sawin laboratory). The PCR program used was as follows: 1] 2 minutes at 95°C, 2] 30 seconds at 95°C, 3] 30 seconds at 45°C, 4] 3 minutes at 72°C, 5] Repeat steps 2-4 34 times, 6] 5 minutes at 72°C. This reaction generated an ~1 Kb DNA fragment. 20 μl of the PCR reaction was run on a 1% agarose gel.

N-terminal gene tagging in *S. pombe*

A number of N-terminal truncations of Mto1 were created, where Mto1 was tagged with GFP and expressed from the nmt81 promoter. The method used is based on techniques described in (Bahler *et al.*, 1998b). Oligonucleotides were used to amplify a region of a plasmid pKS715 that contains the sequence for nourseothricin resistance, the *nmt81* promoter and the GFP tag; these oligonucleotides also have homology to *mto1*, allowing the cassette generated to integrate via homologous recombination. The oligonucleotide pair OKS444/ OKS1940 was used to generate *nmt81:GFP-mto1(801-n)* truncations (KS5227 *nmt81:GFP-mto1(801-1115)*, KS5293 *nmt81:GFP-mto1(801-1051)*), with OKS444/ OKS1941 used to generate *nmt81:GFP-mto1(919-n)* truncations (KS5228 *nmt81:GFP-mto1(919-1115)*, KS5230 *nmt81:GFP-mto1(919-1051)*). Two strains were used for the strain construction, the wild-type strain KS516 and the KS1957 *mto1(1-1051)::ura4+* strain so that a single PCR cassette could be used to create truncations of the *mto1* gene that finished at either the 1115 amino acid or 1051 amino acid position, depending on which yeast strain the cassette was inserted into. For the strain KS1581 *nmt81:GFP-mto1(481-1115)*, OKS444/ OKS448 were used to amplify a region of plasmid pKS170 that contains the sequence for kanamycin resistance, the *nmt81* promoter and the GFP tag, and the cassette was inserted into the wild-type KS516 strain.

50 μl PCR reactions were prepared as follows: distilled water to 50 μl, 20 ng of plasmid template DNA, 5 μl Buffer IV (10 × stock: 750 mM Tris-HCl pH 8.8, 200 mM $(NH_4)_2SO_4$, 0.1% Tween 20), 2.5 μl of 10 mM dNTPs, 7 μl of 25 mM $MgCl_2$,

0.1 μl of each oligonucleotide (100 μM stock), 0.4 units Taq polymerase (Sawin laboratory), 7.6 units Pwo polymerase (Sawin laboratory). The PCR program used was as follows: 1] 2 minutes at 95°C, 2] 15 seconds at 95°C, 3] 30 seconds at 56°C or 60°C, 4] 7 minutes at 72°C, 5] Repeat steps 2-4 29 times, 6] 5 minutes at 70°C. This reaction generated an ~3.1 Kb DNA fragment. 0.5 μl of the PCR reaction was run on a 1% agarose gel to confirm the reaction was successful. The DNA was then cleaned up using phenol/chloroform/isoamyl (PCI). 0.5 ml of PCI solution (25:24:1) was added to an equal volume of PCR product, vortexed, centrifuged for 5 minutes at 13K rpm and the supernatant recovered. This step was repeated first with PCI and then with chloroform alone. One-tenth volume of 3 M NaOAc was added to the final recovered supernatant, and two volumes of ethanol. This mixture was then centrifuged at 4°C for 10 minutes at 13K rpm. The pellet was washed with 1ml 70% ethanol and centrifuged for 5 minutes at 13K rpm. The pellet was then air-dried and resuspended in TE (10 mM Tris pH 7.5, 1 mM EDTA). Samples of the purified DNA were run on an agarose gel to estimate the DNA concentration.

The DNA cassettes were then transformed into yeast. Cultures were grown to mid-exponential growth, with 20 ml of culture used per transformation. Cells were harvested by centrifugation for 5 minutes at 3K rpm. The cells were then washed in an equal volume of distilled water, spun again before being re-suspended in 1 ml of 1M LiOAc pH7.5/TE. The cells were centrifuged for 1 minute at 13K rpm, resuspended to 2 x 10^9 cells in 1M LiOAc pH7.5/TE and dispensed into 100 μl aliquots. ~20 μg of purified PCR product was used per transformation and incubated for 10 minutes at room temperature. 260 μl of freshly prepared PEG^{3350}/LiOAc/TE

was added and gently pipetted to mix before incubating at room temperature for 30 minutes. 43 μl of DMSO was then added and the cells heat shocked for 5 minutes at 42°C. They were then centrifuged for 1 minute at 13 000 rpm and washed with 1 ml of distilled water. Finally cells were resuspended in 400 μl distilled water and plated to 2 x YE5S plates. Incubate plates at 32°C overnight, replica plate to YE5S/ appropriate antibiotic plates (nourseothricin: 100 μg/ml or G418: 100 μg/ml), grown for 2 days then replica plated to fresh YE5S/ antibiotic plates and incubated overnight. Colonies were streaked to YE5S, incubated for 2 days and then replica plated to YE5S/ antibiotic plates to check stable integration.

Colony PCR was used to check that the cassettes had integrated at the correct position in the genome, using oligonucleotides with homology to the GFP tag and to *mto1*. DNA was prepared from freshly grown cells (1 day old). A pinhead amount of cells was added to 25 μl of 0.25% SDS/TE. The cells were boiled for 5 minutes, centrifuged to pellet cell debris and the supernatant retained. 25 μl PCR reactions were prepared as follows: distilled water to 25 μl, 1 μl DNA, 2.5 μl Buffer IV (10 × stock: 750 mM Tris-HCl pH 8.8, 200 mM $(NH_4)_2SO_4$, 0.1% Tween 20), 0.5 μl of 10 mM dNTPs, 1.5 μl of 25 mM $MgCl_2$, 1.25 μl of 20% Triton X-100, 0.125 μl each of forward and reverse oligonucleotides (100 μM stock), 5 units Taq polymerase (Sawin laboratory), 0.075 units Pwo polymerase (Sawin laboratory). The oligonucleotides OKS506/ OKS358 were used for to test KS1581 and OKS358/ OKS1796 for all other strains. OKS506 has homology to the KanMx region of the PCR cassette, OKS1796 to the NatMx region and OKS358 has homology to sequence upstream of *mto1*. The PCR program used was as follows: 1] 2 minutes at

94°C, 2] 30 seconds at 94°C, 3] 30 seconds at 47°C, 4] 3.5 minutes at 68°C, 5] Repeat steps 2-4 34 times, 6] 10 minutes at 68°C. This reaction generated an ~1.3 Kb DNA fragment (~800 bp for KS1581). 5 μl of the PCR reaction was run on a 1% agarose gel.

Expression was further confirmed using PAGE on an 8% acrylamide gel to run boiled extracts prepared from the strains (using the standard protocol described below), followed by Western blotting using anti-GFP at 1:300 (3.0, Sawin laboratory). The strains were then imaged using wide field microscopy to further check the expression of the tagged protein and to determine the localisation of the truncated *mto1* alleles.

Plasmid shuffle system

Sub-cloning was used to construct the Pcp1 plasmids used in the plasmid shuffle system. pKS310 contains a 9.5 Kb genomic region encompassing the *pcp1* gene in the *pBSKS* vector. A 7.6 Kb section was excised using XbaI/XhoII, the fragment blunted and 'tailed' by the T4 polymerase mediated addition of nucleotides. This fragment was then inserted into *pGEM-T* (Promega). The fragment could insert in two distinct orientations relative to the different multiple cloning regions present on either side of the insertion site. From one orientation, a fragment of *pcp1* containing the promoter region and the coding region was sub-cloned into pUR19 using a SalI site present in *pGEM-T* and a HpaI site present downstream from the *pcp1* stop codon, to create pKS477. The alternative orientation was used as a basis for constructing the second plasmid. This plasmid was designed to have coding region

under the control of the endogenous promoter, with a carboxyl-terminus GFP tag. First the final 800 nucleotides of the pcp1 cloning sequence were amplified by PCR. This fragment was subcloned into *pGEM-T-pcp1* using a BglII site present in *pcp1*, and a SalI site introduced during the PCR. This created new plasmid where the insert finished at the end of the *pcp1*-coding region with the stop codon removed. Then the promoter and the coding region were subcloned into *pALKS-GFP* using ApaI/SalI sites to create pKS480. pKS477 has a URA3 selectable marker and pKS480 has a LEU2 marker. Pcp1 is expressed under the control of the endogenous promoter as over expression of Pcp1 has been shown to lead to the formation of super-numerary SBP-like structures (Flory et al., 2002). pKS477 was used to generate the haploid *pcpΔ* strain KS2973 with the genomic deletion 'covered' by a plasmid-based copy of *pcp1*. The construction of this strain is described in the text.

Yeast two-hybrid screening

The bait plasmid pKS481 *pBTM116-mto1(769-1115)* was used in the yeast two-hybrid screen and was constructed by digesting pKS282 *pGEM-T.Mto1* with NruI and Not1 and inserting the fragment released into the two-hybrid LexA bait vector pBTM116 and transformed into the *S. cerevisiae* test strain KS3048 *L40Δgal*. Expression of the bait protein was confirmed via Western blotting of yeast protein extracts with both anti-LexA (Santa Cruz, sc-7544) and anti-Mto1 (Sawin laboratory, S897). A meiotic *S. pombe* library (KS158, the kind gift of T Nakamura, Osaka City University, Japan) was sequentially transformed into the bait-plasmid containing strain. This library contains ~ 1 million independent cDNA fragments inserted into the prey vector *pGAD424*. The transformation method used is based on that

described by Gietz and Woods, 2006. A 250 ml culture of *L40Δgal* containing pKS481 was grown overnight at 30°C in minimal medium lacking tryptophan. This culture was used to inoculate a 250 ml culture of pre-warmed YPDA to reach mid-exponential growth after ~ 4 hrs. Cells were harvested by centrifuging 50 ml aliquots for 5 minutes at 3 000 rpm, re-suspending in 25 ml dH_2O, centrifuging as before, before re-suspending in 1 ml dH_2O and centrifuged for 2 minutes at 3 000 rpm before removing the supernatant. The cells were then resuspended in 3.4 ml transformation mix (2.4 ml PEG^{3350}, 360 µl 1M LiOAc, 90 µl dH_2O with 500 µl of carrier DNA (Salmon Testes DNA, Sigma, 2 mg/ml in TE (10 mM Tris-HCl pH8.0, 1 mM EDTA) boiled for 5 minutes and cooled on ice before it was added to the transformation mix). 50 µl of the meiotic cDNA library was added to each transformation reaction and the transformation reactions vortexed for 30 seconds. The reactions were then heat shocked for 20 minutes at 42°C, inverting the tubes every 5 minutes to re-distribute the mixture. The reactions were centrifuged for 2 minutes at 3 000 rpm, re-suspended in 1 ml dH_2O and finally 100 µl of cell suspension plated to selective medium lacking tryptophan (to select for the bait plasmid), leucine (to select for the prey plasmid) and histidine. Plates were incubated at 30°C. 10 µl of cell suspension was plated to selective medium lacking tryptophan and leucine to estimate the efficacy of the transformation. ~3.4 x 10^6 prey plasmids were screened for Mto1(769-1115)-interacting clones. Interaction was determined by induced expression of both His and LacZ reporter genes. To identify expression of the LacZ reporter gene, an X-gal overlay assay was performed (Fromont-Racine et al., 2002). For each agar plate 10 ml of overlay mixture heated to 50°C was added directly onto the plate surface (5 ml 0.5 M Na_2HPO_4 pH 7.5, 4.7 ml 1% (w/v) agar,

200 µl 2% w/v) X-Gal in dimethylformamide (DMF), 100 µl 10% (w/v) SDS). Plates were checked after 23 hrs at 30°C. In colonies expressing LacZ 5,5'-dibromo-4,4'-dichloro-indigo is produced and the colonies become blue; positive colonies were then picked through the overlay agar using toothpicks.

Interacting plasmids were sequenced to identify the gene they contained. Colony PCR was used to amplify the inserts of prey plasmids to be identified. DNA was prepared from freshly grown cells (1 day old) as follows. A repeat pipettor was used to add 25 µl of 0.25% SDS/TE to the wells of a 96-well plate. A pinhead quantity of cells was added to each well and the plate boiled for 5 minutes. The plate was then centrifuged to pellet cell debris and 20 µl of the supernatant for each sample retained. This DNA was used in PCR reactions. For each 25 µl PCR reaction the following was prepared: distilled water to 25 µl, 1 µl DNA, 2.5µl Buffer IV (10 × stock: 750 mM Tris-HCl pH 8.8, 200 mM $(NH_4)_2SO_4$, 0.1% Tween 20), 1.25µl of 10 mM dNTPs, 3.5 µl of 25 mM $MgCl_2$, 2.5 of 10% Triton X-100, 0.25 µl each of OKS1111/ OKS1112 (100 µM stock), 1 units Taq polymerase (Sawin laboratory). The following PCR program was used: 1] 2 minutes at 94°C, 2] 20 seconds at 94°C, 3] 30 seconds at 50°C, 4] 2 minutes at 74°C, 5] Repeat steps 2-4 34 times, 6] 10 minutes at 74°C. Colony PCR was also used to specifically identify (and exclude) prey plasmids that contained the *his5*+ gene. This was performed as above, substituting oligonucleotides OKS1123/ OKS1124. Where the prey insert was not amplified by the first round of PCR, colony PCR was repeated using different oligonucleotides (OKS113/114), increasing the extension time to 6 minutes and decreasing the annealing temperature to 68°C.

5 μl of the PCR was run in a 1% agarose gel to confirm the PCR. The remaining PCR product was used for sequencing reactions, To 6 μl of the PCR product was added 1 μl ExoI (NEB) and 1 μl Antartic phosphatase (NEB) to degrade excess oligonucleotides and cleave 5' phosphates. No additional buffer was required. The mixture was incubated at 37°C for 15 minutes, then heated to 80°C for 15 minutes to inactivate enzyme activity. The DNA was then used directly for sequencing. 2 μl of DNA was added to 2 μl of Big Dye 3.1 (Applied Biosystems), 1 μl of OKS1113 (6.7 μM stock) and 5 μl 'better buffer' (20 mM Tris-HCl pH8.0, 5 mM $MgCl_2$). The sequencing reaction was performed as follows: 96°C for 1 minute, then 25 cycles of: 96°C for 10 seconds, 50°C for 5 seconds, 60°C for 4 minutes and samples were sent for sequencing to the University of Edinburgh sequencing service. The sequence was then identified by BLAST search of the NCBI database.

To retrieve prey plasmids from *S. cerevisiae*, cultures were grown in selective medium minus leucine for 2-3 days at 30°C. 1 ml of culture was then centrifuged for 30 seconds at 13 000 rpm and the cell pellet was resuspended in 100 μl lysis buffer (2.5 M LiCl, 50 mM Tris-HCl pH 8.0, 4% Triton X-100, 62.5 mM EDTA). The samples were bead beaten with zirconium beads for 2 x 30 seconds at setting 5.0. A hole was pierced in the bottom of each tube and the liquid collected into a second tube by brief centrifugation. The plasmid DNA was then purified using a Qiagen Miniprep kit, eluting in 30 μl buffer EB provided. The plasmid DNA was then transformed into XL1-blue *E. coli* cells. 50 - 100 μl of cell suspension was added to the eluted DNA and the cells incubated for 30 minutes on ice before a 90 second heat

shock was applied at 42°C. The cells were returned to 4°C for 5 minutes, 1 ml LB media added, then incubated at 37°C for 1 hr prior to plating to selective media. Colony PCR using oligonucleotides with homology to the GAL4 activation domain was then used to distinguish between bacterial colonies containing prey and bait plasmids. For each reaction: distilled water to 25 µl, 2.5µl Buffer IV(10 × stock: 750 mM Tris-HCl pH 8.8, 200 mM $(NH_4)_2SO_4$, 0.1% Tween 20), 0.5 µl of 10 mM dNTPs, 1.5 µl of 25 mM $MgCl_2$, 2.5 of 10% Triton X-100, 0.125 µl each of OKS1249/ OKS1250 with homology to the GAL4 activation domain (100 µM stock), 1.8 units Taq polymerase (Sawin laboratory) and 0.01 units Pwo polymerase (Sawin laboratory). The PCR program used was: 1] 5 minutes at 95°C, 2] 15 seconds at 95°C, 3] 30 seconds at 50°C, 4] 2 minutes at 72°C, 5] Repeat steps 2-4 34 times, 6] 5 minutes at 72°C, producing a 400 bp product. Template DNA was provided by inserting a pipette tip into the bacterial colony of interest and dipping it into the PCR reaction mix.

Plasmids containing a series of *mto1* C-terminal truncated at different points within the Mto1 localising region were created to test whether this region was required for interaction with genes that had previously interacted with Mto1(769-1115). These plasmids are pKS507 *pBTM116-mto1(769-1051)*, pKS759 *pBTM116-mto1(769-1065)*, pKS760 *pBTM116-mto1(769-1075)*, pKS762 *pBTM116-mto1(769-1095)* and pKS918 *pBTM116-mto1(769-1085)*. PCR was used to amplify the required regions of *mto1* using oligonucleotides that introduced SmaI and SalI restriction sites at the 5' and 3' ends of the fragments respectively. Each fragment was ligated into *pGEM-T*, sequenced, and digested with SmaI and SalI, prior to insertion into *pGAD424*.

Expression was confirmed by Western blotting using anti-Mto1(Sawin laboratory, S897).

To map the region of Cdc11 required for interaction with Mto1 in *S. cerevisiae L40Δgal*, a series of plasmids (pKS752-758) containing fragments of *cdc11* were constructed. PCR was used to amplify the required regions of *cdc11* using oligonucleotides that introduced SmaI and BamHI restriction sites at the 5' and 3' ends of the fragments respectively. Each fragment was ligated into *pGEM-T* and sequenced, then digested with SmaI and BamHI and sub-cloned into *pGAD424*. The presence of each insert was confirmed using colony PCR.

A number of prey plasmids containing candidate genes to test for interaction with Mto1 were constructed using the Gateway system (Invitrogen). *pDONR201* donor vector plasmids were obtained from the ORFeome collection ((Matsuyama et al., 2006)). *myp2* and *rng3* were recombined into *pACT2.2gtwy* using LR II recombinase to form pKS873 and pKS872. *pACT2.2gtwy* contains the Gal4 activation domain followed by a HA tag and has the LEU2 selectable marker. The donor plasmids used for *spn1* and *cdc4* were the kind gift of Hiro Yamano, Marie Curie Research Institute, UK and contained cDNA sequence rather than genomic gene sequence, as these genes contain introns. *spn1* and *cdc4* were also inserted into *pACT2.2gtwy* to give pKS915 and pKS916. Successful recombination was confirmed by restriction digest.

cdc12 was inserted into *pGAD424* to test for interaction with Mto1. The reading frame of *pGAD424* was shifted by the insertion of a linker region formed from two

oligonucleotides into the multiple cloning site. *pGAD424* was digested with EcoRI and SalI, gel purified then ligated in the presence of OKS1314 and OKS1315 to create *pGAD424-1*. Insertion of the linker region was confirmed by sequencing. *pGAD424-1* (pKS630) was then digested with BamHI and SalI and *cdc12* excised from *pUR19.nmt1.cdc12* using BamHI and XhoI was inserted. Insertion was confirmed by colony PCR and restriction digest.

Semi-quantitative assays of β-galactosidase expression were carried out using 2-nitrophenol-β-D-galactopyranoside (ONPG; Sigma) as a substrate. 5 ml cultures in appropriate selective media were grown overnight at 30°C, before being diluted 1:5 in YPD medium. The diluted cultures were grown for 3-5 hrs at 30°C until they reached OD_{600} 0.5-0.8. When cultures had reached the appropriate OD, 1.5 ml of each sample was centrifuged at 13 000 rpm for 30 seconds and the cell pellets resuspended in 1.5 ml of Z buffer (60 mM $Na_2HPO_4.2H_2O$, 40 mM $NaH_2PO_4.2H_2O$, 100 mM KCl, 100 mM $MgSO_4$.7H2O, adjusted to pH 7.0) and centrifuged at 13 000 rpm for 30 seconds. The supernatant was removed and the cell pellet resuspended in 300 µl of Z buffer. Two samples of 100 µl were taken from this and snap-frozen in liquid nitrogen before being thawed by heating to 37°C. This freeze-thaw cycle was repeated twice more and 700 µl Z buffer with 270 µl 2-mercaptoethanol per 100 ml Z buffer was added to each tube. 160 µl of ONPG (4 mg/ml in Z buffer) was then added to the tubes. The samples were incubated at 30°C. Samples were inspected regularly for the appearance of a yellow colour; when this colour appeared in one sample, 400 µl of 1 M Na2CO3 was added to all the samples. Tubes were centrifuged for 10 min at 13 000 rpm to pellet cell debris and the OD_{420} measured

relative to a blank control sample. Samples were adjusted so that the readings were within OD_{420} 0.02-1.0, to be within the linear range of the assay and the adjustment added in to the concentration factor used to for calculating β -galactosidase units. β -galactosidase units = 1 000 x OD_{420}/(t x V x OD_{600}) where t = elapsed time (in min) of incubation, V = 0.1 ml x concentration factor and OD_{600} = A_{600} of 1 ml of culture.

Microscopy

Equipment and image analysis

Wide-field microscopy used a Nikon 100x/1.40 NA Plan Apo objective on a Nikon TE300 inverted microscope. This was connected to a Coolsnap HQ CCD camera (Photometrics). For spinning-disc confocal microscopy, a Nikon 100x/1.45 NA Plan Apo objective was used on a Nikon TE2000 inverted microscope, connected to a Yokogawa CSU-10 spinning disc confocal head (Visitech) and a Coolsnap HQ CCD camera. Image acquisition, processing and analysis were carried out using Metamorph software (Molecular Devices). Maximal projections are shown for all imaging. Microscope images were adjusted using only linear contract enhancement with Metamorph (Molecular Devices) or Photoshop (Adobe) software. Time-lapse images to compare samples were imaged under identical illumination conditions; the brightness and contrast was later scaled using consistent values to allow accurate comparisons to be made.

Mto1 localisation to the equator

To examine whether Mto1 localisation to the equator requires actin, KS3692 *hht2*-

GFP nmt81:GFP-mto1(784-1115) cells were treated with Latrunculin B (to 100 μM, 20 mM stock solution, Calbiochem) or DMSO (solvent, equal volume) for 30 minutes at 25°C prior to imaging by wide field microscopy.

PAA formation in Myp2Δ cells

Time-lapse wide-field microscopy was used to examine PAA formation in *myp2* and *myp2Δ* cells expressing GFP-atb2 under the control of the *nmt81* promoter. Cells were grown in minimal medium at room temperature (25°C). 1 μl of pelleted cells resuspended in a little media was spotted on to an EMM/ 2% agarose pad on a standard microscope slide before imaging. 7 z-sections, 0.6 μm apart were acquired at 30-second intervals using Metamorph software. Video sequences were deconvolved using the Softworx (Applied Precision) and maximum projections were used for movies at 10 frames per second (300-fold increase in speed) using Quicktime 7.4.1 (Apple) and H.264 video compression. Image stills also show deconvolved maximal projections.

nda3-KM311 arrest

To observe whether Mto1 was present at the equator during *nda3-KM311* arrest using immunostaining, *nda3-KM311* cells were grown in YE5S media for 9 hrs at 18°C. Samples were collected prior to the transfer to the permissive temperature and 10 and 20 minutes after transfer to the permissive temperature of 36°C. Samples were collected for immunofluorescence using rapid filtration, the filter then being immersed into cold (-80°C) methanol. Samples were further processed by washing

twice in 1 ml PEM (0.1 M NaPipes pH6.8, 1 mM EGTA, 1 mM $MgCl_2$), the cell wall digested by incubation with 1 ml freshly prepared PEMS (PEM + 1.2 M sorbitol) with 1 mg/ml zymolysase (ICN) for 30 minutes – 1hr at 37°C. Digestion was confirmed by mixing a sample of cells with 10% SDS and observing loss of refractility using phase contrast microscopy. Cells were then washed twice with PEM, once with PEM + 1% Triton X-100, and washed twice more with PEM, before being incubated with PEMBAL (PEM + 1% BSA, 0.1% NaN_3, 100 mM lysine (monohydrochloride)), rotating, for 1 hr. Anti-tubulin staining used the TAT1 antibody (Woods et al., 1989), kindly provided by Prof. Keith Gull (Oxford University), at 1:40 dilution, followed by extended (1 – 2 hr) washes in 500 µl PEMBAL. Alexa 488 labelled donkey anti-mouse secondary antibody (Molecular Probes Europe BV) was used at 1:50 dilution, followed by three further extended washes with PEMBAL. Samples were re-processed for staining with anti-Mto1 (Sawin laboratory, anti-mod20 B, affinity purified against C-terminus of Mto1) using the blocking solution KOM1 (100 mM NaPIPES (pH 6.8), 1 mM MgCl2, 2% nonfat milk, 100 mM lysine (monohydrochloride) 5% glycerol and 0.05% NaN_3) to give low fluorescent background. KOM1 was filter-sterilized before use to remove precipitated milk protein. The secondary antibody used was Alexa 568 donkey anti-sheep (Molecular Probes Europe BV) at 1:30 dilution. Cells were then observed using wide field microscopy. The experiment was then repeated as before, with an extra time point taken 30 minutes after the transfer to 36°C and sampling wild-type cells grown in YE5S media for 9 hrs at 18°C. Cells were immunostained as previously, and also stained with DAPI (4,6-diamino-2-phenylindole, 1µg/ml). For

imaging, cells were spun onto coverslips previously coated with poly-L-lysin (10 mg/ml).

To observe whether Mto1 was present at the equator during *nda3-KM311* arrest using live cells, cultures were grown in YE5S media for 9 hrs at 18°C. KS4939 *nmt41:GFP-mto1 nda3-KM311 rlc1-mCherry* cells and the control strain KS4942 *nmt41:GFP-mto1 rlc1-mCherry* were then centrifuged in a chilled centrifuge (18°C) to pellet cells. Images were then taken at room temperature. For strain KS4939 the culture was also warmed in a shaking water bath (36°C) to release the arrest. Cells were centrifuged in a centrifuge to pellet cells and the slide placed on a pre-heated block while being transported to the microscope. Imaging was carried using a wide field microscope fitted with an objective heater (Bioptechs) set at 36°C.

Imaging of temperature-sensitive mutant strains

To study the accumulation of cut cells over time for strains with mutations in the anaphase promoting complex, cultures were grown in YE5S media at 25°C until they reached mid-exponential growth and were then transferred to 36°C. A sample of each culture was collected by rapid filtration and fixed in -80°C methanol every 30 minutes before being stained with DAPI stain (1μg/ml) and calcofluor (50 μg/ml, Sigma F-6259) to stain the nucleus and septum.

To study nuclear accumulation in strains with mutations in the septation initiation network, cultures were grown in minimal media at 25°C until they reached mid-exponential growth and were then transferred to 36°C. At 30-minute intervals a

sample of each culture was collected and fixed with formaldehyde (133 µl 30% formaldehyde solution was added to 1 ml of culture and left for 1 hr at room temperature. Cells were washed three times in an equivalent volume of PEM (0.1 M NaPipes pH6.8, 1 mM EGTA, 1 mM $MgCl_2$) extracted for 30 seconds with PEM/1% Triton X-100 and washed three additional times in PEM. 300 U of Alexa fluor 568 phalloidin (Molecular Probes Europe BV) was re-suspended in 1.5 ml methanol. 15 µl aliquots were evaporated using a speed-vacuum and stored at -80°C. To stain cells, 7 µl was added to a 1µl pellet of fixed, extracted cells. 0.5 µl of the stained cells were then mixed with 2.5 µl PEM and placed on a microscope slide for imaging. Cells were co-stained with DAPI (1µg/ml).

Time-lapse spinning-disc confocal microscopy was used to determine the effect of regulatory pathways on Mto1 localisation. Cultures of temperature-sensitive SIN and APC strains were grown to mid-exponential growth at the permissive temperature (25°C) before being transferred to the restrictive temperature. APC mutant strains were grown in YE5S media. SIN mutant strains expressing GFP-atb2 were grown in EMM and SIN mutants strains expressing GFP-Mto1 were grown in EMM + 15 µM thiamine to repress the expression of GFP-Mto1 from the *nmt41* promoter. Imaging at the restrictive temperature was carried out using the Delta T system (Bioptechs). The Delta T system uses thermal transfer from the surface of the slide directly to the sample, in contrast to other methods that use peripheral heating. Agarose pads were pre-cast onto 19 mm diameter coverslips, by sandwiching ~16 µl of 2% agarose dissolved in the appropriate media in-between two coverslips separated with scotch tape. This was left to set and the coverslips were later separated by sliding them

apart. Cells were collected from the culture at the restrictive temperature and centrifuged for ~10 seconds in a pre-warmed eppendorf tube to pellet cells. Care was taken throughout to keep cells at the appropriate temperature to maintain the arrest state. The tube was immediately replaced in a metal heat block heated to the appropriate temperature and taken to a heated room (37°C) where slide construction took place. 1 µl of pelleted cells resuspended in a little media was spotted onto the agarose pad on the coverslip, and the coverslip then gently laid onto the Delta T slide. The finished slide was placed into a metal carrying chamber (shown in Figure 7) to maintain the temperature as the slide was taken from the heated room to the slide. The Delta T slide is then mounted on the confocal microscope using an adaptor. An objective heater (Bioptechs) was also used in conjuncture with the Delta T system. 8 z-sections, 0.6 µm apart were acquired at either 30- or 60-second intervals.

Preliminary time-lapse microscopy to study Mto1 localisation in wild-type and *cut4.533* strains after 2 hrs at the restrictive temperature used lectin to attach cells directly to the Delta T slide. 5 µl of lectin solution (0.3 mg/ml in water, Sigma L1395) was added to the slide surface. 5 µl of pelleted cells resuspended in a little media were mixed with the lectin and the suspension spread over the surface of the slide using a pipette tip. This was left for 3 min at 37°C to allow cells to adhere to the glass. The slide was then rinsed with 3 x 1 ml pre-warmed media, 1 ml pre-warmed media was added to the slide and the slide placed into the metal carrying chamber for

Figure 7 Pre-warmed chamber for Delta T slide transportation

Metal carrying chamber used to maintain cells at the restrictive temperature during transport to the microscope. The chamber is pre-warmed to the desired temperature and Delta T slides fit tightly inside.

transport to the microscope as before. Cell density is significantly improved using agarose pads, compared to this method.

Imaging of Mto1-GFP localisation during *cps1-191* arrest also used the Bioptechs system described above in association with the confocal microscope to maintain samples at the restrictive temperature. Cultures were grown at 25°C until they reached mid-exponential growth and then shifted to the 36°C for 2hr 45 minutes to induce arrest. Slides were prepared as described above, and imaging started from 3 hrs after the shift to 36°C. Settings used: 488 nm laser, 800 ms at 35% power, bin 2, 8 x 0.6 μm sections. A sample of each culture was collected by rapid filtration and fixed in -80°C methanol before being stained with Hoechst stain 33342 (1 μg/ml) to confirm the arrest based on the accumulation of binucleate cells. Images were identically adjusted to allow direct comparison.

Measuring CAR position

To determine the role of the PAA in centring the CAR the strains KS5065 *mto1-427 rlc1-mCherry uch2-mCherry* and KS5067 *rlc1-mCherry uch2-mCherry* were imaged. The position of the CAR in binucleate cells was determined by measuring from the CAR to each cell tip using the Metamorph software calliper tool. These measurements were used to calculate the displacement value of the CAR by dividing the shorter of the two distances between the CAR and the cell tips by the total cell length i.e. a/ (a+b) where a and b = distance from CAR to the cell tips, where a<b. 50 cells were measured for KS5065 *mto1-427 rlc1-mCherry uch2-mCherry* and KS5067

rlc1-mCherry uch2-mCherry. The displacement values were ordered according to increasing value and the results graphed.

Biochemical methods

Tandem affinity purification

Native extracts for tandem affinity purification were prepared from cell pellets frozen in liquid nitrogen then ground to a powder. 135 g of cell powder for each strain was resuspended in 270ml LBN buffer (15 mM Na2HPO4, 10 mM NaH_2PO_4, 150 mM NaCl, 2 mM EDTA, 1 mM DTT, 2 mM benzamidine, 1 mM PMSF, 2 mM AESBF, 5 μg/ml chymostatin, leupetin, antipain, aprotinin, pepstatin, E64). NP-40 was added to 1% final concentration before 10 minutes incubation at 4°C. The extract was centrifuged at 4 000rpm for 10 minutes at 4°C) to remove insoluble cellular debris, the supernatant retained and re-centrifuged. 10 μl of pre-equilibrated fractogel IgG beads (Sawin laboratory) were added per 2 g of cell powder to the clarified extract, followed by rotating incubation for 1.5 hrs at 4°C. The extract was then loaded on to a 25 ml disposable column (Bio-Rad) and washed with 5 x 15 ml WBN (25 mM Tris-HCl pH 8.0, 150 mM NaCl, 0.1% NP-40, 1 mM DTT). The fractogel beads were then recovered in 5 ml TEV cleavage buffer (25 mM Tris-HCl pH 8.0, 150 mM NaCl, 0.1% NP40, 0.5 mM EDTA, 1 mM DTT). 500 μl of TEV (Sawin laboratory) was added, the slurry incubated with end-over-end rotation for 2 hrs at 4°C and the supernatant recovered by centrifugation. S-protein agarose (Novagen) pre-equilibrated in WBN was added to the supernatant, using 1 μl of S-protein agarose per gram of starting cells, then incubated with end-over-end rotation

for 1.5 hrs at 4°C. The S-protein agarose was recovered by centrifuging at 2 000rpm for 30 seconds at 4°C, and loaded onto a 5 ml disposable column (Bio-Rad), washed with 3 x 4 ml WBN, then transferred to an eppendorf tube and washed with 2 x 1 ml WBN without NP40. Material was eluted from the beads using 50µl Laemmli sample buffer (2% SDS, 10% glycerol, 0.125 M Tris-HCl pH 6.8, 0.002% bromophenol blue, 5% 2-mercaptoethanol), boiled for 5 minutes. 3 µl of each sample was run on an 8% poly-acrylamide gel. The gel was silver stained using the Invitrogen SilverQuest silver staining kit. The remainder of the sample was given to Flavia de Lima Alves (Rappsilber Laboratory, University of Edinburgh) for mass spectrometry.

Immunoprecipitation

Native extracts for immunoprecipitation were prepared from cell pellets frozen in liquid nitrogen then ground to a powder. Extracts were made with extract buffer (50mM NaHepes pH 7.5, 75mM KCL, 1mM $MgCl_2$, 1mM EGTA, 0.5mM DTT, 0.1% Triton X-100, and protease inhibitors: 5µg/ml CLAAPE, 2mM AEBSF, 1mM benzamidine); 1ml buffer was added to ~500mg of ground cells. Each sample was vortexed to resuspend the cell powder, centrifuged (13 000 rpm for 15 minutes at 4°C,) to remove insoluble cellular debris, the supernatant retained and if necessary adjusted to equivalent protein concentrations. 10µl of Protein G Dynabeads (Invitrogen) pre-loaded with 3µl anti-GFP antibody (Sawin laboratory, 3.0) was added to 950µl of protein extract. Following incubation with rotation for 1hr at 4°C, beads were washed six times with 1ml of extract buffer and resuspended in Laemmli sample buffer prior to SDS-PAGE and Western blotting. Relative loading is

described in figure legends of respective figures. NuPAGE 4 - 12% pre-cast Bis-Tris gels were used to optimise the transfer of the large Myp2-YFP protein. Ponceau staining was used as a loading control and to confirm even transfer in the region of interest. Membranes were blocked in a solution of 5% skim milk powder/ TBS/ 0.01% Tween-20 for 1 hr, then incubated in primary antibody diluted in the same solution (anti-Mto1 1:2000 (Sawin laboratory, S897) or anti-GFP 1:300 (Sawin laboratory, 3.0)) for 1 hr prior to washing three times with 0.01% Tween-20/ TBS. The membranes were then incubated with secondary antibodies (anti-sheep 1:10 000) and washed three times in 0.01% Tween-20/ TBS before development with ECL.

Samples for co-immunoprecipitation experiments using *cps1-191* mitotic arrest were grown at 25°C until they reached mid-exponential growth before being transferred to 36°C for 3 hrs. A sample of each culture was collected by rapid filtration and fixed in -80°C methanol before being stained with Hoechst 33342 (1 μg/ml) or DAPI stain (1μg/ml) to confirm the arrest based on the accumulation of binucleate cells. Membranes imaged using the Li-Cor system were blocked in a solution of 5% skim milk powder/ TBS/ 0.01% Tween-20 for 1 hr, then incubated in primary antibody diluted in the same solution (anti-Mto1 1:2000 (Sawin laboratory, S897) or anti-GFP 1:300 (Sawin laboratory, 3.0), for each also co-straining for anti-tubulin TAT1 1:1000 (kind gift of Keith Gull, University of Oxford, UK)) for 1 hr prior to washing three times with 0.01% Tween-20/ TBS. The membranes were then incubated with secondary antibodies (IRDye 680 anti-goat 1:10 000 (Li-Cor)/ IRDye 800 anti-mouse 1:20 000 (Li-Cor)), then washed twice in 0.01% Tween-20/ TBS with a final wash in TBS prior to scanning.

To correct for variations in loading of cell extracts, intensity readings for proteins in the cell extract were adjusted relative to KS4680 (the sample with the most protein loaded), based on quantification of tubulin using the TAT-1 antibody. The respective tubulin readings were divided by 32.4 (the amount of tubulin present for KS4680), then the readings for Mto1 were in turn divided by this number. For example, for KS4957 *cps1-191 myp2-YFP mto1-427* the amount of tubulin loaded was 29.07 intensity units. 29.07/32.4 = 0.897. The amount of Mto1 co-immunoprecipitated was 72.06 intensity units. 72.06/0.897 = 80.31 intensity units of Mto1, correcting for loading variations.

Boiled protein extracts from yeast

5ml cultures were grown overnight to mid-exponential growth in appropriate media. The cultures were centrifuged for 5 minutes at 4 000 rpm to pellet cells, the supernatant removed and the cell pellet resuspended in 1ml TBS/ 1 mM EDTA/ 2mM PMSF. The samples were then centrifuged for 1 minute at 13 000 rpm, the supernatant removed and the cell pellets boiled for 5 minutes. The samples were bead beaten with zirconium beads for 2 x 30 seconds. A hole was pierced in the bottom of each tube and the liquid collected by brief centrifugation into a second tube containing 150µl 2x laemmli sample buffer (2% SDS, 10% glycerol, 0.125 M Tris-HCl pH 6.8, omitting β-mercaptoethanol and bromophenol blue). The samples were then boiled for 5 minutes and centrifuged for 5 minutes at 13 000 rpm to remove insoluble cell debris. Protein concentration was determined via BCA assay (Sigma-Aldrich) and appropriate amounts used for SDS-PAGE and Western blotting analysis.

Antibody production

To raise antibodies against Alp4 and Alp6 the amino and carboxyl termini of these proteins were sub-cloned into GST-expression vectors as follows. To sub-clone the amino terminus of *alp6*, the region *alp6(1 - 1165)* was excised from pKS410 *pGEM-T.alp6* using BamHI and Sal1, and inserted into *the pGex-5x-3* vector digested with BamHI and Sal1 to create pKS739. To sub-clone the carboxyl terminus of *alp6*, the region *alp6(1311 - 2448)* was excised from pKS410 *pGEM-T.alp6* using a second SalI site present in Alp6 and also Not1. The fragment was inserted into *pGex-5x-3* digested with BamHI and Sal1 to create pKS740. The amino terminus of *alp4* was sub-cloned from pKS403 *pGEM-T.alp4*. *Alp4*(1-1041) was excised with BglII and Mfe1, and inserted into *pGex-5x-3* digested with BamHI and EcoRI to create pKS743. To sub-clone the carboxyl terminus of *alp4*, the region *alp4(889-2352)* was excised from pKS403 using BamHI and Not1. This was inserted into *pGex-5x-3* digested with BamHI and Not1 to create pKS744. Plasmid construction was confirmed by diagnostic digest. The plasmids were then transformed into BL21 DE3 *E. coli* cells..

Protein expression was induced by the addition of 1 mM IPTG to the culture media for 2 hrs. Cells were harvested by centrifugation and resuspended in 3 volumes of lysis buffer (20 mM Tris-HCl pH 8.0, 1 mM EDTA, 5 mM $MgCl_2$, 0.3 mM PMSF, 8 U/ml Benzonase. 400 µg/ml lysozyme). To purify inclusion bodies the cell mixture was passed through the French press three times at 15K psi, before NaCl was added to a final concentration of 300 mM and Triton TX-100 to a final concentration 1%.

The sample was then mixed with an equal volume of resuspension buffer (50 mM Tris-HCl 8.0, 300 mM NaCl, 1 mM EDTA, 1% Triton X-100, 0.3 mM PMSF). The sample was centrifuged for 20 minutes at 10K rpm. The supernatant was discarded and the pellet resuspended in ~15 cell volumes of resuspension buffer, using a Dounce pestle. The centrifugation/ resuspension process was repeated three times.

A sample of the purified inclusion bodies was resolved by 10% SDS-PAGE against BSA standards to estimate the concentration of the fusion proteins. The remainder of each sample was again resolved by 10% SDS-PAGE, using an over-sized gel (gel dimensions 150 mm x 6mm x 200 mm, a separate gel was used for each fusion protein), running a maximum of 13.7 mg of protein per gel. Each gel was run at 200 mA for 6 hrs. They were then surface staining with aqueous Coomassie (0.05% Coomassie-R250 in dH_2O, left for 10 minutes at room temperature, then destained in dH_2O) prior to excision of the band of interest. These gel slices were frozen at -20°C, lyophilized and finely ground by pestle and mortar. The samples were then given to the Scottish National Blood Service to inject into sheep. The sheep used were selected as having low pre-existing immunity to *S. pombe* epitopes.

Table 1. Yeast Strains

Strain Number	*Genotype*	Source
KS515	*h+ ade6-216 leu1-32 ura4-D18*	ICRF
KS516	*h- ade6-210 leu1-32 ura4-D18*	ICRF
KS762	*h- mto1GFP::kanMX*	Sawin laboratory
KS1236	*h- kanMX::nmt81::GFP-atb2 ade6-216 leu1-32 ura4-D18*	Sawin laboratory
KS1238	*h- nda3-km311 ade6-210 leu1-32 ura4-D18*	Sawin laboratory
KS1581	*h- kanMx::nmt81:GFP-mto1(481-1115) ade6-M210 leu1-32 ura4-D18*	This study
KS1890	*h- mto2-GFP::kanMX6 ade6-216 leu1-32 ura4-D18*	Sawin laboratory
KS1956	*h- mto1(1-800)::ura4+ ade6-210 leu1-32*	Sawin laboratory
KS1957	*h– mto1(1-1051)::ura4+ ade6-210 leu1-32*	Sawin laboratory
KS2760	*h- hphMX6::nmt81:GFP-atb2 ade6-216 leu1-32 ura4-D18*	Sawin laboratory
KS2973	*h- pcp1Δ::natMX6 ade6-216 leu1-32 ura4-D18 + pUR19-pcp1*	This study
KS2976	*h- myp2-YFP::kanMX6 ade6-210 leu1-32 ura4-D18*	T. Pollard
KS2987	*h - spn1-mYFP::kanMX6 ade6-210 leu1-32 ura4-D18*	T. Pollard
KS2989	*h - ain1-mYFP::kanMX6 ade6-210 leu1-32 ura4-D18*	T. Pollard
KS3078	*MAT a his3Δ200 trp1-901 leu2-3112 ade2 LYS2::(4lexAop-HIS3) URA3::(8lexAop-lacZ) Δgal4::KAN*	J. Beggs
KS3162	*h- kanMX6::nmt81:GFP-mto1(784-1115) ade6-210 leu1-32 ura4-D18*	Sawin laboratory
KS3465	*h- rga7Δ::ura4 mto1-GFP ade6-216 leu1-32 ura4-D18*	This study

KS3466	*h+ ain1Δ::kanMX6 mto1-GFP::kanMX6*	This study
KS3474	*h+ mto1(1-1051)-TAPS::kanMX6 ade6-216 leu1-32 ura4-D18*	Sawin laboratory
KS3524	*h+ mto1-TAPS::kanMX6 ade6-216 leu1-32 ura4-D18*	Sawin laboratory
KS3693	*h+ hht2-GFP::ura4+ kanMX6::nmt81:GFP-mto1(784-1115) ade6-210 leu1-32*	This study
KS3724	*h- cps1-191 ade6-210 leu1-32 lys1-131 ura4-D18*	P. Nurse
KS3583	*h- pdk1::ura4+ mto1GFP:kanMx leu1-32 ura4D18*	This study
KS4099	*h+ cut9.665 ade6-210 leu1-32 ura4-DSE his1-102*	K. Hardwick
KS4111	*h- cut8.563 leu1-32*	C. Gordon
KS4113	*h+ cut4.533 leu1-32 ura4-D18*	C. Gordon
KS4191	*h- cut8.563 alp4-tdT:natMx6 mto1-GFP::kanMX ade6-210 leu1-32*	This study
KS4192	*h+ cut9.665 alp4-tdT:natMx6 mto1-GFP::kanMX ade6-210 leu1-31 ura1-D18/DSE*	This study
KS4231	*h- cut4.533 alp4-tdT:natMx6 mto1-GFP::kanMX ade6-210 leu1-32 ura4-D18*	This study
KS4290	*h+ nmt41-GFP-CHD:leu1+ kanMX6::nmt81:mto1-tdRFP::natMX6 ade6-210 leu1-32 ura4-D18*	This study
KS4314	*h+ hsp9Δ::kanMX6 mto1-GFP leu1-32*	This study
KS4410	*h+ myp2Δ::kanMx ade6-216 leu1-32 ura4-D18*	This study
KS4413	h- *ain1Δ::kanMX6 hsp9Δ::kanMX6 mto1GFP::natMX*	This study
KS4494	*h+ spn1Δ::kanMx mto1GFP:natMx ade6-216*	This study
KS4496	*h+ acp2Δ::kanMx mto1GFP:natMx ade6-216*	This study

KS4498	*h+ myp2Δ::kanMx mto1GFP:kanMx*	This study
KS4577	*h- mto1-GFP::kanMx6 rlc1Δ::kanMx4 ade6-210 leu1-32 ura4-D18*	This study
KS4677	*h+ mto1Δ::kanMX6 myp2-YFP::kanMX6 ade6-210 leu1-32 ura4-D18*	This study
KS4680	*h- mto1-427 myp2-YFP::kanMX6 ade6-216 leu1-32 ura4-D18*	This study
KS4771	*h+ nmt41:GFP-mto1::kanMx6 rlc1-mCherry::ura4 uch2-mCherry::ura4 ade6-210 leu1-32 ura4-D18*	This study
KS4806	*h+ myp2Δ::kanMx hphMX6::nmt81:GFP-atb2 ade6-216 leu1-32 ura4-D18*	This study
KS4812	*h+ sid4-SA1 kanMX::nmt41:GFP-mto1 rlc1-mCherry::ura4+ uch2-mCherry::ura4+ ade6-210 leu1-32 ura4-D18*	This study
KS4837	*h- cut4.533 kanMX::nmt41:GFP-mto1 rlc1-mCherry::ura4+ uch2-mCherry::ura4+ ade6-216 leu1-32 ura4-D18*	This study
KS4843	*h+ cut8.563 myp2-YFP::kanMx6 rlc1-mCherry::ura4+ uch2-mCherry::ura4+ ade6-210 leu1-32 ura4?*[a]	This study
KS4908	*h+ sid4-SA1 kanMx::nmt81:GFP-atb2 ade6-216 leu1-32 ura4-D18*	This study
KS4910	*h+ mto1(1-1051):ura4+ myp2-YFP:kanMx6 ad6-210 leu1-21 ura4-D18*	This study
KS4935	*h+ myp2-YFP mto1(1-800):ura4+ ade6-210 leu1-32 ura4-D18*	This study
KS4939	*h- nda3-KM311 kanMx::nmt41:GFP-mto1 rlc1-mCherry::ura4+ ade6-210 leu1-32 ura4-D18*	This study
KS4942	*h+ kanMx::nmt41:GFP-mto1 rlc1-mCherry::ura4+ ade6-216 leu1-32 ura4-D18*	This study
KS4956	*h- leu1-32::SV40-GFP-atb2 [LEU1] leu1-32 ura4-D18 ade6-216*	F. Chang

KS4957	*h+ mto1.427 myp2-YFP::kanMx6 cps1-191 ade6-216 leu1-32 ura4-D18*	This study
KS4959	*h- myp2-YFP:kanMx6 cps1-191 ade6216 leu1-32 lys1-131 ura4-D18*	This study
KS4961	*h- cut8.563 nmt41:GFP-mto1::kanMx rlc1-mCherry::ura4+ uch2-mCherry::ura4+ ade6-21X^{b} leu1-32 ura4?*	This study
KS4963	*h+ cut4.533 myp2-YFP::kanMx rlc1-mCherry::ura4+ uch2-mCherry::ura4+ leu1-32 ura4-D18*	This study
KS5059	*h+ cut9.665 alp4-GFP::natMx6 rlc1-mCherry::ura4+ uch2-mCherry::ura4+ ade6-216 leu1-32 ura4-D18*	This study
KS5062	*h- cut4.533 leu1-32::SV40-GFP-atb2 [LEU1] ade-21X leu1-32 ura4-D18*	This study
KS5064	*h- leu1-32::SV40-GFP-atb2 [LEU1] leu1-32 ura4-D18 ade6-216*	This study
KS5065	*h- rlc1-mCherry::ura4+ uch2-mCherry::ura4+ ade6-210 leu1-32 ura4-D18*	This study
KS5067	*h+ mto1-427 rlc1-mCherry::ura4+ uch2-mCherry::ura4+ ade6-216 leu1-32 ura4-D18*	This study
KS5083	*h- cut9.665 nmt41:GFP-mto1::kanMx6 rlc1-mCherry::ura4 uch2-mCherry::ura4 ade6-21X leu1-32 ura4-D18*	This study
KS5084	*h+ cdc11-123 kanMX::nmt81:GFP-atb2 leu1-32*	This study
KS5086	*h- cdc7-24 kanMX::nmt81:GFP-atb2 leu1-32*	This study
KS5088	*h- cut8.563 leu1-32::SV40-GFP-atb2 [LEU1] leu1-32*	This study
KS5106	*h- cut9.665 leu1-32::SV40-GFP-atb2 [LEU1] ade6-21X leu1-32 ura4-D18/DSE*	This study
KS5109	*h- mto1-427 ade6-216 leu1-32 ura4-D18*	This study

KS5122	*h- mto1-427-GFP::kanMx6 cps1-191 ad6-216 leu1-32 lys1-131 ura4-D18*	This study
KS5124	*h- myp2-YFP::kanMx6 mto1(1-800):ura4+ cps1-191 ade6-216 leu1-32 ura4-D18*	This study
KS5136	*h- mto1(1-800):ura4+ cps1-191 ade6-216 lys1-131 leu1-32 ura4-D18*	This study
KS5140	*h- cps1-191 mto1-GFP:kanMx ade6-216 leu1-32 ura4-D18*	This study
KS5177	*h+ cut4.533 rlc1-mCherry::ura4+ uch2-mCherry::ura4 leu1-32:SV40-GFP-atb2 [LEU1] leu1-32 ura4-D18*	This study
KS5179	*h- cut9.665 rlc1-mCherry::ura4+ uch2-mCherry::ura4 leu1-32:SV40-GFP-atb2 [LEU1] ade6-216 ura4-D18*	This study
KS5180	*h- cut8.563 uch2-mCherry::ura4+ leu1-32::SV40-GFP-atb2 [LEU1] ade6-210 leu1-32 ura4?*	This study
KS5189	*h- mto1-427 cps1-191 ade6-216 leu1-32 ura-D18*	This study
KS5203	*h- rlc1-mCherry::ura4 uch2-mCherry::ura4 leu1-32:SV40-GFP-atb2 [LEU1] ade6-210 leu1-32 ura4-D18*	This study
KS5205	*h- cut8.563 rlc1-mCherry::ura4 uch2-mCherry::ura4 leu1-32:SV40-GFP-atb2 [LEU1] ade6-210 leu1-32 ura4-D18*	This study
KS5227	*h- natMX6::nmt81:GFP-mto1(801-1115) ade6-210 leu1-32 ura4-D18*	This study
KS5228	*h- natMX6::nmt81:GFP-mto1(919-1115) ade6-210 leu1-32 ura4-D18*	This study
KS5230	*h- natMX6::nmt81:GFP-mto1(919-1051)::ura4+ ade6-210 leu1-32 ura4-D18*	This study
KS5293	*h- natMX6::nmt81:GFP-mto1(801-1051)::ura4+ ade6-210 leu1-32 ura4-D18*	This study

[a] Not determined whether *ura4-D18* or *ura4+*.

[b] Not determined whether *ade210* or *ade216*.

Table 2. Plasmids

Plasmid Name	Vector	Insert	Source
pKS135	pGAD424	-	H. Ohkura
pKS158	pGAD424	meiotic cDNA library	T. Nakamura
pKS170	pFA6a-kanMX6-P81nmt1-GFP	-	
pKS282	pGEM-T	*mto1*	Sawin laboratory
pKS310	pBSKS	9.5Kb genomic fragment containing *pcp1*	Sawin laboratory
pKS403	pGEM-T	*alp4*	Sawin laboratory
pKS410	pGEM-T	*alp6*	Sawin laboratory
pKS414	pBMT116+1	*mto2*	Sawin laboratory
pKS477	pUR19	*pcp1*	This study
pKS480	pALKS-GFP	*pcp1*	This study
pKS481	pBTM116	*mto1(769-1115)*	
pKS507	pBTM116-1	*mto1(769-1051)*	This study
pKS630	pGAD424-1	-	This study
pKS637	pGAD424-1	*cdc12*	This study
pKS715	pFA6a-P81nmt-GFP	-	R. Allshire
pKS739	pGex-5x-3	*alp6 (1-1165)*	This study
pKS740	pGex-5x-3	*alp6 (1311-2448)*	This study
pKS743	pGex-5x-3	*alp4 (1-1041)*	This study
pKS744	pGex-5x-3	*alp4 (889-2352)*	This study
pKS752	pGAD424	*cdc11(562-1045)*	This study
pKS753	pGAD424	*cdc11(701-1045)*	This study

pKS754	pGAD424	*cdc11(801-1045)*	This study
pKS755	pGAD424	*cdc11(901-1045)*	This study
pKS756	pGAD424	*cdc11(562-700)*	This study
pKS757	pGAD424	*cdc11(562-800)*	This study
pKS758	pGAD424	*cdc11(562-900)*	This study
pKS759	pBTM116	*mto1(769-1065)*	This study
pKS760	pBTM116	*mto1(769-1075)*	This study
pKS762	pBTM116	*mto1(769-1095)*	This study
pKS776	pDUAL-GFH41c	*hsp9*	This study
pKS777	pDUAL-GFH81c	*hsp9*	This study
pKS872	pACT2.2gtwy	*rng3*	This study
pKS873	pACT2.2gtwy	*myp2*	This study
pKS915	pACT2.2gtwy	*cdc4*	This study
pKS916	pACT2.2gtwy	*spn1*	This study
pKS918	pBTM116	*mto1(769-1085)*	This study

Table 3. Oligonucleotides

Oligo Name	Sequence
OKS358	ATAATGTAAACGAGTGTGTGCAAATGT
OKS444	ACTACATATATGCCATAGCGTATCAATAGGCATATCTTCG ATCCCATACTTTCTTTTAACAATTAACAATTTAAGAAAGA GAATTCGAGCTCGTTTAAAC
OKS448	TCCTTTTTATTCTCATCTTTTAGTTTTCTTATCTGTTGTACC AAATGGTTAACCGAGCAGTGGGTGACCTGTTTATCAAATT TGTATAGTTCATCCATGC
OKS503	CACGTTGTGCCTGAATAAAACTCGATTC
OKS506	GGTTGCATTCGATTCCTGTTTGTAATTG
OKS1111	ACGGCTAGTAAAATTGATGATGGT
OKS1112	TTCTGAATAAGCCCTCGTAATA
OKS1113	ATAACGCGTTTGGAATCACTACAG
OKS1114	TTACATAAAAGAAGGCAAAACGAT
OKS1123	CTCAAGCGCTTTCACAACCAA
OKS1124	TGATTTTCGTTTCGTTCGTATTTC
OKS1138	TTCTCTGGCACCCAACTTGTC
OKS1249	GATAAAGCGGAATTAATTCCCGA
OKS1250	GTTTGGTGGGGTATCTTCATC
OKS1314	AATTCGGATCCCCCGGGG
OKS1315	TCGACCCCGGGGGATCCG
OKS1796	GCCCAGAATACCCTCCTTGA
OKS1856	CACTTCTCTTTACTCTTTGACCCTCCAG
OKS1875	CAAGCATCTGAAAAACGCCTT
OKS1876	AGTGAAACTTTTAGGCGCTG

OKS1940 CTTTGCTCACAATGGTAGATTTTTTTCATCAACTTATCAGT
ACCAGACTGATCCTTTTTATTCTCATCTTTTAGTTTTCTTTT
GTATAGTTCATCCATGC

OKS1941 ACTGCCTGATTCATGCTTGAAATTGTCGTCAATGCTTCAAC
GTTGGTATTTACAGGCTTACTTCCCGTATTCAGTTGGGTTTT
GTATAGTTCATCCATGC

Chapter III - Search for the interacting protein(s) that target Mto1 to the cytokinetic ring

The C-terminus of Mto1 is sufficient for localisation to the cell equator

In light of the finding that the extreme C-terminus of Mto1 is required for its localisation (S. Rincon, personal communication) we asked whether the N-terminus of Mto1 is required for localisation to MTOCs. A series of Mto1 truncations were made under the control of the *nmt81* promoter, which increases expression ~3x relative to the endogenous *mto1* promoter (K. Sawin, personal communication), with GFP fused at the amino-terminus. GFP-Mto1(481-1115), GFP-Mto1(784-1115), GFP-Mto1(801-1115) and GFP-Mto1(919-1115) can be seen at discrete spots corresponding to both interphase and mitotic SPBs, at rings at the cell equator corresponding to the eMTOC and decorating interphase microtubules (Figure 8). GFP-Mto1(784-1115), GFP-Mto1(801-1115) and GFP-Mto1(919-1115) also localise to the mitotic spindle. Mto1 is known to bind to microtubules, and as such can be expected to bind to the microtubules of the spindle if it is present in the nucleus. The GFP-Mto1(784-1115) fragment is ~64KDa in size. Although this exceeds the size limit for free diffusion into the nucleus (the size limit for free diffusion of proteins through nuclear pores is ~40KDa (Peters, 1984)) protein morphology plays an

important role in nuclear transport and the structure of this fragment may be sufficiently narrow for free entry across nuclear pores, while the larger Mto1(481-1115) fragment is restricted to the cytoplasm. As expected from previous findings, Mto1 truncations that lack the 1051-1115 localisation domain do not localise to the cell equator; nor are they seen at SPBs. GFP-Mto1(801-1051) and GFP-Mto1(919-1051) both show diffuse cytoplasmic localisation, with enrichment at the nucleus (Figure 8). I conclude that Mto1(919-1115) is sufficient for localisation to the equator and the N-terminus is not required.

(These results are in agreement with more recent findings (I. Samejima, personal communication) that Mto1(1028-1095) is sufficient for localisation to the eMTOC, interphase SPB and mitotic SPB).

Mto1 localisation to the cell equator requires F-actin

Since F-actin is required for γ-tubulin recruitment to the eMTOC (Heitz et al., 2001), we asked whether the same is true for the equatorial localisation of Mto1. A fluorescently labelled histone, Hht2-GFP, was used as a nuclear marker to identify binucleate cells; these cells can be expected to have Mto1 at the equator, as the mitotic spindle is longer than 8μm (see Introduction). GFP-Mto1(784-1115) was expressed from the *nmt81* promoter to provide a stronger signal to balance the strong nuclear signal. Cells were incubated with Latrunculin B (Lat B) at 25°C for 30

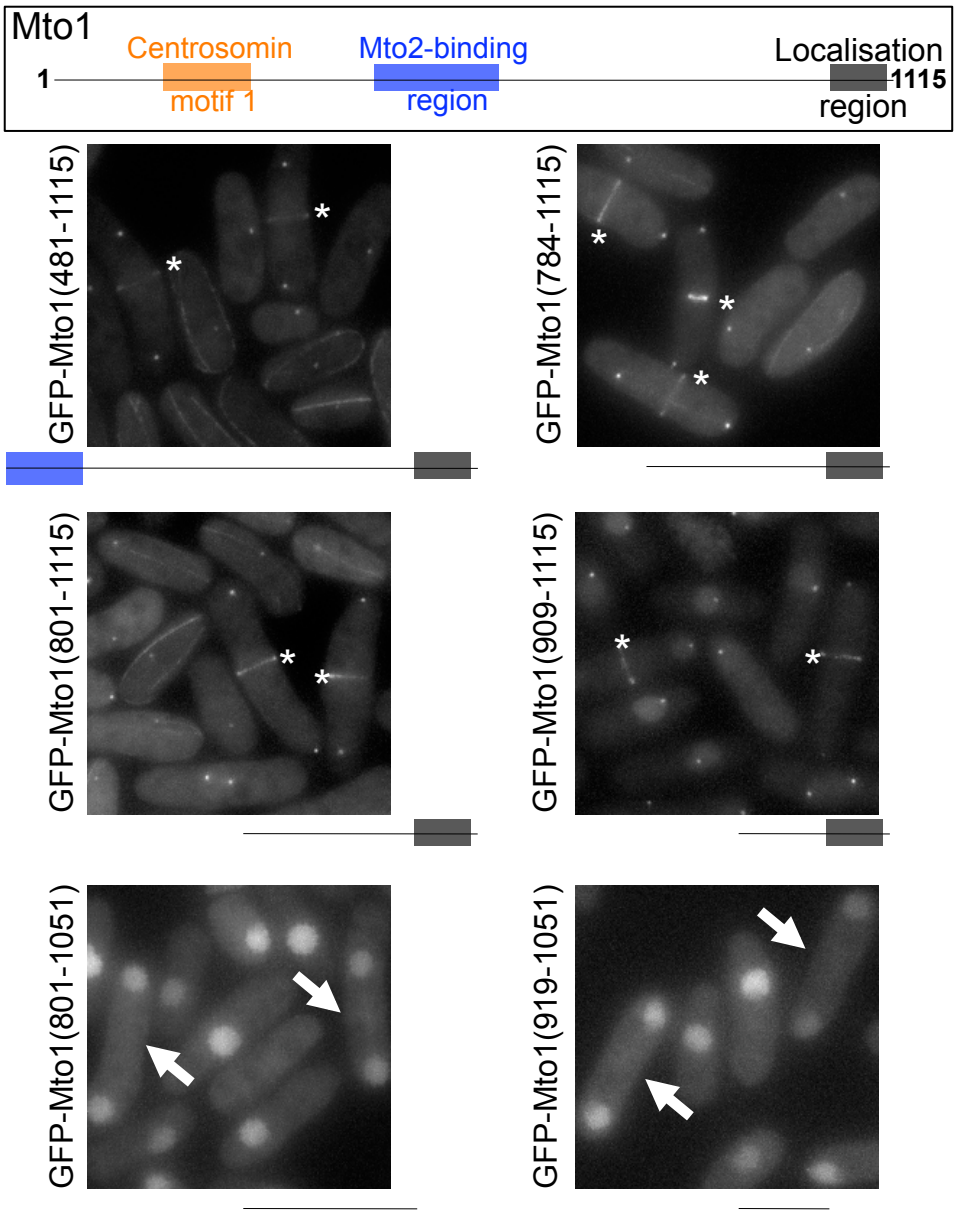

Figure 8 The C-terminus of Mto1 is sufficient and necessary for localisation to the cell equator

Wide field microscopy showing the localisation of *nmt81:*GFP-Mto1(481-1115)*, nmt81:*GFP-Mto1(784-1115*)*, *nmt81:*GFP-Mto1 (801-1115)*, nmt81:*GFP-Mto1(919-1115), *nmt81:*GFP-Mto1(801-1051) and *nmt81:*GFP-Mto1(919-1051). Truncations that include the 1051-1115 'localisation domain' at the extreme C-terminus of Mto1 localise to the equator (*); this localisation is abolished for truncations that lack the localisation domain (arrows). A schematic of Mto1 is shown at the top and for each fragment.

minutes to depolymerise F-actin then examined. 0% of binucleate cells treated with Lat B had GFP-Mto1(784-1115) at the equator compared to 96% of binucleate cells treated with DMSO alone (Figure 9). Thus Mto1 localisation to the equator requires F-actin.

Mto1 co-localises with the CAR

As Mto1 forms a contractile ring (Sawin et al., 2004) and requires F-actin to localise to the cell equator, we asked whether Mto1 would co-localise with the CAR. The strain *mto1-tdRFP CHD-GFP* was used to check for co-localisation; CHD (calponin homology domain), derived from the CAR protein Rng2, binds actin and shows the position of the CAR. Images of live cells were taken in the red and the green channels and the images combined (Figure 10). Mto1 and the CAR co-localise, suggesting that Mto1 may interact with a component of the CAR.

Further examples of Mto1 co-localising with the CAR can be seen in Chapter V.

A yeast two-hybrid screen for Mto1-interacting proteins

Screen design

It was decided to begin by screening to find proteins that interact with Mto1. Biochemical interactions have been shown between Mto1 and some other proteins (γ-TuC: Sawin et al., 2004; Venkatram et al., 2004; Mto2: (Sawin *et al.*, 2004; Venkatram *et al.*, 2004; Zimmerman *et al.*, 2004b; Samejima *et al.*, 2005; Venkatram *et al.*, 2005) Rsp1: Zimmerman et al., 2004), but no comprehensive screen had

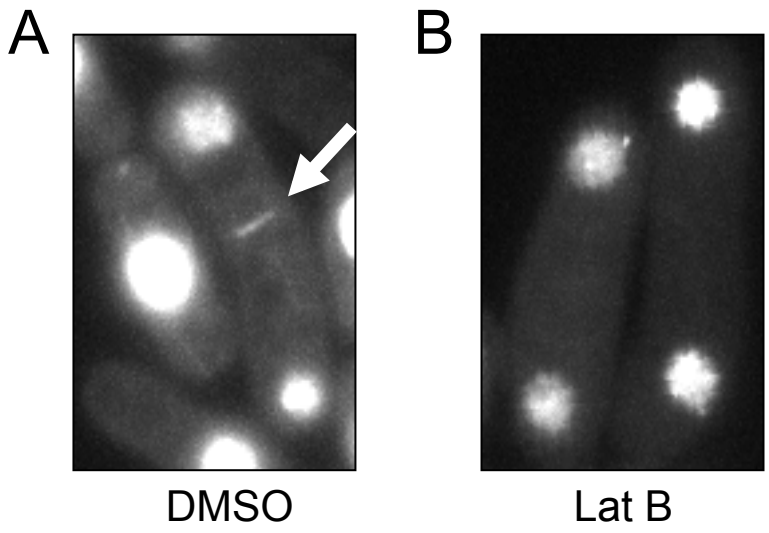

C

Mto1 at equator in binucleate cells		
	Yes	No
Lat B	0%	100%
Control	96%	4%

n = 200 cells

Figure 9 Mto1 localisation to the equator requires F-actin

Wide field images showing localisation of *nmt81:*GFP-Mto1(784-1115) in binucleate cells treated with (A) Lat B and (B) DMSO (control). (C) *nmt81:*GFP-Mto1(784-1115) is present at the cell equator in 96% of binucleate cells for the control sample (arrow in (A)); localisation of Mto1 to the equator is abolished by the addition of LatB.

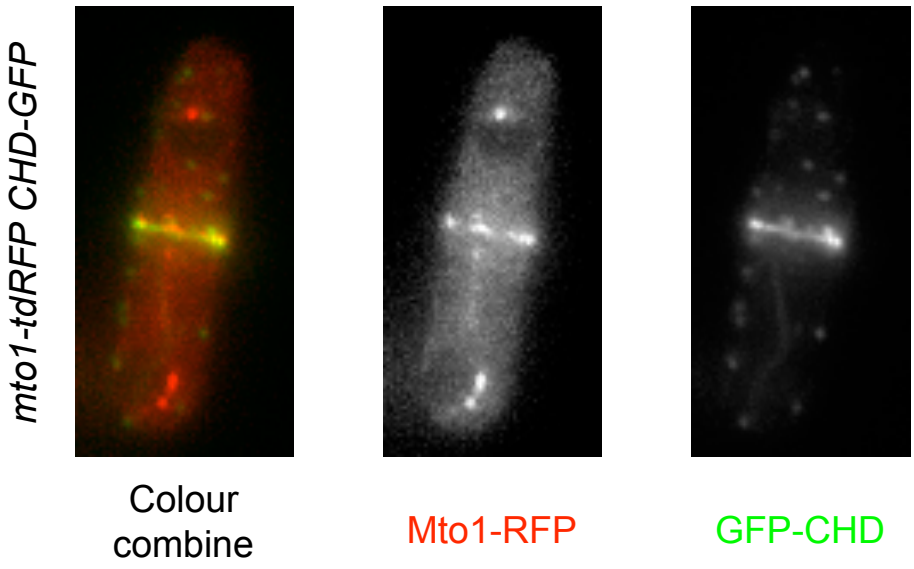

Figure 10 Mto1 co-localises with the CAR

Wide field images of *mto1-tdRFP CHD-GFP* cells. CHD, the actin-binding domain of Rng2, marks the CAR, actin cables and actin patches. Mto1 localises to the equator, co-localising with the CAR.

previously been done. The protein or proteins that recruit Mto1 to the site of the eMTOC could then be identified from the interacting proteins identified.

Many different screening approaches are available. It was initially decided to do a yeast 2-hybrid screen as the yeast 2-hybrid system is a versatile method that can be used to screen many possible interactions (Fields and Song, 1989). The system has the advantage of being unbiased since the screen is genome-wide, rather than being restricted to selected candidates. It also identifies direct protein-protein interactions. However as the screening is carried out in *S. cerevisiae* key protein post-translational modifications may be missing, leading to false negatives. False positives are also a possibility, where two proteins interact in the screen but are not able to interact within *S. pombe,* for example where the proteins are expressed at different times in the cell cycle or have distinct cellular localisations.

It can be useful to employ a smaller fragment of the bait protein in a yeast two-hybrid screen to reduce the number of non-physiological interactions identified. Mto1 is a large protein (~128 kDa) and also contains several coiled-coil regions and so may have a propensity towards promiscuous interaction as coiled-coil regions can mediate protein-protein interactions (Burkhard et al., 2001). Having shown that Mto1(784-1115) is sufficient to localise to the equator, it was decided to use a piece of a similar length in the screen. Accordingly LexA-Mto1(769-1115) was used as bait; the starting position is the location of a convenient restriction site. The Shimoda meiotic cDNA prey library was used as it provides good coverage over the genome. Interaction was determined by induced expression of both the His and LacZ reporter

genes, permitting growth on media lacking histidine and producing a blue colour when tested by X-gal overlay assay. I suspected that the interaction between Mto1 and the localising protein might be controlled by post-translational modifications within the cell (to potentially restrict the interaction to a specific time within the cell cycle) and therefore the interaction could be weak in the context of the yeast-two hybrid screen. I therefore opted to use a method of selection with comparatively low stringency.

Test transformations were performed to investigate optimal transformation conditions, before a large-scale transformation was performed. I found that the length of heat shock affected the transformation efficiency, with 20 minutes at 42°C being optimal. The amino acid mixture used in the media also affected the number of colonies obtained, with Kaiser drop-out mix (Formedium) giving consistently better results than the equivalent drop-out mixture from Qbiogene.

~3.4 million transformants were tested in the large-scale screen, a three-fold over-sampling of the prey library. Of these, 833 colonies grew on media lacking tryptophan, leucine and histidine and produced a blue colour with the LacZ overlay assay within 23 hrs. Colony PCR was used to amplify the prey plasmid insert, using primers to either side of the cloning site of the *pGAD424* vector. These PCR products were purified and sequenced. The gene within the prey plasmid was then identified using the BLAST program and NCBI database. A number of the hits were found to contain the *S. pombe his5* gene. *his5* is able to complement *HIS3Δ* in *S. cerevisiae*; the colonies also became blue in the LacZ assay. Colony PCR using

primers to *pGAD424* and *his5* was used to identify prey plasmids with *his5* prior to sequencing, leaving 583 colonies. A complete list of genes identified from this screen is given at the end of the chapter. 334 prey inserts were identified, with around 200 colonies that either contained *his5* fragments that were not identified by colony PCR, contained empty vector (where the prey insert may have been excised) or where the prey insert was not amplified by PCR.

Colonies from the large-scale screen were tested against increasing levels of 3'aminotriazole (3-AT) to determine the strength of the interaction between the prey insert and Mto1(769-1115). 3-AT is a competitive inhibitor of the *HIS3* gene product. Adding 3-AT to the media raises the stringency of the *HIS3* selection. Patched colonies were replica-plated to selective medium lacking tryptophan, leucine (to select for the prey plasmid) and histidine, with 3-AT added at concentrations of 5, 10, 25 and 50 mM. An overlay assay was also performed, recording the time taken for the blue colour to become noticeable (plates were checked at 1.5, 4.5, 6.5 and 21.5 hrs after the start of the assay. This found 80 proteins that 'strongly' interact with Mto1(769-1115); a list is given in Table 4. Descriptions of gene functions are taken from the *S. pombe* GeneDB database (http://www.genedb.org/ genedb/pombe/index.jsp), supplemented by the Biobase Pombe Knowledge Library (http://biobase-international.com/). Hypothetical genes refer to a protein whose existence is predicted, but for which no experiment evidence of expression *in vivo.* Sequence orphans are sequences with no significant similarity to other sequences.

Table 4 List of strong interactors from yeast two-hybrid screen

Sample number	Gene name	Function	Timepoint blue colour appears (hrs)	Intensity at 21.5 hrs (1= weak, 5 = strong)	Highest [3-AT] with growth
424	adh1	Alcohol dehydrogenase	21.5	1	10
102	agl1	Alpha-glucosidase	21.5	1	10
169	ain1	Alpha-actinin	1.5	5	0
513	arg7	Argininosuccinate lyase	4.5	2	0
744	bgs2	1,3-beta-glucan synthase	4.5	2	0
773	bgs2	1,3-beta-glucan synthase	4.5	2	0
329	cdc11	SIN pathway component	1.5	3	0
354	cdc11	SIN pathway component	1.5	5	0
902	cdc11	SIN pathway component	1.5	5	0
683	crn1	Coronin	21.5	1	25
384	ef1-b	Translation elongation factor 1 alpha-E	6.5	2	0
734	eno1	Phosphopyruvate hydratase	21.5	1	25
736	eno1	Enolase	6.5	3	25
733	gar1	Small nucleolar protein required for pre-rRNA processing	21.5	1	25
539	hxk2	Hexokinase 2	21.5	1	10
558	if-2	Translation initiation factor	21.5	1	50
38	meu25	Meiosis expression upregulated	21.5	1	5
850	mfm1	Mating factor precursor	21.5	1	50
273	ndc10	Subunit b of the Cbf3 kinetochore protein complex	1.5	3	0
264	pcn1	Auxiliary protein of DNA polymerase delta	4.5	2	0
919	plb1	Phospholipase B	4.5	3	0
68	pli1	SUMO E3 ligase involved in centromere organization and telomere maintenance	1.5	5	0

318	pli1	SUMO E3 ligase involved in centromere organization and telomere maintenance	1.5	5	0
858	pli1	SUMO E3 ligase involved in centromere organization and telomere maintenance	1.5	5	0
1	pli1	SUMO E3 ligase involved in centromere organization and telomere maintenance	1.5	3	5
128	pms1	Mitotic cohesin complex subunit	1.5	3	0
590	prp45	Component of the Cdc5p-associated complex, possibly involved in pre-mRNA splicing	1.5	5	50
396	psm1	Subunit of the cohesin complex, involved in sister chromatid cohesion and normal progression through mitosis	1.5	2	0
830	psm1	Subunit of the cohesin complex, involved in sister chromatid cohesion and normal progression through mitosis	1.5	3	0
181	pyr1	Hydroxymethylglutaryl-CoA lyase	21.5	1	10
94	rad18	DNA damage ds break repair	21.5	1	50
88	rpb7	RNA polymerase II subunit	21.5	1	50
949	rpl3701	60S ribosomal protein	21.5	1	50
531	rpl3701	60S ribosomal protein	4.5	3	25
417	rpo41	Mitochondrial DNA-directed RNA polymerase	21.5	1	10
1094	rps1501	40S ribosomal protein	21.5	1	50
222	rps29	40S ribosomal protein	21.5	1	50
6	rps4	hypothetical, contains ribosomal S4E domain	21.5	1	10
210	rpt1	Hypothetical protein, similar to *S. cerevisiae* Rpt1 (ATPase component of 25S ribosome)	21.5	1	25
97	rsp1	Required for disassembly and assembly of MTOCs	21.5	1	50

383	rsp1	Required for disassembly and assembly of MTOCs	1.5	5	50
718	rsp1	Required for disassembly and assembly of MTOCs	1.5	5	50
896	rsp1	Required for disassembly and assembly of MTOCs	1.5	5	50
913	rsp1	Required for disassembly and assembly of MTOCs	1.5	5	5
1039	rsp1	Required for disassembly and assembly of MTOCs	1.5	5	50
1086	rsp1	Required for disassembly and assembly of MTOCs	21.5	1	50
993	sdh3	Succinate dehydrogenase	21.5	1	25
196	SPAC10F6.11c	Predicted kinase activater	1.5	4	0
349	SPAC14C4.04	Hypothetical protein of unknown function	21.5	2	0
489	SPAC14C4.11	Polyphosphate synthetase	21.5	1	5
492	SPAC14C4.11	Polyphosphate synthetase	21.5	1	10
973	SPAC1687.18c	Cohesin loading factor	6.5	3	0
729	SPAC19G12.09	NADH/NADPH dependent indole-3-acetaldehyde reductase	21.5	1	25
367	SPAC25G10.06	40S ribosomal protein	4.5	2	0
502	SPAP8A3.02c	Protein containing a 2OG-Fe(II) oxygenase superfamily domain	21.5	1	5
471	SPBC13G1.09	Bystin-family protein	21.5	1	50
75	SPBC1685.04	Sequence orphan	4.5	2	5
180	SPBC1703.13c	Mitochondrial carrier protein	21.5	1	10
340	SPBC17G9.06c	Acetyltransferase	4.5	4	50
400	SPBC23G7.06c	Unknown function	21.5	1	10
835	SPBC24C6.03	Proline-tRNA ligase	21.5	1	25
1066	SPBC2D10.07c	Protein containing a peptidase family S24 domain	21.5	1	50

87	SPBC2G2.14	Unknown function	21.5	1	50
536	SPBC409.13	6,7-dimethyl-8-ribityllumazine synthase (DMRL synthase), involved in riboflavin biosynthesis	21.5	1	5
547	SPBC409.13	6,7-dimethyl-8-ribityllumazine synthase (DMRL synthase), involved in riboflavin biosynthesis	21.5	2	50
167	SPCC1393.08	hypothetical protein, has 2 GATA-type zinc fingues, homology to mouse transcriptional activator	21.5	1	50
202	SPCC1672.04c	Mitochondial copper ion transfer protein	4.5	2	0
407	SPCC1672.04c	Mitochondial copper ion transfer protein	21.5	2	0
418	SPCC1672.04c	Mitochondial copper ion transfer protein	1.5	4	25
434	SPCC24B10.18	UPF0390 family	21.5	1	10
709	SPCC330.04c	Unknown function	1.5	5	0
797	SPCC330.04c	Unknown function	1.5	5	0
806	SPCC576.14	Similarity to diphthamide methyltransferase			50
559	SPCC613.07	SnoRNA biogenesis protein	21.5	1	50
443	SPCC794.04c	Sugar transporter	21.5	1	10
491	SPCC830.08c	Similarity to *S. cerevisiae* Yop1p, involved in membrane trafficking	21.5	2	0
486	SPCP1E11.07c	Component of the Cdc5p-associated complex, possibly involved in pre-mRNA splicing	21.5	1	10
67	tas3	Protein required for heterochromatin assembly and silencing at centromeric repeats	1.5	3	0
856	tea3	Cell end marker required for initiation of bipolar growth and proper septum placement	1.5	5	0
641	wtf23	Member of the WTF protein family	21.5	1	25

This screen was carried out specifically to find the protein or proteins that target Mto1 to the cell equator. Candidates to investigate further were therefore selected on the basis of their localisation to the equator. Localisation data was taken from the *S. pombe* Postgenome Database ((Matsuyama et al., 2006), http://www.riken.jp/SPD/index.html). This database features localisation data for 90% of *S. pombe* genes. 271 genes were listed as present at the site of septum localisation. The localisation images were examined for these genes, and 90 were found to have localisation related to the CAR rather than the septum. Five of these genes were identified in the yeast two-hybrid screen.

Crn1, a protein of unknown function localises to actin patches, cables and the CAR (Pelham and Chang, 2001); Pdk1 is a kinase involved in mitotic spindle function that localises to the SPBs and the CAR (Bimbo *et al.*, 2005); Pob1 is required for cell polarity, elongation, and separation (Toya *et al.*, 1999); Rga7 is a Rho GTPase activator (Nakano *et al.*, 2001) and Rad24 is a cytokinesis checkpoint control protein (Mishra *et al.*, 2005).

To this list were added two additional proteins on the basis of function. Ain1, an actinin is a known component of the CAR, bundling and cross-linking actin (Wu *et al.*, 2001). The localisation of Ain1 was not determined due to cloning difficulties. Hsp9 is a heat shock protein thought to have a role in CAR stabilisation (Jang *et al.*, 1996). In the RIKEN database Hsp9-YFP localises throughout the cell. This may be a consequence of over-expression as the RIKEN localisation data was based on strains expressing the protein of interest from the strong *nmt1* promoter. Protein

localisation as reported in the database may be altered due to the C-terminal YFP tag. These proteins were all identified in the yeast two-hybrid once, with the exception of *hsp9*, which was identified 5 times. All the proteins were so-called 'weak' interactors, with the exception of Ain1.

The intrinsic limitations of the yeast-two hybrid system require that any interaction must be confirmed independently of the system by biochemical means or showing an *in vivo* requirement for the interaction. False positives in the yeast two-hybrid assay may be generated by incorrect folding, or bringing together two proteins that are able to interact but are expressed at different times in the cell or have distinct cellular localisations. The limitations of the yeast two-hybrid system can also generate false negatives due to incorrect folding and the absence of post-translational modification. To further investigate the selected candidates, I looked to see if they were required for Mto1 to localise to the cell equator gene-deletion strains. I also tested the prey plasmids against *LexA-mto1(769-1051)* by yeast two-hybrid, as I predicted that the 1051-1115 region of Mto1 necessary for the localisation of Mto1 would also be required for interaction with the localising protein.

Mto1-GFP localisation was studied in *ain1Δ, hsp9Δ, pdk1Δ* and *rga7Δ* deletion strains. Mto1 localisation was not examined in the *pob1Δ* strain as this gene is required for viability; the *crn1Δ* strain was not tested as microtubule organisation was previously reported normal in this strain and PAA formation would not occur in the absence of Mto1 at the cell equator (Pelham and Chang, 2001) and the *rad24Δ* strain was not tested as the null strains was not available. Mto1-GFP localised to the

cell equator in all strains tested (Figure 11). In the yeast two-hybrid assays, prey plasmids isolated in the yeast two-hybrid screen containing Ain1 and Hsp9 showed an interaction with *LexA-mto1(769-1115)* by growth on media minus histidine and expression of a blue colour in a LacZ overlay assay, but not with *LexA-mto1(769-1051)* (Figure 12, A and B). The LacZ overlay was extended by carrying out an ONPG assay to quantify the β-galactosidase expression. β-galactosidase activity in cells expressing *Gal4AD-ain1* and *LexA-mto1(769-1115)* was 3.14 Miller Units and for *Gal4AD-hsp9* and *LexA-mto1(769-1115)* was 0.51 Miller Units after 19 hrs; β-galactosidase activity in cells expressing *Gal4AD-ain1* or *Gal4AD-hsp9* with *LexA-mto1(769-1051)* was below the threshold of the assay, supporting the conclusion of the LacZ overlay assay and the growth assay. I considered that a redundant mechanism might be in place to localise Mto1 with both Ain1 and Hsp9 being independently able to target Mto1 to the cell equator, and so constructed the double deletion *ain1Δhsp9Δ*. However, Mto1-GFP also localised to the cell equator in this strain (Figure 12, C).

Of the other genes identified in the yeast two-hybrid screen, many are commonly found as false positives in yeast two-hybrid screens, regardless of the bait protein used. These include ribosomal proteins and mitochondrial proteins (Van Criekinge and Beyaert, 1999) and are of limited interest. Other genes identified are unlikely to show a functional interaction with Mto1 *in vivo* given what is known of their function and localisation. However two genes identified were of particular interest and the interaction with Mto1 was investigated further. Rsp1, a protein involved in eMTOC disassembly has previously been shown to interact with Mto1 by yeast two-

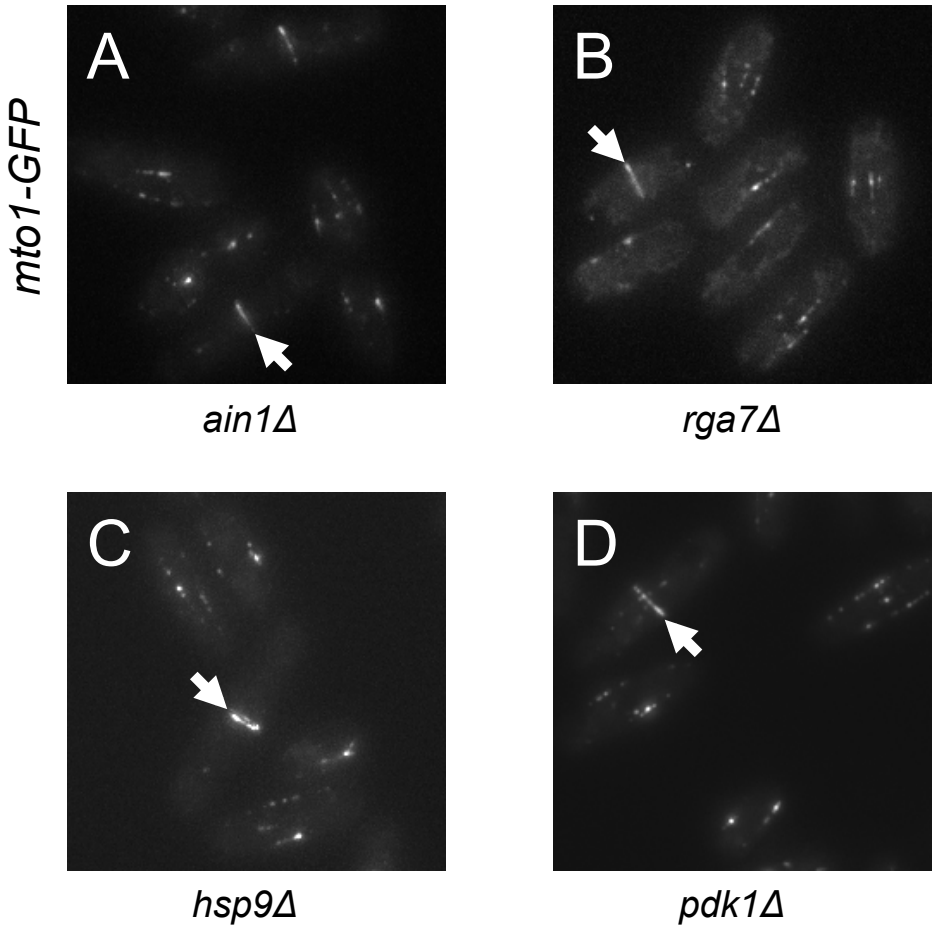

Figure 11 Mto1 localisation in candidate gene-deletion strains

Mto1-GFP localisation in (A) *ain1Δ,* (B) *hsp9Δ,* (C) *pdk1Δ* and (D) *rga7Δ* cells. Mto1 is present at the cell equator in these strains (arrows).

Figure 12 Mto1 interaction with Ain1 and Hsp9 from yeast two-hybrid screen.

(A) Growth of *Gal4AD-rga7 vs* (i) *LexA-mto1(769-1115)* and (ii) *LexA-mto1(769-1051); Gal4AD-hsp9 vs* (iii) *LexA-mto1(769-1115)* and *(iv) LexA-mto1(769-1051), Gal4AD-ain1 vs* (i) *LexA-mto1(769-1115)* and (ii) *LexA-mto1(769-1051)* on -WL and -WLH media. Ain1 and Hsp9 show growth on media lacking histidine with *LexA-Mto1(769-1115)*, but not with *LexA-Mto1(769-1051),* while Rga7 shows an interaction with both Mto1 truncations. (B) LacZ overlay assays. Ain1 and Hsp9 produce a blue colour with *LexA-mto1(769-1115)*, but not with *LexA-mto1(769-1051). Gal4AD vs LexA-mto2* was included as a positive control (LexA-Mto2 is strongly self-activating, the empty prey vector was included to allow growth on media lacking leucine). Both bait fragment were tested for autoactivation against the empty prey vector and found not to interact. (C) Mto1-GFP localises to the cell equator in *ain1Δ hsp9Δ* cells (arrows).

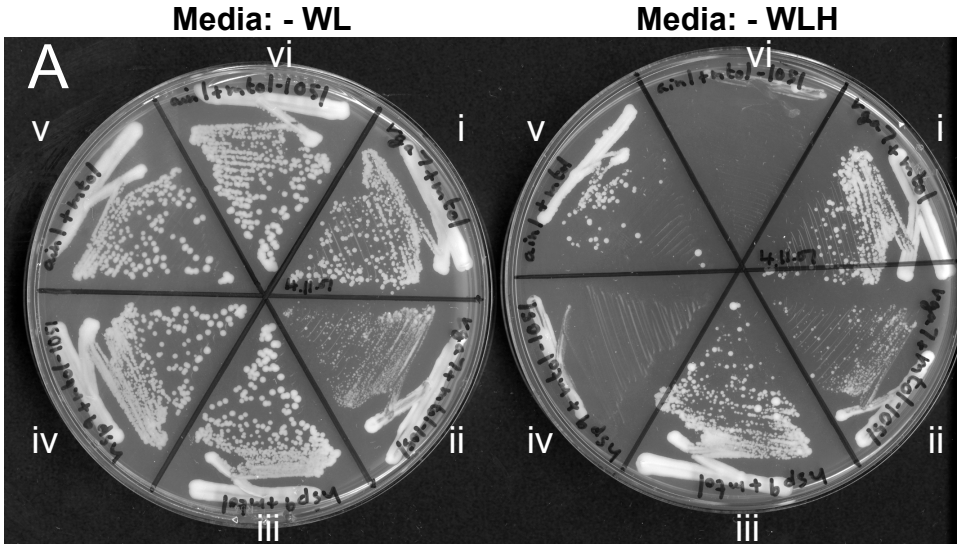
A
Media: - WL
Media: - WLH
vi
i
ii
iii
iv
v

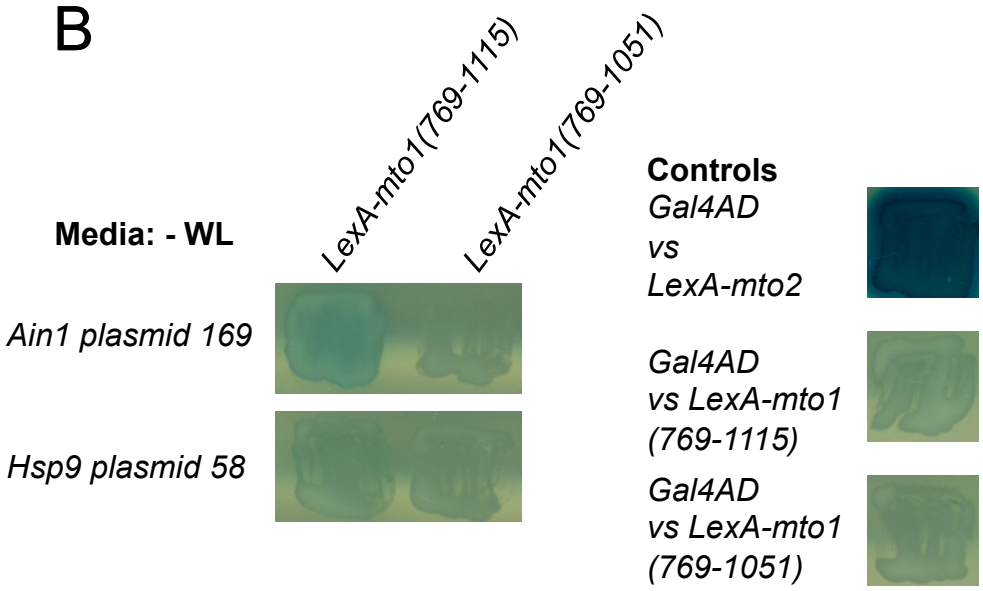
B
LexA-mto1(769-1115)
LexA-mto1(769-1051)
Media: - WL
Ain1 plasmid 169
Hsp9 plasmid 58
Controls
Gal4AD
vs
LexA-mto2
Gal4AD
vs LexA-mto1
(769-1115)
Gal4AD
vs LexA-mto1
(769-1051)

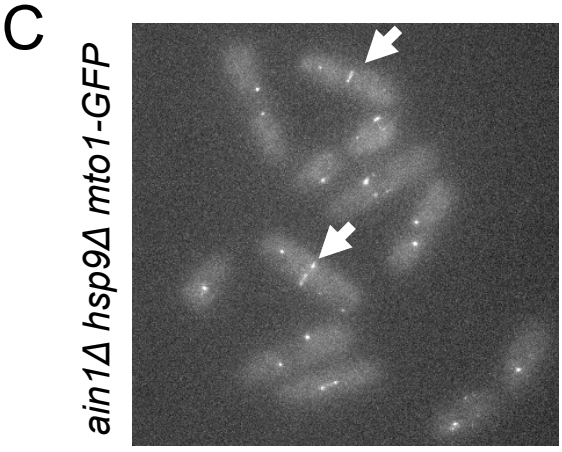
C
ain1Δ hsp9Δ mto1-GFP

hybrid (Zimmerman and Chang, 2005) and appeared seven times in my screen, strongly interacted with Mto1 based on the 3-AT and LacZ data. Cdc11, a component of the SIN pathway, forms a scaffold for signalling at the SPB and is of interest as a potential candidate for the protein that interacts with Mto1 at the mitotic SPB (an area of interest to other members of the laboratory).

Plasmid 354 from the yeast two-hybrid screen (the first *cdc11* prey plasmid identified) was sequenced and found to contain the region *cdc11(561-1046)*, the C-terminal half of the protein. This plasmid was tested against *LexA-mto1(769-1115)* and *LexA-mto1(769-1051)* and found to interact by growth on media minus histidine and by LacZ overlay assay with *LexA-mto1(769-1115)*, but not with *LexA-mto1(769-1051)*, consistent with the requirement of the Mto1 localisation domain for the interaction (Figure 13, A). This plasmid was then re-made as pKS752 to ensure that no mutations were present in the sequence and tested against a series of Mto1 truncations: *LexA-mto1(769-1115), LexA-mto1(769-1095)* and *LexA-mto1(769-1065)* (Figure 13, B). I found that there was an interaction with *LexA-mto1(769-1115)*, *LexA-mto1(769-1095)*, but not with *LexA-mto1(769-1065)* based on growth on media minus histidine and by LacZ overlay assay. This corresponds with previous findings that the region 1085-1095 is necessary for the localisation of Mto1 to the mitotic SPB (I. Samejima, personal communication). I then tested pKS752 *Gal4AD-cdc11(561-1046)*, against *LexA-mto1(769-1115), LexA-mto1(769-1095), LexA-mto1(769-1085), LexA-mto1(769-1075), LexA-mto1(769-1065)* and *LexA-mto1(769-1051)* (Figure 13, C) based on growth on media minus histidine and by ONPG assay

Figure 13 Mto1 interaction with Cdc11 and Rsp1 by yeast two-hybrid screen

(A) Plasmid 354 *Gal4AD-cdc11(561-1046)* tested against *LexA-mto1(769-1115)* and *LexA-mto1(769-1051)* by growth on media minus histidine and by LacZ overlay assay. (B) pKS752 (equivalent to plasmid 354) similarly tested against *LexA-mto1(769-1115), LexA-mto1(769-1095)* and *LexA-mto1(769-1065)* and (C) pKS752 tested against *LexA-mto1(769-10115), LexA-mto1(769-1095), LexA-mto1(769-1085), LexA-mto1(769-1075), LexA-mto1(769-1065)* and *LexA-mto1(769-1051)*. (D) *LexA-mto1(769-1115)* tested against the smaller truncations *Gal4AD-cdc11(701-1046)*, *Gal4AD-cdc11(801-1046), Gal4AD-cdc11(901-1046), Gal4AD-cdc11(561-700), Gal4AD-cdc11(561-800)* and *Gal4AD-cdc11(561-900)*. (E) Rsp1 (plasmid 896, isolated in the yeast two-hybrid screen) tested against *LexA-mto1(769-1115)* and *LexA-mto1(769-1051)* by growth on media minus histidine and by LacZ overlay assay. (F) Rsp1 (plasmid 1086, isolated in the yeast two-hybrid screen) tested against *LexA-mto1(769-1115), LexA-mto1(769-1095)* and *LexA-mto1(769-1065)* and (G) against *LexA-mto1(769-10115), LexA-mto1(769-1095), LexA-mto1(769-1085), LexA-mto1(769-1075), LexA-mto1(769-1065)* and *LexA-mto1(769-1051). Mto1(1051-1065)* is necessary for interaction with Rsp1 and Mto1(1085-1095) region is necessary for interaction with Cdc11

A

Gal4AD-cdc11(561-1046) vs LexA-mto1(769-1115)

Gal4AD-cdc11(561-1046) vs LexA-mto1(769-1051)

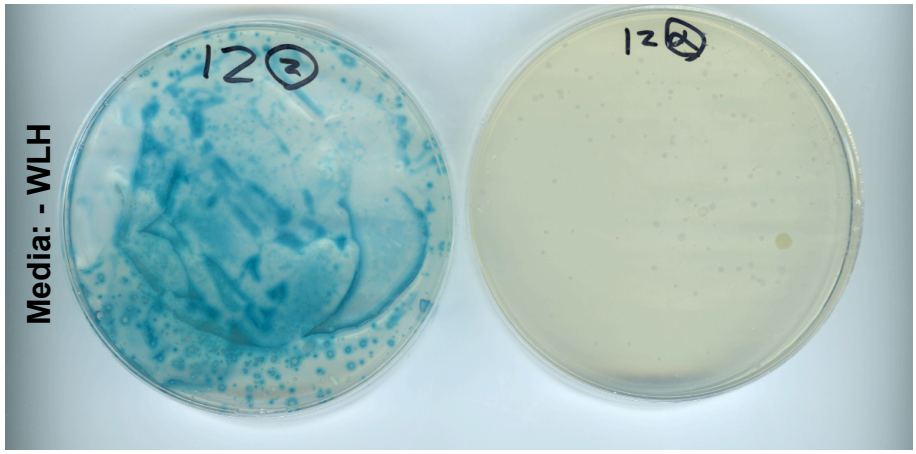

B

Media: - WLH

Gal4AD-cdc11 (561-1046) (pKS752)

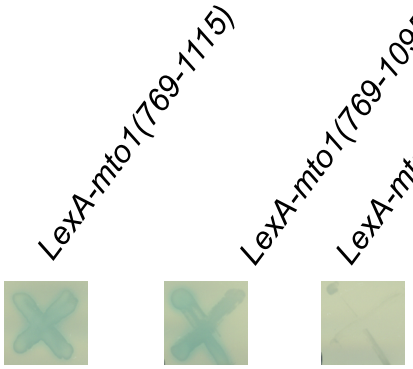

C

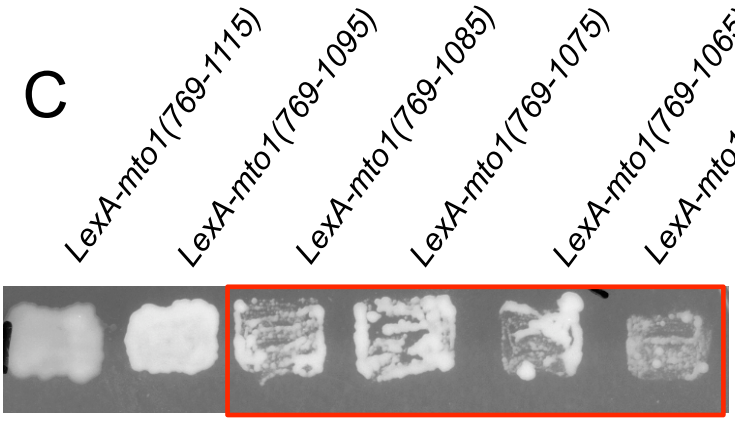

Media: - WLH

Gal4AD-cdc11, plasmid 1086 from screen

ONPG readings Miller units after 55 mins

5.64 *3.44* *Other samples below limit of assay (LexA-mto1(769-1085) not tested)*

D *LexA-mto1(769-1115) vs cdc11 truncations*

Media: - WLH

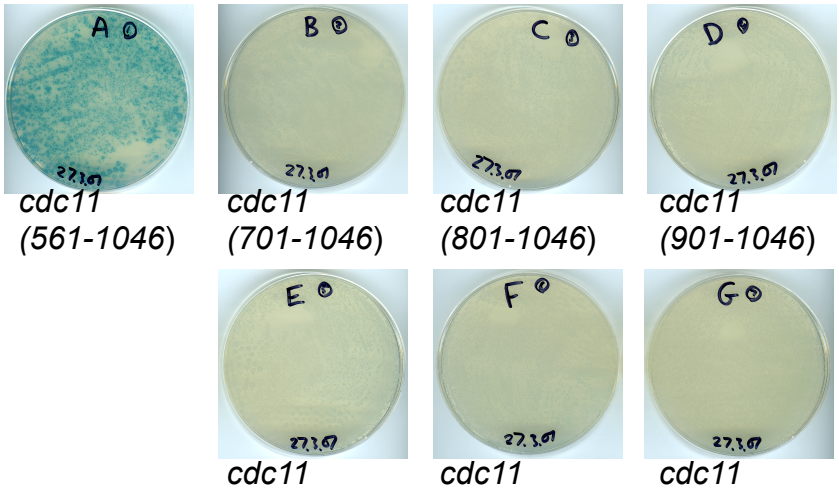

cdc11 (561-1046) *cdc11 (701-1046)* *cdc11 (801-1046)* *cdc11 (901-1046)*

cdc11 (561-700) *cdc11 (561-800)* *cdc11 (561-900)*

E

Gal4AD-rsp1, plasmid 896 *vs LexA-mto1(769-1115)*

Gal4AD-rsp1, plasmid 896 *vs LexA-mto1(769-1051)*

Media: - WLH

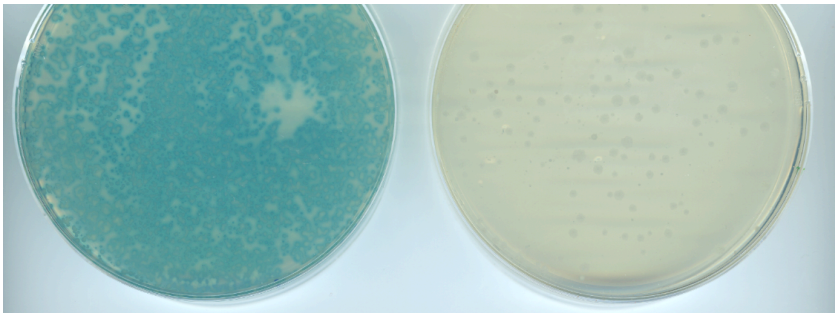

F

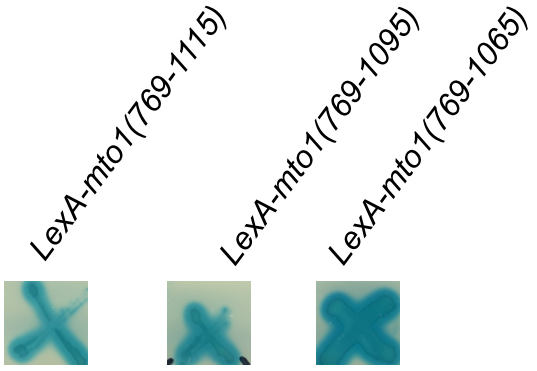

Media: - WLH

Gal4AD-rsp1, plasmid 1086 from screen

G

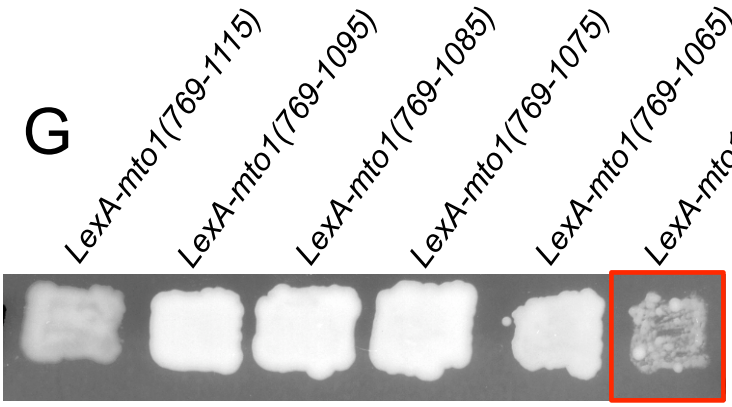

Media: - WLH

Gal4AD-rsp1, plasmid 1086 from screen

16.94	*35.3*	*37.5*	*25.0*	*Both below limit of assay: LexA-mto1(769-1065) should be retested as this contradicts 'F'.*	***ONPG readings Miller units after 55 mins***

As before, the 1085-1095 region is necessary for interaction with Cdc11, supporting the idea that Cdc11 may localise Mto1 to the mitotic SPB.

I also made a series of plasmids with Cdc11 fragments in the pGad424 vector to map the region of Cdc11 necessary to interact with Mto1 using the yeast two-hybrid assay. A series of plasmids were made as follows: *Gal4AD-cdc11(701-1046)*, *Gal4AD-cdc11(801-1046), Gal4AD-cdc11(901-1046), Gal4AD-cdc11(561-700), Gal4AD-cdc11(561-800)* and *Gal4AD-cdc11(561-900)*. These were tested for interaction with *LexA-mto1(769-1115)*; all gave growth on media minus histidine, but only pKS752 *Gal4AD-cdc11(561-1046)* gave a blue colour in the LacZ overlay assay (Figure 13 D). Expression of *Gal4AD-cdc11(561-1046)*, *Gal4AD-cdc11(901-1046)* and *Gal4AD-cdc11(561-900)* was tested by Western blotting using anti-Cdc11 antibody (Sawin Laboratory) and anti-GAL4 (Santa Cruz, sc-46680), but no specific bands were seen for any sample tested and so the experiment was inconclusive (data not shown). The sequence of the Cdc11 C-terminus shows that it contains 14-16 leucine-rich repeats, from ~605-988 aas (K Sawin, personal communication). These short 20-30 amino acid motifs are known to form horseshoe-like structures (Kobe and Kajava, 2001). Making truncations within this region may affect protein stability. Alternatively, as ligands for leucine-rich regions typically bind to the inside of the horseshoe structure, residues from spatially distant parts of Cdc11 may be required and the area seen is the minimum necessary for the interaction with Mto1.

Rsp1 (plasmid 1086, isolated in the yeast two-hybrid screen) was also tested first against *LexA-mto1(769-1115), LexA-mto1(769-1095)* and *LexA-mto1(769-1065)*

(Figure 13, E) and later against *LexA-mto1(769-1115), LexA-mto1(769-1095), LexA-mto1(769-1085), LexA-mto1(769-1075), LexA-mto1(769-1065)* and *LexA-mto1(769-1051)* (Figure 13, F). I found that the 1085-1095 region is necessary for interaction with Rsp1, the implications of which are discussed below.

Tandem affinity purification of Mto1

The next method used to identify proteins that interact with Mto1 was tandem affinity purification (TAP) (Puig et al., 2001). Two-step purification reduces the number of non-specific interactions present in the final sample. The sample is digested with TEV protease after the first purification step to expose the second affinity tag; a second purification step is then performed. Mass spectrometry (MS) analysis can then be used to identify proteins bound to the protein of interest. This method has the advantage that *in vivo* protein modifications are present in the sampled extract, and it is an unbiased screen. However indirect interactions mediated through other proteins are included in the results and the complex must be soluble to be available for precipitation. Also the interaction must be sufficiently stable to survive a lengthy purification.

In this screen the TAPS tag was fused to the C-terminus of Mto1 expressed under the endogenous promoter. Two alleles of Mto1 were used: full length Mto1-TAPS and a truncation, Mto1(1-1051)-TAPS, that lacks the C-terminal localising domain. Mto1(1-1051) does not localise to the eMTOC; as the C-terminus of Mto1 is necessary for localisation to the equator, any protein that interacts with Mto1(1-1051) is unlikely to

be the eMTOC recruitment factor. Comparing the list of interacting proteins for the truncation versus full-length Mto1 will help to exclude non-specific interactions. An untagged control sample was also used to control for non-specific interactions with the beads used during the purification.

Following TAP/MS, various proteins interacting with Mto1 were identified (a complete list is given in Table 6 at the end of the chapter). Figure 14 shows a silver-stained agarose gel run with an aliquot of the protein sample used for mass spectrometry analysis. 193 proteins were found for Mto1-TAPS, 167 proteins for Mto1(1-1051)-TAPS and 29 for the untagged control. Proteins known to localise to the equator were found (Crn1, cornonin; Fim1, fimbrin; Rad24, a DNA damage and cytokinesis checkpoint protein) but these proteins interacted with both Mto1(1-1051)-TAPS and Mto1-TAPS and on this basis were not considered further. No potential candidates showing an interaction with Mto1-TAPS, but not Mto1(1-1051)-TAPS were found. Of the other proteins known to interact with Mto1, Mto2 was present for both alleles of Mto1 (as expected), but the γ-TuC proteins were not detected despite Mto1 previously being shown to affinity purify with Alp4 and Alp6 (Venkatram et al., 2004). This suggests that the method may require additional optimisation. Rsp1, a protein involved in the breakdown of the eMTOC and also previously shown to interact with Mto1 was found to interact with Mto1-TAPS, but interestingly not with Mto1(1-1051)-TAPS. Potential implications of this finding for the mechanism of eMTOC disassembly are discussed below.

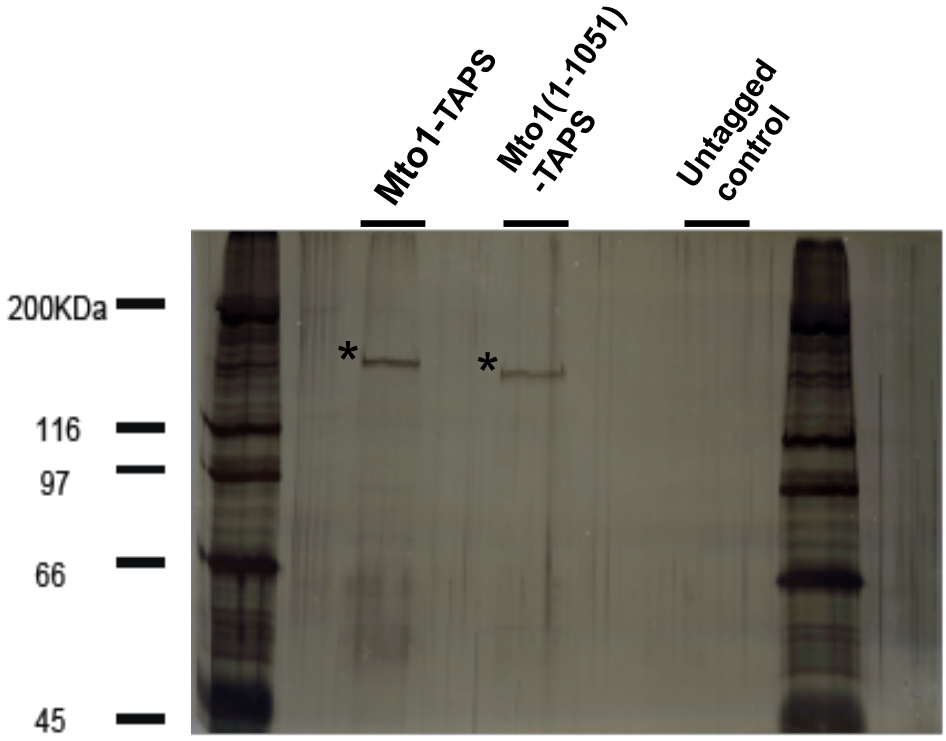

Figure 14 Tandem affinity purification of Mto1 and Mto1(1-1051)

Silver stained acrylamide gel showing the purification of KS3524 *mto1-TAPS*, KS3474 *mto1(1-1051)-TAPS* and wild-type KS516 as an untagged control strain. Each sample is equal to 6 % of the total sample. * indicates primary bands for Mto1-TAPS and Mto1(1-1051)-TAPS.

Discussion

Localisation of Mto1 to the cell equator

Here I have shown that the C-terminus of Mto1 Mto1(919-1115) is sufficient for localisation to both the SPB and the eMTOC. This region includes the 1051-1115aa localisation region that was previously identified as necessary for the localisation of Mto1. I also found that Mto1 co-localises with the CAR and requires F-actin to localise to the equator. Taken together with the previous finding that the Mto1 ring that forms at the equator is contractile (Sawin *et al.*, 2004), these strongly suggest an interaction between Mto1 and the CAR, leading me to hypothesise that the protein or proteins that target Mto1 to the cell equator is a component of the CAR. I carried out a yeast two-hybrid screen using a C-terminal fragment of Mto1 and tandem affinity purification of Mto1(1-1115) and Mto1(1-1051). Despite identifying a number of proteins that appear to interact with Mto1 and localise to the cell equator, none of the proteins tested were found to be required for the localisation of Mto1 to the cell equator. It is possible that redundant mechanisms of localisation may be present, but testing combinations of the proteins so-far identified would be time-consuming and could lead to false negatives due to synthetic effects of deleting genes in combination, especially on the CAR. Crn1 and Rad24 were identified in both the yeast to-hybrid screen and by tandem affinity purification, suggesting that these interactions may be real, although their function is unknown. Further experiments to identify the protein that localises Mto1 to the cell equator are described in the next chapter, based on the CAR component hypothesis.

eMTOC disassembly: Mto1 and Rsp1

My screening also identified *in vivo* evidence of the physical interaction between Mto1 and Rsp1, a protein required for PAA breakdown. Mto1 and Rsp1 have previously been shown to interact by yeast two-hybrid (Zimmerman and Chang, 2005). I have repeated this finding, show that it takes place *in vitro* using tandem affinity purification and show by both methods that this interaction requires the C-terminal localisation region of Mto1. This suggests a potential mechanism for disassembly, where Rsp1 competitively binding to the 1051-1065aa region of Mto1, disrupting the interaction with the Mto1 localising protein and so disassembling the eMTOC. Rsp1 contains a J-domain (Zimmerman et al., 2004b). J-domains bind and activate Hsp70 chaperones (Kelley, 1999). Another J-domain protein, auxilin, initiates clathrin disassembly after endocytosis via the recruitment of Hsp70 (Kelley, 1998). The eMTOC may be deconstructed via a similar mechanism. Further investigation of the mechanism and control of eMTOC disassembly presents an interesting area for future study.

Table 5 Results of yeast two-hybrid screen

Sample number	Gene name	Function
7	act1	Actin
424	adh1	Alcohol dehydrogenase
102	agl1	Alpha-glucosidase
56	agn1	Endo-(1,3)-alpha-glucanase involved in degradation of septum edging during cell separation
741	aif1	Oxidoreductase activity, regulates apoptosis
169	ain1	Alpha-actinin
184	apl4	Member of the adaptin N-terminal region-containing family, which are components of coated vesicles
327	arc3	Actin related protein, part of Arp2/3 complex, actin cortical patches
450	arc3	Actin related protein, part of Arp2/3 complex, actin cortical patches
133	arg4	Arginine specific carbamoyl-phosphate synthase
113	arg5	Arginine specific carbamoyl-phosphate synthase
513	arg7	Argininosuccinate lyase
40	arp2	Actin-related protein 2, a component of the Arp2/Arp3 complex required for actin cortical patch assembly
111	ats1	Acetyltransferase, histone acetylation
455	bem46	Predicted esterase/lipase
108	bgs2	1,3-beta-glucan synthase component, required for proper spore cell wall biosynthesis
409	bgs2	1,3-beta-glucan synthase component, required for proper spore cell wall biosynthesis
744	bgs2	1,3-beta-glucan synthase component, required for proper spore cell wall biosynthesis
773	bgs2	1,3-beta-glucan synthase component, required for proper spore cell wall biosynthesis
451	bgs2	1,3-beta-glucan synthase component, required for proper spore cell wall biosynthesis
207	bgs3	1,3-beta-glucan synthase component, required for proper spore cell wall biosynthesis
1092	bgs4	1,3-beta-glucan synthase component, required for proper spore cell wall biosynthesis
109	cct4	Component of Chaperonin-containing T-complex
234	cda1	Chitin deacetylase
329	cdc11	SIN pathway component
354	cdc11	SIN pathway component
902	cdc11	SIN pathway component
468	cid16	Member of the PAP or 25A associated domain containing and nucleotidyltransferase domain containing families
135	clr4	Histone H3 methyltransferase
690	cox13	Cytochrome c oxidase subunit
151	cox13	Cytochrome c oxidase subunit

565	cpc2	Protein required for normal mating, sporulation, and protein translation
683	crn1	Protein of unknown function that localizes to actin patches, actin cables, and the actin contractile ring
115	cut23	Subunit of the APC/cyclosome complex
967	cwf25c	Component of the Cdc5p-associated complex, possibly involved in pre-mRNA splicing
122	ef1-b	Translation elongation factor 1 alpha-E, involved in regulating cell polarity
384	ef1-b	Translation elongation factor 1 alpha-E, involved in regulating cell polarity
386	ef1-b	Translation elongation factor 1 alpha-E, involved in regulating cell polarity
337	eft-2	Translation elongation factor 2
57	eno1	Enolase, phosphopyruvate hydratase activity
62	eno1	Enolase, phosphopyruvate hydratase activity
734	eno1	Enolase, phosphopyruvate hydratase activity
736	eno1	Enolase, phosphopyruvate hydratase activity
265	erg2	C-8 sterol isomerase (predicted)
1020	erg24	Sterol reductase
586	erg5	Biosynthesis of ergosterol
1048	fba1	Fructose-bisphosphate aldolase
733	gar1	Small nucleolar protein required for pre-rRNA processing
3	ght5	Hexose trabsporter
369	ght8	Predicted hexose transporter
385	glu2	NAD-specific isocitrate dehyrogenase subunit
224	gpd3	Glyceraldehyde 3-phosphate dehydrogenase
361	gpd3	Glyceraldehyde 3-phosphate dehydrogenase
10	gpi14	Mannosyltransferase
416	gps2	UDP-galactose synthesis and protein glycosylation
172	grt1	Transcription factor
397	hht2	Histone H3.2
490	hht3	Histone H3.3
58	hsp9	Heat shock-induced protein, may stabilise contractile ring
64	hsp9	Heat shock-induced protein, may stabilise contractile ring
220	hsp9	Heat shock-induced protein, may stabilise contractile ring
1075	hsp9	Heat shock-induced protein, may stabilise contractile ring
659	hsp9	Heat shock-induced protein, may stabilise contractile ring
539	hxk2	Hexokinase 2, catalyzes glucose phosphorylation
557	its3	1-phosphatidylinositol-4-phosphate 5-kinase
706	lsm1	Predicted mRNA decapping complex subunit
191	map3	Pheromone M factor receptor
38	meu25	Meiosis expression upregulated

39	meu4	Meiosis expression upregulated
1098	meu4	Meiosis expression upregulated
441	mfm1	Mating factor precursor
460	mfm1	Mating factor precursor
478	mfm1	Mating factor precursor
658	mfm1	Mating factor precursor
850	mfm1	Mating factor precursor
862	mfm1	Mating factor precursor
179	mfm3	Mating factor precursor
275	mfm3	Mating factor precursor
1013	mfm3	Mating factor precursor
440	mok11	Glucan biosynthesis
526	mok11	Putative cell wall alpha-glucan synthase.
285	mpf1	Predicted meiotic PUF family protein
170	mrp19	Mitochondrial ribosome
582	mug135	Cell surface glycoprotein
709	mug136	Cell surface glycoprotein
797	mug137	Cell surface glycoprotein
442	mug174	Unknown function
798	mug40	DinB translesion DNA repair polymerase
160	mug51	unknown function
278	mug56	Predicted spore wall assembly protein
273	ndc10	Component of the Cbf3 kinetochore protein complex that binds DNA
282	ndc10	Component of the Cbf3 kinetochore protein complex that binds DNA
21 (group 1)	ndk1	Nucleaotide diphosphase kinase, nucleotide transport
1105	nmt1	Thiamine biosynthesis
517	nuc2	Anaphase-promoting complex subunit
848	nup146	Protein with weak similarity to S. cerevisiae Nup159p, a nuclear pore protein
502	ofd2	2 OG-Fe(II) oxygenase superfamily protein
716	ofd3	3 OG-Fe(II) oxygenase superfamily protein
23	pam17	Unknown function
264	pcn1	Auxiliary protein of DNA polymerase delta
276	pcn1	Proliferating cell nuclear antigen
21	pcy1	Vacuolar carboxypeptidase Y
5	pda1	Pyruvate dehydrogenase
91	pfk1	6-Phosphofructokinase beta subunit
317	pfk1	6-Phosphofructokinase beta subunit
142	pgi1	Cytosolic glucose-6-phosphate isomerase
40 (group 1)	pka1	cAMP dependant protein kinase
2	pkl1	ATPase involved in mitotic spindle function
919	plb1	Phospholipase B, preferentially deacylates phosphatidylinositol
140	pld1	Predicted phospholipase
68	pli1	SUMO E3 ligase
318	pli1	SUMO E3 ligase
858	pli1	SUMO E3 ligase
1	pli1	SUMO E3 ligase

203	pmp3	Plasma membrane proteolipid Pmp3
206	pmp3	Plasma membrane proteolipid Pmp4
256	pmp3	Plasma membrane proteolipid Pmp5
128	pms1	Mitotic cohesin complex subunit
1054	pob1	Essential protein required for cell polarity, elongation, and separation
104	ppk21	Serine/threonine protein kinase
154	ppk33	Serine/threonine protein kinase
590	prp45	Component of the Cdc5p-associated complex, possibly involved in pre-mRNA splicing
106	prs1	Ribose-phosphate pyrophosphokinase
19	psm1	Mitotic cohesin complex subunit
396	psm1	Subunit of the cohesin complex
830	psm1	Subunit of the cohesin complex
6	ptr2	Peptide permease
181	pyr1	Hydroxymethylglutaryl-CoA lyase
291	qcr10	Ubiquinol-cytochrome-c reductase complex subunit
467	qcr7	Similarity to ubiquinol cytochrome c reductase subunit 7
94	rad18	DNA damage ds break repair
346	rad24	Cytokinesis checkpoint control
427	rad25	14-3-3- protein involved in G2/M phase transition and DNA damage checkpoint control
909	rec10	Protein with roles in meiotic recombination and chromosome segregation
32	rga7	Rho GTPase activator
103	rga7	Rho GTPase activator
411	rgs1	Regulator of G protein signalling in mating pathway
187	rhp6	Putative E2 ubiquitin-conjugating enzyme required for DNA repair
88	rpb7	RNA polymerase II subunit
884	rpb7	RNA polymerase II subunit
554	rpl12-1	60S ribosomal protein L12A
801	rpl22	60S ribosomal protein
904	rpl22	60S ribosomal protein
499	rpl3602	60S ribosomal protein L36
392	rpl3701	60S ribosomal protein L37A
949	rpl3701	60S ribosomal protein L37A
531	rpl3701	60S ribosomal protein L37A
255	rpl902	60S ribosomal protein
417	rpo41	Mitochondrial DNA-directed RNA polymerase
1094	rps1501	40S ribosomal protein S15
4	rps2	40S ribosomal protein S2
178	rps25-1	40S ribosomal protein S25
222	rps29	40S ribosomal protein
6 (group 1)	rps402	ribosomal protein S4
475	rps403	ribosomal protein S5
476	rps901	40S ribosomal protein
795	rps901	40S ribosomal protein

795	rps901	40S ribosomal protein S9A
210	rpt1	Predicted 19S proteasome regulatory subunit
393	rsm18	Mitochondrial ribosomal protein subunit S18
97	rsp1	Required for disassembly and assembly of MTOCs
148	rsp1	Required for disassembly and assembly of MTOCs
353	rsp1	Required for disassembly and assembly of MTOCs
383	rsp1	Required for disassembly and assembly of MTOCs
717	rsp1	Required for disassembly and assembly of MTOCs
718	rsp1	Required for disassembly and assembly of MTOCs
896	rsp1	Required for disassembly and assembly of MTOCs
913	rsp1	Required for disassembly and assembly of MTOCs
1039	rsp1	Required for disassembly and assembly of MTOCs
1086	rsp1	Required for disassembly and assembly of MTOCs
993	sdh3	Succinate dehydrogenase cytochrome B subunit
859	sfr1	Swi five-dependent recombination repair protein 1
548	shm2	Protein with high similarity to serine hydroxymethyltransferase
556	shm2	Serine hydroxymethyltransferase
829	sod1	Manganese-containing, mitochondrial superoxide dismutase precursor
1014	sod2	Manganese-containing, mitochondrial superoxide dismutase precursor
1088	SPAC1039.10	Protein containing an endoribonuclease L-PSP domain
196	SPAC10F6.11c	Predicted kinase activater
1057	SPAC1296.06	Oxidoreductase activity
246	SPAC1486.07c	Mitochondrial ribosomal protein subunit L19
297	SPAC14C4.04	Golgi/ vacuolar associated protein
349	SPAC14C4.04	Hypothetical protein of unknown function
348	SPAC14C4.04	Unknown function
489	SPAC14C4.11	Polyphosphate synthetase
489	SPAC14C4.11	Polyphosphate synthetase
492	SPAC14C4.11	Polyphosphate synthetase
83	SPAC167.05	Hypothetical protein of unknown function
333	SPAC16A10.01	Hypothetical protein of unknown function
1031	SPAC16E8.17c	Succinate-CoA ligase alpha subunit
56	SPAC1851.04c	Predicted guanyl-nucleotide exchange factor
335	SPAC186.06	Hypothetical protein of unknown function
728	SPAC19G12.09	Aldehyde reductase

729	SPAC19G12.09	NADH/NADPH dependent indole-3-acetaldehyde reductase
321	SPAC1F8.07c	Predicted pyruvate decarboxylase
1077	SPAC227.05	Predicted prefoldin4 subunit
1080	SPAC227.05	Predicted prefoldin4 subunit
413	SPAC22F3.07c	Mitochondrial ATP synthase subunit
197	SPAC22F8.08	Secreation GTPase
357	SPAC23C4.03	Putative haspin
26	SPAC24C9.06c	Aconitate hydratase
26 (group 1)	SPAC24C9.07c	Predicted 1,3 beta glucan synthase
30 (group 1)	SPAC24C9.07c	Predicted 1,3 beta glucan synthase
1102	SPAC24H6.01c	Membrane bound O-acyl transferase
367	SPAC25G10.06	40S ribosomal protein S28A
1074	SPAC27E2.11c	Sequence orphan
301	SPAC29B12.05c	S-adenosylmethionine-dependent methyltransferase
1016	SPAC2F3.14c	Hypothetical protein of unknown function
453	SPAC2G11.05c	Unknown function
834	SPAC31G5.19	Member of the ATPase family
271	SPAC343.06c	Predicted phospholipid scramblase
814	SPAC3G6.13c	60S ribosomal protein L41
1095	SPAC3G6.13c	60S ribosomal protein L41
703	SPAC4G8.01c	Hypothetical protein of unknown function
422	SPAC4G9.15	Predicted ketoreductase
12	SPAC4G9.15	Predicted ketoreductase
336	SPAC57A7.12	Predicted heat shock protein
158	SPAC589.06c	Hypothetical protein of unknown function
479	SPAC644.08	Predicted methionine salvage haloacid dehalogenase-like hydrolase
98	SPAC6B12.14c	Unknown function
794	SPAC6F12.13c	Putative farnesyl pyrophosphate synthetase
1120	SPAC922.04	Sequence orphan
173	SPAC922.06	Oxidoreductase
1112	SPAC9E9.04	Unknown function, appears to localise to membranes
165	SPAC9E9.09c	Aldehyde dehydrogenase
286	SPAC9E9.09c	Aldehyde dehydrogenase
630	SPACUNK4.11c	Sequence orphan
284	SPAP8A3.02c	1 OG-Fe(II) oxygenase superfamily
294	SPAP8A3.02c	2 OG-Fe(II) oxygenase superfamily
705	SPAPJ691.03	Unknown function
2 (group 1)	SPBC106.16	20S proteosome subunit
66	SPBC1198.06c	Predicted mannan endo-1,6-alpha-mannosidate
243	SPBC1271.15c	Translation initiation factor
310	SPBC1271.15c	Translation initiation factor
558	SPBC1271.15c	Translation initiation factor
471	SPBC13G1.09	Predicted bystin family U3 and U14 snoRNA associated protein
459	SPBC1539.06	Predicted acyl-coenzyme A binding protein
861	SPBC1539.06	Predicted acyl-coenzyme A binding protein
406	SPBC1683.02	Predicted adenine deaminase

75	SPBC1685.04	sequence orphan
84	SPBC16E9.09c	COPII vesicle transport
15	SPBC16G5.05c	Predicted ER membrane protein
146	SPBC1703.07	Predicted ATP citrate synthase subunit
180	SPBC1703.13c	Predicted mitochondrial carrier protein
340	SPBC17G9.06c	Predicted siderophore-iron biosynthesis protein
340	SPBC17G9.06c	Predicted siderophore-iron biosynthesis protein
444	SPBC19G7.03c	40S ribosomal protein S30B
567	SPBC19G7.03c	40S ribosomal protein S30B
258	SPBC215.10	Predicted haloacid dehalogenase-like hydrolase
320	SPBC21C3.19	Unknown function
400	SPBC23G7.06c	Unknown function
810	SPBC244.02c	Predicted U3 snoRNP-associated protein
835	SPBC24C6.03	Predicted proline-tRNA ligase
368	SPBC29A10.08	Glycolipid-anchored surface protein precursor
405	SPBC29A3.19	Hypothetical cycloisomerase
687	SPBC2D10.03c	Hypothetical protein of unknown function
1066	SPBC2D10.07c	Predicted mitochondrial inner membrane peptidase complex catalytic subunit
124	SPBC2D10.11c	Predicted nucleosome assembly protein
18	SPBC2D10.20	Predicted ubiquitin protein ligase
87	SPBC2G2.14	Sequence orphan
157	SPBC2G2.14	Sequence orphan
344	SPBC32H8.09	Hypothetical protein, contains WD repeats
536	SPBC409.13	6,7-dimethyl-8-ribityllumazine synthase
547	SPBC409.13	6,7-dimethyl-8-ribityllumazine synthase
334	SPBC577.04	Human THOC5 homologue
247	SPBC646.08c	Predicted oxysterol binding
214	SPBC660.11	Component of the ribosome assembly chaperone (RAC) complexrequired for pre-rRNA maturation
249	SPBC713.11c	Unknown
33	SPBC83.02c	60S ribosomal subunit
150	SPBC887.17	Uracil permease
176	SPBC887.17	Uracil permease
311	SPBC8D2.04	Histone H3
36	SPBC8D2.18c	Adenosylhomocysteinase activity [P]; Trialkylsulfonium hydrolase activity
818	SPBC8E4.02	Predicted agmatinase
927	SPBC8E4.03	Predicted agmatinase
153	SPBC8E4.04	Aldehyde reductase
439	SPBC947.06c	Sugar transporter
28	SPBP165F5.08c	Predicted flavoprotein
71	SPBP19A11.02c	Sequence orphan
155	SPBP8B7.15c	Ubiquitin-protein ligase E3
31	SPBP8B7.25	Cyclophilin family peptidyl-prolyl cis-trans isomerase
144	SPCC1020.08	Predicted wybutosine biosynthesis protein
1013	SPCC126.12	Hypothetical protein, predicted NGG1p interacting factor 3 family
167	SPCC1393.08	Predicted transcription factor

341	SPCC1450.15	Phosphoethanolamine N-methyltransferase family
118	SPCC1672.04c	Predicted mitochondrial copper chaperone
168	SPCC1672.04c	Predicted mitochondrial copper chaperone
257	SPCC1672.04c	Predicted mitochondrial copper chaperone
259	SPCC1672.04c	Predicted mitochondrial copper chaperone
279	SPCC1672.04c	Predicted mitochondrial copper chaperone
407	SPCC1672.04c	Predicted mitochondrial copper chaperone
418	SPCC1672.04c	Predicted mitochondrial copper chaperone
681	SPCC1672.04c	Predicted mitochondrial copper chaperone
9	SPCC16C4.10	Predicted 6-phosphoglucolactonase
34	SPCC1739.04c	Sequence orphan
644	SPCC1906.05	Zinc finger protein
434	SPCC24B10.18	Human Leydig cell tumor 10 kDa protein homologue
11	SPCC285.05	Purine nucleoside permease
322	SPCC569.01c	Unknown function
806	SPCC576.14	Predicted diphthine synthase
324	SPCC594.04c	Predicted steroid oxidoreductase
559	SPCC613.07	snoRNA biogenesis
195	SPCC757.07c	Catalase
443	SPCC794.04c	Sugar transporter
491	SPCC830.08c	ER membrane protein
917	SPCC830.08c	ER membrane protein
1083	SPCC830.08c	Golgi membrane protein
486	SPCP1E11.07c	Component of the Cdc5p-associated complex, possibly involved in pre-mRNA splicing
11 (group 1)	spi1	Ran GTPase
37	spi1	Ran GTPase
312	spt16	FACT complex component
973	ssl3	Cohesin loading factor
30 (group 1)	stt3	Oligosaacharyltransferase
67	tas3	Protein required for heterochromatin assembly and silencing at centromeric repeats
856	tea3	Cell tip protein required for initiation of bipolar growth and proper septum placement
580	tif225	Putative translation initiation factor
35	tip1	CLIP170 family involved in organisation of cytoskeleton
612	tip1	CLIP170 family involved in organisation of cytoskeleton
790	tip1	CLIP170 family involved in organisation of cytoskeleton
331	tor1	Target of rapamycin, member of the phosphatidylinositol kinase-related kinase protein family
175	tpi1	Triosephosphate
375	ubi1	Ribosomal-ubiquitin fusion protein
96	ubi4	Ubiquitin family protein required for meiosis
868	ubl1	Ubiquitin-like protein required for the activation of SCF ubiquitin-ligase

1055	ubp25	Ubiquitin carboxyl-terminal hydrolase
79	ufe1	SNARE protein
426	uvi15	Protein essential for stationary phase survival
313	vip1	RNA-binding protein
1061	vip2	RNA-binding protein
217	vip3	RNA-binding protein
281	vip4	RNA-binding protein
1069	vps45	Predicted vacuolar sorting protein
253	wos2	p23 family, interacts with cdc2 in M-G1 transition
641	wtf23	Unknown function
819	zip1	Transcription factor

Table 6 Results of tandem affinity purification

Sample	acc Num	Mass	Peptides	Score	Protein Description
Mto1(3474)	SPCC1827.03c	56752	2	98	|||acetyl-CoA ligase |Schizosaccharomyces pombe|chr 3|||Manual
Mto1(3474)	SPAC24C9.06c	85482	2	93	|||aconitate hydratase|Schizosaccharomyces pombe|chr 1|||Manual
Mto1(3524)	SPCC1281.06c	54632	2	55	|||acyl-coA desaturase |Schizosaccharomyces pombe|chr 3|||Manual
Mto1(3474)	SPBC8D2.18c	47866	7	328	|||adenosylhomocysteinase |Schizosaccharomyces pombe|chr 2|||Manual
Mto1(3524)	SPBC8D2.18c	47866	6	271	|||adenosylhomocysteinase |Schizosaccharomyces pombe|chr 2|||Manual
Mto1(3474)	SPAC9E9.09c	55475	9	415	|||aldehyde dehydrogenase|Schizosaccharomyces pombe|chr 1|||Manual
Mto1(3524)	SPAC9E9.09c	55475	7	307	|||aldehyde dehydrogenase|Schizosaccharomyces pombe|chr 1|||Manual
Mto1(3474)	SPAC977.14c	40346	3	129	|||aldo/keto reductase, unknown biological role|Schizosaccharomyces pombe|chr 1|||Manual
Mto1(3524)	SPAC977.14c	40346	5	167	|||aldo/keto reductase, unknown biological role|Schizosaccharomyces pombe|chr 1|||Manual
Mto1(3524)	SPACUNK4.16c	107549	3	127	|||alpha,alpha-trehalose-phosphate synthase |Schizosaccharomyces pombe|chr 1|||Manual
Mto1(3474)	SPCC1827.06c	38925	2	70	|||aspartate semialdehyde dehydrogenase|Schizosaccharomyces pombe|chr 3|||Manual
Mto1(3524)	SPCC1827.06c	38925	3	126	|||aspartate semialdehyde dehydrogenase|Schizosaccharomyces pombe|chr 3|||Manual
Mto1(3474)	SPCC1223.07c	66914	3	119	|||aspartate-tRNA ligase |Schizosaccharomyces pombe|chr 3|||Manual
Mto1(3524)	SPCC1223.07c	66914	2	65	|||aspartate-tRNA ligase |Schizosaccharomyces pombe|chr 3|||Manual
Mto1(3474)	SPBC1703.07	67845	2	125	|||ATP citrate synthase subunit 1 |Schizosaccharomyces pombe|chr 2|||Manual
Mto1(3524)	SPBC1703.07	67845	2	101	|||ATP citrate synthase subunit 1 |Schizosaccharomyces pombe|chr 2|||Manual
Mto1(3474)	SPAC22A12.16	54137	2	121	|||ATP-citrate synthase subunit 2 |Schizosaccharomyces pombe|chr 1|||Manual
Mto1(3524)	SPBC1711.08	37568	2	61	|||chaperone activator Aha1 |Schizosaccharomyces pombe|chr 2|||Manual
Mto1(3524)	SPCC970.03	33759	2	61	|||cytochrome b5 reductase |Schizosaccharomyces pombe|chr 3|||Manual
Mto1(3474)	SPBC24C6.04	60466	3	200	|||delta-1-pyrroline-5-carboxylate dehydrogenase|Schizosaccharomyces pombe|chr 2|||Manual
Mto1(3524)	SPBC24C6.04	60466	3	170	|||delta-1-pyrroline-5-carboxylate dehydrogenase|Schizosaccharomyces pombe|chr 2|||Manual
Mto1(3474)	SPCC794.07	52199	13	782	|||dihydrolipoamide S-acetyltransferase E2 |Schizosaccharomyces pombe|chr 3|||Manual
Mto1(3524)	SPCC794.07	52199	12	647	|||dihydrolipoamide S-acetyltransferase E2 |Schizosaccharomyces pombe|chr 3|||Manual
Mto1(3474)	SPBC776.15c	49161	3	95	|||dihydrolipoamide S-succinyltransferase, e2 component of oxoglutarate dehydrogenase complex |Schi
Mto1(3524)	SPBC776.15c	49161	3	110	|||dihydrolipoamide S-succinyltransferase, e2 component of oxoglutarate dehydrogenase complex |Schi
Mto1(3524)	SPBC1734.11	45420	3	108	|||DNAJ domain protein Mas5 |Schizosaccharomyces pombe|chr 2|||Manual
Mto1(3474)	SPAC6F12.13c	39833	2	72	|||farnesyl pyrophosphate synthetase|Schizosaccharomyces pombe|chr 1|||Manual
Mto1(3474)	SPAC17A5.15c	80984	3	137	|||glutamate-tRNA ligase |Schizosaccharomyces pombe|chr 1|||Manual
Mto1(3524)	SPAC17A5.15c	80984	2	76	|||glutamate-tRNA ligase |Schizosaccharomyces pombe|chr 1|||Manual
Mto1(3474)	SPAC24C9.12c	52113	9	402	|||glycine hydroxymethyltransferase |Schizosaccharomyces pombe|chr 1|||Manual
Mto1(3524)	SPAC24C9.12c	52113	2	122	|||glycine hydroxymethyltransferase |Schizosaccharomyces pombe|chr 1|||Manual
Mto1(3524)	SPAC1B2.03c	38768	2	82	|||GNS1/SUR4 family protein|Schizosaccharomyces pombe|chr 1|||Manual
Mto1(3524)	SPBC16E9.15	8297	2	105	|||heat shock factor binding protein |Schizosaccharomyces pombe|chr 2|||Manual
Mto1(3474)	SPBC16D10.08c	100617	5	201	|||heat shock protein Hsp104 |Schizosaccharomyces pombe|chr 2|||Manual
Mto1(3524)	SPBC16D10.08c	100617	6	284	|||heat shock protein Hsp104 |Schizosaccharomyces pombe|chr 2|||Manual
Mto1(3474)	SPAC57A7.12	61419	2	88	|||heat shock protein Pdr13 |Schizosaccharomyces pombe|chr 1|||Manual
Mto1(3474)	SPBC1703.13c	34221	2	93	|||inorganic phosphate transporter |Schizosaccharomyces pombe|chr 2|||Manual
Mto1(3524)	SPBC1703.13c	34221	2	107	|||inorganic phosphate transporter |Schizosaccharomyces pombe|chr 2|||Manual
Mto1(3524)	SPAC23C11.05	32675	2	105	|||inorganic pyrophosphatase |Schizosaccharomyces pombe|chr 1|||Manual
Mto1(3474)	SPBC8D2.06	123408	2	71	|||isoleucine-tRNA ligase |Schizosaccharomyces pombe|chr 2|||Manual
Mto1(3474)	SPAC26F1.13c	127511	2	94	|||leucine-tRNA ligase |Schizosaccharomyces pombe|chr 1|||Manual

Mto1(3524)	SPBC17A3.04c	89680	2	63	|||methionine-tRNA ligase |Schizosaccharomyces pombe|chr 2|||Manual
Mto1(3474)	SPCC622.12c	49158	2	101	|||NADP-specific glutamate dehydrogenase |Schizosaccharomyces pombe|chr 3|||Manual
Mto1(3474)	SPBC21C3.08c	48673	3	181	|||ornithine aminotransferase|Schizosaccharomyces pombe|chr 2|||Manual
Mto1(3524)	SPBC21C3.08c	48673	2	102	|||ornithine aminotransferase|Schizosaccharomyces pombe|chr 2|||Manual
Mto1(3474)	SPBC660.16	54216	9	327	|||phosphogluconate dehydrogenase, decarboxylating |Schizosaccharomyces pombe|chr 2|||Manual
Mto1(3524)	SPBC660.16	54216	9	473	|||phosphogluconate dehydrogenase, decarboxylating |Schizosaccharomyces pombe|chr 2|||Manual
Mto1(3474)	SPAC1F12.07	42999	4	161	|||phosphoserine aminotransferase |Schizosaccharomyces pombe|chr 1|||Manual
Mto1(3524)	SPAC1F12.07	42999	2	74	|||phosphoserine aminotransferase |Schizosaccharomyces pombe|chr 1|||Manual
Mto1(3524)	SPBC19C7.06	79396	2	87	|||proline-tRNA ligase |Schizosaccharomyces pombe|chr 2|||Manual
Mto1(3474)	SPAC1F5.02	55244	2	104	|||protein disulfide isomerase|Schizosaccharomyces pombe|chr 1|||Manual
Mto1(3524)	SPAC1F5.02	55244	2	80	|||protein disulfide isomerase|Schizosaccharomyces pombe|chr 1|||Manual
Mto1(3474)	SPCC736.15	39952	3	102	|||protein kinase inhibitor |Schizosaccharomyces pombe|chr 3|||Manual
Mto1(3474)	SPAC1F8.07c	65316	18	1034	|||pyruvate decarboxylase |Schizosaccharomyces pombe|chr 1|||Manual
Mto1(3524)	SPAC1F8.07c	65316	17	924	|||pyruvate decarboxylase |Schizosaccharomyces pombe|chr 1|||Manual
Mto1(516)	SPAC1F8.07c	65316	5	260	|||pyruvate decarboxylase |Schizosaccharomyces pombe|chr 1|||Manual
Mto1(3474)	SPBC16H5.08c	69284	2	101	|||ribosome biogenesis ATPase, Arb family |Schizosaccharomyces pombe|chr 2|||Manual
Mto1(3524)	SPBC16H5.08c	69284	2	104	|||ribosome biogenesis ATPase, Arb family |Schizosaccharomyces pombe|chr 2|||Manual
Mto1(3474)	SPBC3B8.03	50477	4	190	|||saccharopine dehydrogenase |Schizosaccharomyces pombe|chr 2|||Manual
Mto1(3524)	SPBC3B8.03	50477	4	153	|||saccharopine dehydrogenase |Schizosaccharomyces pombe|chr 2|||Manual
Mto1(3524)	SPAC17G6.13	49107	2	83	|||sequence orphan|Schizosaccharomyces pombe|chr 1|||Manual
Mto1(3524)	SPBC365.16	30558	2	56	|||sequence orphan|Schizosaccharomyces pombe|chr 2|||Manual
Mto1(3474)	SPCC584.01c	111797	4	205	|||sulfite reductase NADPH flavoprotein subunit |Schizosaccharomyces pombe|chr 3|||Manual
Mto1(3524)	SPCC584.01c	111797	2	80	|||sulfite reductase NADPH flavoprotein subunit |Schizosaccharomyces pombe|chr 3|||Manual
Mto1(3474)	SPBC2G5.05	75762	6	273	|||transketolase |Schizosaccharomyces pombe|chr 2|||Manual
Mto1(3524)	SPBC2G5.05	75762	9	398	|||transketolase |Schizosaccharomyces pombe|chr 2|||Manual
Mto1(3474)	SPAC29A4.02c	46014	10	453	|||translation elongation factor EF-1 gamma subunit |Schizosaccharomyces pombe|chr 1|||Manual
Mto1(3524)	SPAC29A4.02c	46014	3	135	|||translation elongation factor EF-1 gamma subunit |Schizosaccharomyces pombe|chr 1|||Manual
Mto1(3524)	SPAC25G10.08	84439	3	99	|||translation initiation factor eIF3b |Schizosaccharomyces pombe|chr 1|||Manual
Mto1(3474)	SPBC4C3.07	33515	2	78	|||translation initiation factor eIF3f|Schizosaccharomyces pombe|chr 2|||Manual
Mto1(3524)	SPBC4C3.07	33515	2	96	|||translation initiation factor eIF3f|Schizosaccharomyces pombe|chr 2|||Manual
Mto1(3474)	SPAC1006.07	44693	8	339	|||translation initiation factor eIF4A|Schizosaccharomyces pombe|chr 1|||Manual
Mto1(3524)	SPAC1006.07	44693	7	364	|||translation initiation factor eIF4A|Schizosaccharomyces pombe|chr 1|||Manual
Mto1(3474)	SPBC646.10c	55525	4	159	|||U3 snoRNP protein Nop56 |Schizosaccharomyces pombe|chr 2|||Manual
Mto1(3474)	SPCC1322.04	56565	2	125	|||UTP-glucose-1-phosphate uridylyltransferase |Schizosaccharomyces pombe|chr 3|||Manual
Mto1(3524)	SPCC1322.04	56565	5	237	|||UTP-glucose-1-phosphate uridylyltransferase |Schizosaccharomyces pombe|chr 3|||Manual
Mto1(3524)	SPCC550.14	141658	2	67	|||vigilin |Schizosaccharomyces pombe|chr 3|||Manual
Mto1(3474)	SPAC1635.01	29692	2	121	|||voltage-dependent anion-selective channel|Schizosaccharomyces pombe|chr 1|||Manual
Mto1(3474)	SPAC1751.03	45228	2	82	||SPAC31A2.01|translation initiation factor eIF3m|Schizosaccharomyces pombe|chr 1|||Manual
Mto1(3474)	SPCC364.07	51193	3	107	||SPCC4G3.01|D-3 phosphoglycerate dehydrogenase |Schizosaccharomyces pombe|chr 3|||Manual
Mto1(3474)	SPBC32H8.12c	42023	9	524	|act1|cps8|actin |Schizosaccharomyces pombe|chr 2|||Manual
Mto1(3524)	SPBC32H8.12c	42023	11	608	|act1|cps8|actin |Schizosaccharomyces pombe|chr 2|||Manual
Mto1(516)	SPBC32H8.12c	42023	5	173	|act1|cps8|actin |Schizosaccharomyces pombe|chr 2|||Manual

Mto1(3474)	SPCC13B11.01	37942	13	744	|adh1|adh|alcohol dehydrogenase Adh1|Schizosaccharomyces pombe|chr 3|||Manual
Mto1(3524)	SPCC13B11.01	37942	11	596	|adh1|adh|alcohol dehydrogenase Adh1|Schizosaccharomyces pombe|chr 3|||Manual
Mto1(516)	SPCC13B11.01	37942	6	343	|adh1|adh|alcohol dehydrogenase Adh1|Schizosaccharomyces pombe|chr 3|||Manual
Mto1(3474)	SPAC5H10.06c	46011	4	171	|adh4||alcohol dehydrogenase Adh4|Schizosaccharomyces pombe|chr 1|||Manual
Mto1(3524)	SPAC5H10.06c	46011	3	107	|adh4||alcohol dehydrogenase Adh4|Schizosaccharomyces pombe|chr 1|||Manual
Mto1(3474)	SPBC530.10c	35112	6	308	|anc1||adenine nucleotide carrier Anc1|Schizosaccharomyces pombe|chr 2|||Manual
Mto1(3524)	SPBC530.10c	35112	4	222	|anc1||adenine nucleotide carrier Anc1|Schizosaccharomyces pombe|chr 2|||Manual
Mto1(3524)	SPBC1921.05	99783	2	94	|ape1||aminopeptidase Ape1|Schizosaccharomyces pombe|chr 2|||Manual
Mto1(3474)	SPAC6F6.10c	37065	2	96	|arc2|arc34|ARP2/3 actin-organizing complex subunit Arc34|Schizosaccharomyces pombe|chr 1|||Manual
Mto1(3474)	SPBC4F6.18c	20663	3	218	|arf1||ADP-ribosylation factor Arf1|Schizosaccharomyces pombe|chr 2|||Manual
Mto1(3524)	SPBC4F6.18c	20663	4	184	|arf1||ADP-ribosylation factor Arf1|Schizosaccharomyces pombe|chr 2|||Manual
Mto1(3474)	SPBC428.05c	46568	2	55	|arg12||argininosuccinate synthase |Schizosaccharomyces pombe|chr 2|||Manual
Mto1(3524)	SPAC1834.02	175040	2	56	|aro1||pentafunctional aromatic polypeptide Aro1 |Schizosaccharomyces pombe|chr 1|||Manual
Mto1(3474)	SPAC222.12c	56898	4	209	|atp2||F1-ATPase beta subunit |Schizosaccharomyces pombe|chr 1|||Manual
Mto1(3524)	SPAC222.12c	56898	3	196	|atp2||F1-ATPase beta subunit |Schizosaccharomyces pombe|chr 1|||Manual
Mto1(3474)	SPAC22A12.15c	73239	9	456	|bip1|bip|BiP |Schizosaccharomyces pombe|chr 1|||Manual
Mto1(3524)	SPAC22A12.15c	73239	10	585	|bip1|bip|BiP |Schizosaccharomyces pombe|chr 1|||Manual
Mto1(3524)	SPCC306.09c	60605	2	71	|cap1|cap|adenylyl cyclase-associated protein Cap1|Schizosaccharomyces pombe|chr 3|||Manual
Mto1(3474)	SPBC1A4.08c	59128	3	107	|cct3||chaperonin-containing T-complex gamma subunit Cct3|Schizosaccharomyces pombe|chr 2|||Manual
Mto1(3524)	SPBC1A4.08c	59128	2	86	|cct3||chaperonin-containing T-complex gamma subunit Cct3|Schizosaccharomyces pombe|chr 2|||Manual
Mto1(3474)	SPBC337.05c	60317	3	112	|cct8||chaperonin-containing T-complex theta subunit Cct8 |Schizosaccharomyces pombe|chr 2|||Manual
Mto1(3474)	SPAC1565.08	90354	5	210	|cdc48|SPAC6F12.01|AAA family ATPase Cdc48|Schizosaccharomyces pombe|chr 1|||Manual
Mto1(3524)	SPAC1565.08	90354	6	254	|cdc48|SPAC6F12.01|AAA family ATPase Cdc48|Schizosaccharomyces pombe|chr 1|||Manual
Mto1(3474)	SPAC26A3.05	190981	6	267	|chc1||clathrin heavy chain Chc1 |Schizosaccharomyces pombe|chr 1|||Manual
Mto1(3524)	SPAC26A3.05	190981	2	88	|chc1||clathrin heavy chain Chc1 |Schizosaccharomyces pombe|chr 1|||Manual
Mto1(3474)	SPAC3C7.11c	63768	2	115	|cnx1|cal1|calnexin |Schizosaccharomyces pombe|chr 1|||Manual
Mto1(3524)	SPAC3C7.11c	63768	2	92	|cnx1|cal1|calnexin |Schizosaccharomyces pombe|chr 1|||Manual
Mto1(3474)	SPAC6B12.15	35228	7	314	|cpc2|rkp1|RACK1 homologue Cpc2|Schizosaccharomyces pombe|chr 1|||Manual
Mto1(3524)	SPAC6B12.15	35228	8	343	|cpc2|rkp1|RACK1 homologue Cpc2|Schizosaccharomyces pombe|chr 1|||Manual
Mto1(516)	SPAC6B12.15	35228	5	194	|cpc2|rkp1|RACK1 homologue Cpc2|Schizosaccharomyces pombe|chr 1|||Manual
Mto1(3474)	SPAC23C4.02	67259	6	215	|crn1||actin binding protein, coronin Crn1|Schizosaccharomyces pombe|chr 1|||Manual
Mto1(3524)	SPAC23C4.02	67259	10	432	|crn1||actin binding protein, coronin Crn1|Schizosaccharomyces pombe|chr 1|||Manual
Mto1(3474)	SPAC56E4.04c	258108	3	99	|cut6||acetyl-CoA carboxylase|Schizosaccharomyces pombe|chr 1|||Manual
Mto1(3524)	SPAC56E4.04c	258108	2	67	|cut6||acetyl-CoA carboxylase|Schizosaccharomyces pombe|chr 1|||Manual
Mto1(3474)	SPBC31A8.01c	33980	2	76	|cwl1|rtn1, SPBC651.13c|reticulon-like protein|Schizosaccharomyces pombe|chr 2|||Manual
Mto1(3524)	SPBC31A8.01c	33980	2	71	|cwl1|rtn1, SPBC651.13c|reticulon-like protein|Schizosaccharomyces pombe|chr 2|||Manual
Mto1(3524)	SPAC22A12.11	62562	3	103	|dak1||dihydroxyacetone kinase Dak1|Schizosaccharomyces pombe|chr 1|||Manual
Mto1(3474)	SPCC1223.08c	51889	2	81	|dfr1||dihydrofolate reductase Dfr1|Schizosaccharomyces pombe|chr 3|||Manual
Mto1(3524)	SPCC1223.08c	51889	4	150	|dfr1||dihydrofolate reductase Dfr1|Schizosaccharomyces pombe|chr 3|||Manual
Mto1(3474)	SPAC1002.09c	55267	2	94	|dld1|dldh|dihydrolipoamide dehydrogenase Dld1|Schizosaccharomyces pombe|chr 1|||Manual
Mto1(3524)	SPBC428.02c	42894	3	106	|eca39|SPBC582.12c|branched chain amino acid aminotransferase Eca49|Schizosaccharomyces pombe|chr 2
Mto1(3474)	SPAC23A1.10	50099	17	851	|ef1a-b||translation elongation factor EF-1 alpha Ef1a-b |Schizosaccharomyces pombe|chr 1|||Manual

Mto1(3524)	SPAC23A1.10	50099	15	797	|ef1a-b||translation elongation factor EF-1 alpha Ef1a-b |Schizosaccharomyces pombe|chr 1|||Manual
Mto1(516)	SPAC23A1.10	50099	8	336	|ef1a-b||translation elongation factor EF-1 alpha Ef1a-b |Schizosaccharomyces pombe|chr 1|||Manual
Mto1(3474)	SPCP31B10.07	93799	21	1172	|eft202||translation elongation factor 2 |Schizosaccharomyces pombe|chr 3|||Manual
Mto1(3524)	SPCP31B10.07	93799	19	928	|eft202||translation elongation factor 2 |Schizosaccharomyces pombe|chr 3|||Manual
Mto1(516)	SPCP31B10.07	93799	4	132	|eft202||translation elongation factor 2 |Schizosaccharomyces pombe|chr 3|||Manual
Mto1(3524)	SPBC25H2.05	18774	2	75	|egd1||nascent polypeptide-associated complex alpha subunit Egd1 |Schizosaccharomyces pombe|chr 2||
Mto1(3474)	SPBC1815.01	47577	16	1043	|eno101|eno1|enolase|Schizosaccharomyces pombe|chr 2|||Manual
Mto1(3524)	SPBC1815.01	47577	12	820	|eno101|eno1|enolase|Schizosaccharomyces pombe|chr 2|||Manual
Mto1(516)	SPBC1815.01	47577	5	276	|eno101|eno1|enolase|Schizosaccharomyces pombe|chr 2|||Manual
Mto1(3474)	SPBC215.09c	41314	5	207	|erg10||acetyl-CoA C-acetyltransferase Erg10 |Schizosaccharomyces pombe|chr 2|||Manual
Mto1(3524)	SPBC215.09c	41314	4	165	|erg10||acetyl-CoA C-acetyltransferase Erg10 |Schizosaccharomyces pombe|chr 2|||Manual
Mto1(3474)	SPAC926.09c	231043	10	420	|fas1||fatty acid synthase beta subunit Fas1|Schizosaccharomyces pombe|chr 1|||Manual
Mto1(3524)	SPAC926.09c	231043	13	513	|fas1||fatty acid synthase beta subunit Fas1|Schizosaccharomyces pombe|chr 1|||Manual
Mto1(3474)	SPAC4A8.11c	202899	12	462	|fas2|lsd1|fatty acid synthase alpha subunit Lsd1 |Schizosaccharomyces pombe|chr 1|||Manual
Mto1(3524)	SPAC4A8.11c	202899	12	470	|fas2|lsd1|fatty acid synthase alpha subunit Lsd1 |Schizosaccharomyces pombe|chr 1|||Manual
Mto1(3474)	SPBC19C2.07	39716	9	456	|fba1||fructose-bisphosphate aldolase Fba1|Schizosaccharomyces pombe|chr 2|||Manual
Mto1(3524)	SPBC19C2.07	39716	13	641	|fba1||fructose-bisphosphate aldolase Fba1|Schizosaccharomyces pombe|chr 2|||Manual
Mto1(516)	SPBC19C2.07	39716	2	55	|fba1||fructose-bisphosphate aldolase Fba1|Schizosaccharomyces pombe|chr 2|||Manual
Mto1(3474)	SPBC1778.06c	68860	2	85	|fim1||fimbrin|Schizosaccharomyces pombe|chr 2|||Manual
Mto1(3474)	SPCC1235.14	60794	2	114	|ght5||hexose transporter Ght5 |Schizosaccharomyces pombe|chr 3|||Manual
Mto1(3474)	SPBC215.05	42482	9	511	|gpd1||glycerol-3-phosphate dehydrogenase Gpd1|Schizosaccharomyces pombe|chr 2|||Manual
Mto1(3524)	SPBC215.05	42482	8	438	|gpd1||glycerol-3-phosphate dehydrogenase Gpd1|Schizosaccharomyces pombe|chr 2|||Manual
Mto1(3474)	SPBC354.12	35823	5	257	|gpd3||glyceraldehyde 3-phosphate dehydrogenase Gpd3|Schizosaccharomyces pombe|chr 2|||Manual
Mto1(3524)	SPBC354.12	35823	5	368	|gpd3||glyceraldehyde 3-phosphate dehydrogenase Gpd3|Schizosaccharomyces pombe|chr 2|||Manual
Mto1(3474)	SPAC26F1.06	23808	6	400	|gpm1||monomeric 2,3-bisphosphoglycerate |Schizosaccharomyces pombe|chr 1|||Manual
Mto1(3524)	SPAC26F1.06	23808	7	415	|gpm1||monomeric 2,3-bisphosphoglycerate |Schizosaccharomyces pombe|chr 1|||Manual
Mto1(516)	SPAC26F1.06	23808	3	150	|gpm1||monomeric 2,3-bisphosphoglycerate |Schizosaccharomyces pombe|chr 1|||Manual
Mto1(3474)	SPBC2F12.14c	57218	2	101	|gua1||IMP dehydrogenase Gua1 |Schizosaccharomyces pombe|chr 2|||Manual
Mto1(3524)	SPBC2F12.14c	57218	2	96	|gua1||IMP dehydrogenase Gua1 |Schizosaccharomyces pombe|chr 2|||Manual
Mto1(3524)	SPAP7G5.02c	60292	2	94	|gua2||GMP synthase [glutamine-hydrolyzing] |Schizosaccharomyces pombe|chr 1|||Manual
Mto1(3524)	SPAC4F8.14c	49721	2	90	|hcs1|hcs|3-hydroxy-3-methylglutaryl-CoA synthase|Schizosaccharomyces pombe|chr 1|||Manual
Mto1(3524)	SPAC222.11	36449	2	76	|hem13||coproporphyrinogen III oxidase |Schizosaccharomyces pombe|chr 1|||Manual
Mto1(3524)	SPBC2G5.06c	51713	3	92	|hmt2|cad1|sulfide-quinone oxidoreductase|Schizosaccharomyces pombe|chr 2|||Manual
Mto1(3474)	SPAC926.04c	80717	22	1302	|hsp90|swo1|heat shock protein Hsp90|Schizosaccharomyces pombe|chr 1|||Manual
Mto1(3524)	SPAC926.04c	80717	18	1051	|hsp90|swo1|heat shock protein Hsp90|Schizosaccharomyces pombe|chr 1|||Manual
Mto1(516)	SPAC926.04c	80717	7	259	|hsp90|swo1|heat shock protein Hsp90|Schizosaccharomyces pombe|chr 1|||Manual
Mto1(3474)	SPAC4F8.07c	51230	7	404	|hxk2||hexokinase 2 |Schizosaccharomyces pombe|chr 1|||Manual
Mto1(3524)	SPAC4F8.07c	51230	7	401	|hxk2||hexokinase 2 |Schizosaccharomyces pombe|chr 1|||Manual
Mto1(3474)	SPBP35G2.07	73375	4	223	|ilv1||acetolactate synthase catalytic subunit|Schizosaccharomyces pombe|chr 2|||Manual
Mto1(3474)	SPBC56F2.12	45274	6	380	|ilv5||acetohydroxyacid reductoisomerase|Schizosaccharomyces pombe|chr 2|||Manual
Mto1(3524)	SPBC56F2.12	45274	6	241	|ilv5||acetohydroxyacid reductoisomerase|Schizosaccharomyces pombe|chr 2|||Manual
Mto1(516)	SPBC56F2.12	45274	3	84	|ilv5||acetohydroxyacid reductoisomerase|Schizosaccharomyces pombe|chr 2|||Manual

Mto1(3524)	SPBC1A4.02c	40107	2	93	|leu1|SPBC1E8.07c|3-isopropylmalate dehydrogenase Leu1|Schizosaccharomyces pombe|chr 2|||Manual
Mto1(3474)	SPAC9E9.03	83415	4	172	|leu2||3-isopropylmalate dehydratase Leu2 |Schizosaccharomyces pombe|chr 1|||Manual
Mto1(3524)	SPAC9E9.03	83415	5	207	|leu2||3-isopropylmalate dehydratase Leu2 |Schizosaccharomyces pombe|chr 1|||Manual
Mto1(3474)	SPBC3E7.16c	64515	3	145	|leu3|SPBC4F6.03c|2-isopropylmalate synthase|Schizosaccharomyces pombe|chr 2|||Manual
Mto1(3524)	SPBC3E7.16c	64515	2	108	|leu3|SPBC4F6.03c|2-isopropylmalate synthase|Schizosaccharomyces pombe|chr 2|||Manual
Mto1(3524)	SPAP7G5.04c	157253	2	69	|lys1||aminoadipate-semialdehyde dehydrogenase |Schizosaccharomyces pombe|chr 1|||Manual
Mto1(3474)	SPAC227.18	41823	2	81	|lys3|SPAC2F7.01|saccharopine dehydrogenase [NAD+, L-lysine forming] |Schizosaccharomyces pombe|chr
Mto1(3474)	SPBC1105.02c	46777	6	248	|lys4||homocitrate synthase |Schizosaccharomyces pombe|chr 2|||Manual
Mto1(3474)	SPCC794.12c	63066	9	384	|mae2||malic enzyme|Schizosaccharomyces pombe|chr 3|||Manual
Mto1(3524)	SPCC794.12c	63066	6	273	|mae2||malic enzyme|Schizosaccharomyces pombe|chr 3|||Manual
Mto1(516)	SPCC794.12c	63066	2	74	|mae2||malic enzyme|Schizosaccharomyces pombe|chr 3|||Manual
Mto1(3524)	SPBC582.06c	38365	4	142	|mcp6|hrs1|meiosis specific coiled-coil protein Mcp6|Schizosaccharomyces pombe|chr 2|||Manual
Mto1(3474)	SPAC12G12.04	62414	12	512	|mcp60|hsp60|mitochondrial heat shock protein Hsp60|Schizosaccharomyces pombe|chr 1|||Manual
Mto1(3524)	SPAC12G12.04	62414	7	319	|mcp60|hsp60|mitochondrial heat shock protein Hsp60|Schizosaccharomyces pombe|chr 1|||Manual
Mto1(3474)	SPAC9.09	85685	7	346	|met26||homocysteine methyltransferase|Schizosaccharomyces pombe|chr 1|||Manual
Mto1(3524)	SPAC9.09	85685	7	332	|met26||homocysteine methyltransferase|Schizosaccharomyces pombe|chr 1|||Manual
Mto1(516)	SPAC9.09	85685	2	65	|met26||homocysteine methyltransferase|Schizosaccharomyces pombe|chr 1|||Manual
Mto1(3474)	SPBC1D7.04	21835	3	154	|mlo3||RNA annealing factor Mlo3|Schizosaccharomyces pombe|chr 2|||Manual
Mto1(3524)	SPBC1D7.04	21835	3	162	|mlo3||RNA annealing factor Mlo3|Schizosaccharomyces pombe|chr 2|||Manual
Mto1(3474)	SPCC1906.01	39922	4	183	|mpg1||mannose-1-phosphate guanyltransferase Mpg1|Schizosaccharomyces pombe|chr 3|||Manual
Mto1(3524)	SPCC1906.01	39922	4	183	|mpg1||mannose-1-phosphate guanyltransferase Mpg1|Schizosaccharomyces pombe|chr 3|||Manual
Mto1(516)	SPCC1906.01	39922	4	141	|mpg1||mannose-1-phosphate guanyltransferase Mpg1|Schizosaccharomyces pombe|chr 3|||Manual
Mto1(3474)	SPCC417.07c	128676	103	6090	|mto1|mbo1, mod20|MT organizer Mto1|Schizosaccharomyces pombe|chr 3|||Manual
Mto1(3524)	SPCC417.07c	128676	107	6407	|mto1|mbo1, mod20|MT organizer Mto1|Schizosaccharomyces pombe|chr 3|||Manual
Mto1(3474)	SPBC902.06	44104	13	765	|mto2||MT organizer Mto2|Schizosaccharomyces pombe|chr 2|||Manual
Mto1(3524)	SPBC902.06	44104	13	860	|mto2||MT organizer Mto2|Schizosaccharomyces pombe|chr 2|||Manual
Mto1(3474)	SPBC26H8.07c	49668	3	91	|nda3|ben1, alp12|tubulin beta |Schizosaccharomyces pombe|chr 2|||Manual
Mto1(3524)	SPBC26H8.07c	49668	2	99	|nda3|ben1, alp12|tubulin beta |Schizosaccharomyces pombe|chr 2|||Manual
Mto1(3524)	SPAC3C7.14c	21885	2	124	|obr1|uhp1|ubiquitinated histone-like protein Uhp1|Schizosaccharomyces pombe|chr 1|||Manual
Mto1(3474)	SPAC57A7.04c	71753	2	76	|pabp||mRNA export shuttling protein |Schizosaccharomyces pombe|chr 1|||Manual
Mto1(3524)	SPAC57A7.04c	71753	3	124	|pabp||mRNA export shuttling protein |Schizosaccharomyces pombe|chr 1|||Manual
Mto1(3474)	SPAC26F1.03	45451	5	236	|pda1||pyruvate dehydrogenase e1 component alpha subunit Pda1|Schizosaccharomyces pombe|chr 1|||Man
Mto1(3524)	SPAC26F1.03	45451	5	189	|pda1||pyruvate dehydrogenase e1 component alpha subunit Pda1|Schizosaccharomyces pombe|chr 1|||Man
Mto1(3474)	SPBC30D10.13c	39769	4	214	|pdb1||pyruvate dehydrogenase e1 component beta subunit Pdb1|Schizosaccharomyces pombe|chr 2|||Manu
Mto1(3524)	SPBC30D10.13c	39769	6	280	|pdb1||pyruvate dehydrogenase e1 component beta subunit Pdb1|Schizosaccharomyces pombe|chr 2|||Manu
Mto1(3474)	SPBC16H5.02	103460	16	880	|pfk1||6-phosphofructokinase |Schizosaccharomyces pombe|chr 2|||Manual
Mto1(3524)	SPBC16H5.02	103460	19	962	|pfk1||6-phosphofructokinase |Schizosaccharomyces pombe|chr 2|||Manual
Mto1(516)	SPBC16H5.02	103460	4	154	|pfk1||6-phosphofructokinase |Schizosaccharomyces pombe|chr 2|||Manual
Mto1(3474)	SPBC1604.05	61017	2	123	|pgi1||glucose-6-phosphate isomerase |Schizosaccharomyces pombe|chr 2|||Manual
Mto1(3524)	SPBC1604.05	61017	3	170	|pgi1||glucose-6-phosphate isomerase |Schizosaccharomyces pombe|chr 2|||Manual
Mto1(3474)	SPBC14F5.04c	44278	19	941	|pgk1||phosphoglycerate kinase|Schizosaccharomyces pombe|chr 2|||Manual
Mto1(3524)	SPBC14F5.04c	44278	21	979	|pgk1||phosphoglycerate kinase|Schizosaccharomyces pombe|chr 2|||Manual

Mto1(516)	SPBC14F5.04c	44278	6	243	|pgk1||phosphoglycerate kinase|Schizosaccharomyces pombe|chr 2|||Manual
Mto1(3474)	SPAC1071.10c	100391	19	1192	|pma1||P-type proton ATPase Pma1 |Schizosaccharomyces pombe|chr 1|||Manual
Mto1(3524)	SPAC1071.10c	100391	13	799	|pma1||P-type proton ATPase Pma1 |Schizosaccharomyces pombe|chr 1|||Manual
Mto1(516)	SPAC1071.10c	100391	5	179	|pma1||P-type proton ATPase Pma1 |Schizosaccharomyces pombe|chr 1|||Manual
Mto1(3474)	SPBC28F2.03	17562	3	107	|ppi1|cyp2|cyclophilin family peptidyl-prolyl cis-trans isomerase Cyp2|Schizosaccharomyces pombe|ch
Mto1(3474)	SPAC110.04c	80554	11	494	|pss1|ssp1, SPAP14E8.01c|heast shock protein Pss1|Schizosaccharomyces pombe|chr 1|||Manual
Mto1(3524)	SPAC110.04c	80554	12	536	|pss1|ssp1, SPAP14E8.01c|heast shock protein Pss1|Schizosaccharomyces pombe|chr 1|||Manual
Mto1(3474)	SPAC4H3.10c	56050	19	1073	|pyk1||pyruvate kinase |Schizosaccharomyces pombe|chr 1|||Manual
Mto1(3524)	SPAC4H3.10c	56050	27	1357	|pyk1||pyruvate kinase |Schizosaccharomyces pombe|chr 1|||Manual
Mto1(516)	SPAC4H3.10c	56050	8	333	|pyk1||pyruvate kinase |Schizosaccharomyces pombe|chr 1|||Manual
Mto1(3474)	SPBC17G9.11c	131519	5	194	|pyr1||pyruvate carboxylase|Schizosaccharomyces pombe|chr 2|||Manual
Mto1(3524)	SPBC17G9.11c	131519	2	84	|pyr1||pyruvate carboxylase|Schizosaccharomyces pombe|chr 2|||Manual
Mto1(3474)	SPAC8E11.02c	30178	4	215	|rad24||14-3-3 protein Rad24|Schizosaccharomyces pombe|chr 1|||Manual
Mto1(3524)	SPAC8E11.02c	30178	2	132	|rad24||14-3-3 protein Rad24|Schizosaccharomyces pombe|chr 1|||Manual
Mto1(3474)	SPAC17A2.13c	30578	2	72	|rad25||14-3-3 protein Rad25|Schizosaccharomyces pombe|chr 1|||Manual
Mto1(3524)	SPAC17A2.13c	30578	2	87	|rad25||14-3-3 protein Rad25|Schizosaccharomyces pombe|chr 1|||Manual
Mto1(3524)	SPBC18E5.04	25756	3	160	|rpl1001|rpl10-1, rpl10|60S ribosomal protein L10|Schizosaccharomyces pombe|chr 2|||Manual
Mto1(3474)	SPAP7G5.05	25742	4	211	|rpl1002|rpl10-2, rpl10|60S ribosomal protein L10|Schizosaccharomyces pombe|chr 1|||Manual
Mto1(3524)	SPCC1183.08c	24016	3	113	|rpl101|rpl1-1, rpl10a-1|60S ribosomal protein L10a|Schizosaccharomyces pombe|chr 3|||Manual
Mto1(3474)	SPBC17G9.10	19936	2	89	|rpl1102|rpl11-2|60S ribosomal protein L11|Schizosaccharomyces pombe|chr 2|||Manual
Mto1(3524)	SPBC17G9.10	19936	3	235	|rpl1102|rpl11-2|60S ribosomal protein L11|Schizosaccharomyces pombe|chr 2|||Manual
Mto1(3474)	SPCC16C4.13c	17713	2	74	|rpl1201|rpl12-1, rpl12.1|60S ribosomal protein L12.1/L12A|Schizosaccharomyces pombe|chr 3|||Manual
Mto1(3524)	SPAC664.05	23515	4	191	|rpl13||60S ribosomal protein L13|Schizosaccharomyces pombe|chr 1|||Manual
Mto1(3474)	SPAC1805.13	15314	2	68	|rpl14||60S ribosomal protein L14|Schizosaccharomyces pombe|chr 1|||Manual
Mto1(3524)	SPAC1805.13	15314	3	107	|rpl14||60S ribosomal protein L14|Schizosaccharomyces pombe|chr 1|||Manual
Mto1(3474)	SPCC576.11	23906	4	159	|rpl15||60S ribosomal protein L15|Schizosaccharomyces pombe|chr 3|||Manual
Mto1(3524)	SPCC576.11	23906	3	180	|rpl15||60S ribosomal protein L15|Schizosaccharomyces pombe|chr 3|||Manual
Mto1(3524)	SPAC23A1.11	22162	4	121	|rpl1602|rpl16-2|60S ribosomal protein L13/L16|Schizosaccharomyces pombe|chr 1|||Manual
Mto1(3474)	SPBC2F12.04	20858	2	79	|rpl1701|rpl17, rpl17-1|60S ribosomal protein L17|Schizosaccharomyces pombe|chr 2|||Manual
Mto1(3524)	SPBC2F12.04	20858	2	76	|rpl1701|rpl17, rpl17-1|60S ribosomal protein L17|Schizosaccharomyces pombe|chr 2|||Manual
Mto1(3524)	SPCC364.03	20871	5	195	|rpl1702|rpl17-2, rpl17|60S ribosomal protein L17|Schizosaccharomyces pombe|chr 3|||Manual
Mto1(3474)	SPBC11C11.07	21177	2	99	|rpl1801|rpl18-1, rpl18|60S ribosomal protein L18|Schizosaccharomyces pombe|chr 2|||Manual
Mto1(3524)	SPBC11C11.07	21177	2	125	|rpl1801|rpl18-1, rpl18|60S ribosomal protein L18|Schizosaccharomyces pombe|chr 2|||Manual
Mto1(3524)	SPBC56F2.02	22767	3	124	|rpl1901|rpl19-1|60S ribosomal protein L19|Schizosaccharomyces pombe|chr 2|||Manual
Mto1(3474)	SPAC3A12.10	20586	4	157	|rpl2001|rpl20-1, rpl20, yl17b, rpl18a-2|60S ribosomal protein L20a|Schizosaccharomyces pombe|chr 1
Mto1(3524)	SPAC3A12.10	20586	4	161	|rpl2001|rpl20-1, rpl20, yl17b, rpl18a-2|60S ribosomal protein L20a|Schizosaccharomyces pombe|chr 1
Mto1(3474)	SPBC365.03c	18426	2	122	|rpl2101|rpl21, rpl21-1|60S ribosomal protein L21|Schizosaccharomyces pombe|chr 2|||Manual
Mto1(3524)	SPAC959.08	18399	3	147	|rpl2102|rpl21-2, rpl21|60S ribosomal protein L21|Schizosaccharomyces pombe|chr 1|||Manual
Mto1(3474)	SPAC11E3.15	13312	3	205	|rpl22|SPAP8A3.01|60S ribosomal protein L22|Schizosaccharomyces pombe|chr 1|||Manual
Mto1(3474)	SPAC3G9.03	15044	4	273	|rpl2301|rpl23-1|60S ribosomal protein L23|Schizosaccharomyces pombe|chr 1|||Manual
Mto1(3524)	SPAC3G9.03	15044	4	237	|rpl2301|rpl23-1|60S ribosomal protein L23|Schizosaccharomyces pombe|chr 1|||Manual
Mto1(3524)	SPBC106.18	15826	5	236	|rpl2501|rpl25a|60S ribosomal protein L25|Schizosaccharomyces pombe|chr 2|||Manual

Mto1(3474)	SPBC29B5.03c	14332	3	111	|rpl26||60S ribosomal protein L26|Schizosaccharomyces pombe|chr 2|||Manual
Mto1(3524)	SPBC29B5.03c	14332	4	141	|rpl26||60S ribosomal protein L26|Schizosaccharomyces pombe|chr 2|||Manual
Mto1(3474)	SPCC74.05	15295	4	132	|rpl2702|rpl27-2|60S ribosomal protein L27|Schizosaccharomyces pombe|chr 3|||Manual
Mto1(3524)	SPCC74.05	15295	2	100	|rpl2702|rpl27-2|60S ribosomal protein L27|Schizosaccharomyces pombe|chr 3|||Manual
Mto1(3474)	SPCC5E4.07	16643	2	58	|rpl2802|rpl28-2|60S ribosomal protein L27a.2/L28A|Schizosaccharomyces pombe|chr 3|||Manual
Mto1(3524)	SPAC9G1.03c	11698	2	71	|rpl3001|rpl30-1, rpl30|60S ribosomal protein L30|Schizosaccharomyces pombe|chr 1|||Manual
Mto1(3524)	SPAPB8E5.06c	43960	6	277	|rpl302|rpl3-2, rpl3-b|60S ribosomal protein L3|Schizosaccharomyces pombe|chr 1|||Manual
Mto1(3524)	SPAC890.08	13253	3	118	|rpl31||60S ribosomal protein L31|Schizosaccharomyces pombe|chr 1|||Manual
Mto1(3524)	SPAC30D11.12	8391	2	70	|rpl3802|rpl38-2, rps38|60S ribosomal protein L38|Schizosaccharomyces pombe|chr 1|||Manual
Mto1(3524)	SPBC1711.06	39943	6	293	|rpl401|rpl4-1, rpl4|60S ribosomal protein L2|Schizosaccharomyces pombe|chr 2|||Manual
Mto1(3474)	SPBP8B7.03c	39800	4	228	|rpl402|rpl4-2, rpl4|60S ribosomal protein L2|Schizosaccharomyces pombe|chr 2|||Manual
Mto1(3524)	SPAC1687.06c	14803	5	194	|rpl44|rpl28|60S ribosomal protein L28/L44|Schizosaccharomyces pombe|chr 1|||Manual
Mto1(3524)	SPAC3H5.12c	33496	3	109	|rpl501|rpl5-1, rpl5|60S ribosomal protein L5|Schizosaccharomyces pombe|chr 1|||Manual
Mto1(3474)	SPCC622.18	21292	4	187	|rpl6||60S ribosomal protein L6|Schizosaccharomyces pombe|chr 3|||Manual
Mto1(3524)	SPCC622.18	21292	3	105	|rpl6||60S ribosomal protein L6|Schizosaccharomyces pombe|chr 3|||Manual
Mto1(3474)	SPBC18H10.12c	28713	3	155	|rpl701||60S ribosomal protein L7|Schizosaccharomyces pombe|chr 2|||Manual
Mto1(3524)	SPBC18H10.12c	28713	4	223	|rpl701||60S ribosomal protein L7|Schizosaccharomyces pombe|chr 2|||Manual
Mto1(3474)	SPBC29A3.04	28646	3	213	|rpl8||60S ribosomal protein L7a |Schizosaccharomyces pombe|chr 2|||Manual
Mto1(3524)	SPBC29A3.04	28646	5	224	|rpl8||60S ribosomal protein L7a |Schizosaccharomyces pombe|chr 2|||Manual
Mto1(3474)	SPAC1F7.13c	27197	2	59	|rpl801|rpl8-1, rpl18, rpk5a, rpl2-1, SPAC21E11.02c|60S ribosomal protein L8|Schizosaccharomyces po
Mto1(3524)	SPAC1F7.13c	27197	2	86	|rpl801|rpl8-1, rpl18, rpk5a, rpl2-1, SPAC21E11.02c|60S ribosomal protein L8|Schizosaccharomyces po
Mto1(3474)	SPAC4G9.16c	21670	2	102	|rpl901|rpl9-1|60S ribosomal protein L9|Schizosaccharomyces pombe|chr 1|||Manual
Mto1(3524)	SPAC4G9.16c	21670	2	69	|rpl901|rpl9-1|60S ribosomal protein L9|Schizosaccharomyces pombe|chr 1|||Manual
Mto1(3524)	SPCC613.06	21540	5	256	|rpl902|rpl9-2|60S ribosomal protein L9|Schizosaccharomyces pombe|chr 3|||Manual
Mto1(3474)	SPCC18.14c	33544	5	231	|rpp0||60S acidic ribosomal protein Rpp0 |Schizosaccharomyces pombe|chr 3|||Manual
Mto1(3524)	SPCC18.14c	33544	4	190	|rpp0||60S acidic ribosomal protein Rpp0 |Schizosaccharomyces pombe|chr 3|||Manual
Mto1(3474)	SPBC685.06	31911	4	215	|rps001|rps0-1, rpsa-1, rps0|40S ribosomal protein S0A |Schizosaccharomyces pombe|chr 2|||Manual
Mto1(3524)	SPBC685.06	31911	4	207	|rps001|rps0-1, rpsa-1, rps0|40S ribosomal protein S0A |Schizosaccharomyces pombe|chr 2|||Manual
Mto1(3474)	SPAPJ698.02c	31515	3	147	|rps002|rpsa-2, rps0-2, rps0|40S ribosomal protein S0B|Schizosaccharomyces pombe|chr 1|||Manual
Mto1(3524)	SPAPJ698.02c	31515	2	85	|rps002|rpsa-2, rps0-2, rps0|40S ribosomal protein S0B|Schizosaccharomyces pombe|chr 1|||Manual
Mto1(3474)	SPBP22H7.08	16490	2	74	|rps1002|rps10-2, rps10B|40S ribosomal protein S10|Schizosaccharomyces pombe|chr 2|||Manual
Mto1(3524)	SPBP22H7.08	16490	4	134	|rps1002|rps10-2, rps10B|40S ribosomal protein S10|Schizosaccharomyces pombe|chr 2|||Manual
Mto1(3524)	SPAC13G6.02c	28641	3	113	|rps101|rps1-1, rps3a-1|40S ribosomal protein S3a|Schizosaccharomyces pombe|chr 1|||Manual
Mto1(3474)	SPAC22H12.04c	28675	4	193	|rps102|rps1-2, rps3a-2|40S ribosomal protein S3a|Schizosaccharomyces pombe|chr 1|||Manual
Mto1(3524)	SPAC22H12.04c	28675	6	256	|rps102|rps1-2, rps3a-2|40S ribosomal protein S3a|Schizosaccharomyces pombe|chr 1|||Manual
Mto1(3474)	SPAC31G5.03	17603	3	109	|rps1101|rps11-1|40S ribosomal protein S11|Schizosaccharomyces pombe|chr 1|||Manual
Mto1(3524)	SPAC31G5.03	17603	7	328	|rps1101|rps11-1|40S ribosomal protein S11|Schizosaccharomyces pombe|chr 1|||Manual
Mto1(3474)	SPCC962.04	16005	2	120	|rps1201|rps12-1, rps12|40S ribosomal protein S12|Schizosaccharomyces pombe|chr 3|||Manual
Mto1(3524)	SPCC962.04	16005	2	138	|rps1201|rps12-1, rps12|40S ribosomal protein S12|Schizosaccharomyces pombe|chr 3|||Manual
Mto1(3474)	SPAC6F6.07c	16999	4	189	|rps13||40S ribosomal protein S13|Schizosaccharomyces pombe|chr 1|||Manual
Mto1(3524)	SPAC6F6.07c	16999	4	242	|rps13||40S ribosomal protein S13|Schizosaccharomyces pombe|chr 1|||Manual
Mto1(3524)	SPAC3H5.05c	14747	4	240	|rps1401|rps14-1, rps14|40S ribosomal protein S14|Schizosaccharomyces pombe|chr 1|||Manual

Mto1(3474)	SPAC1071.07c	17623	2	89	|rps1502|rps15-2, rps15|40S ribosomal protein S15|Schizosaccharomyces pombe|chr 1|||Manual
Mto1(3524)	SPAC1071.07c	17623	2	89	|rps1502|rps15-2, rps15|40S ribosomal protein S15|Schizosaccharomyces pombe|chr 1|||Manual
Mto1(3474)	SPBC18H10.14	15499	2	100	|rps1601|rps16-1|40S ribosomal protein S16|Schizosaccharomyces pombe|chr 2|||Manual
Mto1(3524)	SPBC18H10.14	15499	4	191	|rps1601|rps16-1|40S ribosomal protein S16|Schizosaccharomyces pombe|chr 2|||Manual
Mto1(3524)	SPBC839.05c	15504	3	147	|rps1701|rps17-1|40S ribosomal protein S17|Schizosaccharomyces pombe|chr 2|||Manual
Mto1(3474)	SPBC16D10.11c	17482	6	281	|rps1801|rps18-1|40S ribosomal protein S18|Schizosaccharomyces pombe|chr 2|||Manual
Mto1(3524)	SPBC16D10.11c	17482	7	289	|rps1801|rps18-1|40S ribosomal protein S18|Schizosaccharomyces pombe|chr 2|||Manual
Mto1(516)	SPBC16D10.11c	17482	3	107	|rps1801|rps18-1|40S ribosomal protein S18|Schizosaccharomyces pombe|chr 2|||Manual
Mto1(3474)	SPBC21C3.13	16197	2	64	|rps1901|rps19-1|40S ribosomal protein S19|Schizosaccharomyces pombe|chr 2|||Manual
Mto1(3524)	SPBC21C3.13	16197	3	136	|rps1901|rps19-1|40S ribosomal protein S19|Schizosaccharomyces pombe|chr 2|||Manual
Mto1(3474)	SPCC576.08c	27791	4	177	|rps2||40S ribosomal protein S2|Schizosaccharomyces pombe|chr 3|||Manual
Mto1(3524)	SPCC576.08c	27791	7	368	|rps2||40S ribosomal protein S2|Schizosaccharomyces pombe|chr 3|||Manual
Mto1(3474)	SPAC5D6.01	14865	2	166	|rps2202|rps22-2, rps15a-2|40S ribosomal protein S15a|Schizosaccharomyces pombe|chr 1|||Manual
Mto1(3524)	SPAC5D6.01	14865	7	339	|rps2202|rps22-2, rps15a-2|40S ribosomal protein S15a|Schizosaccharomyces pombe|chr 1|||Manual
Mto1(516)	SPAC5D6.01	14865	3	100	|rps2202|rps22-2, rps15a-2|40S ribosomal protein S15a|Schizosaccharomyces pombe|chr 1|||Manual
Mto1(3474)	SPBP4H10.13	15760	2	82	|rps2302|rps23-2|40S ribosomal protein S23|Schizosaccharomyces pombe|chr 2|||Manual
Mto1(3524)	SPBP4H10.13	15760	2	58	|rps2302|rps23-2|40S ribosomal protein S23|Schizosaccharomyces pombe|chr 2|||Manual
Mto1(3474)	SPBC17G9.07	15586	2	85	|rps2402|rps24-2|40S ribosomal protein S24|Schizosaccharomyces pombe|chr 2|||Manual
Mto1(3524)	SPBC17G9.07	15586	3	123	|rps2402|rps24-2|40S ribosomal protein S24|Schizosaccharomyces pombe|chr 2|||Manual
Mto1(3474)	SPBC3D6.15	9813	2	98	|rps2501|rps25-1|40S ribosomal protein S25|Schizosaccharomyces pombe|chr 2|||Manual
Mto1(3524)	SPBC3D6.15	9813	2	97	|rps2501|rps25-1|40S ribosomal protein S25|Schizosaccharomyces pombe|chr 2|||Manual
Mto1(3524)	SPAC1805.11c	14082	3	104	|rps2602|rps26-2|40S ribosomal protein S26|Schizosaccharomyces pombe|chr 1|||Manual
Mto1(3524)	SPBC1685.10	9508	2	65	|rps27||40S ribosomal protein S27|Schizosaccharomyces pombe|chr 2|||Manual
Mto1(3474)	SPBC16G5.14c	27764	7	350	|rps3||40S ribosomal protein S3|Schizosaccharomyces pombe|chr 2|||Manual
Mto1(3524)	SPBC16G5.14c	27764	12	573	|rps3||40S ribosomal protein S3|Schizosaccharomyces pombe|chr 2|||Manual
Mto1(516)	SPBC16G5.14c	27764	2	135	|rps3||40S ribosomal protein S3|Schizosaccharomyces pombe|chr 2|||Manual
Mto1(3474)	SPBC19F8.08	29784	3	148	|rps401|rps4-1, rps4, SPBC25H2.17c|40S ribosomal protein S4|Schizosaccharomyces pombe|chr 2||Manua
Mto1(3524)	SPBC19F8.08	29784	8	324	|rps401|rps4-1, rps4, SPBC25H2.17c|40S ribosomal protein S4|Schizosaccharomyces pombe|chr 2||Manua
Mto1(3474)	SPAC8C9.08	22382	7	392	|rps5||40S ribosomal protein S5|Schizosaccharomyces pombe|chr 1|||Manual
Mto1(3524)	SPAC328.10c	22514	7	426	|rps502|rps5-2|40S ribosomal protein S5|Schizosaccharomyces pombe|chr 1|||Manual
Mto1(3474)	SPAC13G6.07c	27596	6	337	|rps601|rps6-1|40S ribosomal protein S6|Schizosaccharomyces pombe|chr 1|||Manual
Mto1(3524)	SPAPB1E7.12	27572	7	364	|rps602|rps6-2, rps6|40S ribosomal protein S6|Schizosaccharomyces pombe|chr 1|||Manual
Mto1(3474)	SPAC18G6.14c	22048	2	87	|rps7||40S ribosomal protein S7|Schizosaccharomyces pombe|chr 1|||Manual
Mto1(3524)	SPAC18G6.14c	22048	6	348	|rps7||40S ribosomal protein S7|Schizosaccharomyces pombe|chr 1|||Manual
Mto1(3524)	SPAC24H6.07	22204	2	109	|rps901|rps9-1, rps9a|40S ribosomal protein S9|Schizosaccharomyces pombe|chr 1|||Manual
Mto1(516)	SPAC24H6.07	22204	3	130	|rps901|rps9-1, rps9a|40S ribosomal protein S9|Schizosaccharomyces pombe|chr 1|||Manual
Mto1(3474)	SPBC29A3.12	22288	4	155	|rps902|rps9-2, rps9b|40S ribosomal protein S9|Schizosaccharomyces pombe|chr 2|||Manual
Mto1(3524)	SPBC29A3.12	22288	7	350	|rps902|rps9-2, rps9b|40S ribosomal protein S9|Schizosaccharomyces pombe|chr 2|||Manual
Mto1(3524)	SPBC11B10.05c	56312	4	204	|rsp1||random septum position protein Rsp1|Schizosaccharomyces pombe|chr 2|||Manual
Mto1(3474)	SPBC14F5.05c	42091	3	199	|sam1||S-adenosylmethionine synthetase |Schizosaccharomyces pombe|chr 2|||Manual
Mto1(3524)	SPBC14F5.05c	42091	2	94	|sam1||S-adenosylmethionine synthetase |Schizosaccharomyces pombe|chr 2|||Manual
Mto1(3474)	SPAC57A7.10c	101329	2	68	|sec21||coatomer gamma subunit Sec21 |Schizosaccharomyces pombe|chr 1|||Manual

Mto1(3524)	SPAC57A7.10c	101329	2	52	|sec21||coatomer gamma subunit Sec21 |Schizosaccharomyces pombe|chr 1|||Manual
Mto1(3474)	SPBC1709.05	67449	18	1287	|sks2|hsc1|heat shock protein Sks2|Schizosaccharomyces pombe|chr 2|||Manual
Mto1(3524)	SPBC1709.05	67449	23	1279	|sks2|hsc1|heat shock protein Sks2|Schizosaccharomyces pombe|chr 2|||Manual
Mto1(516)	SPBC1709.05	67449	3	158	|sks2|hsc1|heat shock protein Sks2|Schizosaccharomyces pombe|chr 2|||Manual
Mto1(3524)	SPAC29B12.04	31611	2	108	|snz1||pyridoxine biosynthesis protein|Schizosaccharomyces pombe|chr 1|||Manual
Mto1(3474)	SPBC1289.03c	24768	2	71	|spi1||Ran GTPase Spi1|Schizosaccharomyces pombe|chr 2|||Manual
Mto1(3524)	SPBC1289.03c	24768	3	100	|spi1||Ran GTPase Spi1|Schizosaccharomyces pombe|chr 2|||Manual
Mto1(3474)	SPAC13G7.02c	70385	3	173	|ssa1||heat shock protein Ssa1|Schizosaccharomyces pombe|chr 1|||Manual
Mto1(3524)	SPAC13G7.02c	70385	6	332	|ssa1||heat shock protein Ssa1|Schizosaccharomyces pombe|chr 1|||Manual
Mto1(3474)	SPCC1739.13	70475	18	996	|ssa2||heat shock protein Ssa2|Schizosaccharomyces pombe|chr 3|||Manual
Mto1(3524)	SPCC1739.13	70475	35	1814	|ssa2||heat shock protein Ssa2|Schizosaccharomyces pombe|chr 3|||Manual
Mto1(516)	SPCC1739.13	70475	9	476	|ssa2||heat shock protein Ssa2|Schizosaccharomyces pombe|chr 3|||Manual
Mto1(3474)	SPBC660.13c	68610	2	133	|ssb1|rpa1, rad11|DNA replication factor A subunit Ssb1 |Schizosaccharomyces pombe|chr 2|||Manual
Mto1(3524)	SPBC660.13c	68610	3	124	|ssb1|rpa1, rad11|DNA replication factor A subunit Ssb1 |Schizosaccharomyces pombe|chr 2|||Manual
Mto1(516)	SPBC660.13c	68610	3	167	|ssb1|rpa1, rad11|DNA replication factor A subunit Ssb1 |Schizosaccharomyces pombe|chr 2|||Manual
Mto1(516)	SPCC1753.01c	30372	2	80	|ssb2|SPCC584.06c|single-stranded DNA binding protein Ssb2|Schizosaccharomyces pombe|chr 3|||Manual
Mto1(3474)	SPAC664.11	73160	9	547	|ssc1|ssp1|Hsp70 chaperone mtHsp70|Schizosaccharomyces pombe|chr 1|||Manual
Mto1(3524)	SPAC664.11	73160	15	789	|ssc1|ssp1|Hsp70 chaperone mtHsp70|Schizosaccharomyces pombe|chr 1|||Manual
Mto1(3474)	SPBC27.08c	54777	7	294	|sua1|SPBC28F2.01c|sulfate adenylyltransferase |Schizosaccharomyces pombe|chr 2|||Manual
Mto1(3524)	SPBC27.08c	54777	5	229	|sua1|SPBC28F2.01c|sulfate adenylyltransferase |Schizosaccharomyces pombe|chr 2|||Manual
Mto1(3524)	SPBC25D12.04	45605	2	66	|suc22||ribonucleotide reductase small subunit Suc22 |Schizosaccharomyces pombe|chr 2|||Manual
Mto1(3474)	SPCC1795.11	70058	14	770	|sum3|ded1, slh3, moc2|ATP-dependent RNA helicase Sum3|Schizosaccharomyces pombe|chr 3|||Manual
Mto1(3524)	SPCC1795.11	70058	13	670	|sum3|ded1, slh3, moc2|ATP-dependent RNA helicase Sum3|Schizosaccharomyces pombe|chr 3|||Manual
Mto1(3474)	SPCC1020.06c	35330	3	107	|tal1||transaldolase |Schizosaccharomyces pombe|chr 3|||Manual
Mto1(3524)	SPCC1020.06c	35330	2	92	|tal1||transaldolase |Schizosaccharomyces pombe|chr 3|||Manual
Mto1(3524)	SPBC660.11	37849	2	76	|tcg1||single-stranded telomeric binding protein Tgc1 |Schizosaccharomyces pombe|chr 2|||Manual
Mto1(3474)	SPBC32F12.11	36018	20	1114	|tdh1|gpd1|glyceraldehyde-3-phosphate dehydrogenase Tdh1|Schizosaccharomyces pombe|chr 2|||Manual
Mto1(3524)	SPBC32F12.11	36018	19	1080	|tdh1|gpd1|glyceraldehyde-3-phosphate dehydrogenase Tdh1|Schizosaccharomyces pombe|chr 2|||Manual
Mto1(516)	SPBC32F12.11	36018	10	563	|tdh1|gpd1|glyceraldehyde-3-phosphate dehydrogenase Tdh1|Schizosaccharomyces pombe|chr 2|||Manual
Mto1(3474)	SPCC417.08	116470	18	898	|tef3||translation elongation factor eEF3|Schizosaccharomyces pombe|chr 3|||Manual
Mto1(3524)	SPCC417.08	116470	16	757	|tef3||translation elongation factor eEF3|Schizosaccharomyces pombe|chr 3|||Manual
Mto1(3474)	SPCC1450.04	23470	3	129	|tef5||translation elongation factor EF-1 beta subunit |Schizosaccharomyces pombe|chr 3|||Manual
Mto1(3524)	SPCC1450.04	23470	2	98	|tef5||translation elongation factor EF-1 beta subunit |Schizosaccharomyces pombe|chr 3|||Manual
Mto1(3474)	SPBC25H2.02	80829	3	116	|ths1||threonine-tRNA ligase Ths1 |Schizosaccharomyces pombe|chr 2|||Manual
Mto1(3524)	SPBC25H2.02	80829	2	111	|ths1||threonine-tRNA ligase Ths1 |Schizosaccharomyces pombe|chr 2|||Manual
Mto1(3524)	SPBC17G9.09	49320	2	89	|tif213||translation initiation factor eIF2 gamma subunit|Schizosaccharomyces pombe|chr 2|||Manual
Mto1(3474)	SPAC3C7.12	52860	6	324	|tip1|noc1|CLIP170 family protein Tip1|Schizosaccharomyces pombe|chr 1|||Manual
Mto1(3524)	SPAC3C7.12	52860	7	463	|tip1|noc1|CLIP170 family protein Tip1|Schizosaccharomyces pombe|chr 1|||Manual
Mto1(3474)	SPBC27B12.13	37814	2	63	|tom40|SPBC8D2.22|mitochondrial TOM complex subunit Tom40|Schizosaccharomyces pombe|chr 2|||Manual
Mto1(3474)	SPCC24B10.21	27324	5	249	|tpi1|tpi|triosephosphate isomerase|Schizosaccharomyces pombe|chr 3|||Manual
Mto1(3524)	SPCC24B10.21	27324	4	214	|tpi1|tpi|triosephosphate isomerase|Schizosaccharomyces pombe|chr 3|||Manual
Mto1(516)	SPCC24B10.21	27324	2	81	|tpi1|tpi|triosephosphate isomerase|Schizosaccharomyces pombe|chr 3|||Manual

Mto1(3474)	SPCC576.03c	21292	5	242	|tpx1||thioredoxin peroxidase Tpx1|Schizosaccharomyces pombe|chr 3|||Manual
Mto1(3524)	SPCC576.03c	21292	4	184	|tpx1||thioredoxin peroxidase Tpx1|Schizosaccharomyces pombe|chr 3|||Manual
Mto1(516)	SPCC576.03c	21292	2	53	|tpx1||thioredoxin peroxidase Tpx1|Schizosaccharomyces pombe|chr 3|||Manual
Mto1(3474)	SPAC19A8.15	76244	2	69	|trp2||tryptophan synthase|Schizosaccharomyces pombe|chr 1|||Manual
Mto1(3524)	SPAC19A8.15	76244	3	125	|trp2||tryptophan synthase|Schizosaccharomyces pombe|chr 1|||Manual
Mto1(3474)	SPBC9B6.04c	48594	2	55	|tuf1||mitochondrial translation elongation factor EF-Tu Tuf1 |Schizosaccharomyces pombe|chr 2|||Ma
Mto1(3474)	SPAC6G10.11c	17475	3	90	|ubi3||ribosomal ubiquitin fusion protein Ubi3|Schizosaccharomyces pombe|chr 1|||Manual
Mto1(3524)	SPAC6G10.11c	17475	2	77	|ubi3||ribosomal ubiquitin fusion protein Ubi3|Schizosaccharomyces pombe|chr 1|||Manual
Mto1(3474)	SPAC22G7.06c	249920	5	204	|ura1||carbamoyl-phosphate synthase |Schizosaccharomyces pombe|chr 1|||Manual
Mto1(3524)	SPAC22G7.06c	249920	3	122	|ura1||carbamoyl-phosphate synthase |Schizosaccharomyces pombe|chr 1|||Manual
Mto1(3524)	SPBC1709.02c	112045	2	123	|vas2|SPBC1734.18c|valine-tRNA ligase Vas2 |Schizosaccharomyces pombe|chr 2|||Manual
Mto1(3524)	SPBC1703.10	22973	2	88	|ypt1||GTPase Ypt1|Schizosaccharomyces pombe|chr 2|||Manual

Chapter IV – Interaction of Myp2 and Mto1

Candidate gene approach: Mto1 localisation to the equator

I next decided to take a candidate gene approach to identifying the Mto1-interacting protein responsible for localising Mto1 to the cell equator. Having shown that Mto1 localisation is dependent on the actin cytoskeleton, and having observed that Mto1 co-localises with the CAR, I hypothesised that the unknown localising factor could be a CAR component. Mto1 localises to the cell equator late in anaphase, at a point when the CAR is nearly fully formed. Mto1 could be directed to the CAR by interacting with any of the components that are part of the CAR at the time when Mto1 first appears. However, I initially focused on proteins that join the CAR at or around the same time as Mto1, based on detailed work from the Pollard laboratory describing the order and timing of CAR assembly (Wu et al., 2003). I looked to see if Mto1 would localise to the equator in strains lacking these selected CAR components (Figure 15). Deleting components that join the CAR when the ring is near completion reduces the likelihood of affecting the localisation of other CAR components by disrupting CAR assembly and thereby affecting Mto1 localisation only indirectly. Little is known about how CAR assembly is regulated and what dependencies may be present within the ordered assembly. Mto1-GFP was imaged in *acp2Δ*, *myp2Δ*, and *spn1Δ* strains. Acp2 is an actin-capping protein that stabilises actin filaments (Kovar et al., 2005), Myp2 is one of two type II myosins found in the CAR (Bezanilla et al., 1997), and Spn1 is a septin involved in cytokinesis (An et al., 2004). Mto1-GFP can be seen to form an equatorial ring in *acp2Δ*, *spn1Δ* and the

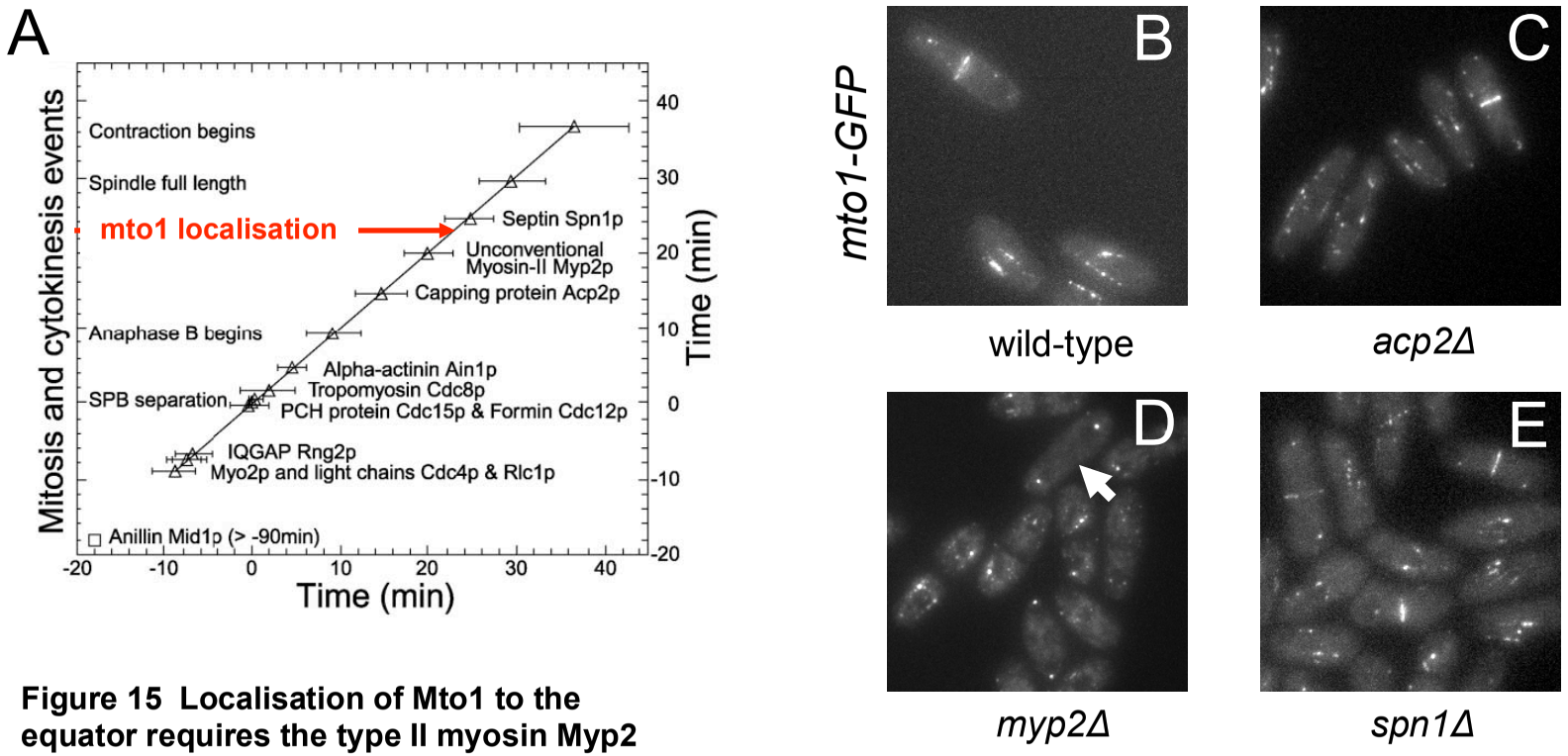

Figure 15 Localisation of Mto1 to the equator requires the type II myosin Myp2

(A) Timing of Mto1 localisation relative to the assembly of the CAR. The appearance of Mto1 at the equator relative to spindle length is plotted on a figure from Wu *et al.* 2003 showing mean time of appearance of CAR proteins at the division site. (B-E) Widefield microscopy showing Mto1-GFP localisation to the equator in (B) wild-type, (C) *acp2Δ, (D) myp2Δ, (E) spn1Δ* cells. Mto1 does not appear at the equator in the *myp2Δ* strain (arrow).

wild-type control strain, but is not found as an equatorial ring in *myp2Δ* (Figure 15, B-D). I conclude that localisation of Mto1 to the equator requires Myp2.

Candidate gene approach: yeast two-hybrid interaction

I then assayed selected CAR genes for interaction with Mto1 using the yeast two-hybrid system. *myp2* and *spn1* genes, previously tested for their roles in Mto1 localisation using gene-deletion strains, were inserted into *pACT2.2gtwy* bait plasmid (plasmid selection: leucine) and tested for interaction with *LexA-mto1(769-1115)* and *LexA-mto1(769-1051)* (plasmid selection: tryptophan). *acp2* was not tested as the gene contains introns and therefore cannot be expressed in *S. cerevisiae*, and the *acp2* cDNA was not available. Two additional CAR genes were also tested. *cdc4*, a myosin light chain essential for viability known to associate with Myp2 (Naqvi et al., 2000) and *rng3*, a protein that promotes myosin function during cytokinesis and localises to the CAR during anaphase B (Lord and Pollard, 2004; Lord et al., 2008). *cdc4* and *rng3* are required for viability and so their role in Mto1 localisation could not be tested in gene-deletion strains. Although none of these proteins were identified as Mto1-interactors in the previous genome-wide yeast two-hybrid screen, it is possible that an interaction might be identified using full-length proteins rather than the gene fragments that are typically present in prey libraries. All of these genes are expressed during meiosis, and would therefore be present in the Shimoda two-hybrid library (Mata *et al.*, 2002).

Interaction between the candidate proteins and both *LexA-mto1(769-1115)* and *LexA-mto1(769-1051)* was assessed by expression of the *HIS3* gene, allowing growth on

media lacking histidine (Figure 16, A). As described previously, the extreme C-terminus of Mto1 is necessary for Mto1 localisation to MTOCs, and I hypothesised that the interacting protein that localises Mto1 to the equator might not interact with *LexA-mto1(76-1051)*. *Gal4AD-HA-spn1*, *Gal4AD-HA-cdc4* and *Gal4AD-HA-rng3* all showed growth on media minus leucine, tryptophan and histidine with both *LexA-mto1(769-1115)* and *LexA-mto1(76-1051)* as bait; *Gal4AD-HA-myp2* showed growth with both *LexA-mto1(769-1115)* and *LexA-mto1(76-1051)* on media minus leucine and tryptophan, but only with *LexA-mto1(769-1115)* on media minus leucine, tryptophan and histidine, suggesting that the Mto1 localisation region 1051-1115 is required for Mto1 to interact with Myp2. These prey plasmids were expressed in *L40Δgal* without the Mto1 bait plasmids and tested for growth on media minus leucine and histidine. No growth was seen, ruling out auto-activation of HIS3 expression (data not shown). While all the proteins tested appear to interact with Mto1, these interactions require additional verification either by biochemical means or by showing a functional interaction *in vivo* due to the limitations of the yeast two-hybrid system. This data could be expanded by also testing the interactions using the LacZ overlay and ONPG assays to assess β-galactosidase expression.

The formin *cdc12* was also tested for interaction with *LexA-mto1(769-1115)*, *LexA-mto1(769-1065)* and *LexA-mto1(76-1051)*. Cdc12 joins the CAR around the time of SPB separation (Wu *et al.*, 2003) and is essential for viability (Chang *et al.*, 1997). There is some evidence that formins influence microtubule nucleation. Mammalian formins localise to microtubules *in vivo* and the over-expression of mDia affects the alignment and stability of cytoplasmic microtubules (Ishizaki *et al.*, 2001; Bartolini

Figure 16 Yeast two-hybrid assays of the interaction of Mto1(769-1115) and Mto1(769-1051) with candidate genes

Interaction between candidate genes and *LexA-mto1(769-1115)* and *LexA-mto1(769-1051)* as measured by growth on -WLH media. Myp2 interacts with *LexA-mto1(769-1115)* but not *LexA-mto1(769-1051)* (red block). (B) Cdc12 does not interact with Mto1 truncations as determined by growth on -WLH media and LacZ overlay assay. Two independent *Gal4AD-cdc12* plasmids were tested. *Gal4AD-cdc11(562-1045*) *vs LexA-mto1(769-1115)* is shown as a positive control for the overlay assay.

A

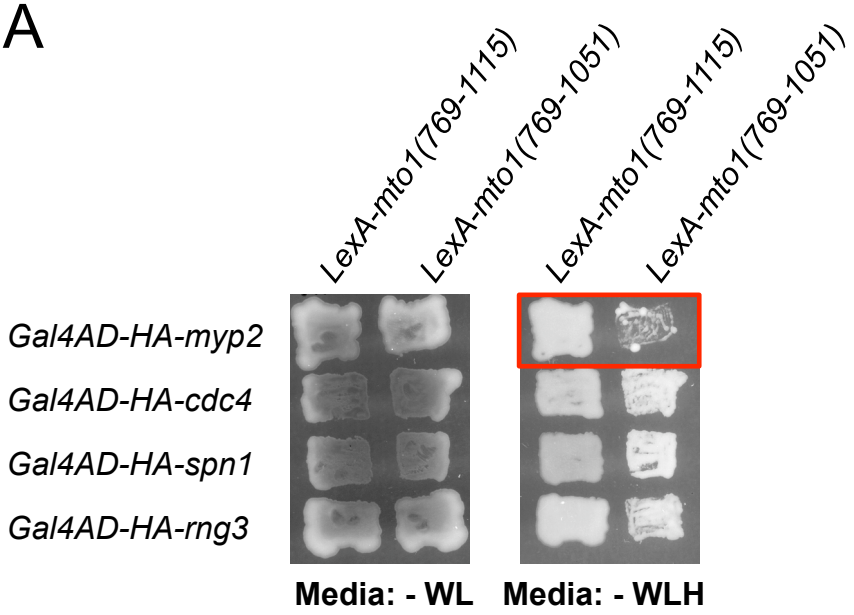

B

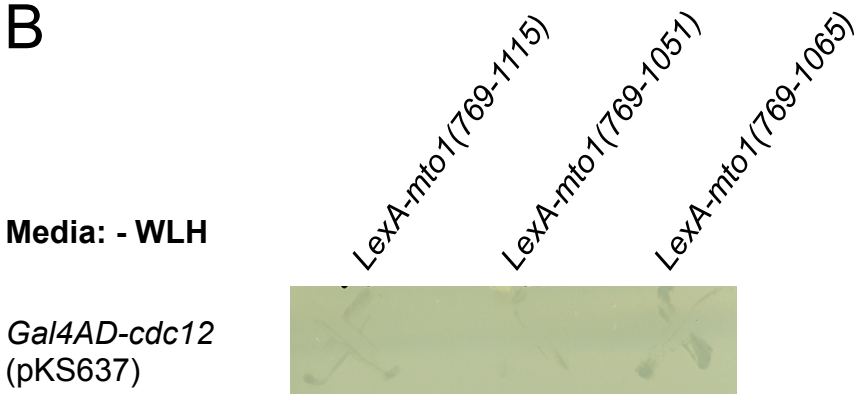

Positive control
Gal4AD-cdc11(562-1045)
vs
LexA-mto1(769-1115)

et al., 2008). In *S. pombe*, deletion of the formin *for3* increases the number of interphase microtubule bundles present in cells (Feierbach and Chang, 2001). Cdc12 is reported to move along both actin cables and microtubules (Chang, 1999), and over-expressed GFP-Cdc12 has been seen to form a filamentous structure reminiscent of the PAA, suggesting that Cdc12 may interact with microtubules (K. Sawin, personal communication). Interaction was assessed by growth on media lacking histidine and by LacZ overlay assay. An *L40Δgal* strain with plasmids expressing Gal4AD-Cdc11(562-1045) and LexA-Mto1(769-1115), previously shown to interact, was included as a control (Figure 16, B). *Gal4AD-cdc12* showed no interaction with *LexA-mto1(769-1115)*, *LexA-mto1(769-1065)* or *LexA-mto1(769-1051)*. Western blotting was used to test expression of Gal4-Cdc12 using both anti-Gal4AD (Santa Cruz, sc-46680) and anti-Cdc12 (Sawin laboratory) antibodies, however no specific bands were seen for either the test or control strains (data not shown). Thus, while it is possible in principle that *cdc12* was not expressed, there is no evidence to suggest an interaction between Mto1 and Cdc12.

Myp2 was then tested for interaction with other Mto1 truncations to define regions within the C-terminal localising domain required for the interaction between Mto1 and Myp2. *Gal4AD-HA-myp2* was tested for interaction with *LexA-mto1(769-1095)*, *LexA-mto1(769-1085)*, *LexA-mto1(769-1075)*, *LexA-mto1(769-1065)*, in addition to *LexA-mto1(769-1115)* and *LexA-mto1(769-1051)*. These additional truncations all contain the region *mto1(1051-1065)*, necessary for localisation to the cell equator. As before, *LexA-mto1(769-1115)* interacts with *Gal4AD-HA-myp2* to give growth on media minus leucine, tryptophan and histidine, but growth was not seen for the other

Mto1 truncations tested, although all the strains tested grew on media minus leucine and tryptophan (Figure 17). The results do not correspond directly with the localisation data, however this could be attributed to an artifact of the yeast two-hybrid assay, perhaps due differences in protein folding in the yeast two-hybrid conditions affecting the interaction of Myp2 with the Mto1 fragments. I conclude that the C-terminal localising region Mto1(1051-1115) is required for the interaction of Mto1 with Myp2.

Myp2 is required for PAA formation

As Mto1 does not localise to the equator in *myp2Δ* cells, the eMTOC should not form and no PAA would be expected to be present. Time-lapse wide-field microscopy was used to monitor live *myp2Δ* cells expressing GFP-Atb2 from the early stages of mitosis through spindle elongation, spindle disassembly and cell division (Figure 18, Movies 1 and 2). *myp2Δ nmt81:GFP-atb2* cells have no PAAs and no signs of microtubule nucleation from the equator were seen. In comparison, 100% of wild-type *nmt81:GFP-atb2* cells formed a PAA (cells with PAA formation: 0/12 cells for *myp2Δ*, 14/14 cells for wild-type). Thus Myp2 is required for the formation of the PAA, consistent with its requirement for the localisation of Mto1 to the cell equator.

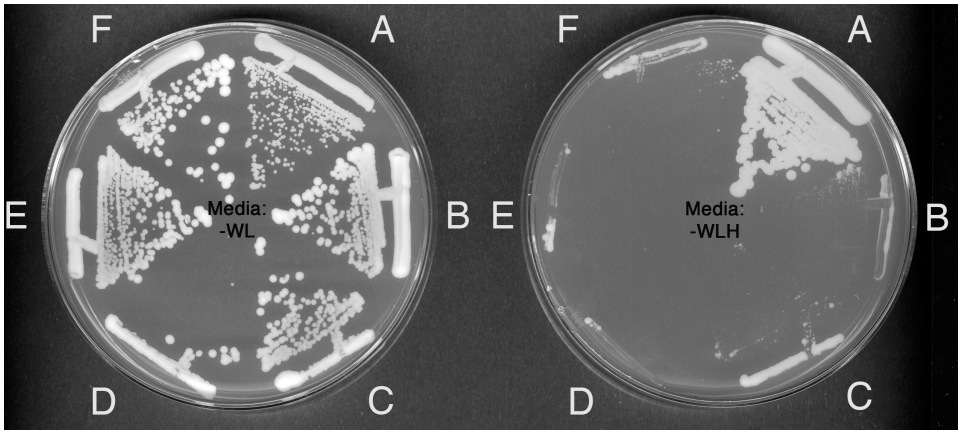

Figure 17 Myp2 interacts with Mto1 by yeast two-hybrid assay

Growth of *Gal4AD-HA-myp2* vs (A) *LexA-mto1(769-1115)*, (B) *LexA-mto1(769-1095)*, (C) *LexA-mto1(769-1085)*, (D) *LexA-mto1(769-1075)*, (E) *LexA-mto1(769-1065)* and (F) *LexA-mto1(769-1051)* on -WL and -WLH media. Myp2 interacts with LexA-Mto1(769-1115), but not with the other Mto1 truncations.

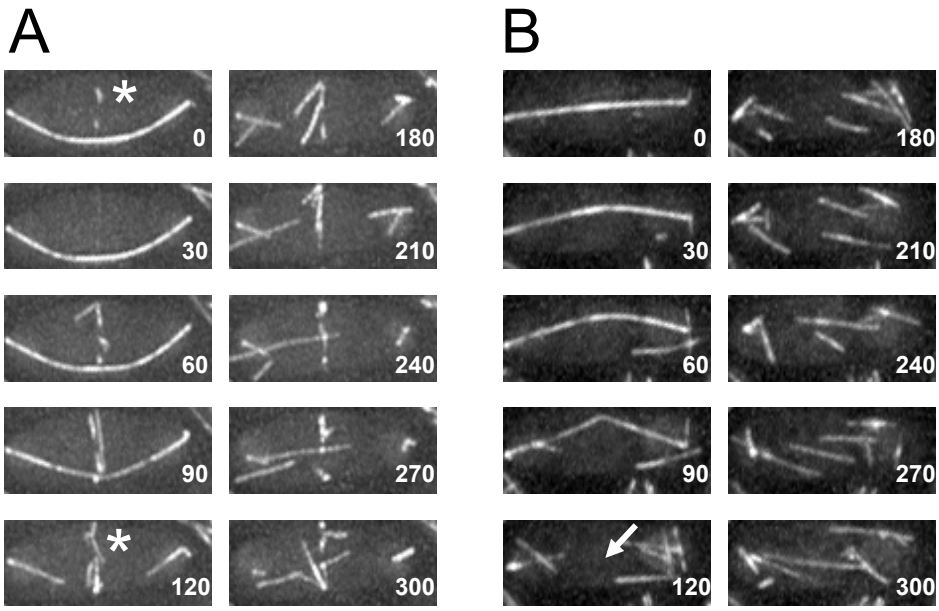

Figure 18 *Myp2Δ* cells do not have a post-anaphase array

Deconvolved time-lapse wide-field microscopy of live (A) *GFP-atb2* cells and (B) *GFP-atb2 myp2Δ* cells. The asterisk indicates the appearance of the PAA and also the continued presence of the PAA following mitotic spindle breakdown. No PAA is seen in the absence of Myp2 (arrow). Numbers in (A) and (B) indicate the time elapsed in seconds since the first frame.

Myp2 localisation to the equator does not require Mto1

As Mto1 localisation to the equator requires Myp2, I asked if Myp2 localisation was similarly dependent on Mto1. As discussed previously, Myp2 and Mto1 appear at the CAR at approximately the same stage of CAR assembly. Therefore I wanted to determine if Myp2 localisation to the CAR could take place independently of Mto1 recruitment, or whether Myp2 localisation required the formation of a Myp2-Mto1 complex. To address this point I examined the localisation of Myp2-YFP in *mto1Δ* cells. Equatorial rings of Myp2-YFP in various stages of contraction were seen in both *myp2-YFP* and *mto1Δ myp2-YFP* cells (Figure 19). I conclude that Myp2 localisation to the CAR does not require Mto1.

The myosin light chain Rlc1 is not required for localisation of Mto1 to the equator

I next asked if the non-essential regulatory light chain Rlc1 was required for localisation of Mto1 to the equator. Rlc1 interacts with both Myo2 and Myp2, and has been found to relieve auto-inhibition of Myo2 (Naqvi et al., 2000). Having established that Myp2 is required for Mto1 localisation to the cell equator, I wondered if this required Rlc1. Mto1-GFP was imaged using wide-field microscopy in *mto1-GFP rlc1Δ* cells. Mto1-GFP can be seen to form an equatorial ring in *rlc1Δ* cells (Figure 20). Therefore localisation of Mto1 to the cell equator does not require Rlc1.

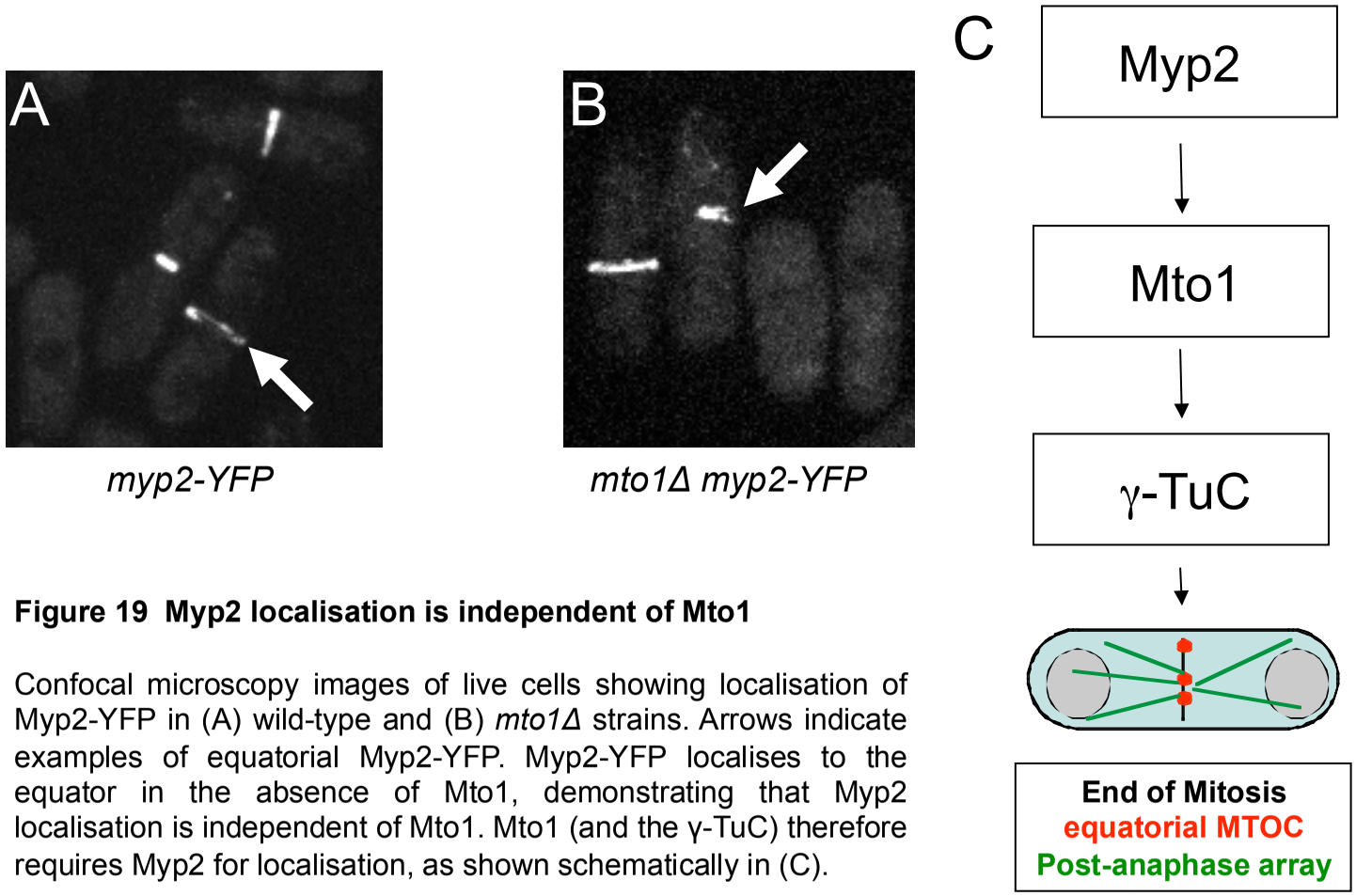

Figure 19 Myp2 localisation is independent of Mto1

Confocal microscopy images of live cells showing localisation of Myp2-YFP in (A) wild-type and (B) *mto1Δ* strains. Arrows indicate examples of equatorial Myp2-YFP. Myp2-YFP localises to the equator in the absence of Mto1, demonstrating that Myp2 localisation is independent of Mto1. Mto1 (and the γ-TuC) therefore requires Myp2 for localisation, as shown schematically in (C).

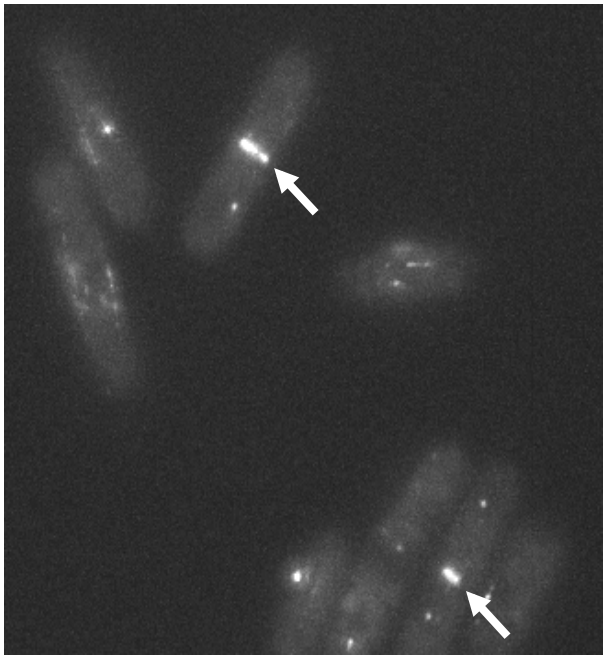

Mto1-GFP rlc1Δ

Figure 20 Mto1 localisation to the equator does not require the regulatory light chain Rlc1

Wide-field microscopy showing Mto1-GFP localisation in *rlc1Δ* cells. Arrows indicate Mto1 at the cell equator.

Mto1 co-immunoprecipitates with Myp2-YFP and Ain1-YFP

To investigate whether Myp2 interacts with Mto1 *in vivo*, I performed immunoprecipitation experiments. Extracts from a number of strains expressing native levels of YFP-tagged cytokinesis proteins were tested to see if they would co-immunoprecipitate Mto1. These strains were the kind gift of Tom Pollard (Wu *et al.*, 2003; Wu and Pollard, 2005). In addition to Myp2, the septin Spn1 and the actinin Ain1 were also included, having been previously shown an interaction with Mto1 in the yeast two-hybrid screen. Mto2-GFP, known to associate with Mto1, was included as a positive control (Samejima et al., 2005; Venkatram et al., 2005). Co-immunoprecipitation experiments were carried out using an anti-GFP antibody (which recognises both GFP and YFP). Myp2-YFP, Ain1-YFP and Mto2-YFP co-immunoprecipitated Mto1, but Mto1 was not co-immunoprecipitated in the untagged wild-type strain or Spn1-YFP (Figure 21). These results indicate that Mto1 interacts with Myp2 and Ain1 *in vitro*.

Two things are apparent from the Western blot. First, Mto1 levels appear to be decreased in the *myp2-YFP* extract. The amount of Mto1 co-immunoprecipitated by Myp2-YFP should therefore be considered relative to the reduced amount of Mto1 available for immunoprecipitation. Secondly Myp2-YFP appears to be less abundant in cell extract than Ain1-YFP, Spn1-YFP or Mto2-GFP. The average number of molecules of various common CAR proteins in a single cell has been measured and ~1.5 times more Myp2 is present in cells than Ain1 (Wu and Pollard, 2005). Why then, is so little Myp2 seen in the cell extract? Myp2 is a large protein, making it prone to degradation and hard to transfer from acrylamide gels into nitrocellulose,

which could explain the discrepancy. These results establish that Myp2 and Ain1, but not Spn1, co-immunoprecipitate Mto1.

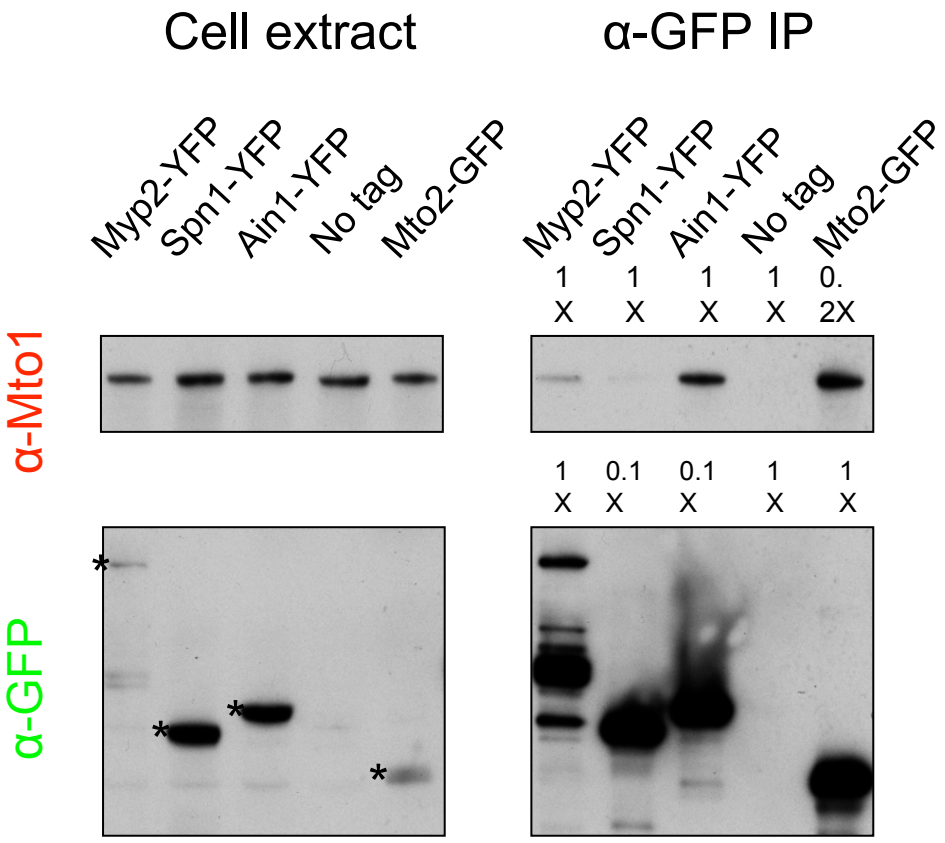

Figure 21 Myp2-YFP co-immunoprecipitates Mto1

Anti-GFP immunoprecipitation of YFP-tagged CAR proteins. Left panel shows the native protein levels of Mto1 and the tagged proteins in cell extract (* indicates primary band for YFP-tagged proteins). Right panel shows the levels recovered by IP. Mto1 is co-immunoprecipitated by Myp2, Ain1 and Mto2 (positive control), but not by Spn1 or the untagged negative control strain. Respective loading amounts are listed above lanes for the anti-GFP immunoprecipitation samples. Cell extracts were loaded at ~35 µg protein for samples probed with anti-Mto1 and 70 µg protein for samples probed with anti-GFP. Immunoprecipitation lanes represent ~110× extract-equivalent loading relative to total cell extract lanes (unless otherwise annotated) for samples probed with anti-Mto1, and ~100× extract-equivalent for samples probed with α-GFP.

Levels of Mto1 protein are reduced in strains expressing Myp2-YFP

It was noted during the above experiments that Mto1 protein levels in the strain KS2976 *myp2-YFP* appeared to be consistently lower than in the other strains used. A dilution series shows that expression in KS2976 is ~0.5 the level of the wild-type strain KS515 (Figure 22, A). I hypothesised that this could be related to the presence of the YFP tag on the Myp2 protein; if so, this could provide supplementary evidence supporting an interaction between Myp2 and Mto1. However, Mto1 expression could also be affected as a result of novel mutations present in the KS2976 strain. I crossed the KS2976 strain against the wild-type strain and compared the expression level of Mto1 in progeny expressing either Myp2 or Myp2-YFP. Expression of Mto1 in strains expressing Myp2-YFP was overall lower than for strains expressing untagged Myp2 (based on 10 samples, Figure 22, B). Thus it is likely that the addition of a C-terminal YFP tag to Myp2 affects Mto1 stability.

Interaction of Myp2-YFP with Mto1 alleles that fail to localise to the equator

Having shown that Myp2-YFP and Mto1 co-immunoprecipitate, I then asked if Myp2 would co-immunoprecipitate *mto1* alleles that fail to localise to the equator. Co-immunoprecipitation experiments were carried out using Mto1(1-1051) and Mto1(1-800) truncations that lack the Mto1(1051-1115) localisation region (Figure 23). Myp2-YFP was also tested to see if it would co-immunoprecipitate Mto1-427,

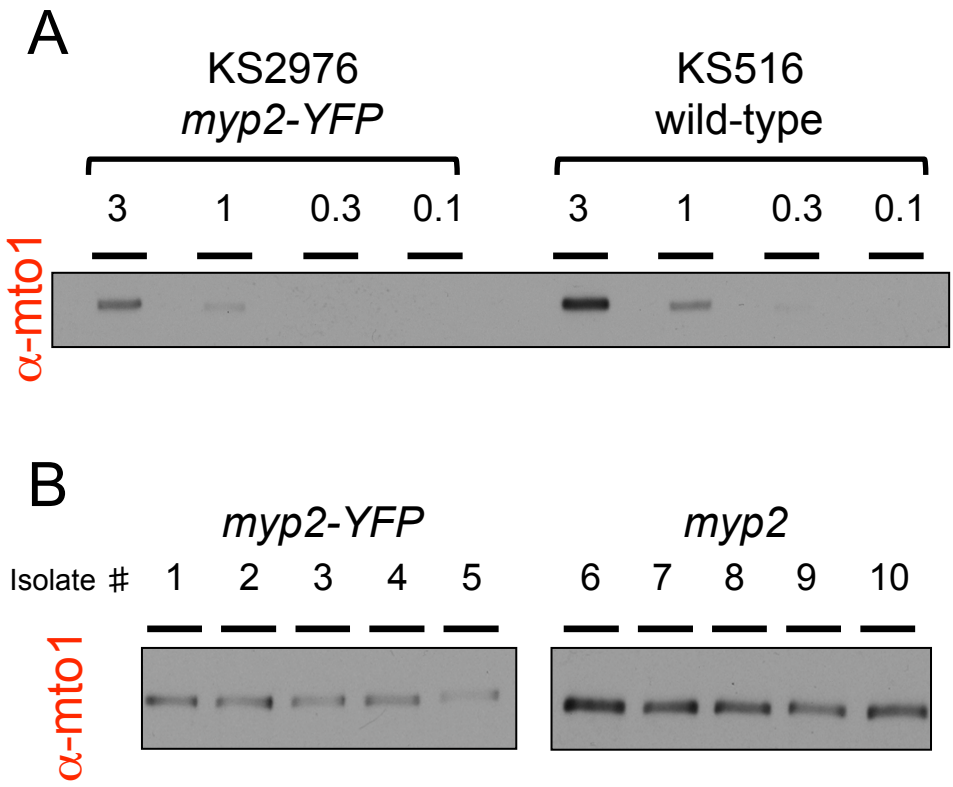

Figure 22 Mto1 levels are reduced in strains expressing Myp2-YFP

(A) Dilution series showing expression of Mto1 in KS2976 *myp2-YFP* strains and wild-type KS516. Numbers over each lane indicates the relative dilution. (B) Expression of Mto1 in progeny derived from out-crossing KS2976 *myp2-YFP* with wild-type strain KS516. Expression of Myp2-YFP correlates with reduced expression of Mto1.

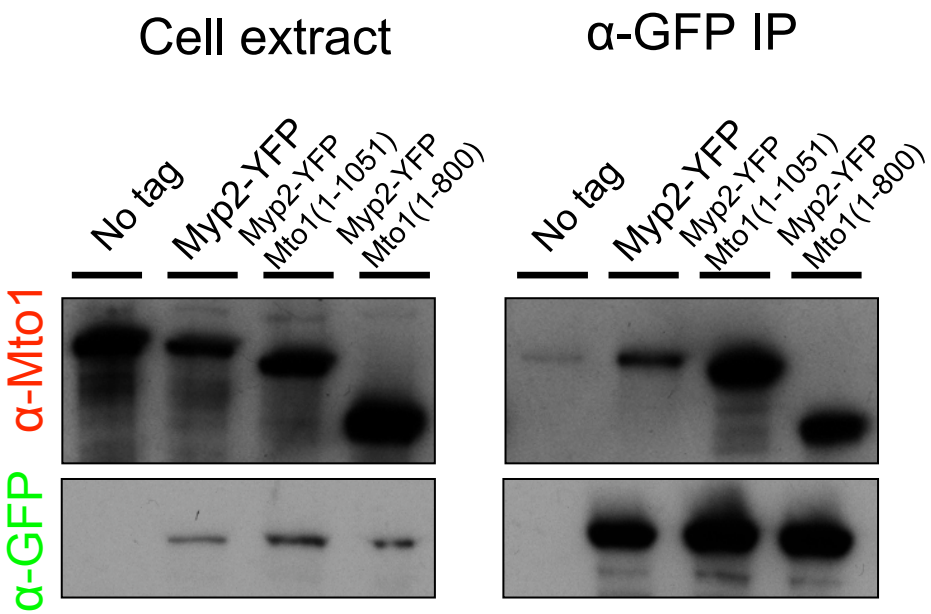

Figure 23 Mto1 alleles that do not localise to the cell equator co-immunoprecipitate with Myp2: Mto1 truncations

Anti-GFP immunoprecipitation of Myp2-YFP. Myp2-YFP co-immunoprecipitates full-length Mto1, Mto1(1-1051) and Mto1(1-800). Immunoprecipitation lanes represent ~100× extract-equivalent loading relative to total cell extract lanes for samples probed with anti-Mto1 , and ~200× extract-equivalent for samples probed with anti-GFP. Cell extracts were loaded at 35 µg protein for samples probed with anti-Mto1 and 70 µg protein for samples probed with anti-GFP.

which contains 3 amino acid substitutions (R1056A, E1059A and E1061A) within the C-terminus of Mto1; these mutations disrupt the localisation of Mto1 to the eMTOC (Figure 24). Surprisingly, I found that all the alleles of Mto1 tested co-immunoprecipitated with Myp2.

The Mto1 alleles were also tested for non-specific interactions with the beads used during the immunoprecipitation experiments. None of the Mto1 alleles immunoprecipitated in strains that expressed untagged Myp2, indicating that the co-immunoprecipitation of Mto1 alleles that fail to localise to the equator with Myp2-YFP cannot be attributed to a non-specific interaction (Figure 25).

Mto1-427 co-immunoprecipitates with Myp2-YFP during mitotic arrest

Having shown that Myp2-YFP co-immunoprecipitates Mto1(1-800), Mto1(1-1051) and Mto1-427, despite none of these *mto1* alleles localising to the equator, I then asked whether these interactions might be restricted to interphase. If so, this would explain why the alleles interacted with Myp2 despite not localising to the equator later in the cell cycle. I asked whether Mto1-427 would co-immunoprecipitate with Myp2-YFP during a *cps1-191* arrest, in which cytokinesis is blocked, after nuclear division and CAR formation has taken place. Co-immunoprecipitation experiments were carried out using a *cps1-191 mto1-427 myp2-YFP* and *cps1-191 myp2-YFP* strains grown for 3 hr at the restrictive temperature of 36°C. Both Mto1 and Mto1-427 co-immunoprecipitated with Myp2-YFP during *cps1-191* arrest (Figure 26).

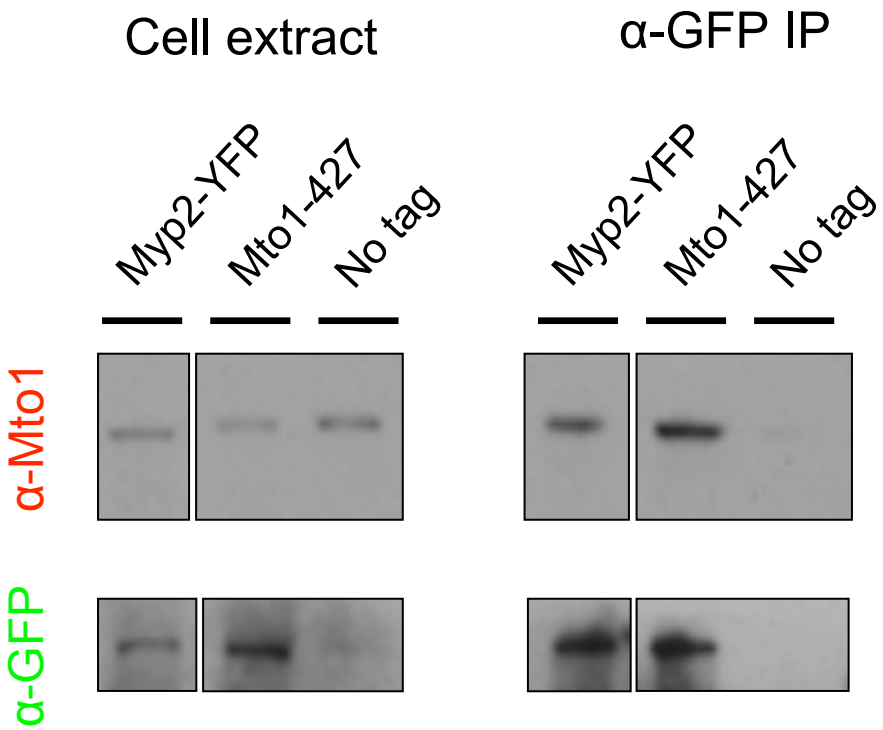

Figure 24 Mto1 alleles that do not localise to the cell equator co-immunoprecipitate with Myp2: Mto1-427

Anti-GFP immunoprecipitation of Myp2-YFP. Left panel shows the native protein levels of Mto1 and Myp2-YFP in cell extract. Both Mto1 and Mto1-427 co-immunoprecipitate with Myp2-YFP. Cell extracts were loaded at ~35 µg protein for samples probed with anti-Mto1 and 70 µg protein for samples probed with anti-GFP. Immunoprecipitation lanes represent ~750× extract-equivalent loading relative to total cell extract lanes for samples probed with anti-Mto1 and ~100× extract-equivalent for samples probed with anti-GFP.

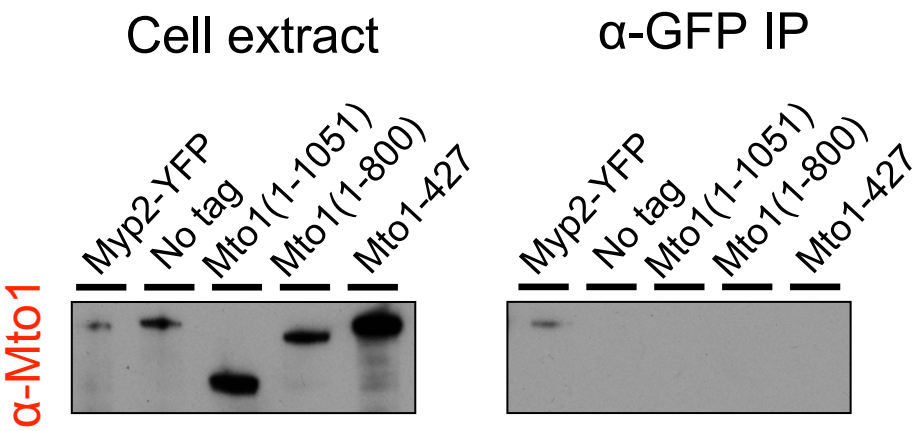

Figure 25 Mto1 truncations do not show non-specific interactions during co-immunoprecipitation

Anti-GFP immunoprecipitation of Myp2-YFP from strains KS2976 *myp2-YFP,* wild-type KS516, KS1956 *mto1(1-800),* KS1957 *mto1(1-1051)* and KS5109 *mto1-427.* Right panel shows levels of Mto1 alleles recovered by IP. Mto1 is co-immunoprecipitated by Myp2, but no protein is seen for the other strains where Myp2 is untagged. Cell extracts were loaded at ~35 µg protein. Immunoprecipitation lanes represent ~200× extract-equivalent loading relative to total cell extract lanes.

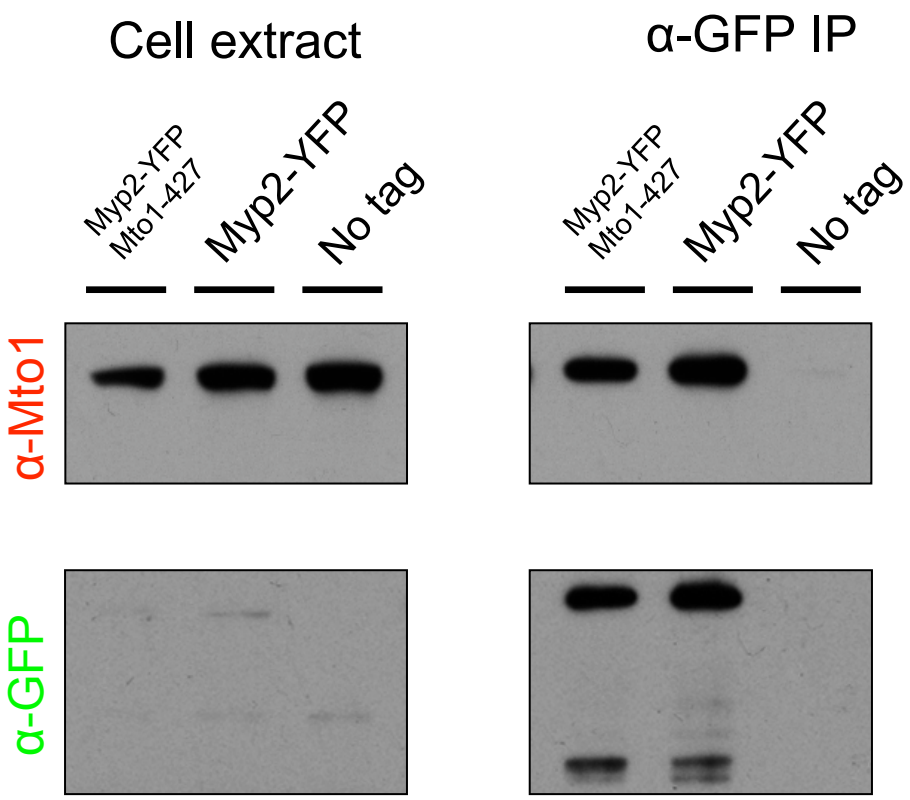

Figure 26 Myp2-YFP co-immunoprecipiates Mto1-427 during *cps1-191* mitotic arrest

Anti-GFP immunoprecipitation of Myp2-YFP. Cell extracts were prepared from cultures grown at 36°C for 3 hrs for strains KS4957 *cps1-191 mto1-427 myp2-YFP,* KS4959 *cps1-191 myp2-YFP* and KS3724 *cps1-191*. Left panel shows the native protein levels of Mto1 and Myp2-YFP. Right panel shows the levels recovered by IP. Both Mto1 and Mto1-427 co-immunoprecipitate with Myp2-YFP. Immunoprecipitation lanes represent ~400× extract-equivalent loading relative to total cell extract lanes for samples probed with anti-Mto1 , and ~50× extract-equivalent for samples probed with anti-GFP. Cell extracts were loaded at ~35 µg protein for samples probed with anti-Mto1 and 70 µg protein for samples probed with anti-GFP.

I then investigated whether the immunoprecipitation of Mto1-427 was from non-arrested cells present in the *cps1-191*-arrested sample, as *cps1-191* arrest does not result in 100% binucleate cells (here *cps1-191* arrest generated an average of 73% binucleate cells). The immunoprecipitation was repeated using the Li-Cor Western system to accurately determine the amount of protein co-immunoprecipitated for each sample. The Li-Cor system uses infra-red detection of dye-coupled secondary antibodies in place of chemiluminescence, allowing quantitative analysis of protein samples. This allowed me to quantitatively compare the relative proportions of Mto1-427 precipitated from cycling and *cps1-191*-arrested cells.

The amount of Mto1-427 co-immunoprecipitated with Myp2-YFP was determined for both *csp1-191*-arrested and cycling cells after 3 hrs growth at 36°C. Immunoprecipitation reactions were also carried out with strains containing untagged *myp2*, to control for any non-specific interaction of the Mto1-427 protein. Intensity levels for bands recognised by anti-Mto1 and anti-GFP (which also recognises YFP) are shown in Table 7; the blot is shown in Figure 27. Similar amounts of Mto1-427 were present in the cell extract for both *myp2-YFP mto1-427* and *cps1-191 myp2-YFP mto1-427*. The amount of tubulin present in the cell extracts was used to determine the amounts of cell extract loaded, and the amount of Mto1-427 present in each cell extract corrected to represent equal loading. More Mto1-427 was present in the control untagged strains *mto1-427* and *cps1-191 mto1-427* relative to the tagged *myp2-YFP mto1-427* and *cps1-191 myp2-YFP mto1-427* strains (~ 27% increase), which agrees with the previous finding that the presence of *myp2-YFP* decreases Mto1 levels (and apparently also levels of Mto1-427). The levels of Myp2 present in

	Cell extracts			α-GFP IP	
Strain	Mto1 input	Tubulin input (loading control)	Corrected Mto1 input*	Myp2-YFP IP	Mto1 IP
myp2-YFP mto1-427	80.90	32.4	80.90	85.96	81.94
mto1-427	87.70	27.76	102.36	-	None detected
cps1-191 myp2-YFP mto1-427	72.06	29.07	80.31	97.10	80.03
cps1-191 mto1-427	82.84	26.40	101.67	-	None detected

Table 7 Intensity levels for the interaction of Mto1-427 with Myp2-YFP in both cycling cells and *cps1-191* arrest

Comparable amounts of Mto1 were present in the initial cell extracts. Similar quantities of Myp2-YFP were immunoprecipitated, and pulled down comparable amounts of Mto1-427. No detectable protein was seen following anti-GFP immunoprecipitation of cell extracts from the control strains *mto1-427* and *cps1-191 mto1-427.* Quantification was carried out using the Li-Cor Odyssey system.

**Values given corrected for differences in loading.*

Figure 27 Mto1-427 co-immunoprecipitates with Myp2-YFP during mitotic arrest: Li-Cor Western

Anti-GFP immunoprecipitation of Myp2-YFP from strains KS460 *mto1-427 myp2-YFP*, KS5109 *mto1-427*, KS4957 *cps1-191 mto1-427 myp2-YFP* and KS5188 *cps1-191 mto1-427.* Cell extracts were prepared from cultures grown at 36°C for 3 hrs. Levels of Myp2-YFP in the cell extract are below the level of detection. TAT-1 (tubulin antibody) was used as a loading control for the cell extracts (green bands). Myp2-YFP is immunoprecipitated for KS460 *mto1-427 myp2-YFP* (cycling cells) and KS4957 *cps1-191 mto1-427 myp2-YFP* (*cps1-191* arrest); both strains co-immunoprecipitate Mto1-427. No Mto1-427 is seen for the other strains where Myp2 is untagged. Immunoprecipitation lanes represent ~100× extract-equivalent loading relative to total cell extract lanes for samples probed with anti-Mto1 antibody, and ~200× extract-equivalent for samples probed with anti-GFP. Cell extracts were loaded at 35 µg protein for samples probed with anti-Mto1 and 70 µg protein for samples probed with anti-GFP. Blot imaged using direct infrared fluorescence detection (Li-Cor system). Intensity levels are given in Table 7.

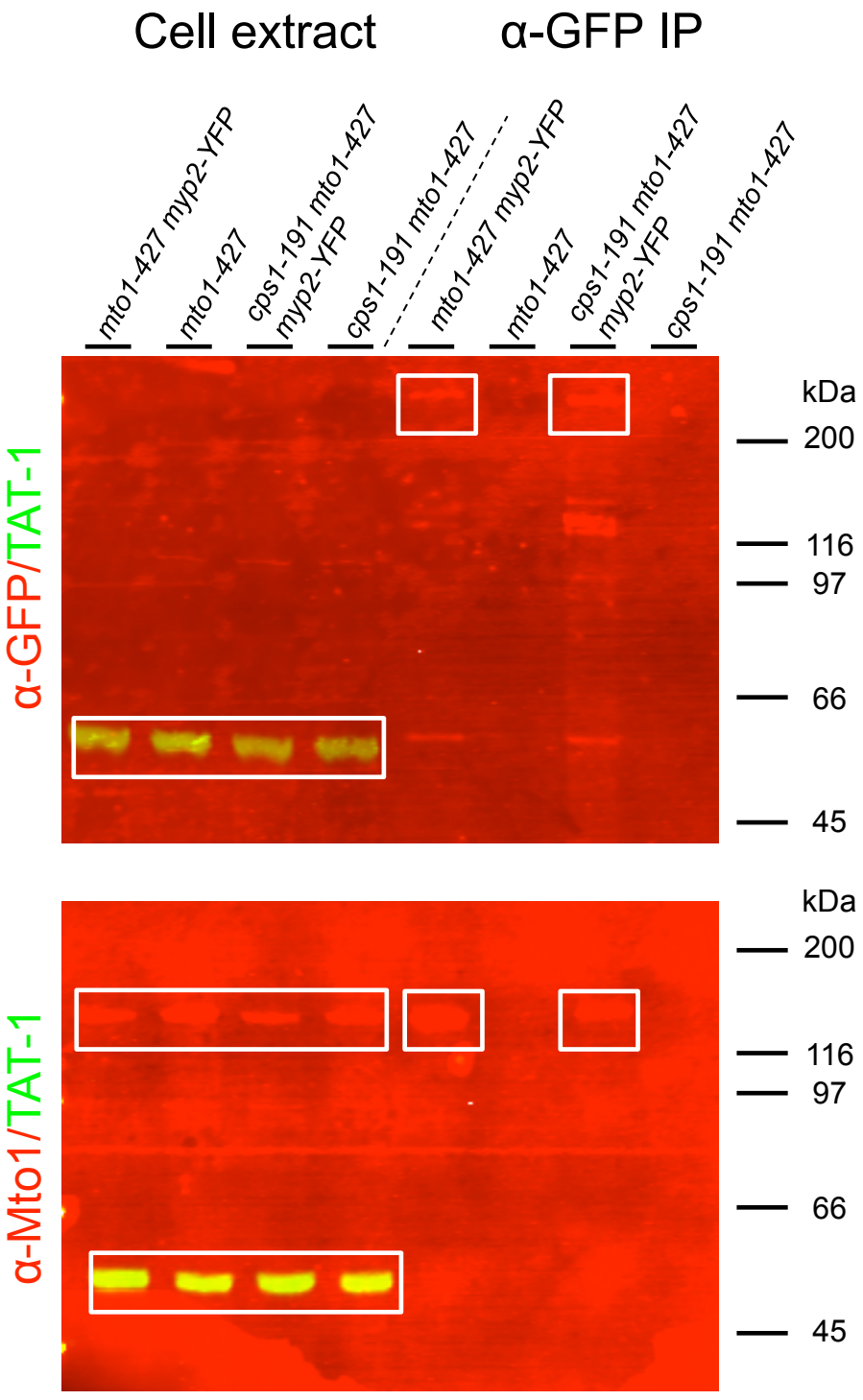
Cell extract
α-GFP IP
mto1-427 myp2-YFP
mto1-427
cps1-191 mto1-427 myp2-YFP
cps1-191 mto1-427
mto1-427 myp2-YFP
mto1-427
cps1-191 mto1-427 myp2-YFP
cps1-191 mto1-427
α-GFP/TAT-1
kDa
200
116
97
66
45
α-Mto1/TAT-1
kDa
200
116
97
66
45

the initial protein extracts were below detection by the Li-Cor system. However comparable amounts of Myp2 were immunoprecipitated (85.96 vs 97.10 intensity units). Near-identical amounts of the Mto1-427 protein were co-immunoprecipitated in cycling cells (97.1 intensity units) and in *cps1-191* cells arrested in mitosis (80.03 intensity units). The amount of Mto1-427 (in intensity units) co-immunoprecipitated per intensity unit of Myp2-YFP is 0.95 for cycling cells and 0.82 for *cps1-191* arrested cells. No detectable amount of Mto1-427 was present in the untagged control samples. As Myp2-YFP co-immunoprecipitates with Mto1-427 at a similar level in both cycling and *cps1-191*-arrested cells, this interaction is therefore present in both interphase and mitotic cells and the hypothesis that the interaction is solely present in interphase can be ruled out. I conclude that Mto-427 physically interacts with Myp2 in both interphase and mitotic cells.

Mto1-427-GFP does not localise to the cell equator during cps1-191 arrest

I next examined the localisation of Mto1-427 during *cps1-191* arrest. Mto1-427 does not localise to the equator under standard growth conditions; however Mto1-427 might appear at the equator during the prolonged arrest conditions. If so, this would invalidate any conclusions applied to the interaction between Mto1-427 and Myp2 during a normal mitosis. The localisation of Mto1-GFP and Mto1-427-GFP in *cps1-191 mto1-GFP* and *cps1-191 mto1-427-GFP* cells was observed after incubation for 3 hr at 36°C. Clear equatorial rings of Mto1-GFP were visible, but no equatorial rings of Mto1-427-GFP were seen (Figure 28). Therefore Mto1-427 does not localise to the equator during *cps1-191* arrest.

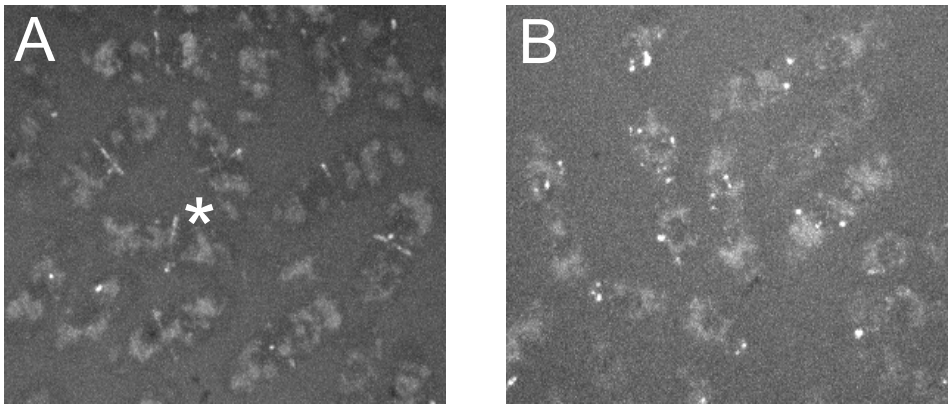

mto1-GFP cps1-191 *mto1-427-GFP cps1-191*

Figure 28 Mto1-427-GFP does not localise to the cell equator during *cps1-191* arrest

Confocal microscopy of live cells showing localisation of (A) Mto1-GFP and (B) Mto1-427-GFP during *cps1-191* arrest. Mto1-GFP localises to the cell equator forming a ring (* marks one example); Mto1-427-GFP is not visible as a ring at the cell equator.

Discussion

Myp2: a non-essential type-II myosin present in the CAR is required for the localisation of Mto1 to the equator

Myp2 (Myosin-II of *pombe*), also known as Myo3, was first identified through its homology to the previously identified type-II myosin in *S. pombe,* Myo2 (Bezanilla et al., 1997; Motegi et al., 1997). Myosins are actin-binding motors; type-II myosins (classified on the basis of sequence similarity (Berg et al., 2001)) provide the contractile force in muscle cells and also for CAR contraction during cytokinesis. In *myp2Δ* cells, Mto1 does not localise to the equator and the PAA does not form. On this basis I conclude that Myp2 is required for Mto1 to localise to the equator. In addition to this genetic dependency, Myp2-YFP and Mto1 co-immunoprecipitate, demonstrating that the proteins interact *in vivo*. Myp2 and Mto1 also interact by yeast-2 hybrid assay, indicating that the proteins can directly interact. I conclude that Myp2 interacts with Mto1 and that this interaction is necessary for Mto1 to localise to the equator. As Myp2 localisation to the CAR does not require Mto1, Myp2 can be placed upstream of Mto1 at the top of the eMTOC formation pathway (shown in Figure 19, C).

Myp2Δ cells are viable and are indistinguishable from wild-type strain on rich media but often appear as multi-septated cells with morphology defects on minimal media, suggesting defects in cytokinesis (Bezanilla et al., 1997). This phenotype is especially prominent when there is a high concentration of chloride ions, and such conditions cause cells to become cold-sensitive. This suggests that Myp2 is

important for cytokinesis under stress conditions. Over-expression of Myp2 produces elongated multi-nucleate cells with few septa. Myp2 shows genetic interactions with several temperature-sensitive mutants of genes involved in cytokinesis: *myp2Δ* shows a synthetic lethal interaction with temperature-sensitive mutations in the formin *cdc12* (Bezanilla et al., 1997) and the tropomyosin *cdc8* (Motegi et al., 1997); colony growth is reduced for *myp2Δ cdc14-118* and *myp2Δ cdc16-116* double mutants (*cdc14* and *cdc16* are components of the septation initiation network) (Bezanilla et al., 1997); and *myp2Δ act1-188* grow only in the presence of sorbitol (unlike *act1-188* cells that were able to grow without sorbitol; *act1* is the *S. pombe* actin gene) (Motegi et al., 1997)). These additive phenotypes suggest that Myp2 plays a role in cell division under normal growth conditions. Both Myo2 and Myp2 are CAR components, but Myo2 localises to the division site early in CAR formation, prior to SPB separation, while Myp2 appears significantly later (Wu et al., 2003). Deletion of Myo2 is lethal, due to severe cytokinesis defects (Kitayama et al., 1997; May et al., 1997). Combining the temperature sensitive *Myo2-E1* mutant with *myp2Δ* produces an additive phenotype, indicating that the two myosins have separate functions during cytokinesis (Bezanilla and Pollard, 2000). Chimera proteins mixing head and tail domains of the two myosins suggest that differences in the tail region may determine function. The precise role of each myosin is not known.

Myp2 follows the general myosin structure but, unusually, has a series of 19 proline residues in the tail region. Myosin heavy chains typically consist of 3 domains. The myosin head contains the motor region, binds actin and performs ATP hydrolysis.

The neck acts as a linker region, and can function as a lever for force transduction. It is also where myosin light chains bind. The tail region contains coiled-coil regions that bind to cargo molecules and allows dimerisation between myosin subunits. In general the head domain is highly conserved, while the tail region varies, generating functional diversity (Goodson and Dawson, 2006). Myosin-IIs typically dimerise though an interaction of the tails, the two tails coming together to form an α-helix. The proline region in the tail of Myp2 divides the tail into two distinct regions that are able to fold back and self-interact to form an anti-parallel coiled-coil. Consistent with this, ultracentrifugation analysis show Myp2 sediments as a monomer, and electron microscopy measurements find the Myp2 tail to be half the length expected (Bezanilla and Pollard, 2000). It is unclear what effect this unusual tail structure has on Myp2 function *in vivo* or how it might affect interaction with Mto1.

Three proteins are known to physically interact with Myp2. Cdc4 and Rlc1 are myosin light chains that interact with Myp2 as well as with Myo2 (Naqvi *et al.*, 1999; Le Goff *et al.*, 2000; Motegi *et al.*, 2000; Naqvi *et al.*, 2000; D'Souza V *et al.*, 2001) and are present at the equator from the time when Myo2 first appears (Wu et al., 2003). Chs2, a transmembrane protein that has homology to chitin synthases, also physically interacts with Myp2 (Martin-Garcia and Valdivieso, 2006). Chs2 localises to the growing edge of the septum and stabilises the CAR during the late stages of cytokinesis. Chs2 localisation is normal in *myp2Δ* cells (Martin-Garcia and Valdivieso, 2006). Rlc1 is not required for localisation of Mto1 to the cell equator, while Cdc4 appears to interact with Mto1(769-1115) and Mto1(769-1051) in a yeast

two-hybrid assay although this result requires further confirmation and it is not clear what the functional implication of such an interaction might be.

Myp2 interaction with *mto1* alleles that fail to localise to the equator

Since the 1051-1065 region of Mto1 is required for Mto1 localisation to the cell equator, I expected that this region would also be necessary for Myp2 and Mto1 to interact. However, Myp2-YFP is able to co-immunoprecipitate Mto1 truncations that lack this C-terminal domain and do not localise to the cell equator. As Myp2-YFP interacts with Mto1(1-800), this suggests that a Myp2-binding domain lies towards the N-terminus of Mto1. The N-terminus of Mto1 contains coiled-coil domains; coiled coil domains are also found in Myp2 and may mediate the interaction between the two proteins. This is not consistent with the my earlier finding that GFP-Mto1(919-1115) localises to the equator. Also Mto1(769-1115) interacts with Myp2 in the yeast 2-hybrid assay, supporting the idea of a C-terminal Myp2-binding domain.

One possible explanation that reconciles the contradictions between the localisation and protein interaction data is that two Myp2-binding domains may be present in Mto1: one domain at the N-terminus and one at the C-terminus. If Mto1(1-800) binds Myp2, why is this fragment unable to localise to the equator? I hypothesise that the C-terminus may be required to stabilise Mto1 once the Myp2-Mto1 complex reaches the ring, either by binding to Myp2 or (less likely) to another protein in the CAR. In the absence of the C-terminus, Mto1 will be recruited to the equator via the N-terminal interaction with Myp2, but will fail to anchor at the CAR. While Ain1 has

been found to both co-immunoprecipitate Mto1 and to interact with Mto1(769-1115) via yeast 2-hybrid assay, an interaction that requires the 1051-1115 region of Mto1, and could anchor Mto1 after it is localised by Myp2, the role of Ain1 in Mto1 localisation is not clear, as Mto1 localises to the equator in *ain1Δ* cells. If Ain1 does anchor Mto1 it would therefore have to be in combination with another protein.

Alternatively, recent work (I. Samejima, personal communication) has shown that Mto1(1028-1095) is sufficient for localisation to the eMTOC, interphase SPB and mitotic SPB it may be useful to look at the interaction between Myp2 and Mto1(801-1027). It is possible that Myp2 might interact with Mto1(1028-1051) even in the absence of the 1051-1115 localisation region. This would explain the interaction with Mto1(1-1051).

Future work studying the ability of Myp2 to co-immunoprecipitate Mto1(801-1115), Mto1(801-1051) and Mto1(801-1027) may give more insight into the mechanism of Myp2-Mto1 interaction. I predict that Myp2 will co-immunoprecipitate with Mto1(801-1115), but not Mto1(801-1051) or Mto1(801-1027). Further N-terminal truncation of Mto1 should also be tested for interaction with Myp2, to establish whether there is an N-terminal interaction domain or if this could somehow be attributed to artifact.

Chapter V - Regulation of Mto1 localisation to the site of eMTOC formation

Understanding how MTOCs are regulated during the cell cycle is a key question. MTOCs must be established not only in the right place (spatial control), but also at the right time (temporal control). Previous work has established that the recruitment of γ-tubulin to the eMTOC requires the activity of the anaphase promoting complex and the septation initiation network (Heitz et al., 2001). To understand how eMTOC formation is regulated I investigated the control of Mto1 localisation to the site of the eMTOC.

Mto1 does not localise to the equator during nda3-KM311 arrest

Mto1 first appears at the site of the prospective eMTOC when the cell is in anaphase B (I. Samejima, personal communication; see Introduction). I considered two hypotheses to explain this temporal regulation of Mto1. First, Mto1 might appear at a fixed amount of time following an earlier cell cycle event such as CAR assembly, independently of the cell undergoing anaphase. Alternatively, the appearance of Mto1 at the equator might be directly regulated by the cell cycle. To distinguish between the two hypotheses, I asked whether Mto1 is present at the equator in cells that are arrested in metaphase using the *nda3-KM311* mutant strain.

nda3 (nuclear division arrested 3) encodes the β-tubulin protein in *S. pombe*; the *KM311* mutation causes microtubules to become reversibly unstable at cold

temperature and *nda3-KM311* cells arrest at a step similar to mitotic prophase with condensed chromosomes, but no spindle (Toda *et al.*, 1983; Hiraoka *et al.*, 1984). The CAR forms and is detectable by phalloidin staining (Chang *et al.*, 1996; Arai and Mabuchi, 2002). Typical arrest conditions incubate the *nda3-KM311* strain for several hours at a low temperature.

To begin with, I examined Mto1 localisation using methanol-fixed *nda3-KM311* arrested cells (this was initially done to determine if the *nda3-KM311* arrest could be used to enrich for Mto1 at the equator to use in TAP purification (related to the experiment described in Chapter III)). Samples were taken after growth at 18°C for 9hrs; samples were also taken 10 and 20 minutes after release to the permissive temperature of 36°C. Samples were stained with both anti-Mto1 and anti-tubulin antibodies staining to visualise Mto1 localisation and to track cell cycle progression based on spindle morphology. In the arrested cells, Mto1 was not present at the equator in 90% of cells; once released by shift to the permissive temperature, the number of cells with Mto1 at the equator sharply increased as cells entered anaphase, decreasing slightly 20 minutes after the release to the permissive temperature (Table 8). While this ruled out the use of *nda3-KM311* arrest to enrich for Mto1 at the cell equator, this result supports the hypothesis that Mto1 localisation to the equator is regulated by cell-cycle progression.

Release from arrest / Cell cycle stage	0 min	10 min	20 min
Cells with mitotic spindle	0%	45%	25%
Cells with PAA	0%	14%	22%
Cells with Mto1 at equator	10%	48%	32%

Table 8 Immunostaining of microtubules and Mto1 in *nda3-KM311* arrested cells

Quantification of *nda3-KM311* cells c0-immunostained with anti-tubulin and anti-Mto1 antibodies. Samples were taken 0, 10 and 20 minutes following release to permissive temperature after arrest at 18°C for 9 hrs. Cells enter mitosis rapidly after release to the permissive temperature. Mto1 appearance at the equator correlates with mitosis. For each time point, n = 100.

I then repeated the time course, including a wild-type strain as a positive control for Mto1 localisation at 18°C. Samples were taken after growth at 18°C for 9hrs and 10, 20 and 30 minutes after release to the permissive temperature of 36°C. Representative images for these time points are shown in Figure 29. Cells were again stained with anti-Mto1 and anti-tubulin, and also with DAPI to visualise the nuclei.

At the restrictive temperature, no microtubules were present for *nda3-KM311* cells and Mto1 was not seen at the equator. Mto1 was found at the equator in wild-type cells at 18°C (7/7 cells with PAAs and 2/5 cells with a long (anaphase) mitotic spindle), but was not seen for any other cell cycle stage. When released to the permissive temperature, *nda3-KM311* cells progressed through the cell cycle. Mto1 was present at the cell equator primarily in cells with a long spindle or with a PAA, but also in a minority of cells with a short (metaphase) mitotic spindle. Mto1 is no longer found at the equator when the cells re-enter interphase at 30 minutes after release to the permissive temperature (Figure 30).

I then examined the localisation of Mto1 during *nda3-KM311* arrest using live cells immediately after release. A fluorescent-tagged myosin regulatory light chain, Rlc1-mCherry, was used to label the CAR. Mto1 was expressed from the *nmt41* promoter under repressed conditions to improve the visibility of Mto1 at the equator during recovery at 36°C, as observations revealed that even in wild-type cells Mto1-GFP is poorly visible at the equator during live imaging at high temperature. Expression of Mto1 from the *nmt41* promoter is approximately double that from the native promoter, based on Western blotting (H. Snaith, Sawin laboratory).

Figure 29 Mto1 localisation to the equator during *nda3-KM311* arrest: fixed cells

Wide-field microscopy of formaldehyde fixed *nda3-KM311* cells after 9 hrs growth at 18°C, and then 10, 20 and 30 minutes after release to 36°C. Also shown are wild-type cells after 9 hrs growth at 18°C. Arrows indicate selected examples of equatorial Mto1.

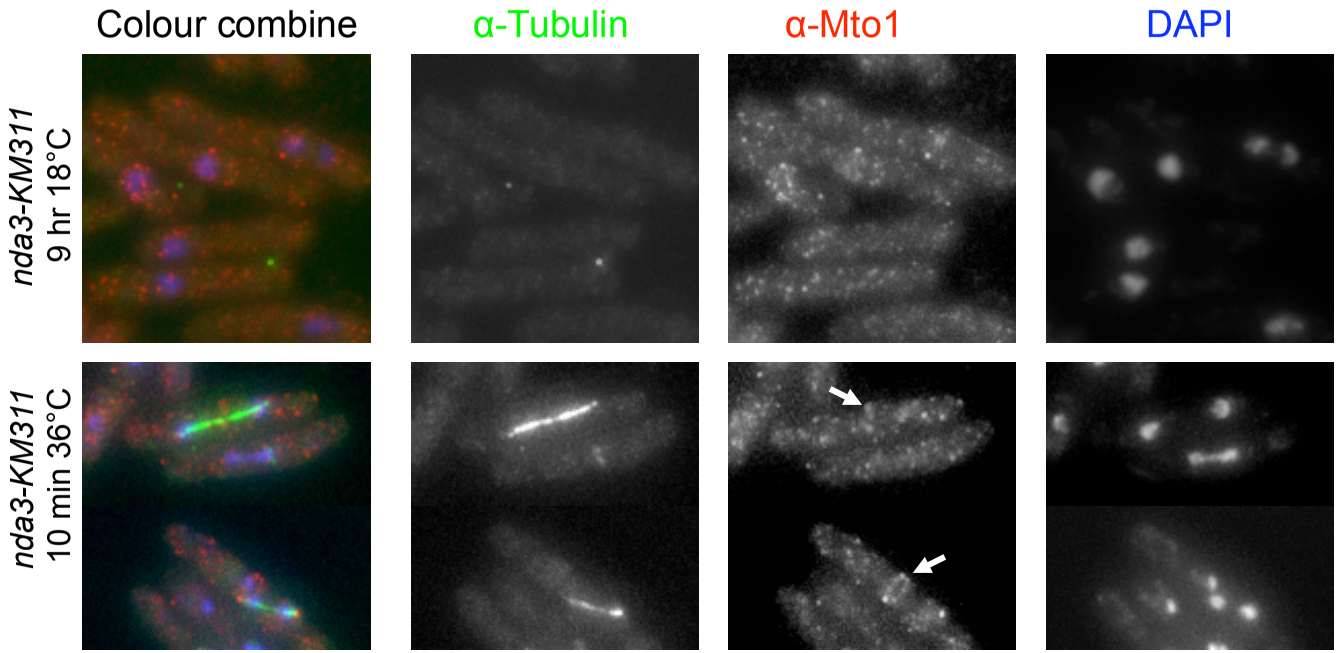

DAPI
α-Mto1
α-Tubulin
Colour combine
wild-type
9 hr 18°C
nda3-KM311
30 min 36°C
nda3-KM311
20 min 36°C

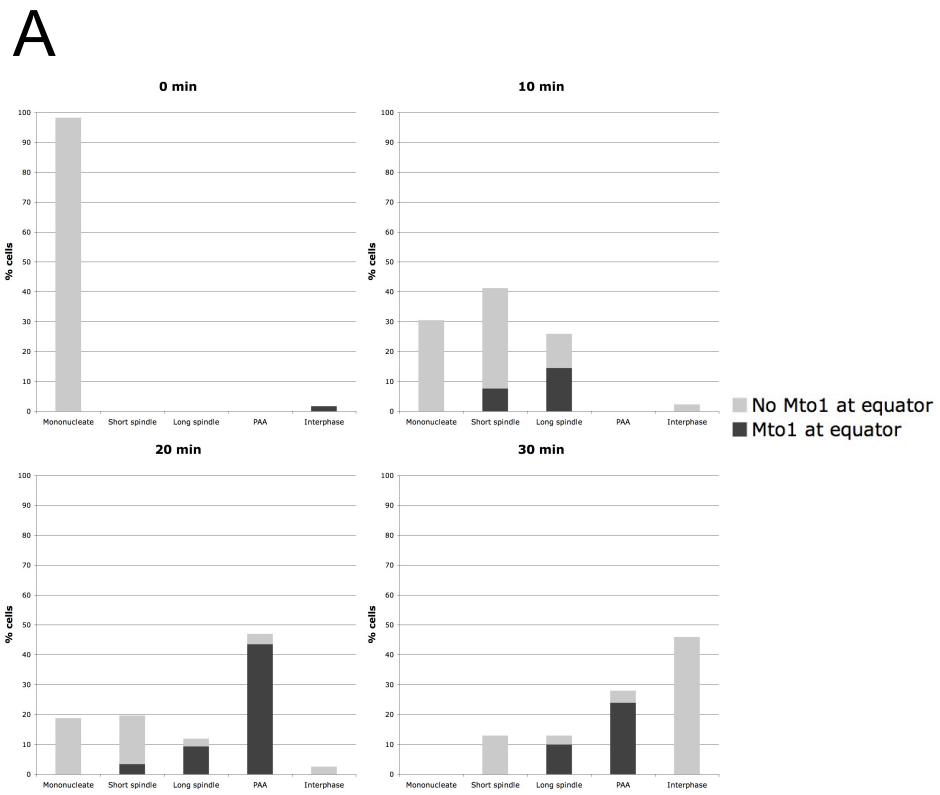

Figure 30 Localisation of Mto1 to the equator after release from *nda3-KM311* arrest (fixed cells)

(A) Cell cycle distribution of *nda3-KM311* cells transferred to 36°C after 9 hrs at 18°C, showing the proportion of cells with and without Mto1 at the equator at each cell cycle stage. (B) Cell cycle stages of cells with Mto1 at the equator.

Cultures were incubated for 9hrs at 18°C. In wild-type *nmt41:GFP-mto1 rlc1-mCherry* cells with a CAR, Mto1 co-localised with the CAR in 72% of cells (GFP-Mto1 is not expected to co-localise with the CAR in all cells with a Rlc1-mCherry ring because Rlc1 appears at the CAR earlier in mitosis than Mto1 (see Figure 15, panel A)). In contrast, 70% of *nmt41:GFP-mto1 nda3-KM311 rlc1-mCherry* cells did not have Mto1 at the equator (98% of these cells had a CAR). This strain was also shifted to the permissive temperature of 36°C for 5 minutes and then imaged at 36°C. Mto1 was present at the CAR in 100% of released cells at 36°C, despite these cells not having entered anaphase (based on SPB separation using Mto1 as an SPB marker). Representative images are shown in Figure 31. I conclude that while Mto1 does not localise to the equator in the majority of *nda3-KM311* arrested cells, it is not necessary for a cell to have entered anaphase for Mto1 to localise to the equator as Mto1 then localises to the equator in all cells immediately when the *nda3-KM311* arrest is released. These results are discussed below.

The anaphase promoting complex is not required for localisation of Mto1 to the equator

A key regulatory pathway active during mitosis, the anaphase promoting complex (APC) initiates the events of anaphase by targeting proteins for destruction by the 26S proteasome (Zachariae and Nasmyth, 1999). Previous work has shown that the APC is required for the localisation of γ-tubulin to the eMTOC (Heitz et al., 2001). I therefore asked whether the localisation of Mto1 to the site of eMTOC formation also requires APC activity, and examined Mto1 localisation in the temperature-

Figure 31 Mto1 localisation to the equator during *nda3-KM311* arrest: live cells

(A) Wide-field microscopy showing GFP-Mto1 localisation in wild-type *nmt41:GFP-mto1 rlc1-mCherry* cells after 9 hrs at 18°C; *nmt41:GFP-mto1 nda3-KM311 rlc1-mCherry* cells after 9 hrs at 18°C and released after 9 hrs at 18°C to 36°C for 5 min. * indicates GFP-Mto1 at the equator in selected cells. (B) Graphical representation of GFP-Mto1 localisation to the equator in these strains in cells containing a CAR. Mto1 is not seen in 100% of cells with a CAR for the wild-type strain as Rlc1-mCherry, used to monitor CAR presence, appears before Mto1.

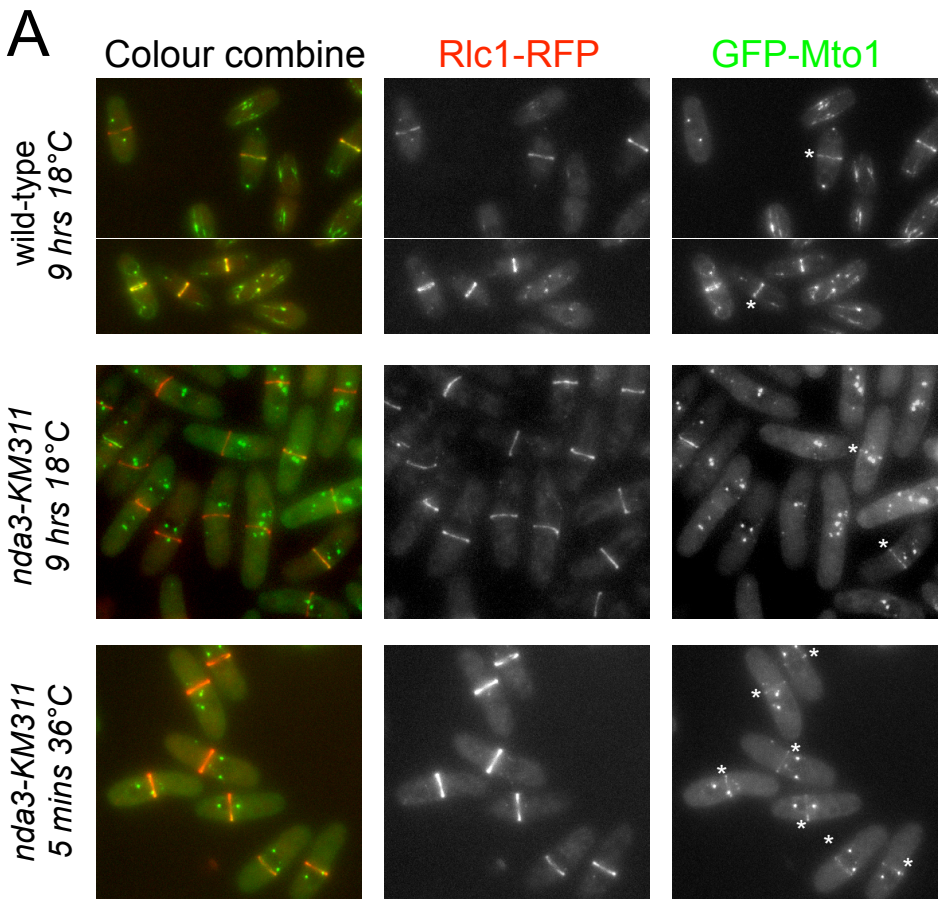
A
Colour combine
Rlc1-RFP
GFP-Mto1
wild-type
9 hrs 18°C
nda3-KM311
9 hrs 18°C
nda3-KM311
5 mins 36°C

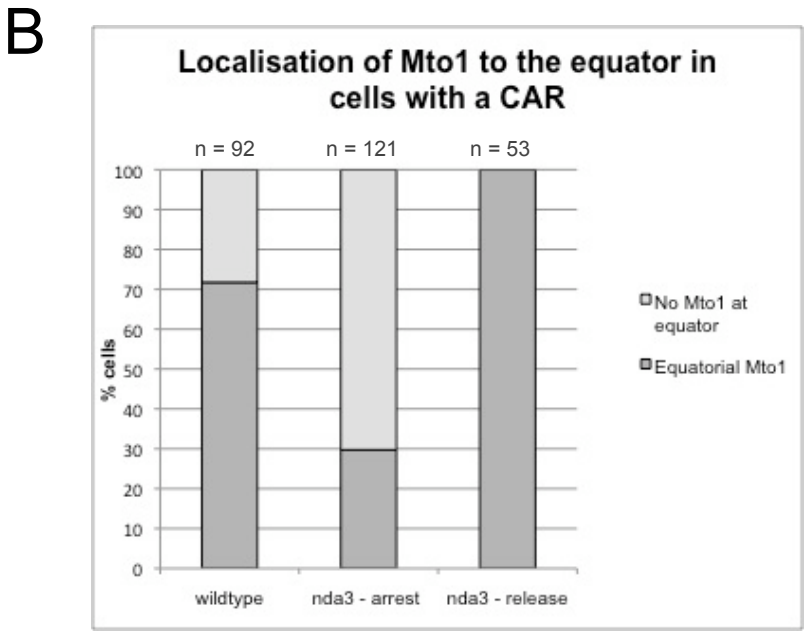
B
Localisation of Mto1 to the equator in cells with a CAR
n = 92
n = 121
n = 53
100
90
80
70
60
50
40
30
20
10
0
% cells
wildtype
nda3 - arrest
nda3 - release
No Mto1 at equator
Equatorial Mto1

sensitive *cut4.533, cut8.563* and *cut9.665* strains at the restrictive temperature. These strains were also used in (Heitz et al., 2001); Cut4 and Cut9 are sub-units of the APC (Yamashita *et al.*, 1996; Yamada *et al.*, 1997), while Cut8 is required to localise the 26S proteasome to the nuclear periphery (Tatebe and Yanagida, 2000).

Inactivation of the APC pathway produces cells that are unable to exit metaphase. The nuclear division cycle is uncoupled from cytokinesis as the CAR continues to form and eventually contracts while the cell is still mononucleate. This typically results in a 'cut' phenotype: the cell is 'untimely torn', and the single nucleus ripped apart (Hirano et al., 1986; Samejima et al., 1993; Yamada et al., 1997; Yanagida, 1998), but can also generate an anucleate cell. Initially, I studied when the cut phenotype appeared in *cut4.533 alp4-tdT:natMx6 mto1-GFP:kanMX, cut8.563 alp4-tdT:natMx6 mto1-GFP:kanMX* and *cut9.665 alp4-tdT:natMx6 mto1-GFP:kanMX* strains grown in YE5S medium. In these strains Alp4 is tagged with tandem dimer Tomato, a red fluorescent protein. Samples were taken at 30 min intervals after cultures were shifted to the restrictive temperature of 36°C. Cells were methanol-fixed and stained with DAPI and calcofluor to monitor nuclear division and septum formation (Figure 32). Cut cells are present from 2 hr after the shift to the restrictive temperature. This information was used to determine the optimal time to observe the cut phenotype after the shift to the restrictive temperature.

The experimental approach used to determine Mto1 localisation in cut mutant strains developed over time. Initially, I planned to quantify Mto1 localisation using single time-point images of live cells. Live cell imaging of fluorescent-tagged proteins in

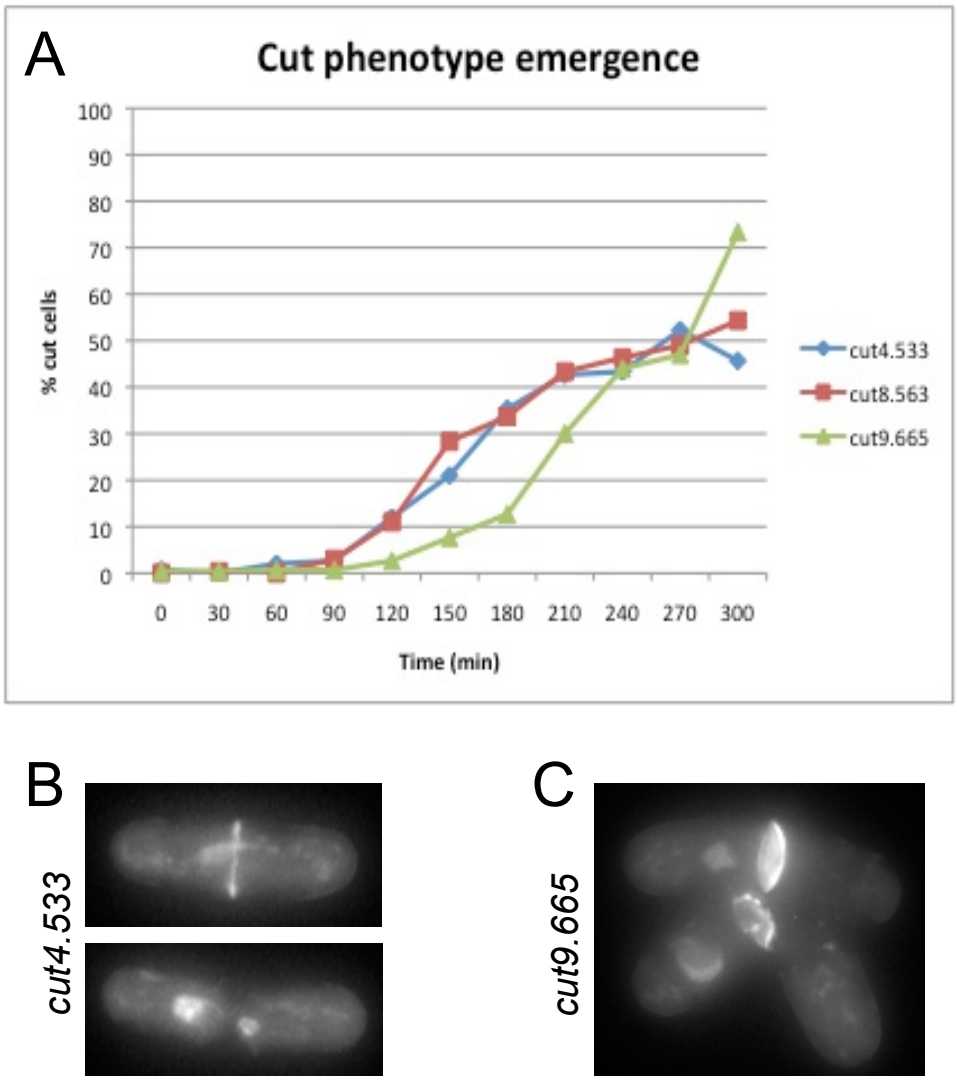

Figure 32 Emergence of the cut phenotype at the restrictive temperature

(A) Quantification of cells with a cut phenotype at 36°C. Cells were methanol-fixed and strained with DAPI and calcofluor. Cut cells are first observed ~120 min after the shift to the restrictive temperature. The number of cut cells begins to plateau after 210 min for *cut4.533* and *cut8.563***.** (B) and (C) Examples of cut phenotype stained with DAPI and calcofluor.

general gives a clearer image with less background staining than the immunostaining of fixed cells, such as was used previously ((Heitz et al., 2001). Alp4-tdT was to be used as an SPB marker to track spindle length, in combination with GFP-tagged Mto1.

A paper from the Oliferenko group, Temasek Life Sciences Laboratory, Singapore (Vjestica et al., 2008) was then published that described Rlc1-mCherry and also a nuclear marker, Uch2-mCherry (a ubiquitin carboxyl-terminal hydrolase, associated with the 26S proteasome). Combining these fluorescent proteins is an excellent approach for observing the cut phenotype, as the CAR can thus be seen to cut the nucleus. I decided to image GFP-tagged Mto1 in combination with Rlc1-mCherry and Uch2-mCherry using time-lapse spinning-disc confocal microscopy. Following Mto1 localisation as the cell cuts demonstrates that the cell does not have a functional APC pathway at the time of imaging. This establishes that any slight temperature fluctuations present during sample preparation have not reversed the arrest. Slide preparation and precautions taken to maintain the restrictive temperature are described in the Materials and Methods section. GFP-Mto1 was expressed from a repressed *nmt41* promoter to improve the signal at the higher temperature (~two-times over-expression relative to the native promoter).

Mto1 localisation to the CAR was monitored in live *nmt41:GFP-mto1 rlc1-mCherry uch2-mCherry* and *cut4.533 nmt41:GFP-mto1 rlc1-mCherry uch2-mCherry* cells from 2hrs after a shift to the restrictive temperature of 36°C. In the wild-type strain, Rlc1-mCherry joined the CAR prior to nuclear division. As the nucleus divided,

GFP-Mto1 appeared at the equator, co-localising with the CAR, and continued to co-localise as the CAR contracted and divided the cell (Figure 33, Movies 3 and 4). GFP-Mto1 localised to the cell equator in 8/8 wild-type cells. In the *cut4.533* strain, the CAR forms as in the wild-type strain. However, the mitotic spindle does not elongate and the nucleus does not divide. As with the wild-type, GFP-Mto1 appeared at the equator, co-localising with the CAR, and continued to co-localise as the CAR contracted. The CAR can clearly be seen to cut the nucleus (Figure 34, Movies 5 and 6). GFP-Mto1 localised to the cell equator in 8/8 *cut4.533* cells. Mto1 localisation to the CAR was then monitored in live wild-type, *cut4.533*, *cut8.563* and *cut9.665* cells expressing *nmt41*:GFP-Mto1, Rlc1-mCherry and Uch2-mCherry from 3hrs after a shift to 36°C. GFP-Mto1 localised to the cell equator for 13/13 wild-type cells (Figure 35, Movies 7 and 8). GFP-Mto1 was clearly observed to co-localise with the CAR in cells with a cut phenotype for 7/7 *cut4.533* cells (Figure 36, Movies 9 and 10), 20/20 *cut8.563* cells (Figure 37, Movies 11 and 12) and 5/5 *cut9.665* cells (Figure 38, Movies 13 and 14). Thus I conclude that the APC is not required for Mto1 localisation to the cell equator.

Next, I examined PAA formation in *cut4.533, cut8.563* and *cut9.665* strains at 36°C. If the PAA does not form, this would support the previous finding that γ-tubulin localisation to the eMTOC requires the APC. Strains were grown and imaged in YE5S media as some cut mutant strains do not exhibit the cut phenotype in minimal media. Temperature-sensitive mutant strains of *cut1- cut9* were originally isolated from cells growing on rich media (Hirano *et al.*, 1986). Media-related differences in phenotype expression may be due to differences in cAMP levels under different

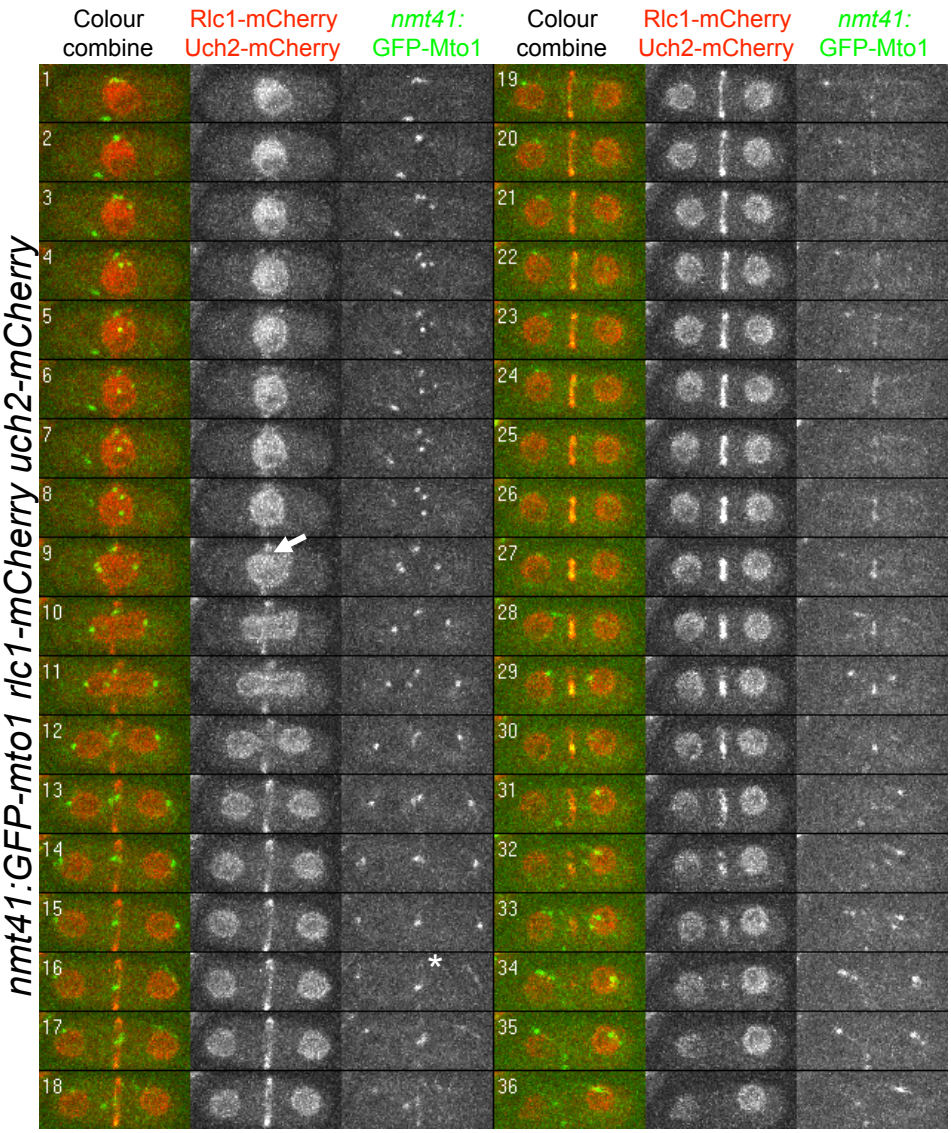

Figure 33 The APC is not required for localisation of Mto1 to the equator: wild-type cell after 2 hrs at 36°C

Time-lapse confocal microscopy of *nmt41:GFP-mto1 rlc1-mCherry uch2-mCherry* cell from 2 hr 06 min at 36°C. GFP-Mto1 can be seen at the SPBs. The CAR forms at the centre of the cell (marked by Rlc1-mCherry, arrow). The nucleus (marked by Uch2-mCherry) divides and GFP-Mto1 appears at the equator (*), co-localising with the CAR. The CAR then contracts, dividing the cell. Numbers indicate time elapsed (in min).

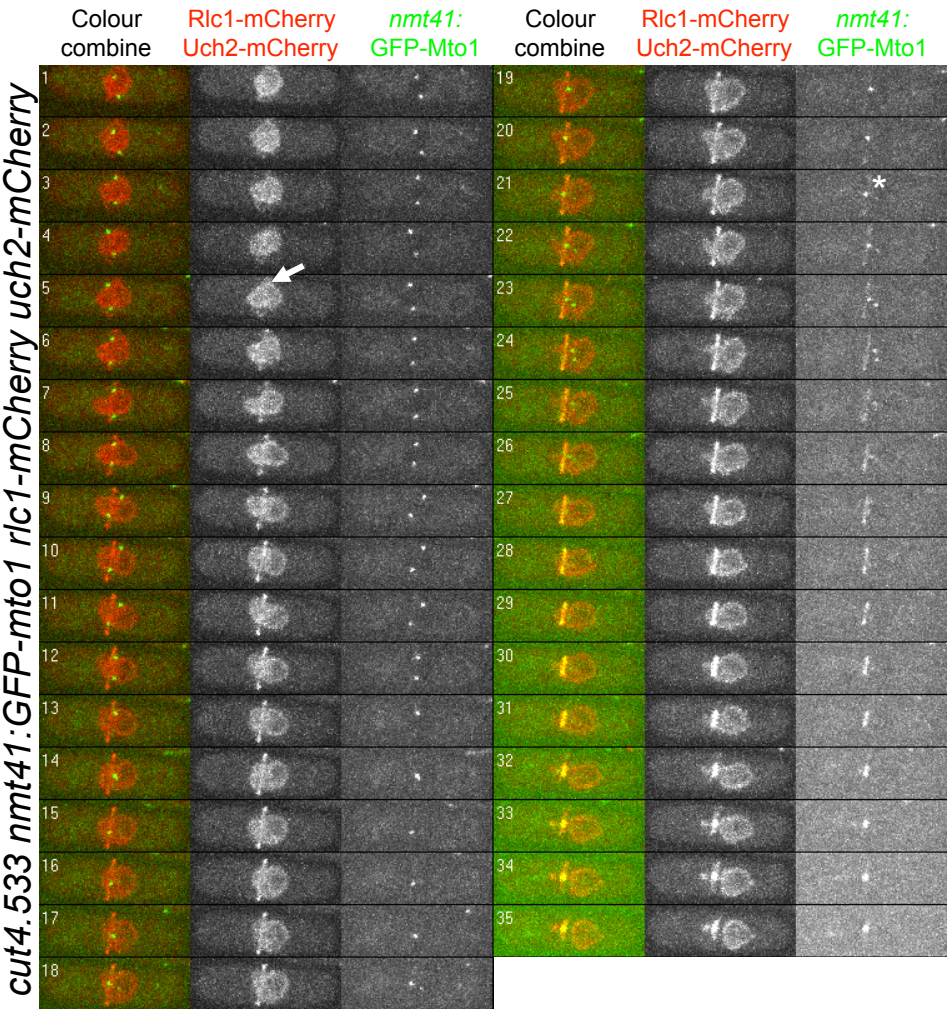

Figure 34 The APC is not required for localisation of Mto1 to the equator: *cut4.533* cell after 2 hrs at 36°C

Time-lapse confocal microscopy of *cut4.533 nmt41:GFP-mto1 rlc1-mCherry uch2-mCherry* cell from *2* hrs at 36°C. The CAR forms (arrow); GFP-Mto1 is present at the SPBs and later appears at the equator (*), co-localising with the CAR. The CAR then contracts, 'cutting' the single nucleus. Numbers indicate time elapsed (in min).

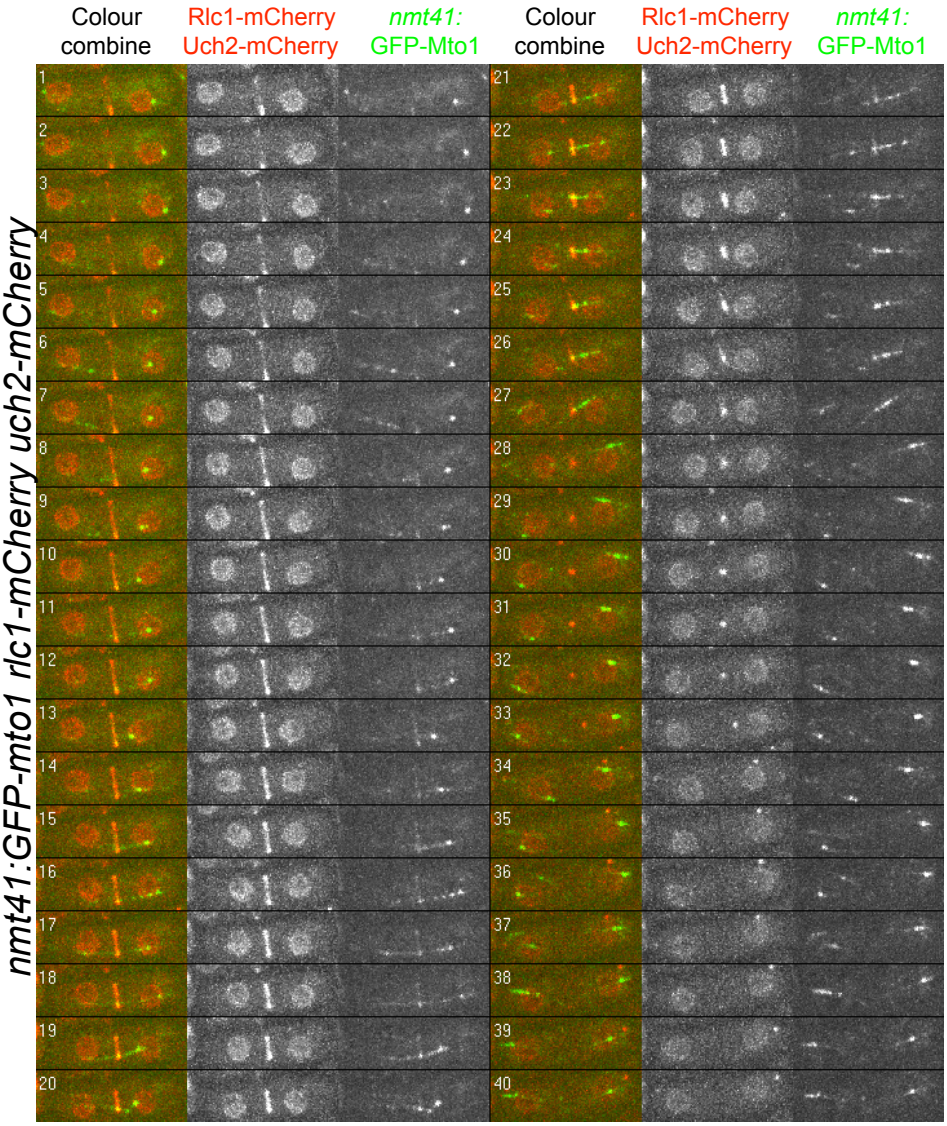

Figure 35 The APC is not required for localisation of Mto1 to the equator: wild-type after 3 hrs at 36°C

Time-lapse confocal microscopy of *nmt41:GFP-mto1 rlc1-mCherry uch2-mCherry* cell from 3 hr 20 hrs at 36°C. The CAR contracts dividing the cell. GFP-Mto1 localises to the cell equator and co-localises with the CAR. Numbers indicate time elapsed (in min).

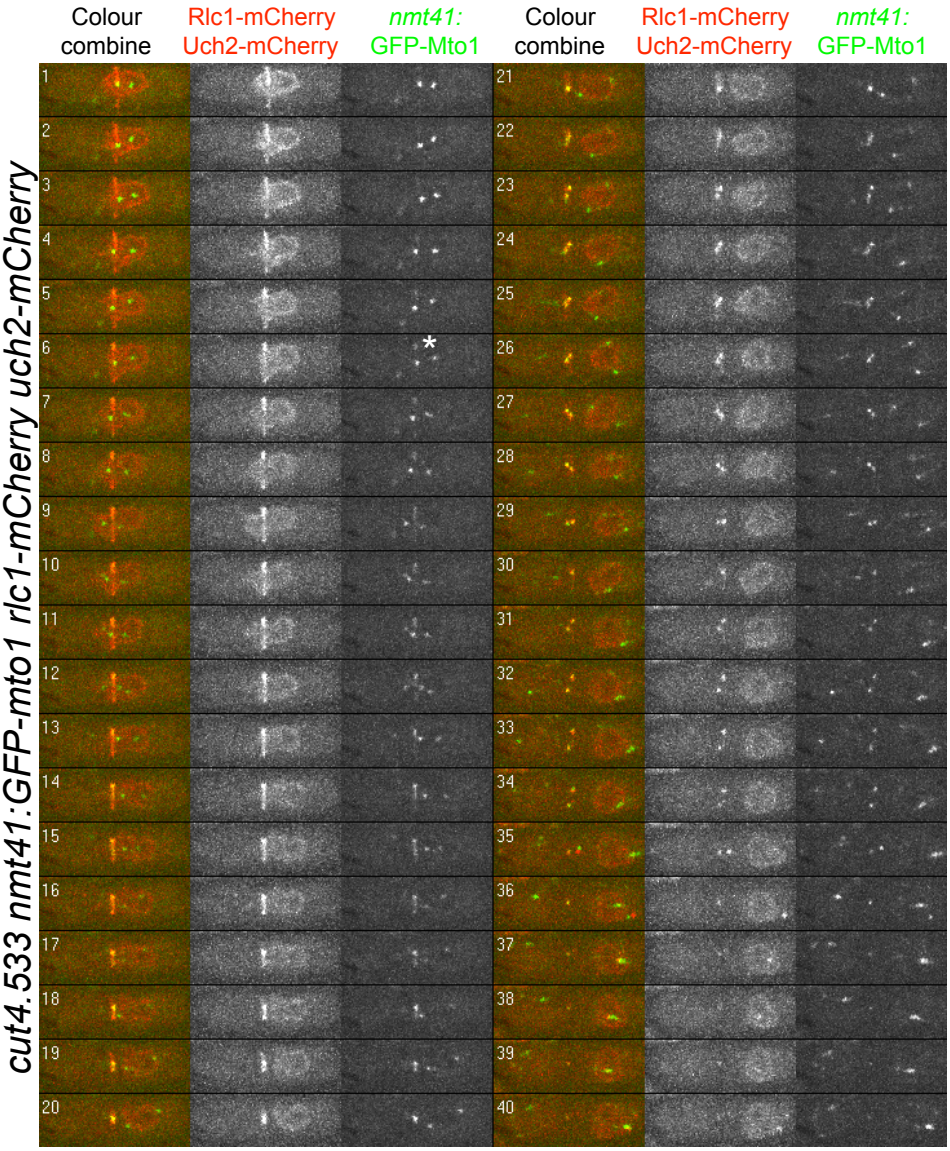

Figure 36 The APC is not required for localisation of Mto1 to the equator: *cut4.533* after 3 hrs at 36°C

Time-lapse confocal microscopy of *cut4.533 nmt41:GFP-mto1 rlc1-mCherry uch2-mCherry* cell from 3 hrs 08 min at 36°C. GFP-Mto1 is present at the SPBs and later appears at the equator (*), co-localising with the CAR. The CAR contracts, producing one mononucleate and one annucleate cell. Numbers indicate time elapsed (in min).

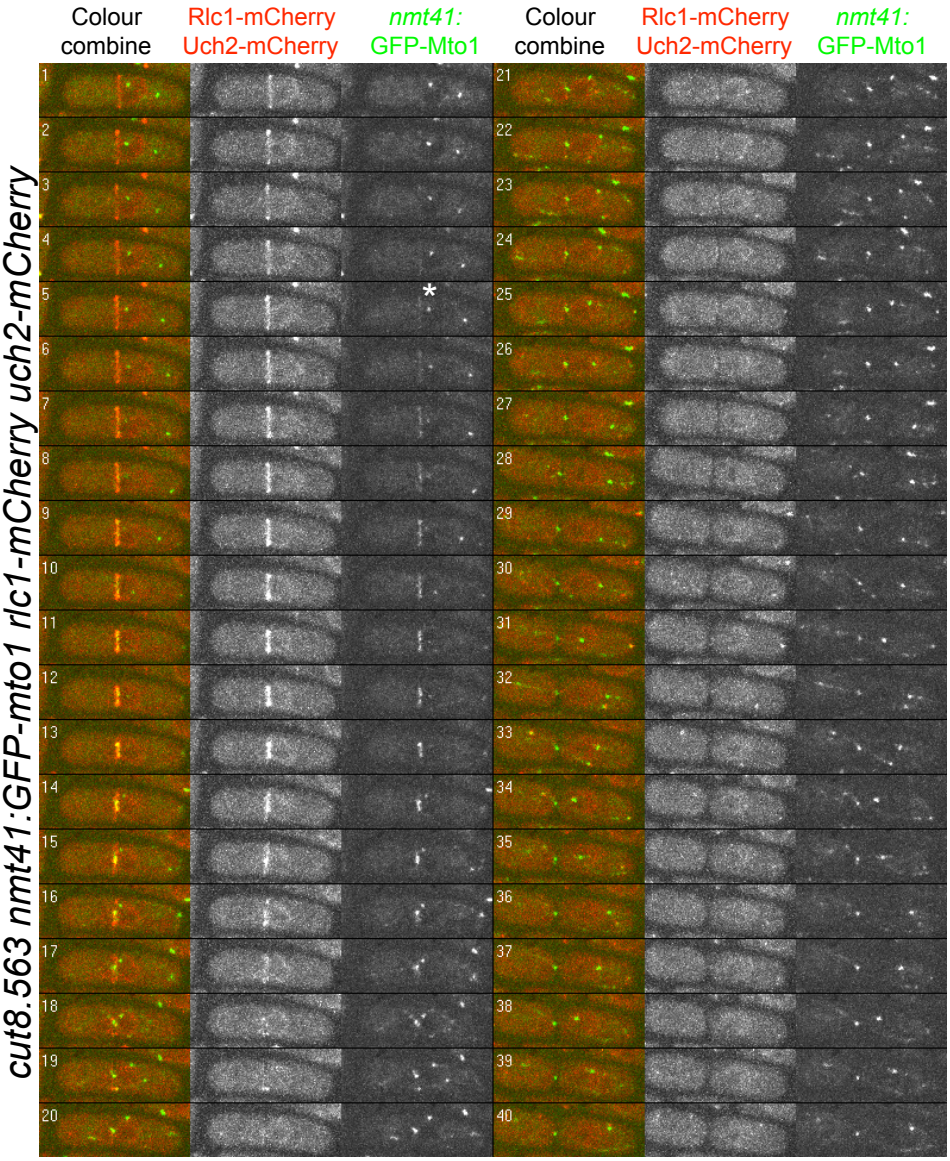

Figure 37 The APC is not required for equatorial localisation of Mto1: *cut8.563* after 3 hrs at 36°C

Time-lapse confocal microscopy of *cut8.563 nmt41:GFP-mto1 rlc1-mCherry uch2-mCherry* cell from 3 hrs 12 min at 36°C. GFP-Mto1 is present at the SPBs (and forms occasional cytoplasmic dots) and appears at the equator (*), co-localising with the CAR. The CAR contracts, cutting the nucleus. Numbers indicate time elapsed (in min).

Figure 38 The APC is not required for localisation of Mto1 to the equator: *cut9.665* after 3 hrs at 36°C

Time-lapse confocal microscopy of *cut9.665 nmt41:GFP-mto1 rlc1-mCherry uch2-mCherry* cell from 3 hrs 19 min at 36°C. GFP-Mto1 appears at the equator (*), prior to the CAR cutting the nucleus. Numbers indicate time elapsed (in min.

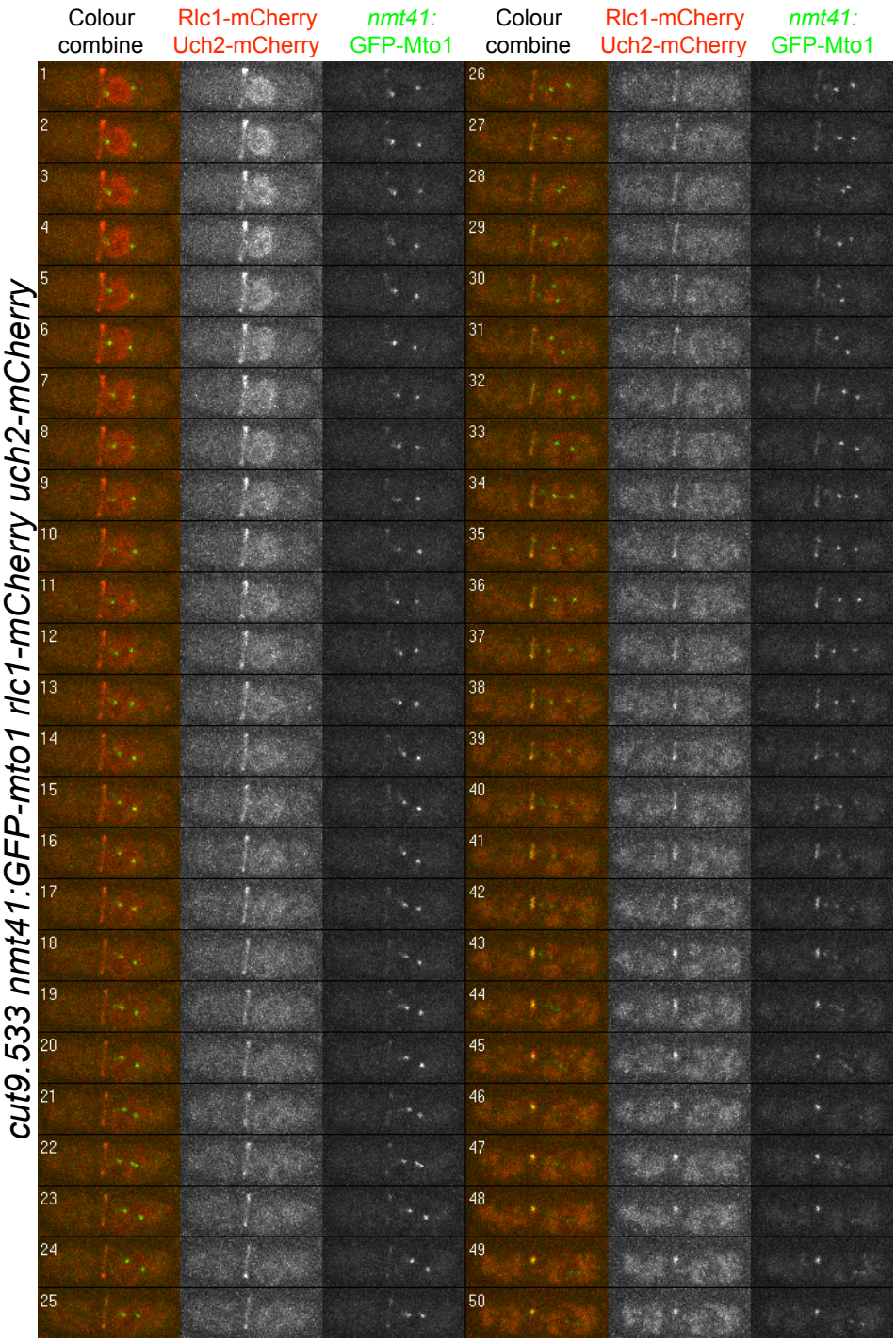
Colour combine
Rlc1-mCherry Uch2-mCherry
nmt41: GFP-Mto1
Colour combine
Rlc1-mCherry Uch2-mCherry
nmt41: GFP-Mto1
cut9.533 nmt41:GFP-mto1 rlc1-mCherry uch2-mCherry

growth conditions. I found that *cut4.533* cells did not show a cut phenotype when grown in minimal media 2, 4 and 5 hrs after transfer to 36ºC (data not shown). *cut8* and *cut9* were not tested. As YE5S media was used, GFP-Atb2 (to label microtubules) was therefore expressed from the *SV40* promoter (Jones et al., 1988) in place of the more commonly used *nmt81* promoter, whose expression would be strongly repressed in rich media. Strains were initially constructed to express *SV40:GFP-atb2* with no other fluorescently-tagged proteins in the cell; unexpectedly, the arrested short metaphase spindles appeared to elongate after an extended metaphase (data not shown).

I then introduced Rlc1-mCherry and Uch2-mCherry to the *SV40:GFP-atb2* APC-mutant strains, to better track the cut phenotype. Observations in these strains confirmed my initial observations as the cells showed a significant metaphase arrest, but the mitotic spindle then elongated either before or during CAR contraction (11/12 dividing cells *cut4.533*, with one dividing cell where the CAR contracted and the mitotic spindle did not elongate, Figure 39, Movies 15 and16; 6/6 dividing cells *cut8.563* Figure 40, Movies 17 and 18 and 7/7 cells *cut9.665* Figure 41, Movies 19 and 20). The nucleus is either cut or in the case of *cut8.563* appears to divide prior to CAR formation. Overall, the strains did not show normal cell division, but neither did they show a classic cut phenotype with nuclear division arrest, despite the strains being temperature sensitive (assessed by growth on solid media containing the dye phloxin B, which preferentially stains dead cells, at 25°C and 36°C) The imaging treatment used was identical to that used previously.

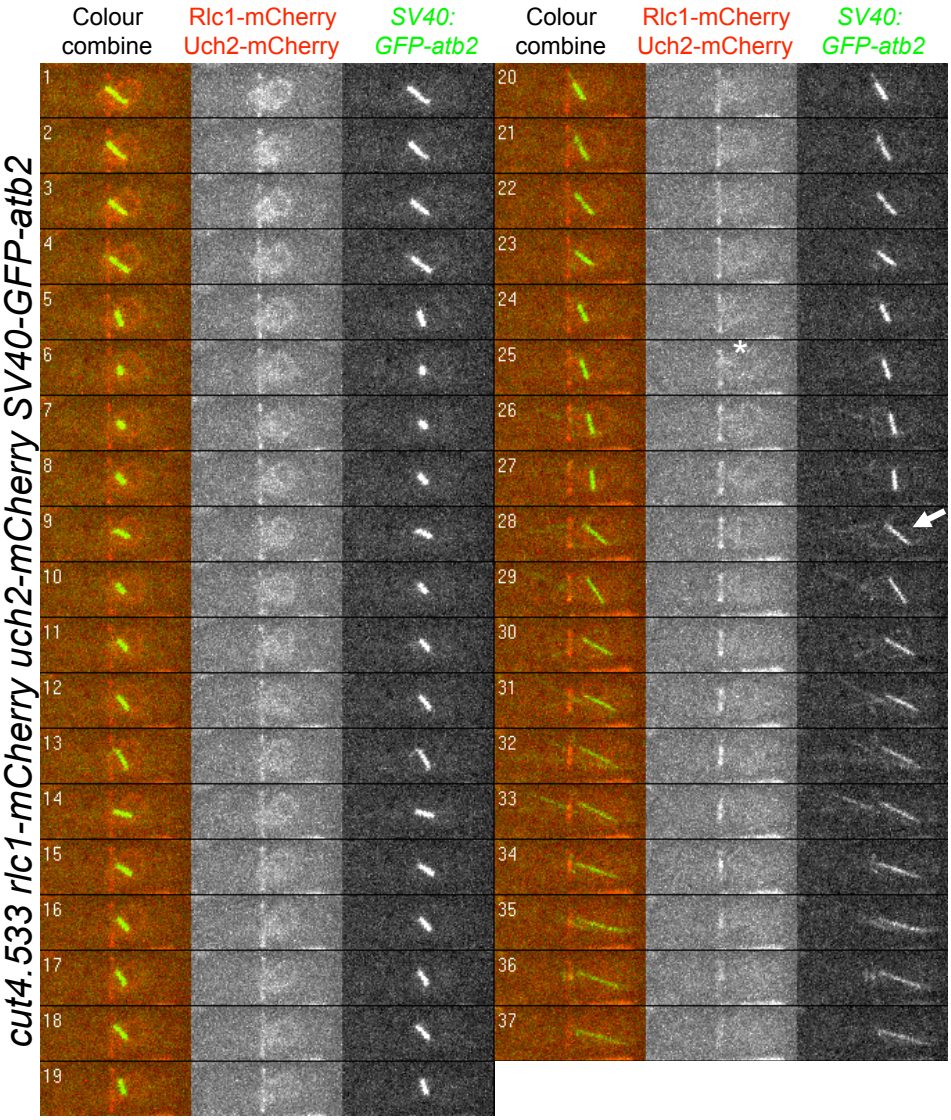

Figure 39 PAA formation: *cut4.533* after 3 hrs at 36°C

Time-lapse confocal microscopy of *cut4.533 rlc1-mCherry uch2-mCherry SV40:GFP-atb2* cell from 3hrs 10 min incubation at 36°C. The CAR starts to contract (*) while the cell is mononucleate, but the mitotic spindle then elongates (arrow). Faint microtubules appear that span the horizontal axis of the cell. Numbers indicate time elapsed (in min).

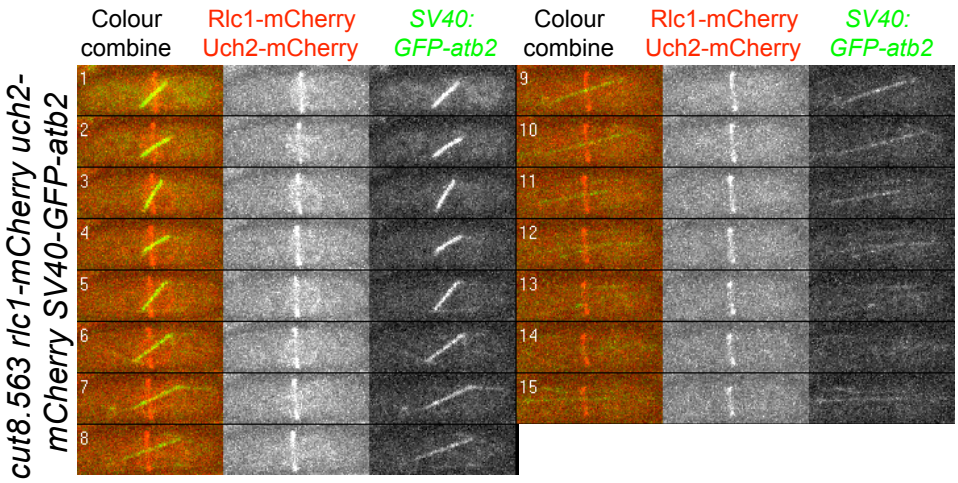

Figure 40 PAA formation: *cut8.563* after 3 hrs at 36°C

Time-lapse confocal microscopy of *cut8.563 rlc1-mCherry uch2-mCherry SV40:GFP-atb2* cell from 3hrs 09 mins incubation at 36°C onwards. The mitotic spindle elongates and the nucleus divides as the CAR contracts. Numbers indicate time elapsed (in min).

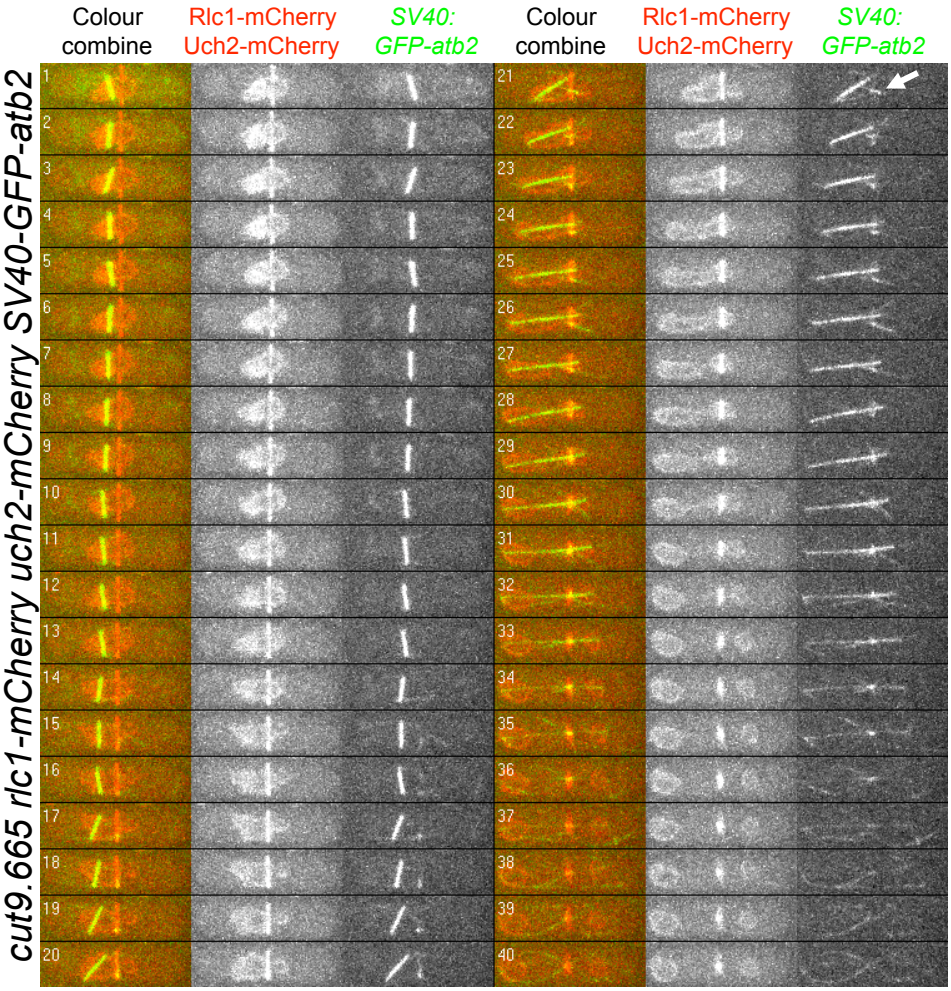

Figure 41 PAA formation: *cut9.665* after 3 hrs at 36°C

Time-lapse confocal microscopy of *cut9.665 rlc1-mCherry uch2-mCherry SV40:GFP-atb2* cell from 3 hr 15 min at 36°C. After an extended metaphase, the mitotic spindle elongates as the CAR contracts, cutting the nucleus. Some microtubule nucleation is seen from the CAR (arrow) Numbers indicate time elapsed (in min).

I then imaged the wild-type *rlc1-mCherry uch2-mCherry SV40:GFP-atb2* strain and found that this strain did not undergo a normal cell division at 36°C . Strikingly, this strain had significant defects in nuclear positioning following nuclear division (6/7 dividing cells, with one cell showing a normal division Figure 42, Movie 21, Movie 23). These defects took the form of one nuclei moving close to the CAR, independently of the movement of the other nucleus. In one notable example a newly separated nucleus moves from the cell tip to the centre of the cell, but then passes through the CAR (Figure 43, Movie 22). It was not clear from the images whether PAAs formed in the wild-type strain. Imaging has not been carried out at 25°C, so it is not known whether defects in cell division are also present at a lower temperature or if the nuclear positioning phenotype is temperature-dependent. The unusual behaviour of the wild-type strain led me to suspect that a suppressor mutation to the cut phenotype may be present in the original *SV40:GFP-atb2* parent strain (KS4956).

KS4956 was the kind gift of Fred Chang, Columbria University, USA (originally numbered FC1234). The strain was constructed by integration of the plasmid pMP103 (Pardo and Nurse, 2005) into strain FC421 *h- leu1- ura4- ade6-* at the *leu1* locus (Bratman and Chang, 2007). Specific integration at this locus was confirmed by backcrossing; there is no mention of the strain being sequenced to additionally confirm the mutation. The *apc10* gene lies ~420 bp upstream of *leu1* and could have been disrupted during the plasmid integration, although the *apc10Δ* null strain is inviable (Kominami et al., 1998).

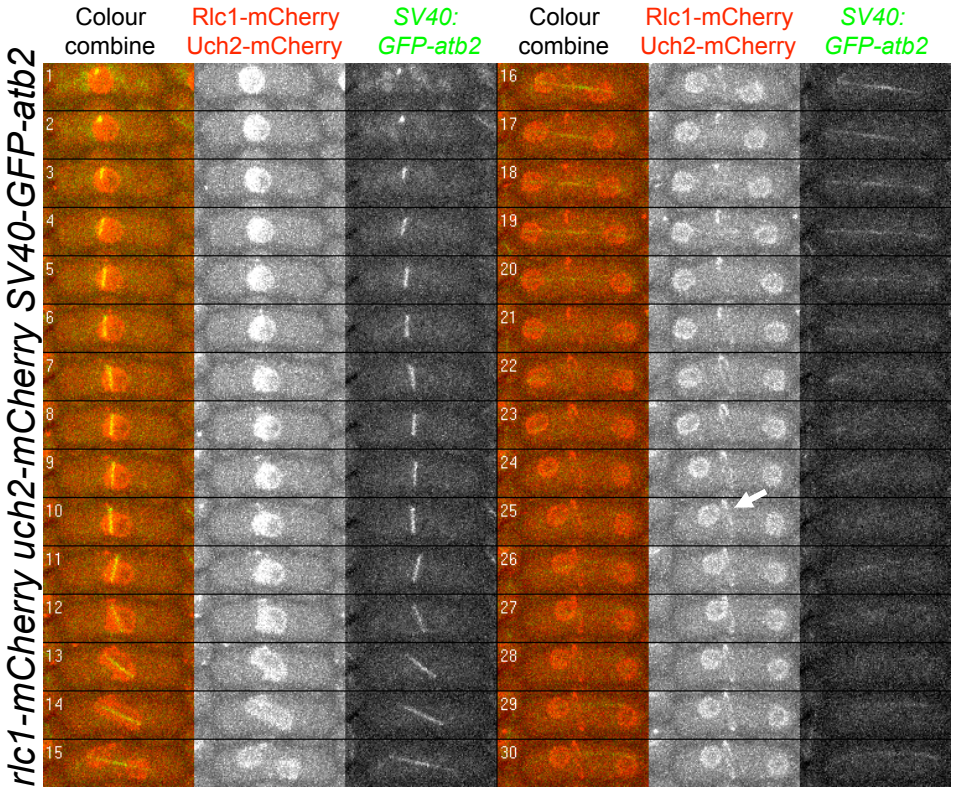

Figure 42 PAA formation: wild-type after 3 hrs at 36°C

Time-lapse confocal microscopy of *rlc1-mCherry uch2-mCherry SV40:GFP-atb2* cells from 3hrs 13 min incubation at 36°C. The mitotic spindle elongates as the cell through pro-metaphase to anaphase. The nucleus divides and the nuclei segregate to the cell ends. The left nucleus then moves back towards the CAR (arrow). Numbers indicate time elapsed (in min).

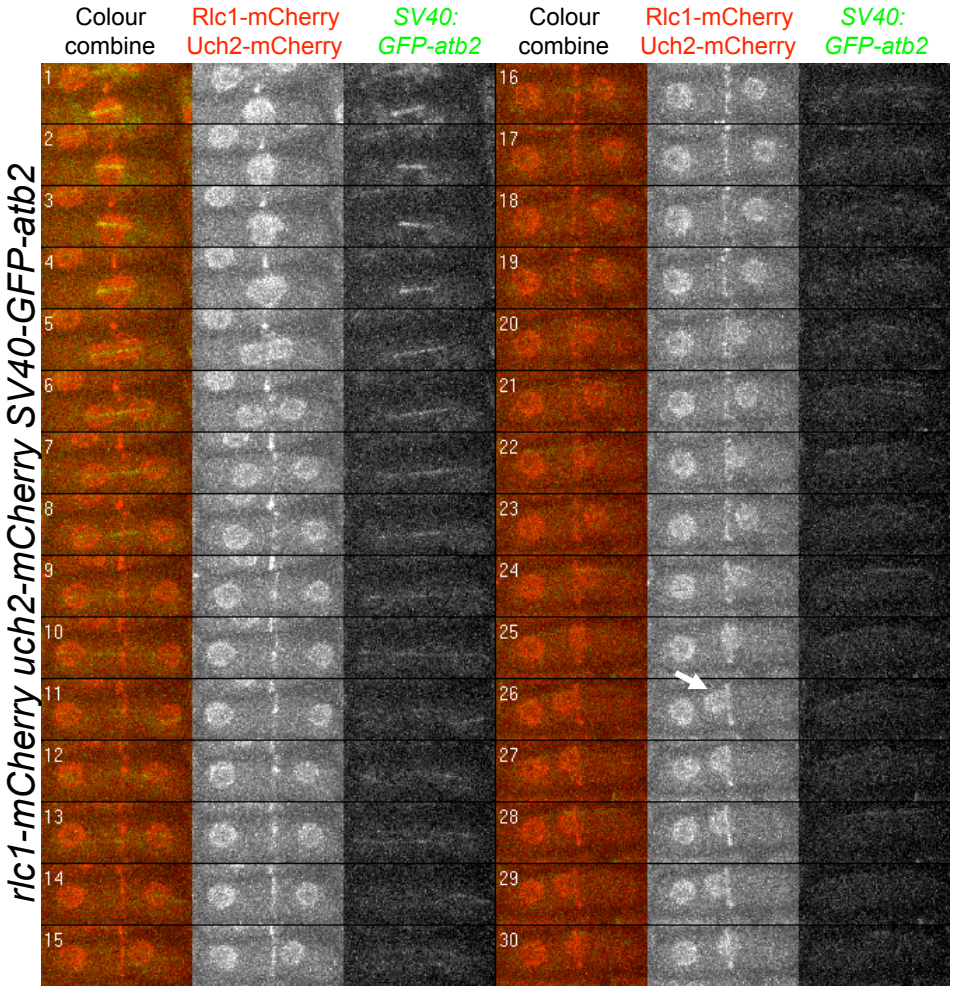

Figure 43 PAA formation: wild-type after 3 hrs at 36°C

Time-lapse confocal microscopy of *rlc1-mCherry uch2-mCherry SV40:GFP-atb2* cells from 3hrs 13 min incubation at 36°C. The right nucleus passes through the CAR (arrow). Numbers indicate time elapsed (in min).

Whatever the mutation in the *SV40:GFP-atb2* strain, it appears to be closely linked to the integrated gene as the parent strain (KS4956) was crossed to multiple strains during the process of constructing the different strains in their final forms. Due to these difficulties, whether APC mutants have a PAA remains an open question.

Requirement of the septation initiation network for PAA formation

The SIN pathway is also required for the localisation of γ-tubulin at the eMTOC (Heitz et al., 2001). I therefore asked whether the appearance of Mto1 at the equator requires an active SIN pathway.

I started by looking at the accumulation of nuclei in SIN mutant strains with time, after transfer to the restrictive temperature. Mutations in the SIN genes create cells that are unable to complete cytokinesis: cells undergo multiple rounds of nuclear division (Balasubramanian et al., 1998). The CAR forms with each set of nuclear division, and disassembles without contracting. Cells were formaldehyde-fixed and stained with DAPI to monitor the number of nuclei present in the cell and phalloidin to visualise CARs. Binucleate cells accumulated over wild-type levels from 3 hr after shift to the restrictive temperature of 36.5° (Figure 44). The proportion of cells with a CAR generally peaked after 3 hr (with the exception of *cdc14.118* where it peaked at 4 hr; this seems to correlate with a slower appearance of binucleate cells in *cdc14.118*), but CAR formation continues at 4 hr after the shift to the restrictive temperature as new binucleate cells develop (Figure 45).

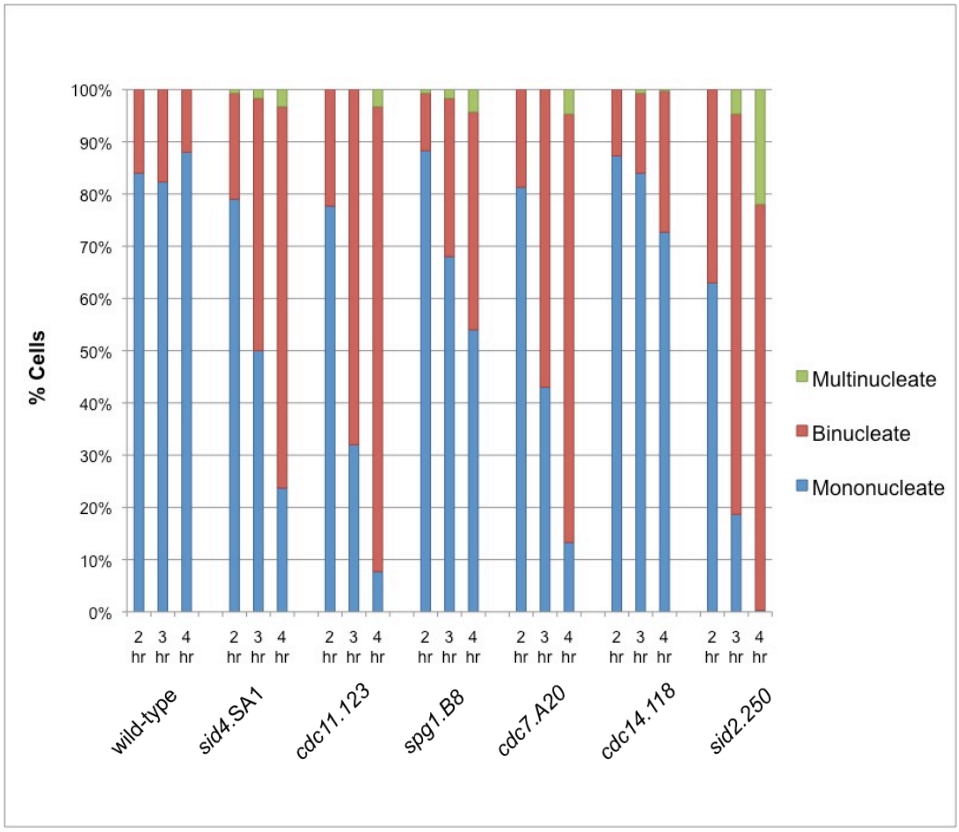

Figure 44 Accumulation of nuclei in SIN mutant strains

Quantification of mononucleate, binucleate and multinucleate cells for SIN mutant strains grown in minimal media after 2, 3 and 4 hr at 36.5°C (restrictive temperature). wild-type cells are predominantly mononucleate, with the proportion of binucleate cells remaining constant over time. The proportion of binucleate cells increases with time for SIN mutant strains; a small number of multinucleate cells seen at later time points. Cells were formaldehyde-fixed and stained with DAPI and phalloidin. N = 300 cells.

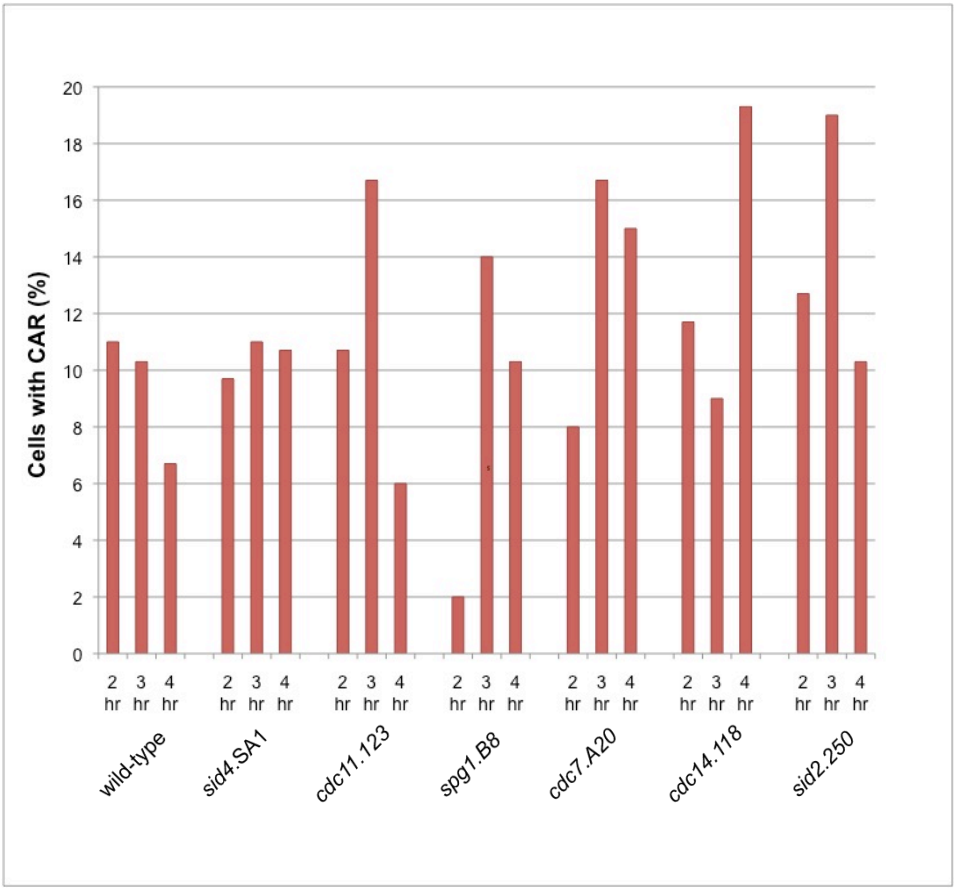

Figure 45 Proportion of cells with a CAR for SIN mutant strains

Quantification of cells with a CAR for SIN mutant strains grown in minimal media after 2, 3 and 4 hr at 36.5°C (restrictive temperature). The number of cells with CARs peaks at 3 hr after the shift to the restrictive temperature. CARs are also seen after 4 hr. Cells were formaldehyde-fixed and stained with DAPI and phalloidin. N = 300 cells.

Next I examined PAA formation in SIN temperature-sensitive mutant strains expressing GFP labelled anti-tubulin from the *nmt81* promoter. At the permissive temperature (25°C), PAAs appeared immediately preceding or at the time of mitotic spindle breakdown for 6/6 *nmt81:GFP-atb2 sid4-SA1* dividing cells, 10/10 *cdc11-123 nmt81:GFP-atb2* dividing cells and 8/8 *cdc7-24 nmt81:GFP-atb2* dividing cells (Figure 46, Movies 24-29).

In contrast, at the restrictive temperature of 36.5°, PAAs were not seen in SIN-deficient mutant strains (3/3 *nmt81:GFP-atb2 sid4-SA1* cells with mitotic spindle breakdown, 9/9 *cdc11-123 nmt81:GFP-atb2* cells with mitotic spindle breakdown and 12/12 *cdc7-24 nmt81:GFP-atb2* cells with mitotic spindle breakdown; Figure 47, Movies 32-37). Time-lapse movies were taken from approximately 2.5 hrs after the shift to 36.5°, to capture the appearance of the maximum number of binucleate cells. PAA formation was seen for 7/7 dividing wild-type *nmt81:GFP-atb2* cells (Figure 47, A, Movies 30 and 31) However, PAA formation was less robust at 36.5°C than at the 25°C and cells did not form microtubule nucleation until some time after mitotic spindle disassembly (Panel A of Figure 47, an 11-minute gap is seen between mitotic spindle disassembly and PAA appearance). At this point septation has begun (based on the width of the PAA, suggesting that CAR contraction had commenced and corresponding pinching in of the cell at the division site). SIN-mutant strains arrest prior to septation as the CAR disassembles without contraction. Since the wild-type control strain did not form a PAA until it had progressed further into the cell cycle than the SIN mutants are able

Figure 46 PAA formation in SIN mutant strains at 25°C

Time-lapse confocal microscopy of (A) *nmt81:GFP-atb2 sid4-SA1* and (B) *cdc11-123 nmt81:GFP-atb2* and (C) *cdc7-24 nmt81:GFP-atb2* cells at 25°C (permissive temperature), showing PAA formation. First nucleation at the cell equator is seen immediately preceding mitotic spindle breakdown. Numbers indicate time elapsed (in min).

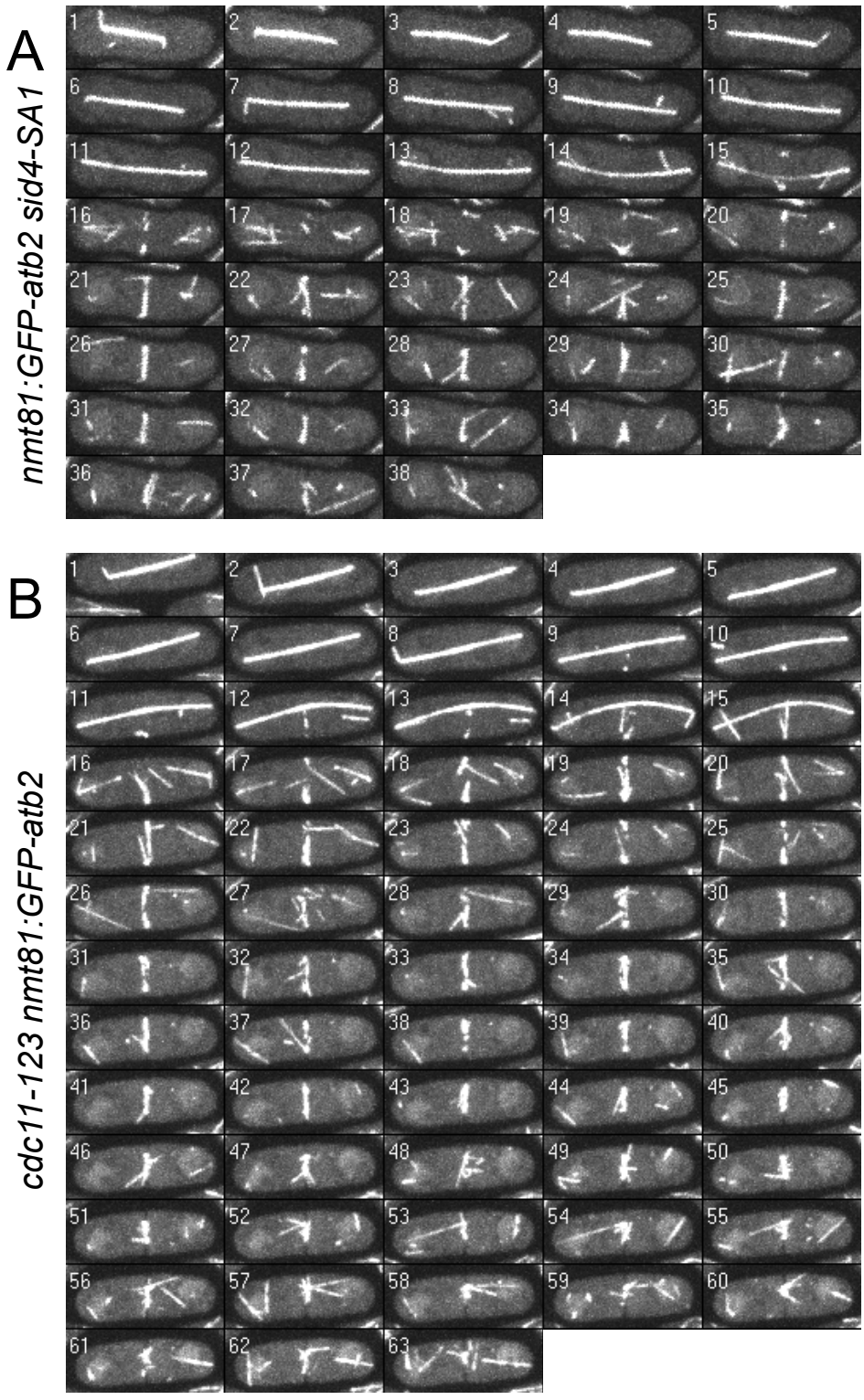
A
nmt81:GFP-atb2 sid4-SA1
B
cdc11-123 nmt81:GFP-atb2

C

cdc7-24 nmt81:GFP-atb2

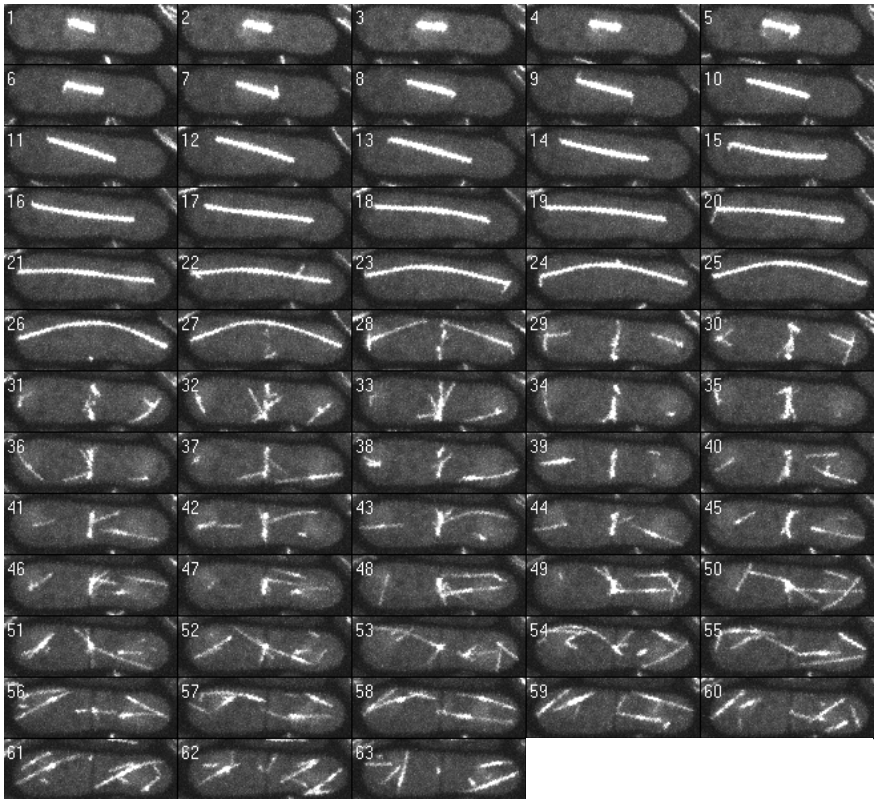

Figure 47 PAA formation in SIN mutant strains at 36.5°C

Time-lapse confocal microscopy of (A) *nmt81:GFP-atb2,* (B) *nmt81:GFP-atb2 sid4-SA1,* (C) *cdc11-123 nmt81:GFP-atb2* and (D) *cdc7-24 nmt81:GFP-atb2* cells at 36.5°C (restrictive temperature). The PAA is present for the wild-type control, but nucleation is delayed relative to PAA at 25°C and does not appear until septum formation can be seen rather than immediately prior to mitotic spindle disassembly. Numbers indicate time elapsed (in min). Filming started 2 hr 55 min, 2 hr 17 min, 2 hr 35 min and 2 hr 17 min after the shift to the restrictive temperature respectively.

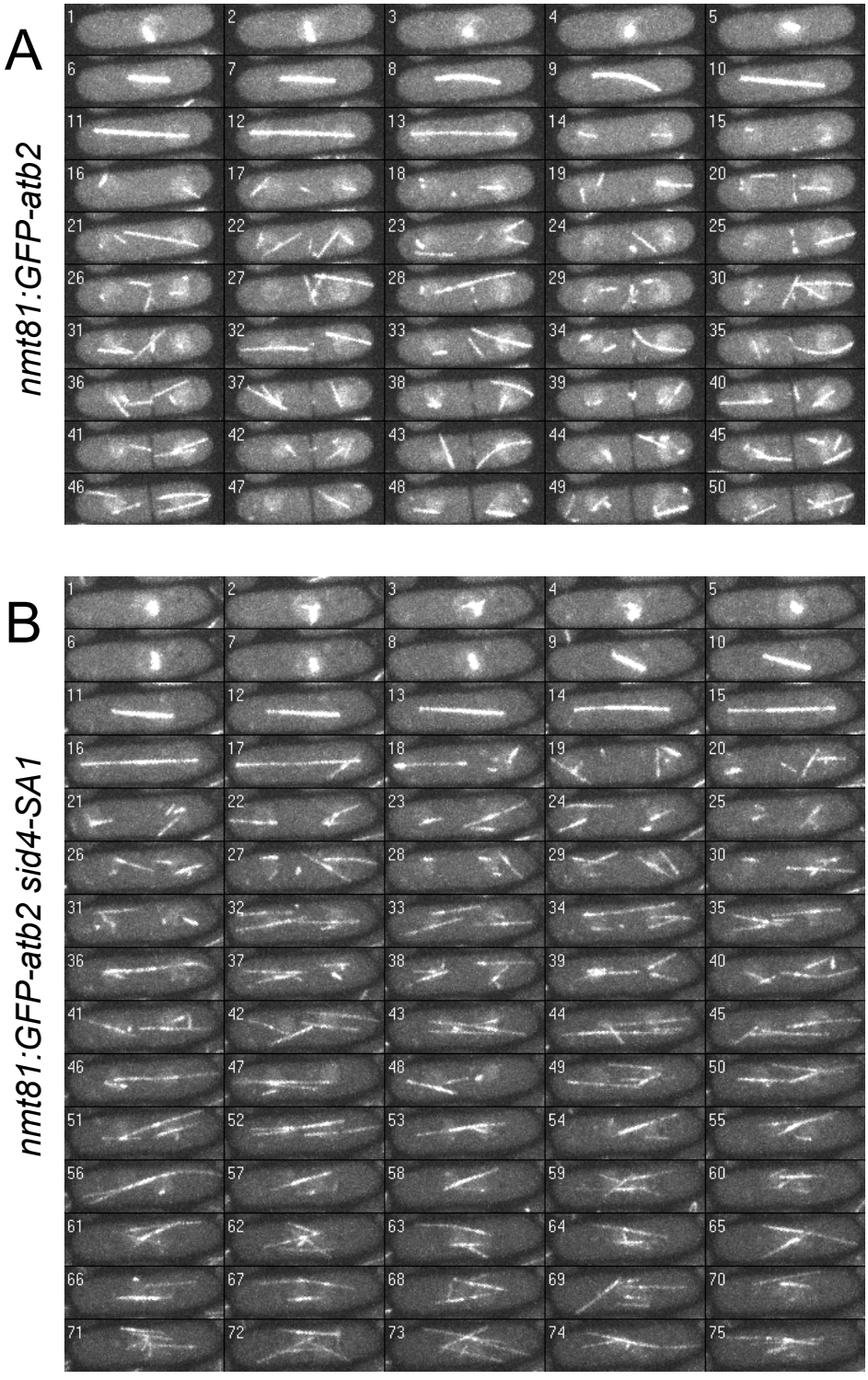
A
nmt81:GFP-atb2
B
nmt81:GFP-atb2 sid4-SA1

C

cdc11-123 nmt81:GFP-atb2

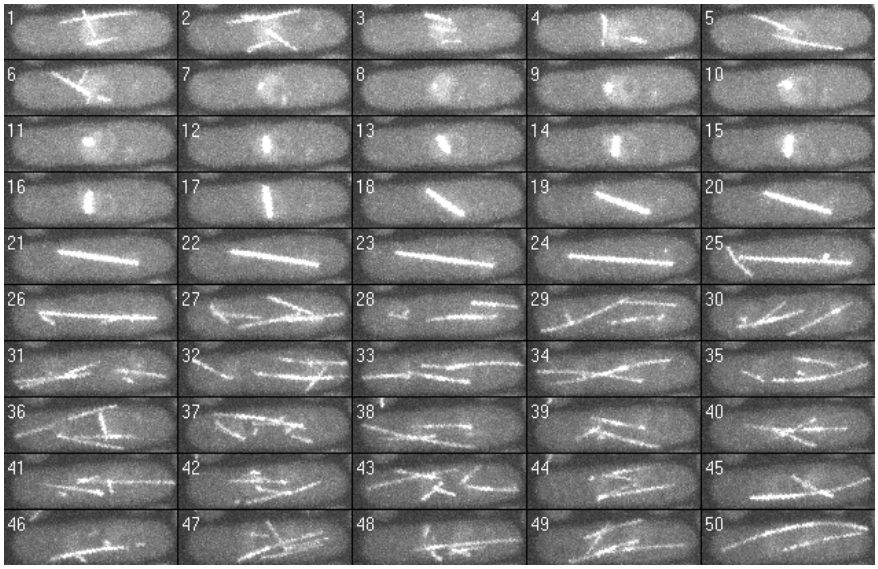

D

cdc7-24 nmt81:GFP-atb2

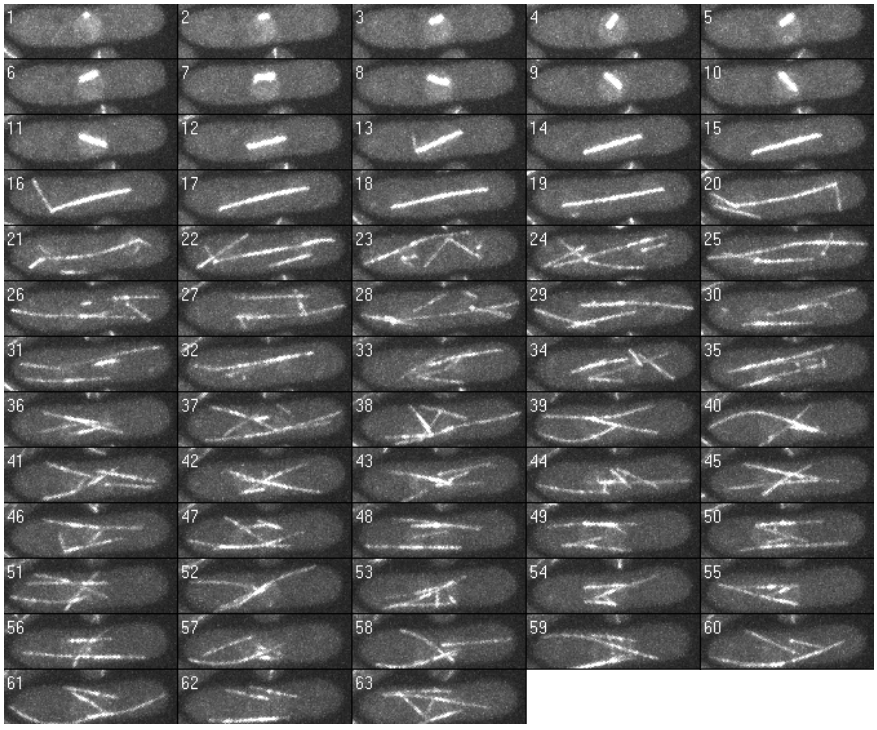

to, I conclude that the lack of PAAs in SIN cannot be attributed to a requirement for the SIN pathway using time-lapse microscopy.

The septation initiation network is not required for localisation of Mto1 to the equator

I then moved on to determine whether the SIN pathway was required for Mto1 localisation. Mto1 localisation to the CAR was monitored using time-lapse spinning-disc confocal microscopy of live *nmt41:GFP-mto1 rlc1-mCherry uch2-mCherry* and *sid4-SA1 nmt41:GFP-mto1 rlc1-mCherry uch2-mCherry* from 2.5 hrs after a shift to the restrictive temperature of 36.5°C. Cells were grown in minimal media with 15 μM thiamine to repress expression of from the *nmt41* promoter. The conditional *sid4-SA1* mutant was selected for analysis because Sid4 functions upstream of the other SIN components; disabling Sid4 therefore disrupts the entire SIN pathway. The mCherry proteins used are the same as those used previously to examine the cut phenotype. Here the nuclear and CAR markers are used to confirm that *sid4-SA1* mutant cells do not complete cytokinesis: in the mutants the CAR forms and the nucleus divides, but the CAR is not triggered to contract and instead disassembles. GFP-Mto1 localised to the cell equator in 13/13 wild-type cells prior to the start of septation (Figure 48, Movies 38, 39). For *sid4-SA1* GFP-Mto1 localised to the cell equator in 9/9 cells with a CAR (Figure 49, Movies 40, 41). Thus Mto1 localisation to the cell equator does not require the SIN.

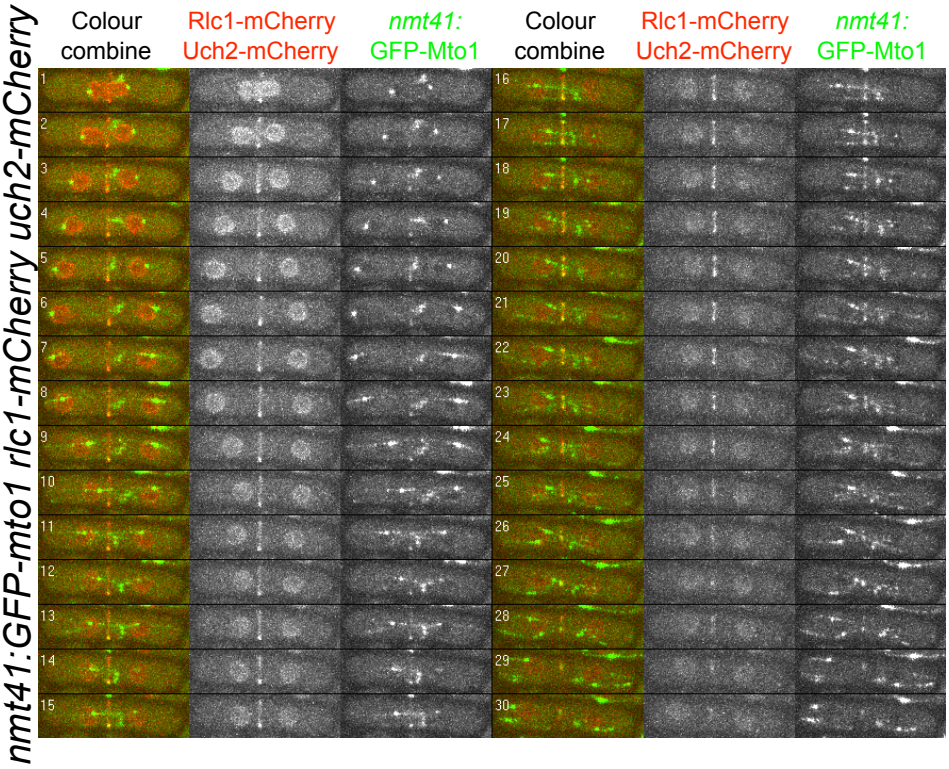

Figure 48 The SIN is not required for localisation of Mto1 to the equator: wild-type cell at 36.5°C

Time-lapse confocal microscopy of *nmt41:GFP-mto1 rlc1-mCherry uch2-mCherry* cell from 2 hrs 08 mins at 36.5°C. Mto1 appears at the equator and is present as the CAR contracts. Numbers indicate time elapsed (in min).

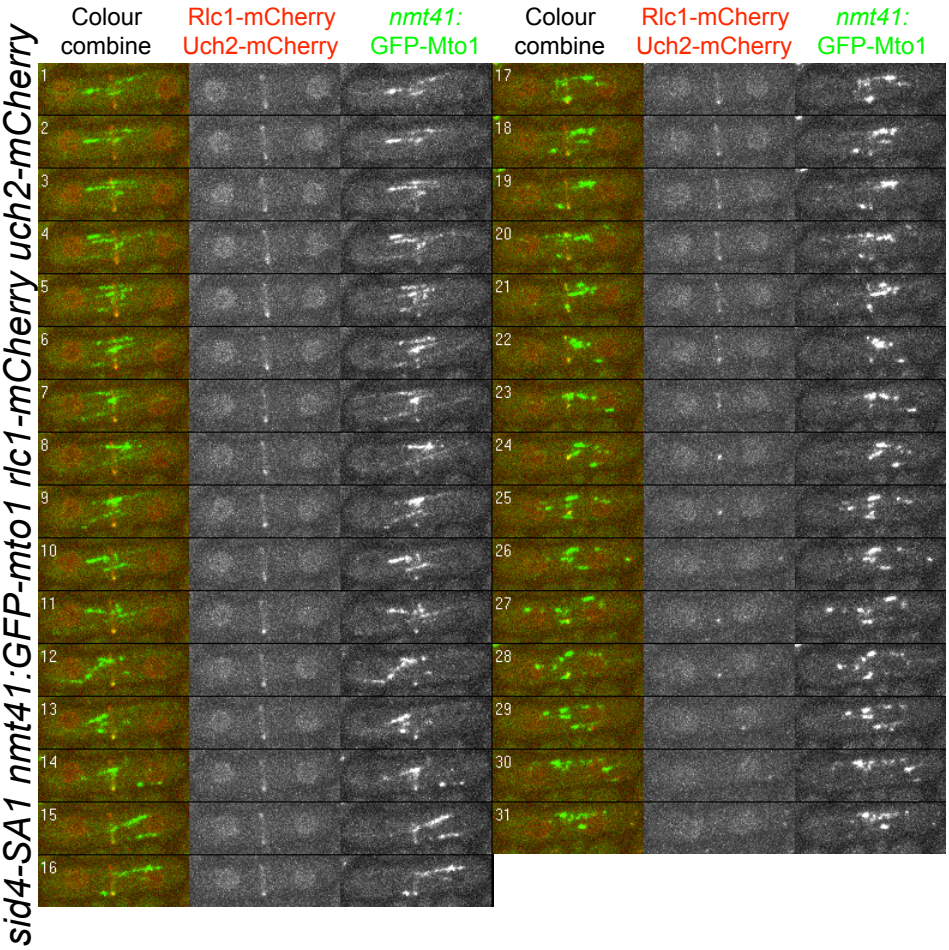

Figure 49 The SIN is not required for localisation of Mto1 to the equator: *sid4-SA1* cell at 36.5°C

Time-lapse confocal microscopy of *sid4-SA1 nmt41:GFP-mto1 rlc1-mCherry uch2-mCherry* cell from 2 hrs 09 mins at 36.5°C. Mto1 is present at the CAR. The CAR then breaks down, leaving a binucleate cell. Numbers indicate time elapsed (in min).

Discussion

Anaphase and Mto1 localisation

In wild-type cells Mto1 localises to the site of the prospective eMTOC during anaphase and this localisation requires the CAR. I found that Mto1 is not present at the cell equator in arrested *nda3-KM311* cells, despite these cells having a CAR. This suggested that the metaphase-anaphase transition is important for regulating Mto1 localisation, possibly due to cell-cycle dependent post-translational modification regulating the Myp2-Mto1 interaction. However, paradoxically, Mto1 is present at the equator in APC mutant cells that do not enter anaphase, suggesting that the cell does not need to have entered anaphase for Mto1 to localise to the equator. Mto1 is also present at the equator in cells released from an *nda3-KM311*-arrest that have a short mitotic spindle. These results are not immediately easy to reconcile. If anaphase is not required for Mto1 localisation to the equator, why is Mto1 not present at the equator during *nda3*-arrest?

It is possible that Mto1 does localise to the equator earlier in the *nda3*-arrest, remaining at the equator for the 30% of *nda3*-arrested cells observed to have Mto1 at the equator when observing live cells, but is no longer present at the equator in the majority of cells after 9 hrs at 18°C. Mto1 was not seen at the equator using immunostaining of fixed cells, perhaps because the punctate staining seen with anti-Mto1 staining, makes it difficult to detect low levels of protein at the equator. Mto1 was also slightly over-expressed in the live cell imaging. It is not clear why Mto1 would disassociate from the cell equator having once localised, but this may be due

to alterations in CAR structure that cause the CAR to be broader during *nda3-KM311* arrest than it is in wild-type cells (Chang *et al.*, 1996).

Alternatively Mto1 may indeed fail to localise to the equator during *nda3-KM311* arrest due to cell-cycle dependent events that take place in the APC mutants, but not during *nda3-KM311* arrest. If so, the *nda3-KM311* arrest may block CAR maturation and impair Mto1 localisation by affecting Myp2 incorporation into the CAR. Future work should determine whether Myp2 is present at the cell equator during *nda3-KM311* arrest.

In the example of mutant cells where Mto1 is present at the equator prior to anaphase (in APC-mutant strains and in some *nda3-KM311*-arrested cells soon after release), the cell has experienced an extended period in metaphase. This time may be necessary for the CAR to develop to the point where Myp2 joins the CAR; Mto1 may not appear earlier in the cell cycle during normal cell division because of the time necessary for the CAR to mature. I conclude that Mto1 localisation does not require the cell to have entered anaphase, ruling out cell cycle direct regulation of Mto1 localisation to the cell equator.

Mto1 localisation is independent of regulation known to affect eMTOC formation

Mto1 is present at the equator in strains that do not have an active APC or SIN pathway. These pathways have both been identified as necessary for eMTOC formation, as γ-tubulin is reportedly absent from the equator when these pathways

are disrupted (Heitz *et al.*, 2001). This data rules out the model that APC and SIN regulation of γ-tubulin recruitment to the eMTOC is enacted through control of Mto1 localisation and suggests that the interaction between Mto1 and the γ-TuC is instead regulated. This is an intriguing hypothesis, but to support the model it is necessary to be confident that γ-tubulin is indeed absent from the eMTOC when the SIN or APC are inactivated.

Previous work suggested that PAA formation requires the SIN (Pardo and Nurse, 2003), consistent with a lack of γ-tubulin. I replicated this work and also found that PAAs do not form in conditional SIN mutant strain at the restrictive temperature. However, defects in PAA development in wild-type strains grown at the restrictive temperature hinder interpretation of the findings and suggest that the lack of PAAs could be artifactual. In wild-type cells at 36.5°C, the PAA did not form until the first signs of septation were seen. Therefore the effects of the high temperature cannot be separated from the inactivation of the SIN and no conclusion can reliably be drawn. It is not clear why PAA formation is altered at high temperature; Mto1 expressed at native levels localises poorly to the equator at high temperature and this may be a contributing factor.

Another approach that could be used to address the question of PAA formation in SIN mutant strains is spore germination of null mutants in the SIN pathway. Spores are unable to undergo cell division in the absence of the SIN, but form CARs and undergo a number of nuclear divisions (Krapp et al., 2001). Recent work by I. Samejima, (Sawin laboratory) observing microtubule nucleation in germinating

cdc11Δ spores showed mitotic spindle formation, but no PAA formation, suggesting that PAA formation does indeed require the SIN.

A role has been identified for the SIN pathway in CAR assembly (Hachet and Simanis, 2008), with SIN mutants failing to form a homogeneous CAR. Defects in CAR assembly could affect eMTOC function and PAA formation, although my findings show that Mto1 localises to the CAR in SIN mutants. Myp2 presence at the CAR is also reported to be SIN-independent (Wu et al., 2003), although the signal intensity of Myp2-YFP is weak in the example shown, with the equatorial ring being indistinct. Whether Myp2 localisation requires the APC is not known.

Whether PAAs form in APC mutant strains remains unknown. As PAA formation is seen in wild-type cells at the restrictive temperature during CAR contraction, and the CAR does contract in APC mutant strains, PAA formation can theoretically be assessed using time-lapse microscopy of temperature-sensitive strains. Alternatively, spore germination of deletion strains could be used.

Why might the interaction between Mto1 and the γ-TuC be regulated? While Mto1 recruits the γ-TuC to MTOCs at several times during the cell cycle, cytoplasmic microtubule nucleation is not constitutively present (Figure 50). No cytoplasmic microtubule nucleation is seen during metaphase, after the disassembly of interphase microtubule bundles and before the appearance of astral microtubules during anaphase B - what were previously thought to be astral microtubules present earlier in mitosis having since been shown to be intranuclear (Zimmerman et al., 2004a).

Regulating the interaction between Mto1 and the γ-TuC may therefore serve to regulate cytoplasmic nucleation.

I speculate that the absence of nucleation in early mitosis could be due to targeted disruption of the interaction between Mto1 and the γ-TuC via phosphorylation by the cyclin dependent kinase, Cdc2. This disruption would later be relieved by activation of the APC, which inactivates Cdc2 via proteolytic destruction of the associated cyclin, Cdc13. Mto1 is again able to interact with the γ-TuC and targets the γ-TuC to the SPB to nucleate astral microtubules and later in anaphase to the eMTOC to nucleate the PAA. However, recent data from the laboratory suggests that Mto1 co-immunoprecipitates the γ-TuC during an *nda3-KM311* arrest, casting the model in doubt, although it is possible that interaction alone is not sufficient to activate the γ-TuC. As Mto1 is present at the SPB through out the cell cycle (Sawin et al., 2004) and the γ-TuC is present on the nuclear face of the SPB it is impossible to determine if γ-tubulin is indeed absent from the cytoplasmic face of the SPB during metaphase using light microscopy. This could instead be addressed using electron microscopy.

Figure 50 Model of APC regulation of microtubule nucleation

Interphase: Mto1/ γ-TuC is present at the SPB to nucleate interphase microtubules. **Metaphase**: no nucleation is seen from the SPB, which we suggest may be due to an absence of γ-TuC from the cytoplasmic face of the SPB at this stage of the cell cycle. I propose that the interaction between Mto1 (blue) and γ-TuC (red) is disrupted by Cdc2 phosphorylation. **Anaphase**: In my model APC activity down-regulates the activity of Cdc2 by targeting Cdc13 for proteolysis. The Mto1-γ-TuC interaction is re-established, and the γ-TuC is then recruited by Mto1 to the SPB to nucleate astral microtubules and also to the eMTOC to nucleate the PAA (not shown).

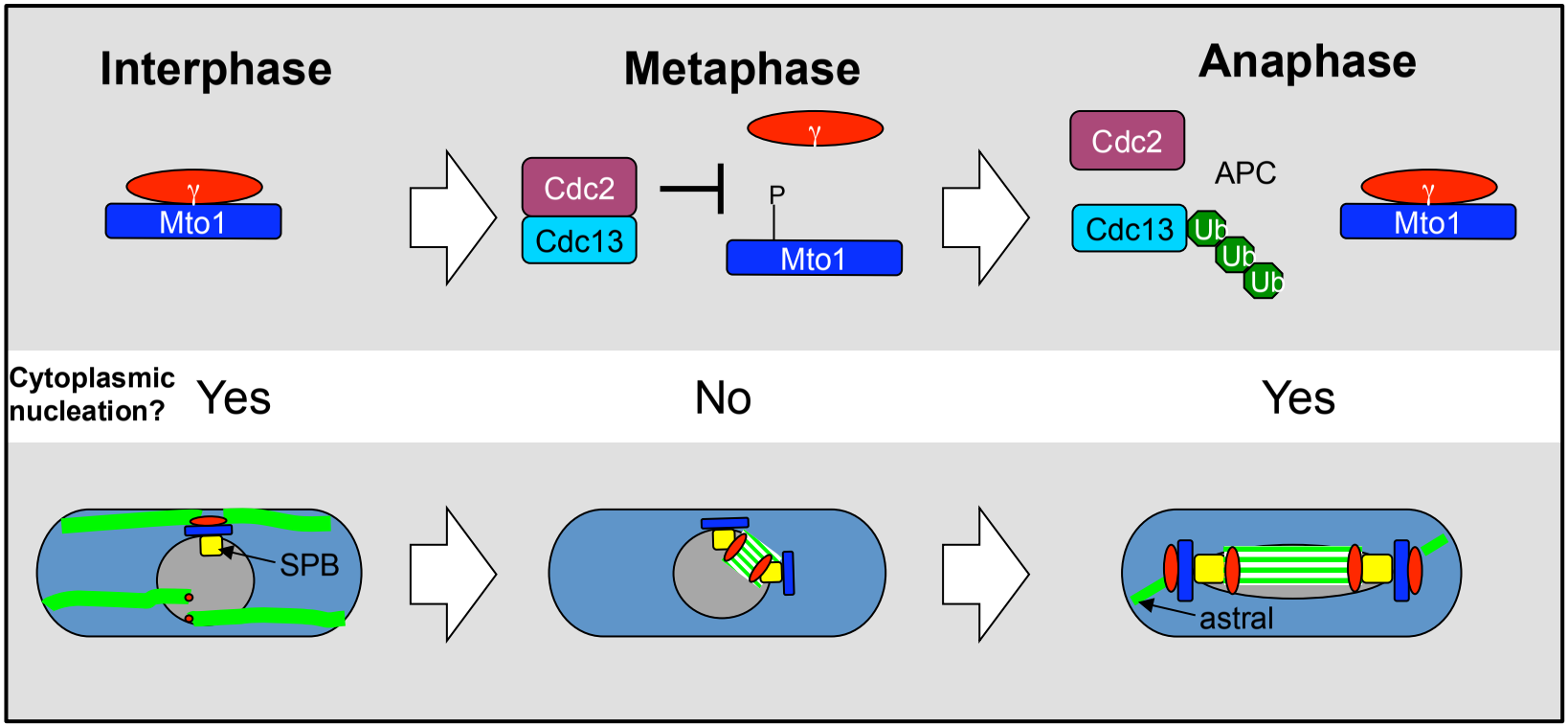
Interphase
Metaphase
Anaphase
γ
Mto1
Cdc2
Cdc13
P
Mto1
γ
Cdc2
APC
Cdc13
Ub
Ub
Ub
γ
Mto1
Cytoplasmic nucleation?
Yes
No
Yes
SPB
astral

Future work

Mto1 interacting proteins

As discussed in Chapter IV, further immunoprecipitation experiments are needed to first determine whether the Mto1 C-terminal truncations that localise to the cell equator will also co-immunoprecipitate with Myp2, and ultimately to map the minimal areas of Mto1 able to interact with Myp2. These experiments should increase our understanding of the function of the localising Mto1(1051-1115) region, by revealing whether this region is necessary for Mto1 to interact with Myp2, or if Mto1(1051-1115) could instead function to anchor Mto1 at the CAR.

Another area to investigate will be to define the minimum region of Myp2 necessary for interaction with Mto1. Given the size and structure of Myp2, it may be useful to use alanine-scanning (sequential substitution of alanine codons within a protein coding region) in addition to testing protein truncations, to preserve Myp2 structure while removing regions of the protein. Continuing on from this, it may be of interest to create a hybrid from the minimal required region of Myp2 with the localisation domain of another protein and see if it is possible to create a novel MTOC by altering the localisation of Mto1.

Once the minimum regions necessary for interaction between Mto1 and Myp2 have been determined, techniques such as surface plasma resonance and isothermal titration calorimetry can be used to show a direct interaction between Myp2 and Mto1 using recombinant proteins. These methods are not suitable for use with the

large full-proteins, and may not detect an interaction using protein fragments if the proteins mis-fold or if post-translation modifications are required. Alternatively, chemical crossing-linking could be used to detect a direct interaction; this has the advantage that this can be carried out with cellular lysate, retaining any necessary post-translational modifications.

Having shown that Rsp1 interacts with Mto1(1-1115), but not Mto1(1-1051) *in vivo*, I speculate that Rsp1-mediated disassembly of the eMTOC may be due to Rsp1 disrupting an interaction between Mto1 and Myp2. This model could be investigated by testing whether competition from Rsp1 can disrupt the interaction between Myp2 and Mto1(769-1115) in a yeast two-hybrid assay.

Regulation of eMTOC formation

Time-lapse microscopy of temperature-sensitive strains in combination with nuclear and CAR markers has proven to be a useful way to show that Mto1 localisation to the equator is independent of the APC and the SIN. It will be important to extend these experiments to look at the localisation of γ-tubulin to the eMTOC using the same system, to verify previous reports that the APC and SIN are necessary for eMTOC formation (Heitz *et al.*, 2001; Pardo and Nurse, 2003) and also to Myp2. Ideally Mto1 and γ-tubulin should be co-imaged within a single cell to demonstrate either that Mto1 is present at the CAR while γ-tubulin is not or that both proteins co-localise to the CAR when the SIN or APC is disrupted. To support these experiments, PAA formation in SIN and APC mutant cells should also be studied,

using spore germination of deletion strains for SIN mutants and either spore germination or time-lapse microscopy for APC mutants.

As discussed in Chapter V, it is not clear why Mto1 is absent from the equator during *nda3*-arrest. Further work could look at Mto1 localisation earlier in the arrest, to see if it is present at the equator initially and then disassociates, and could also determine whether Myp2 is present at the CAR during *nda3-KM311* arrest.

It may also be informative to map post-translation modification of Mto1 and see how this changes at different cell cycle stages. One useful approach could be to compare post-translational modifications of Mto1 in wild-type strains compared to APC and SIN mutant strains. It would also be interesting to learn how Myp2 incorporation into the CAR is regulated and more generally how the precise order of CAR assembly is controlled.

I have hypothesised that the Mto1-γ-TuC interaction may be disrupted early in mitosis, accounting for the absence of astral microtubule nucleation at this time. As mentioned in Chapter V, electron microscopy could be used to determine if γ-tubulin is absent from the cytoplasmic face of the SPB at this time. If so, further work could look at whether astral microtubules are present in temperature-sensitive *cdc2* or *cdc13* mutants, to confirm the model I present that the Mto1-γ-TuC interaction is disrupted by Cdc2-Cdc13, and this disruption is later relieved by the action of the APC .

Concluding remarks

Until recently, relatively little was known about how the γ-TuC was recruited to prospective MTOCs. The discovery of Mto1, the first protein identified as playing a direct role in recruiting the γ-TuC to non-centrosomal MTOCs, put *S. pombe* at the forefront of research into MTOC formation. Here I have identified Myp2 as a protein that interacts with Mto1 *in vivo* to recruit Mto1 and so the γ-TuC complex to the eMTOC. I have also sought to determine how Mto1 recruitment to the eMTOC is regulated, within the context of previous findings that eMTOC formation required the SIN and APC. I have shown that Mto1 localisation to the equator is independent of both the SIN and APC, ruling out the hypothesis that the SIN and/or APC act to regulate eMTOC formation by controlling the localisation of Mto1. A model of eMTOC formation based on my findings is shown in Figure 51. More work remains to be done to clarify the role of the SIN and APC in eMTOC formation. Learning more about the interactions between Myp2, Mto1 and γ-TuC and how these interactions are regulated may generate insights into non-centrosomal MTOCs construction and regulation in higher eukaryotes.

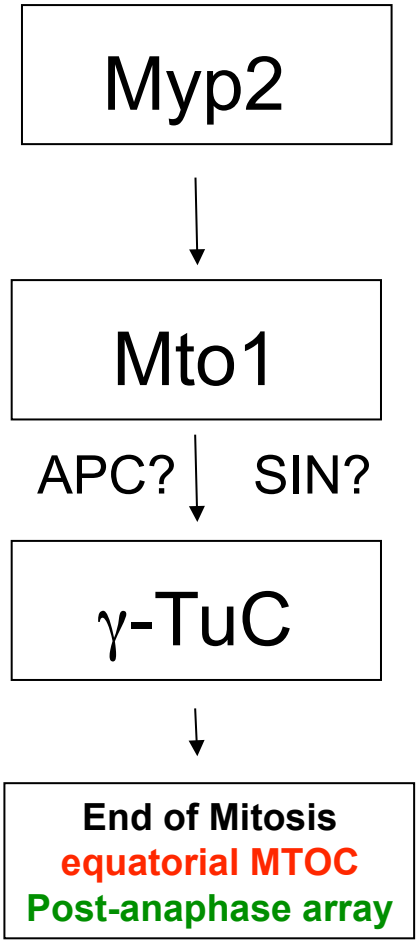

Figure 51 Current model of eMTOC formation

Myp2 localises Mto1 and thus the γ-TuC to the site of the eMTOC. Mto1 localisation is independent of the APC and SIN; γ-tubulin localisation to the eMTOC is reported to require the APC and SIN, suggesting that the APC and SIN regulate the interaction between Mto1 and the γ-TuC.

Appendix 1 - Role of the PAA in maintaining CAR position in non-arrested cells

Following on from the previous finding (Pardo and Nurse, 2003) that the PAA acts to maintain the CAR in a central position when cytokinesis is delayed, we asked whether the PAA is required to maintain the CAR in the middle of the cell in normally cycling cells.

mto1Δ cells are known to have misplaced septa (Venkatram et al., 2004) indicating that the CAR is off-centre in these cells. However, *mto1Δ* cells lack all cytoplasmic nucleation and, in addition to lacking the PAA, also have defective interphase bundles. In *S. pombe* interphase microtubule bundles centre the nucleus (Tran *et al.*, 2001; Daga *et al.*, 2006); nuclear position in turn establishes the position of the division site at the centre of the cell via the Mid1 protein (Paoletti and Chang, 2000; Daga and Chang, 2005). *Mto1Δ* cells have off-centred nuclei (Sawin et al., 2004) and therefore it can be expected that the CAR will in turn be mis-positioned, making it difficult to specifically evaluate the effect of the absent PAA.

To assess the role of the PAA in maintaining the CAR at the centre of the cell, the CAR position was measured using the *mto1-427* allele. *mto1-427* contains mutations in the Mto1 localisation domain (R1056A, E1059A and E1061A), which affect localisation to the cell equator (I. Samejima, personal communication). *mto1-427* cells specifically lack the PAA, but have normal interphase and astral microtubules.

The ring component Rlc1-mCherry and the nuclear marker Uch2-mCherry were used to examine CAR position in binucleate cells (Figure 52). At this stage of the cell cycle wild-type cells have formed the PAA. Cells grown at 25°C were imaged and the position of the ring determined by measuring the distance from the CAR to each cell tip. These measurements were used to calculate a ratio of the smaller length over the total cell length i.e. a/ (a+b) where a<b. If the CAR is perfectly centred the ratio will be 0.5. Increasing deviation away from the centre will give a progressively smaller value.

No significant difference was seen between the two strains: the graphs overlap for 84% of the readings and shown negligible divergence for the remaining 16%. Thus the PAA is not required to maintain the CAR in the middle of the cell in normally cycling cells, as in cells lacking the PAA the CAR remains centred.

Discussion

The function of the PAA is not completely understood. Previous work suggests a role for the PAA in positioning the CAR at the centre of the cell when cytokinesis is interrupted (Pardo and Nurse, 2003). However no requirement for the PAA during normal cell division has been identified. Removing the PAA does not cause deviant positioning of the CAR in cells growing under standard laboratory conditions and *mto1-427* cells grown on phloxin B media (to selectively stain dead cells) are no sicker than wild-type (K. Sawin, personal communication). Nor are any obvious

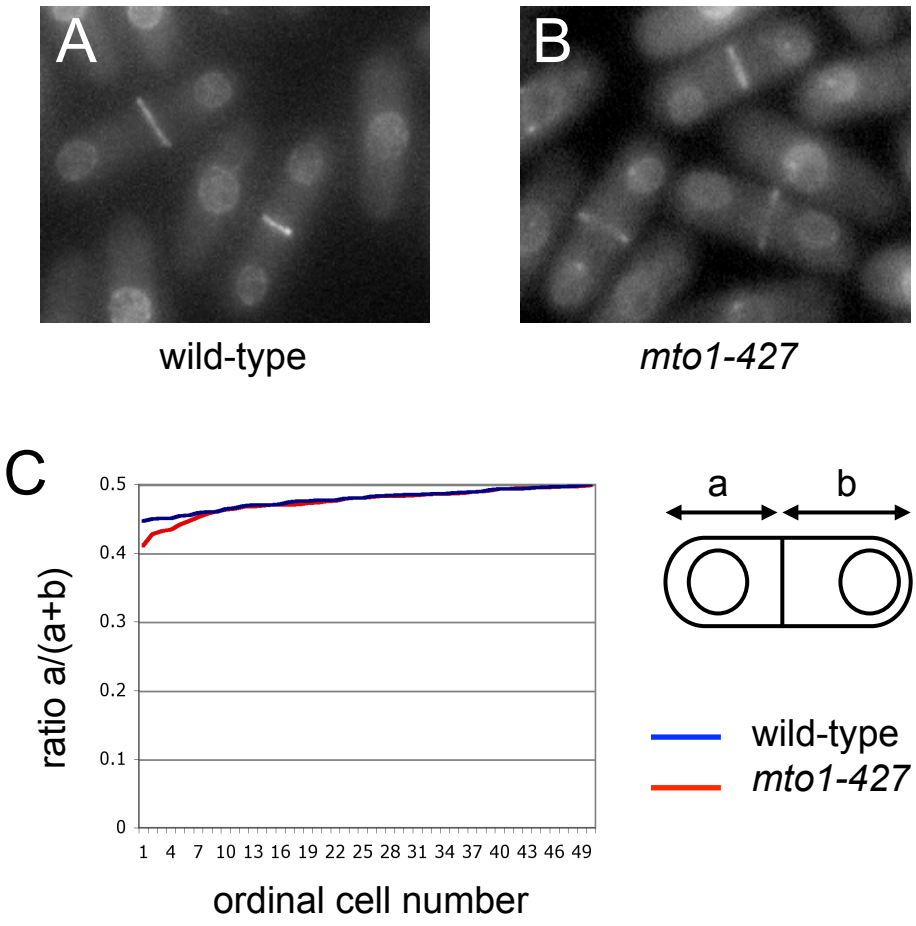

Figure 52 CAR position is not altered by PAA absence

Wide-field images of (A) wild-type *rlc1-mCherry uch2-mCherry* cells and (B) *mto1-427 rlc1-mCherry uch2-mCherry* cells. The *mto1-427 rlc1-mCherry uch2-mCherry* strain does not nucleate a PAA. (C) Measurements of CAR eccentricity for 50 asynchronous wild-type and *mto1-427* cells, in ascending order of the ratio *a*/(*a*+*b*) where *a* is the shorter distance from the CAR to the cell tip and *b* is the longer distance. CAR placement is indistinguishable from wild-type in 84% of *mto1-427* cells and shows no significant difference for the other 16%.

defects seen in the behaviour or morphology of either the mitotic spindle or interphase microtubule bundles when the PAA is absent.

A 'cytokinesis checkpoint' has been identified in *S. pombe*. *S. pombe* strains with mutations in the cytokinetic machinery exhibit a prolonged G2 delay after failing to complete cytokinesis in the previous cell cycle (Nurse *et al.*, 1976; Chang *et al.*, 1996; Balasubramanian *et al.*, 1998; Le Goff *et al.*, 1999; Liu *et al.*, 1999; Liu *et al.*, 2000; Mishra *et al.*, 2004). The Cdc14-family phosphatase Clp1 is required to block the nuclear cycle (Mishra et al., 2004). F-actin must also be present (Liu et al., 1999), indicating that the persistence of the CAR is important for maintaining the arrest. The SIN pathway is also necessary; the multi-nucleate phenotype seen in SIN mutant strains is epistatic to the G2 nuclear arrest (Le Goff et al., 1999; Liu et al., 2000). By blocking entry into mitosis until cytokinesis is completed, the checkpoint is proposed to allow additional time for mild defects in the cytokinesis machinery to be repaired, while preventing the cell from accumulating multiple nuclei. The PAA has been shown to act during this time to maintain the position of the CAR. It may well be that the PAA has no role in standard cell division and is only required if the cytokinesis checkpoint is activated.

How does the PAA centre the CAR during a delay in cytokinesis? CAR displacement requires membrane trafficking (Pardo and Nurse, 2003). Lipid rafts are established adjacent to the CAR late in anaphase (Wachtler et al., 2003). These sterol-rich membrane regions are found in many cell types and are thought to act as platforms to facilitate interactions within specific areas of the membrane, for

example for signal transduction (Simons and Ikonen, 1997). How lipid rafts are established and positioned within cell membranes is not known. However, microtubule structures in higher organisms, including the midbody in animal cells and the phragmoplast in plants (Otegui et al., 2005), are known to target membrane secretion to the site of cell division during cytokinesis (McCollum, 2005). Lipid rafts in *S. pombe* are hypothesised to be involved in maintaining and/or positioning the CAR (Wachtler et al., 2003). The PAA is not required to establish lipid rafts at the division site, as lipid rafts are present in cells without PAAs (Pardo and Nurse, 2003; Wachtler et al., 2003). However, the microtubules of the PAA could potentially traffic membrane vesicles to maintain the position of lipid raft. Any model explaining the mechanism for PAA maintenance of CAR position will need to explain why the CAR is only displaced in one direction and also why re-establishing the PAA does not re-centre the CAR once it is mis-positioned (Pardo and Nurse, 2003). It will be interesting to see whether the CAR drifting seen during *cps1-191* arrest in cells treated with the microtubule-depolymerising drug carbendazim is also seen in *cps1-191 mto1-427* cells that lack the PAA. Further understanding the function of the PAA in *S. pombe* may generate insights into the function of microtubules in cell division in other organisms.

Appendix 2 - Raising antibodies against Alp4 and Alp6

Antibodies were raised to the γ-TuSC components, Alp4 and Alp6. This work was undertaken as the first stage of a larger project that was later abandoned. Production of the antibodies was continued, as these are of general value for the ongoing work of the laboratory. The amino and carboxyl termini of Alp4 and Alp6 were sub-cloned into GST-fusion vectors. These fusion proteins were expressed in *E.coli*, SDS-PAGE-purified from purified inclusion bodies and used to immunise sheep. The antibodies produced were serum or blot-affinity purified before being used for western blotting (Samejima et al., 2008).

Appendix 3 - Pcp1 plasmid shuffle system

Pcp1 anchors the γ-TuC to the nuclear face of the SPB (Flory et al., 2002). We are interested in the hypothetical phenotype of a *mto1Δ pcp1Δ* double knock-out strain, specifically whether such cells will be completely deficient in microtubule nucleation or if other forms of microtubule nucleation (associated with chromatin or from soluble γ-TuCs) will be uncovered. As Pcp1 is an essential gene it was decided to create temperature sensitive alleles of Pcp1 and select specifically for cells that show no nucleation from the nuclear face of the SPB.

Plasmid shuffle is one method used to generate conditional mutations (Forsburg, 2001). This system can be used to screen a library of mutagenised plasmids. As a prelude to the 'shuffle' a plasmid with a copy of an essential gene and a selectable marker is transformed into a diploid strain with one copy of the gene of interest already deleted. The cells are sporulated and subjected to selection to obtain haploids that lack a genomic copy of the gene, but remain viable because the deletion is 'covered' by the plasmid copy of the gene. In the 'shuffle', a second plasmid is transformed into the 'covered' strain and the cells are plated onto media that both selects for the second plasmid while selecting against the first. By replica plating to plates containing Phloxin B that preferentially stains dead cells, and comparing colony growth at the permissive and restrictive temperatures it is possible to identify temperature-sensitive mutants for further investigation.

To generate the haploid *pcpΔ* strain KS2973 with the genomic deletion 'covered' by a plasmid-based copy of *pcp1*, pKS477 pUR19-pcp1 (selection: Ura+) was transformed into the diploid strain *pcp1/pcpΔ::natMX6* and random spore analysis was used to identify haploid cells that were $Nat^{R}Ura^{+}$ (i.e. had the plasmid covering the deletion of genomic *pcp1*). pKS480 pALKS-pcp1-GFP (selection: Leu+) was then transformed into this strain, plated onto plates containing 0.1% FOA (5-fluorouracil-6-carboxylic acid), which were also selective for Leu+ colonies. Colonies formed on this plate were replica plated to confirm that they were Leu+ and Ura-, which in turn confirmed that the plasmid shuffle had been successful and the first plasmid had been lost.

High transformation efficiency is needed to screen mutagenised libraries. Electroporation, the Bähler method of LiOAc transformation (Bahler *et al.*, 1998b) and the 'Long' LiOAc transformation protocol (Okazaki et al., 1990) were trialled; all gave transformation efficiencies of ~ 2 x 10^4 transformants/ μg DNA/ 10^8 cells.

We hypothesise that targeting mutagenesis to the CM1 region of Pcp1 will generate alleles that fail to bind the gamma-tubulin complex at the restrictive temperature, and consequently abolish microtubule nucleation. The Mutazyme II error-prone polymerase [Stratagene] was used to amplify megaprimers for the targeted mutagenesis. Primers were designed both to the amino-terminus and specifically to the CM1 region within the amino-terminus, generating products of 1Kb and 250bp respectively. These megaprimers were then used to prime a Quikchange reaction and amplify the pKS480 plasmid. This was expected to generate a library of plasmids

with mutations restricted to the amino-terminus of Pcp1, but the efficiency of the Quikchange reaction was poor.

XL1-Red error-prone competent cells [Stratagene] were also used to complement the target mutagenesis approach. These cells are deficient in DNA repair pathways so plasmids cultured within them accumulate mutations; this means that mutations could be introduced anywhere in the *pcp1* gene. pKS480 was transformed into XL1-Red competent cells and the cells were cultured for times between 24 hours and one week, but preliminary results making an empirical measurement of the mutation rate from inactivation of the Leu+ marker suggested that the mutation rate was insufficient for my purpose and the experiment was put aside. Previous mutations generated in the Pcp1 homologue, SPC110 suggest that multiple mutations may be needed to produce a phenotype (Sundberg *et al.*, 1996; Sundberg and Davis, 1997).

Alternative methods of mutagenesis that could be used include introducing errors to PCR by altering the ratios of deoxynucleotides supplied/ adding a sub-optimal cation, or hydroxylamine mutagenesis. Unlike the previous methods used these have the disadvantage of being biased towards producing specific mutations. Any method used must generate a large number of alleles that can then be screened.

Bibliography

Alfa, C.E., and Hyams, J.S. (1990). Distribution of tubulin and actin through the cell division cycle of the fission yeast Schizosaccharomyces japonicus var. versatilis: a comparison with Schizosaccharomyces pombe. J Cell Sci *96 (Pt 1)*, 71-77.

An, H., Morrell, J.L., Jennings, J.L., Link, A.J., and Gould, K.L. (2004). Requirements of fission yeast septins for complex formation, localization, and function. Mol Biol Cell *15*, 5551-5564.

Anders, A., Lourenco, P.C., and Sawin, K.E. (2006). Noncore components of the fission yeast gamma-tubulin complex. Mol Biol Cell *17*, 5075-5093.

Arai, R., and Mabuchi, I. (2002). F-actin ring formation and the role of F-actin cables in the fission yeast Schizosaccharomyces pombe. J Cell Sci *115*, 887-898.

Bahler, J., Steever, A.B., Wheatley, S., Wang, Y., Pringle, J.R., Gould, K.L., and McCollum, D. (1998a). Role of polo kinase and Mid1p in determining the site of cell division in fission yeast. J Cell Biol *143*, 1603-1616.

Bahler, J., Wu, J.Q., Longtine, M.S., Shah, N.G., McKenzie, A., 3rd, Steever, A.B., Wach, A., Philippsen, P., and Pringle, J.R. (1998b). Heterologous modules for efficient and versatile PCR-based gene targeting in Schizosaccharomyces pombe. Yeast *14*, 943-951.

Balasubramanian, M.K., Helfman, D.M., and Hemmingsen, S.M. (1992). A new tropomyosin essential for cytokinesis in the fission yeast S. pombe. Nature *360*, 84-87.

Balasubramanian, M.K., McCollum, D., Chang, L., Wong, K.C., Naqvi, N.I., He, X., Sazer, S., and Gould, K.L. (1998). Isolation and characterization of new fission yeast cytokinesis mutants. Genetics *149*, 1265-1275.

Bartolini, F., Moseley, J.B., Schmoranzer, J., Cassimeris, L., Goode, B.L., and Gundersen, G.G. (2008). The formin mDia2 stabilizes microtubules independently of its actin nucleation activity. J Cell Biol *181*, 523-536.

Basto, R., Brunk, K., Vinadogrova, T., Peel, N., Franz, A., Khodjakov, A., and Raff, J.W. (2008). Centrosome amplification can initiate tumorigenesis in flies. Cell *133*, 1032-1042.

Berg, J.S., Powell, B.C., and Cheney, R.E. (2001). A millennial myosin census. Mol Biol Cell *12*, 780-794.

Berger, B., Wilson, D.B., Wolf, E., Tonchev, T., Milla, M., and Kim, P.S. (1995). Predicting coiled coils by use of pairwise residue correlations. Proc Natl Acad Sci U S A *92*, 8259-8263.

Bezanilla, M., Forsburg, S.L., and Pollard, T.D. (1997). Identification of a second myosin-II in Schizosaccharomyces pombe: Myp2p is conditionally required for cytokinesis. Mol Biol Cell *8*, 2693-2705.

Bezanilla, M., and Pollard, T.D. (2000). Myosin-II tails confer unique functions in Schizosaccharomyces pombe: characterization of a novel myosin-II tail. Mol Biol Cell *11*, 79-91.

Bimbo, A., Liu, J., and Balasubramanian, M. (2005). Roles of Pdk1p, a fission yeast protein related to phosphoinositide-dependent protein kinase, in the regulation of mitosis and cytokinesis. Mol Biol Cell *16*, 3162-3175.

Bouckson-Castaing, V., Moudjou, M., Ferguson, D.J., Mucklow, S., Belkaid, Y., Milon, G., and Crocker, P.R. (1996). Molecular characterisation of ninein, a new coiled-coil protein of the centrosome. J Cell Sci *109 (Pt 1)*, 179-190.

Bratman, S.V., and Chang, F. (2007). Stabilization of overlapping microtubules by fission yeast CLASP. Dev Cell *13*, 812-827.

Burkhard, P., Stetefeld, J., and Strelkov, S.V. (2001). Coiled coils: a highly versatile protein folding motif. Trends Cell Biol *11*, 82-88.

Busch, K.E., and Brunner, D. (2004). The microtubule plus end-tracking proteins mal3p and tip1p cooperate for cell-end targeting of interphase microtubules. Curr Biol *14*, 548-559.

Carazo-Salas, R.E., Antony, C., and Nurse, P. (2005). The kinesin Klp2 mediates polarization of interphase microtubules in fission yeast. Science *309*, 297-300.

Chang, F. (1999). Movement of a cytokinesis factor cdc12p to the site of cell division. Curr Biol *9*, 849-852.

Chang, F., Drubin, D., and Nurse, P. (1997). cdc12p, a protein required for cytokinesis in fission yeast, is a component of the cell division ring and interacts with profilin. J Cell Biol *137*, 169-182.

Chang, F., Woollard, A., and Nurse, P. (1996). Isolation and characterization of fission yeast mutants defective in the assembly and placement of the contractile actin ring. J Cell Sci *109 (Pt 1)*, 131-142.

Charles, J.F., Jaspersen, S.L., Tinker-Kulberg, R.L., Hwang, L., Szidon, A., and Morgan, D.O. (1998). The Polo-related kinase Cdc5 activates and is destroyed by the mitotic cyclin destruction machinery in S. cerevisiae. Curr Biol *8*, 497-507.

Chew, T.G., and Balasubramanian, M.K. (2008). Nuc2p, a subunit of the anaphase-promoting complex, inhibits septation initiation network following cytokinesis in fission yeast. PLoS Genet *4*, e17.

Cullen, C.F., May, K.M., Hagan, I.M., Glover, D.M., and Ohkura, H. (2000). A new genetic method for isolating functionally interacting genes: high plo1(+)-dependent

mutants and their suppressors define genes in mitotic and septation pathways in fission yeast. Genetics *155*, 1521-1534.

Cuschieri, L., Miller, R., and Vogel, J. (2006). Gamma-tubulin is required for proper recruitment and assembly of Kar9-Bim1 complexes in budding yeast. Mol Biol Cell *17*, 4420-4434.

D'Souza V, M., Naqvi, N.I., Wang, H., and Balasubramanian, M.K. (2001). Interactions of Cdc4p, a myosin light chain, with IQ-domain containing proteins in Schizosaccharomyces pombe. Cell Struct Funct *26*, 555-565.

Daga, R.R., and Chang, F. (2005). Dynamic positioning of the fission yeast cell division plane. Proc Natl Acad Sci U S A *102*, 8228-8232.

Daga, R.R., Yonetani, A., and Chang, F. (2006). Asymmetric microtubule pushing forces in nuclear centering. Curr Biol *16*, 1544-1550.

Dammermann, A., Desai, A., and Oegema, K. (2003). The minus end in sight. Curr Biol *13*, R614-624.

Desai, A., and Mitchison, T.J. (1997). Microtubule polymerization dynamics. Annu Rev Cell Dev Biol *13*, 83-117.

Descombes, P., and Nigg, E.A. (1998). The polo-like kinase Plx1 is required for M phase exit and destruction of mitotic regulators in Xenopus egg extracts. EMBO J *17*, 1328-1335.

Dictenberg, J.B., Zimmerman, W., Sparks, C.A., Young, A., Vidair, C., Zheng, Y., Carrington, W., Fay, F.S., and Doxsey, S.J. (1998). Pericentrin and gamma-tubulin form a protein complex and are organized into a novel lattice at the centrosome. J Cell Biol *141*, 163-174.

Ding, R., West, R.R., Morphew, D.M., Oakley, B.R., and McIntosh, J.R. (1997). The spindle pole body of Schizosaccharomyces pombe enters and leaves the nuclear envelope as the cell cycle proceeds. Mol Biol Cell *8*, 1461-1479.

Donaldson, M.M., Tavares, A.A., Hagan, I.M., Nigg, E.A., and Glover, D.M. (2001). The mitotic roles of Polo-like kinase. J Cell Sci *114*, 2357-2358.

Doxsey, S.J., Stein, P., Evans, L., Calarco, P.D., and Kirschner, M. (1994). Pericentrin, a highly conserved centrosome protein involved in microtubule organization. Cell *76*, 639-650.

Drummond, D.R., and Cross, R.A. (2000). Dynamics of interphase microtubules in Schizosaccharomyces pombe. Curr Biol *10*, 766-775.

Eng, K., Naqvi, N.I., Wong, K.C., and Balasubramanian, M.K. (1998). Rng2p, a protein required for cytokinesis in fission yeast, is a component of the actomyosin ring and the spindle pole body. Curr Biol *8*, 611-621.

Erickson, H.P. (2000). Gamma-tubulin nucleation: template or protofilament? Nat Cell Biol *2*, E93-96.

Erickson, H.P., and Stoffler, D. (1996). Protofilaments and rings, two conformations of the tubulin family conserved from bacterial FtsZ to alpha/beta and gamma tubulin. J Cell Biol *135*, 5-8.

Fankhauser, C., Reymond, A., Cerutti, L., Utzig, S., Hofmann, K., and Simanis, V. (1995). The S. pombe cdc15 gene is a key element in the reorganization of F-actin at mitosis. Cell *82*, 435-444.

Fava, F., Raynaud-Messina, B., Leung-Tack, J., Mazzolini, L., Li, M., Guillemot, J.C., Cachot, D., Tollon, Y., Ferrara, P., and Wright, M. (1999). Human 76p: A new member of the gamma-tubulin-associated protein family. J Cell Biol *147*, 857-868.

Feierbach, B., and Chang, F. (2001). Roles of the fission yeast formin for3p in cell polarity, actin cable formation and symmetric cell division. Curr Biol *11*, 1656-1665.

Fields, S., and Song, O. (1989). A novel genetic system to detect protein-protein interactions. Nature *340*, 245-246.

Fish, J.L., Kosodo, Y., Enard, W., Paabo, S., and Huttner, W.B. (2006). Aspm specifically maintains symmetric proliferative divisions of neuroepithelial cells. Proc Natl Acad Sci U S A *103*, 10438-10443.

Flory, M.R., Morphew, M., Joseph, J.D., Means, A.R., and Davis, T.N. (2002). Pcp1p, an Spc110p-related calmodulin target at the centrosome of the fission yeast Schizosaccharomyces pombe. Cell Growth Differ *13*, 47-58.

Fong, K.W., Choi, Y.K., Rattner, J.B., and Qi, R.Z. (2008). CDK5RAP2 is a pericentriolar protein that functions in centrosomal attachment of the gamma-tubulin ring complex. Mol Biol Cell *19*, 115-125.

Forsburg, S.L. (1999). The best yeast? Trends Genet *15*, 340-344.

Forsburg, S.L. (2001). The art and design of genetic screens: yeast. Nat Rev Genet *2*, 659-668.

Fromont-Racine, M., Rain, J.C., and Legrain, P. (2002). Building protein-protein networks by two-hybrid mating strategy. Methods Enzymol *350*, 513-524.

Fujita, A., Vardy, L., Garcia, M.A., and Toda, T. (2002). A fourth component of the fission yeast gamma-tubulin complex, Alp16, is required for cytoplasmic microtubule integrity and becomes indispensable when gamma-tubulin function is compromised. Mol Biol Cell *13*, 2360-2373.

Furge, K.A., Cheng, Q.C., Jwa, M., Shin, S., Song, K., and Albright, C.F. (1999). Regions of Byr4, a regulator of septation in fission yeast, that bind Spg1 or Cdc16 and form a two-component GTPase-activating protein with Cdc16. J Biol Chem *274*, 11339-11343.

Furge, K.A., Wong, K., Armstrong, J., Balasubramanian, M., and Albright, C.F. (1998). Byr4 and Cdc16 form a two-component GTPase-activating protein for the Spg1 GTPase that controls septation in fission yeast. Curr Biol *8*, 947-954.

Gachet, Y., Tournier, S., Millar, J.B., and Hyams, J.S. (2004). Mechanism controlling perpendicular alignment of the spindle to the axis of cell division in fission yeast. EMBO J *23*, 1289-1300.

Giansanti, M.G., Gatti, M., and Bonaccorsi, S. (2001). The role of centrosomes and astral microtubules during asymmetric division of Drosophila neuroblasts. Development *128*, 1137-1145.

Goodson, H.V., and Dawson, S.C. (2006). Multiplying myosins. Proc Natl Acad Sci U S A *103*, 3498-3499.

Goshima, G., Mayer, M., Zhang, N., Stuurman, N., and Vale, R.D. (2008). Augmin: a protein complex required for centrosome-independent microtubule generation within the spindle. J Cell Biol *181*, 421-429.

Gould, K.L., and Simanis, V. (1997). The control of septum formation in fission yeast. Genes Dev *11*, 2939-2951.

Guertin, D.A., Chang, L., Irshad, F., Gould, K.L., and McCollum, D. (2000). The role of the sid1p kinase and cdc14p in regulating the onset of cytokinesis in fission yeast. EMBO J *19*, 1803-1815.

Guertin, D.A., Venkatram, S., Gould, K.L., and McCollum, D. (2002). Dma1 prevents mitotic exit and cytokinesis by inhibiting the septation initiation network (SIN). Dev Cell *3*, 779-790.

Gunawardane, R.N., Martin, O.C., Cao, K., Zhang, L., Dej, K., Iwamatsu, A., and Zheng, Y. (2000). Characterization and reconstitution of Drosophila gamma-tubulin ring complex subunits. J Cell Biol *151*, 1513-1524.

Gunawardane, R.N., Martin, O.C., and Zheng, Y. (2003). Characterization of a new gammaTuRC subunit with WD repeats. Mol Biol Cell *14*, 1017-1026.

Hachet, O., and Simanis, V. (2008). Mid1p/anillin and the septation initiation network orchestrate contractile ring assembly for cytokinesis. Genes Dev *22*, 3205-3216.

Hagan, I., and Yanagida, M. (1997). Evidence for cell cycle-specific, spindle pole body-mediated, nuclear positioning in the fission yeast Schizosaccharomyces pombe. J Cell Sci *110 (Pt 16)*, 1851-1866.

Hagan, I.M. (1998). The fission yeast microtubule cytoskeleton. J Cell Sci *111 (Pt 12)*, 1603-1612.

Hagan, I.M., and Hyams, J.S. (1988). The use of cell division cycle mutants to investigate the control of microtubule distribution in the fission yeast Schizosaccharomyces pombe. J Cell Sci *89 (Pt 3)*, 343-357.

Haren, L., Remy, M.H., Bazin, I., Callebaut, I., Wright, M., and Merdes, A. (2006). NEDD1-dependent recruitment of the gamma-tubulin ring complex to the centrosome is necessary for centriole duplication and spindle assembly. J Cell Biol *172*, 505-515.

Hayles, J., and Nurse, P. (2001). A journey into space. Nat Rev Mol Cell Biol *2*, 647-656.

Heitz, M.J., Petersen, J., Valovin, S., and Hagan, I.M. (2001). MTOC formation during mitotic exit in fission yeast. J Cell Sci *114*, 4521-4532.

Hirano, T., Funahashi, S.I., Uemura, T., and Yanagida, M. (1986). Isolation and characterization of Schizosaccharomyces pombe cutmutants that block nuclear division but not cytokinesis. EMBO J *5*, 2973-2979.

Hiraoka, Y., Toda, T., and Yanagida, M. (1984). The NDA3 gene of fission yeast encodes beta-tubulin: a cold-sensitive nda3 mutation reversibly blocks spindle formation and chromosome movement in mitosis. Cell *39*, 349-358.

Hoog, J.L., Schwartz, C., Noon, A.T., O'Toole, E.T., Mastronarde, D.N., McIntosh, J.R., and Antony, C. (2007). Organization of interphase microtubules in fission yeast analyzed by electron tomography. Dev Cell *12*, 349-361.

Horio, T., Kimura, N., Basaki, A., Tanaka, Y., Noguchi, T., Akashi, T., and Tanaka, K. (2002). Molecular and structural characterization of the spindle pole bodies in the fission yeast Schizosaccharomyces japonicus var japonicus. Yeast *19*, 1335-1350.

Horio, T., Uzawa, S., Jung, M.K., Oakley, B.R., Tanaka, K., and Yanagida, M. (1991). The fission yeast gamma-tubulin is essential for mitosis and is localized at microtubule organizing centers. J Cell Sci *99 (Pt 4)*, 693-700.

Huang, Y., Chew, T.G., Ge, W., and Balasubramanian, M.K. (2007). Polarity determinants Tea1p, Tea4p, and Pom1p inhibit division-septum assembly at cell ends in fission yeast. Dev Cell *12*, 987-996.

Ishizaki, T., Morishima, Y., Okamoto, M., Furuyashiki, T., Kato, T., and Narumiya, S. (2001). Coordination of microtubules and the actin cytoskeleton by the Rho effector mDia1. Nat Cell Biol *3*, 8-14.

Jang, Y.J., Park, S.K., and Yoo, H.S. (1996). Isolation of an HSP12-homologous gene of Schizosaccharomyces pombe suppressing a temperature-sensitive mutant allele of cdc4. Gene *172*, 125-129.

Janson, M.E., Setty, T.G., Paoletti, A., and Tran, P.T. (2005). Efficient formation of bipolar microtubule bundles requires microtubule-bound gamma-tubulin complexes. J Cell Biol *169*, 297-308.

Jaspersen, S.L., and Winey, M. (2004). The budding yeast spindle pole body: structure, duplication, and function. Annu Rev Cell Dev Biol *20*, 1-28.

Job, D., Valiron, O., and Oakley, B. (2003). Microtubule nucleation. Curr Opin Cell Biol *15*, 111-117.

Jones, R.H., Moreno, S., Nurse, P., and Jones, N.C. (1988). Expression of the SV40 promoter in fission yeast: identification and characterization of an AP-1-like factor. Cell *53*, 659-667.

Kamasaki, T., Osumi, M., and Mabuchi, I. (2007). Three-dimensional arrangement of F-actin in the contractile ring of fission yeast. J Cell Biol *178*, 765-771.

Kapitein, L.C., Janson, M.E., van den Wildenberg, S.M., Hoogenraad, C.C., Schmidt, C.F., and Peterman, E.J. (2008). Microtubule-driven multimerization recruits ase1p onto overlapping microtubules. Curr Biol *18*, 1713-1717.

Keating, T.J., and Borisy, G.G. (1999). Centrosomal and non-centrosomal microtubules. Biol Cell *91*, 321-329.

Keating, T.J., and Borisy, G.G. (2000). Immunostructural evidence for the template mechanism of microtubule nucleation. Nat Cell Biol *2*, 352-357.

Kelley, W.L. (1998). The J-domain family and the recruitment of chaperone power. Trends Biochem Sci *23*, 222-227.

Kelley, W.L. (1999). Molecular chaperones: How J domains turn on Hsp70s. Curr Biol *9*, R305-308.

Khodjakov, A., Cole, R.W., Oakley, B.R., and Rieder, C.L. (2000). Centrosome-independent mitotic spindle formation in vertebrates. Curr Biol *10*, 59-67.

Khodjakov, A., La Terra, S., and Chang, F. (2004). Laser microsurgery in fission yeast; role of the mitotic spindle midzone in anaphase B. Curr Biol *14*, 1330-1340.

Khodjakov, A., and Rieder, C.L. (1999). The sudden recruitment of gamma-tubulin to the centrosome at the onset of mitosis and its dynamic exchange throughout the cell cycle, do not require microtubules. J Cell Biol *146*, 585-596.

Khodjakov, A., and Rieder, C.L. (2001). Centrosomes enhance the fidelity of cytokinesis in vertebrates and are required for cell cycle progression. J Cell Biol *153*, 237-242.

Kitayama, C., Sugimoto, A., and Yamamoto, M. (1997). Type II myosin heavy chain encoded by the myo2 gene composes the contractile ring during cytokinesis in Schizosaccharomyces pombe. J Cell Biol *137*, 1309-1319.

Knop, M., and Schiebel, E. (1998). Receptors determine the cellular localization of a gamma-tubulin complex and thereby the site of microtubule formation. EMBO J *17*, 3952-3967.

Kobe, B., and Kajava, A. (2001). The leucine-rich repeat as a protein recognition motif. Curr Opin Struct Biol *11*, 725-732.

Kollman, J.M., Zelter, A., Muller, E.G., Fox, B., Rice, L.M., Davis, T.N., and Agard, D.A. (2008). The structure of the gamma-tubulin small complex: implications of its architecture and flexibility for microtubule nucleation. Mol Biol Cell *19*, 207-215.

Kominami, K., Seth-Smith, H., and Toda, T. (1998). Apc10 and Ste9/Srw1, two regulators of the APC-cyclosome, as well as the CDK inhibitor Rum1 are required for G1 cell-cycle arrest in fission yeast. EMBO J *17*, 5388-5399.

Kovar, D.R., Wu, J.Q., and Pollard, T.D. (2005). Profilin-mediated competition between capping protein and formin Cdc12p during cytokinesis in fission yeast. Mol Biol Cell *16*, 2313-2324.

Krapp, A., Gulli, M.P., and Simanis, V. (2004). SIN and the art of splitting the fission yeast cell. Curr Biol *14*, R722-730.

Krapp, A., Schmidt, S., Cano, E., and Simanis, V. (2001). S. pombe cdc11p, together with sid4p, provides an anchor for septation initiation network proteins on the spindle pole body. Curr Biol *11*, 1559-1568.

Lawo, S., Bashkurov, M., Mullin, M., Ferreria, M.G., Kittler, R., Habermann, B., Tagliaferro, A., Poser, I., Hutchins, J.R., Hegemann, B., Pinchev, D., Buchholz, F., Peters, J.M., Hyman, A.A., Gingras, A.C., and Pelletier, L. (2009). HAUS, the 8-subunit human Augmin complex, regulates centrosome and spindle integrity. Curr Biol *19*, 816-826.

Le Goff, X., Motegi, F., Salimova, E., Mabuchi, I., and Simanis, V. (2000). The S. pombe rlc1 gene encodes a putative myosin regulatory light chain that binds the type II myosins myo3p and myo2p. J Cell Sci *113 Pt 23*, 4157-4163.

Le Goff, X., Woollard, A., and Simanis, V. (1999). Analysis of the cps1 gene provides evidence for a septation checkpoint in Schizosaccharomyces pombe. Mol Gen Genet *262*, 163-172.

Liu, J., Wang, H., and Balasubramanian, M.K. (2000). A checkpoint that monitors cytokinesis in Schizosaccharomyces pombe. J Cell Sci *113 (Pt 7)*, 1223-1230.

Liu, J., Wang, H., McCollum, D., and Balasubramanian, M.K. (1999). Drc1p/Cps1p, a 1,3-beta-glucan synthase subunit, is essential for division septum assembly in Schizosaccharomyces pombe. Genetics *153*, 1193-1203.

Loiodice, I., Staub, J., Setty, T.G., Nguyen, N.P., Paoletti, A., and Tran, P.T. (2005). Ase1p organizes antiparallel microtubule arrays during interphase and mitosis in fission yeast. Mol Biol Cell *16*, 1756-1768.

Lord, M., and Pollard, T.D. (2004). UCS protein Rng3p activates actin filament gliding by fission yeast myosin-II. J Cell Biol *167*, 315-325.

Lord, M., Sladewski, T.E., and Pollard, T.D. (2008). Yeast UCS proteins promote actomyosin interactions and limit myosin turnover in cells. Proc Natl Acad Sci U S A *105*, 8014-8019.

Luders, J., Patel, U.K., and Stearns, T. (2006). GCP-WD is a gamma-tubulin targeting factor required for centrosomal and chromatin-mediated microtubule nucleation. Nat Cell Biol *8*, 137-147.

Luders, J., and Stearns, T. (2007). Microtubule-organizing centres: a re-evaluation. Nat Rev Mol Cell Biol *8*, 161-167.

Lupas, A.N., and Gruber, M. (2005). The structure of alpha-helical coiled coils. Adv Protein Chem *70*, 37-78.

Magidson, V., Chang, F., and Khodjakov, A. (2006). Regulation of cytokinesis by spindle-pole bodies. Nat Cell Biol *8*, 891-893.

Martin, O.C., Gunawardane, R.N., Iwamatsu, A., and Zheng, Y. (1998). Xgrip109: a gamma tubulin-associated protein with an essential role in gamma tubulin ring complex (gammaTuRC) assembly and centrosome function. J Cell Biol *141*, 675-687.

Martin, S.G., McDonald, W.H., Yates, J.R., 3rd, and Chang, F. (2005). Tea4p links microtubule plus ends with the formin for3p in the establishment of cell polarity. Dev Cell *8*, 479-491.

Martin-Garcia, R., and Valdivieso, M.H. (2006). The fission yeast Chs2 protein interacts with the type-II myosin Myo3p and is required for the integrity of the actomyosin ring. J Cell Sci *119*, 2768-2779.

Masuda, H., Hirano, T., Yanagida, M., and Cande, W.Z. (1990). In vitro reactivation of spindle elongation in fission yeast nuc2 mutant cells. J Cell Biol *110*, 417-425.

Masuda, H., Toda, T., Miyamoto, R., Haraguchi, T., and Hiraoka, Y. (2006). Modulation of Alp4 function in Schizosaccharomyces pombe induces novel phenotypes that imply distinct functions for nuclear and cytoplasmic gamma-tubulin complexes. Genes Cells *11*, 319-336.

Mata, J., Lyne, R., Burns, G., and Bahler, J. (2002). The transcriptional program of meiosis and sporulation in fission yeast. Nat Genet *32*, 143-147.

Mata, J., and Nurse, P. (1997). tea1 and the microtubular cytoskeleton are important for generating global spatial order within the fission yeast cell. Cell *89*, 939-949.

Matsuyama, A., Arai, R., Yashiroda, Y., Shirai, A., Kamata, A., Sekido, S., Kobayashi, Y., Hashimoto, A., Hamamoto, M., Hiraoka, Y., Horinouchi, S., and Yoshida, M. (2006). ORFeome cloning and global analysis of protein localization in the fission yeast Schizosaccharomyces pombe. Nat Biotechnol *24*, 841-847.

May, K.M., Reynolds, N., Cullen, C.F., Yanagida, M., and Ohkura, H. (2002). Polo boxes and Cut23 (Apc8) mediate an interaction between polo kinase and the anaphase-promoting complex for fission yeast mitosis. J Cell Biol *156*, 23-28.

May, K.M., Watts, F.Z., Jones, N., and Hyams, J.S. (1997). Type II myosin involved in cytokinesis in the fission yeast, Schizosaccharomyces pombe. Cell Motil Cytoskeleton *38*, 385-396.

McCollum, D. (2005). Cytokinesis: breaking the ties that bind. Curr Biol *15*, R998-1000.

McKim, K.S., and Hawley, R.S. (1995). Chromosomal control of meiotic cell division. Science *270*, 1595-1601.

Meireles, A.M., Fisher, K.H., Colombie, N., Wakefield, J.G., and Ohkura, H. (2009). Wac: a new Augmin subunit required for chromosome alignment but not for acentrosomal microtubule assembly in female meiosis. J Cell Biol *184*, 777-784.

Mishra, M., Karagiannis, J., Sevugan, M., Singh, P., and Balasubramanian, M. (2005). The 14-3-3 protein rad24p modulates function of the cdc14p family phosphatase clp1p/flp1p in fission yeast. Curr Biol *15*, 1376-1383.

Mishra, M., Karagiannis, J., Trautmann, S., Wang, H., McCollum, D., and Balasubramanian, M.K. (2004). The Clp1p/Flp1p phosphatase ensures completion of cytokinesis in response to minor perturbation of the cell division machinery in Schizosaccharomyces pombe. J Cell Sci *117*, 3897-3910.

Mitchison, T., and Kirschner, M. (1984). Dynamic instability of microtubule growth. Nature *312*, 237-242.

Mogensen, M.M., and Tucker, J.B. (1987). Evidence for microtubule nucleation at plasma membrane-associated sites in Drosophila. J Cell Sci *88 (Pt 1)*, 95-107.

Moreno, S., Klar, A., and Nurse, P. (1991). Molecular genetic analysis of fission yeast Schizosaccharomyces pombe. Methods Enzymol *194*, 795-823.

Moritz, M., Braunfeld, M.B., Guenebaut, V., Heuser, J., and Agard, D.A. (2000). Structure of the gamma-tubulin ring complex: a template for microtubule nucleation. Nat Cell Biol *2*, 365-370.

Moritz, M., Braunfeld, M.B., Sedat, J.W., Alberts, B., and Agard, D.A. (1995). Microtubule nucleation by gamma-tubulin-containing rings in the centrosome. Nature *378*, 638-640.

Morrell, J.L., Tomlin, G.C., Rajagopalan, S., Venkatram, S., Feoktistova, A.S., Tasto, J.J., Mehta, S., Jennings, J.L., Link, A., Balasubramanian, M.K., and Gould, K.L. (2004). Sid4p-Cdc11p assembles the septation initiation network and its regulators at the S. pombe SPB. Curr Biol *14*, 579-584.

Motegi, F., Mishra, M., Balasubramanian, M.K., and Mabuchi, I. (2004). Myosin-II reorganization during mitosis is controlled temporally by its dephosphorylation and spatially by Mid1 in fission yeast. J Cell Biol *165*, 685-695.

Motegi, F., Nakano, K., Kitayama, C., Yamamoto, M., and Mabuchi, I. (1997). Identification of Myo3, a second type-II myosin heavy chain in the fission yeast Schizosaccharomyces pombe. FEBS Lett *420*, 161-166.

Motegi, F., Nakano, K., and Mabuchi, I. (2000). Molecular mechanism of myosin-II assembly at the division site in Schizosaccharomyces pombe. J Cell Sci *113 (Pt 10)*, 1813-1825.

Mulvihill, D.P., and Hyams, J.S. (2002). Cytokinetic actomyosin ring formation and septation in fission yeast are dependent on the full recruitment of the polo-like kinase Plo1 to the spindle pole body and a functional spindle assembly checkpoint. J Cell Sci *115*, 3575-3586.

Mulvihill, D.P., Petersen, J., Ohkura, H., Glover, D.M., and Hagan, I.M. (1999). Plo1 kinase recruitment to the spindle pole body and its role in cell division in Schizosaccharomyces pombe. Mol Biol Cell *10*, 2771-2785.

Murata, T., Sonobe, S., Baskin, T.I., Hyodo, S., Hasezawa, S., Nagata, T., Horio, T., and Hasebe, M. (2005). Microtubule-dependent microtubule nucleation based on recruitment of gamma-tubulin in higher plants. Nat Cell Biol *7*, 961-968.

Murone, M., and Simanis, V. (1996). The fission yeast dma1 gene is a component of the spindle assembly checkpoint, required to prevent septum formation and premature exit from mitosis if spindle function is compromised. EMBO J *15*, 6605-6616.

Murphy, S.M., Preble, A.M., Patel, U.K., O'Connell, K.L., Dias, D.P., Moritz, M., Agard, D., Stults, J.T., and Stearns, T. (2001). GCP5 and GCP6: two new members of the human gamma-tubulin complex. Mol Biol Cell *12*, 3340-3352.

Murphy, S.M., Urbani, L., and Stearns, T. (1998). The mammalian gamma-tubulin complex contains homologues of the yeast spindle pole body components spc97p and spc98p. J Cell Biol *141*, 663-674.

Nakano, K., Mutoh, T., and Mabuchi, I. (2001). Characterization of GTPase-activating proteins for the function of the Rho-family small GTPases in the fission yeast Schizosaccharomyces pombe.
. Genes Cells *6*, 1031-1042.

Naqvi, N.I., Eng, K., Gould, K.L., and Balasubramanian, M.K. (1999). Evidence for F-actin-dependent and -independent mechanisms involved in assembly and stability of the medial actomyosin ring in fission yeast. EMBO J *18*, 854-862.

Naqvi, N.I., Wong, K.C., Tang, X., and Balasubramanian, M.K. (2000). Type II myosin regulatory light chain relieves auto-inhibition of myosin-heavy-chain function. Nat Cell Biol *2*, 855-858.

Niccoli, T., Arellano, M., and Nurse, P. (2003). Role of Tea1p, Tea3p and Pom1p in the determination of cell ends in Schizosaccharomyces pombe. Yeast *20*, 1349-1358.

Nigg, E.A. (1998). Polo-like kinases: positive regulators of cell division from start to finish. Curr Opin Cell Biol *10*, 776-783.

Nurse, P., Thuriaux, P., and Nasmyth, K. (1976). Genetic control of the cell division cycle in the fission yeast Schizosaccharomyces pombe. Mol Gen Genet *146*, 167-178.

Oakley, C.E., and Oakley, B.R. (1989). Identification of gamma-tubulin, a new member of the tubulin superfamily encoded by mipA gene of Aspergillus nidulans. Nature *338*, 662-664.

Oegema, K., Wiese, C., Martin, O.C., Milligan, R.A., Iwamatsu, A., Mitchison, T.J., and Zheng, Y. (1999). Characterization of two related Drosophila gamma-tubulin complexes that differ in their ability to nucleate microtubules. J Cell Biol *144*, 721-733.

Ohkura, H., Hagan, I.M., and Glover, D.M. (1995). The conserved Schizosaccharomyces pombe kinase plo1, required to form a bipolar spindle, the actin ring, and septum, can drive septum formation in G1 and G2 cells. Genes Dev *9*, 1059-1073.

Okazaki, K., Okazaki, N., Kume, K., Jinno, S., Tanaka, K., and Okayama, H. (1990). High-frequency transformation method and library transducing vectors for cloning mammalian cDNAs by trans-complementation of Schizosaccharomyces pombe. Nucleic Acids Res *18*, 6485-6489.

Oliferenko, S., and Balasubramanian, M.K. (2002). Astral microtubules monitor metaphase spindle alignment in fission yeast. Nat Cell Biol *4*, 816-820.

Otegui, M.S., Verbrugghe, K.J., and Skop, A.R. (2005). Midbodies and phragmoplasts: analogous structures involved in cytokinesis. Trends Cell Biol *15*, 404-413.

Padte, N.N., Martin, S.G., Howard, M., and Chang, F. (2006). The cell-end factor pom1p inhibits mid1p in specification of the cell division plane in fission yeast. Curr Biol *16*, 2480-2487.

Paluh, J.L., Nogales, E., Oakley, B.R., McDonald, K., Pidoux, A.L., and Cande, W.Z. (2000). A mutation in gamma-tubulin alters microtubule dynamics and organization and is synthetically lethal with the kinesin-like protein pkl1p. Mol Biol Cell *11*, 1225-1239.

Paoletti, A., and Chang, F. (2000). Analysis of mid1p, a protein required for placement of the cell division site, reveals a link between the nucleus and the cell surface in fission yeast. Mol Biol Cell *11*, 2757-2773.

Pardo, M., and Nurse, P. (2003). Equatorial retention of the contractile actin ring by microtubules during cytokinesis. Science *300*, 1569-1574.

Pardo, M., and Nurse, P. (2005). The nuclear rim protein Amo1 is required for proper microtubule cytoskeleton organisation in fission yeast. J Cell Sci *118*, 1705-1714.

Pelham, R.J., and Chang, F. (2001). Role of actin polymerization and actin cables in actin-patch movement in Schizosaccharomyces pombe. Nat Cell Biol *3*, 235-244.

Peters, J.M. (2002). The anaphase-promoting complex: proteolysis in mitosis and beyond. Mol Cell *9*, 931-943.

Peters, J.M. (2006). The anaphase promoting complex/cyclosome: a machine designed to destroy. Nat Rev Mol Cell Biol *7*, 644-656.

Peters, R. (1984). Nucleo-cytoplasmic flux and intracellular mobility in single hepatocytes measured by fluorescence microphotolysis. EMBO J *3*, 1831-1836.

Puig, O., Caspary, F., Rigaut, G., Rutz, B., Bouveret, E., Bragado-Nilsson, E., Wilm, M., and Seraphin, B. (2001). The tandem affinity purification (TAP) method: a general procedure of protein complex purification. Methods *24*, 218-229.

Rajagopalan, S., Bimbo, A., Balasubramanian, M.K., and Oliferenko, S. (2004). A potential tension-sensing mechanism that ensures timely anaphase onset upon metaphase spindle orientation. Curr Biol *14*, 69-74.

Rauch, A., Thiel, C.T., Schindler, D., Wick, U., Crow, Y.J., Ekici, A.B., van Essen, A.J., Goecke, T.O., Al-Gazali, L., Chrzanowska, K.H., Zweier, C., Brunner, H.G., Becker, K., Curry, C.J., Dallapiccola, B., Devriendt, K., Dorfler, A., Kinning, E., Megarbane, A., Meinecke, P., Semple, R.K., Spranger, S., Toutain, A., Trembath, R.C., Voss, E., Wilson, L., Hennekam, R., de Zegher, F., Dorr, H.G., and Reis, A. (2008). Mutations in the pericentrin (PCNT) gene cause primordial dwarfism. Science *319*, 816-819.

Raynaud-Messina, B., and Merdes, A. (2007). Gamma-tubulin complexes and microtubule organization. Curr Opin Cell Biol *19*, 24-30.

Reddy, S.K., Rape, M., Margansky, W.A., and Kirschner, M.W. (2007). Ubiquitination by the anaphase-promoting complex drives spindle checkpoint inactivation. Nature *446*, 921-925.

Rieder, C.L., Faruki, S., and Khodjakov, A. (2001). The centrosome in vertebrates: more than a microtubule-organizing center. Trends Cell Biol *11*, 413-419.

Rosenberg, J.A., Tomlin, G.C., McDonald, W.H., Snydsman, B.E., Muller, E.G., Yates, J.R., 3rd, and Gould, K.L. (2006). Ppc89 links multiple proteins, including the septation initiation network, to the core of the fission yeast spindle-pole body. Mol Biol Cell *17*, 3793-3805.

Samejima, I., Lourenco, P.C., Snaith, H.A., and Sawin, K.E. (2005). Fission yeast mto2p regulates microtubule nucleation by the centrosomin-related protein mto1p. Mol Biol Cell *16*, 3040-3051.

Samejima, I., Matsumoto, T., Nakaseko, Y., Beach, D., and Yanagida, M. (1993). Identification of seven new cut genes involved in Schizosaccharomyces pombe mitosis. J Cell Sci *105 (Pt 1)*, 135-143.

Samejima, I., Miller, V.J., Groocock, L.M., and Sawin, K.E. (2008). Two distinct regions of Mto1 are required for normal microtubule nucleation and efficient association with the gamma-tubulin complex in vivo. J Cell Sci *121*, 3971-3980.

Sawin, K.E., Lourenco, P.C., and Snaith, H.A. (2004). Microtubule nucleation at non-spindle pole body microtubule-organizing centers requires fission yeast centrosomin-related protein mod20p. Curr Biol *14*, 763-775.

Sawin, K.E., and Nurse, P. (1998). Regulation of cell polarity by microtubules in fission yeast. J Cell Biol *142*, 457-471.

Sawin, K.E., and Snaith, H.A. (2004). Role of microtubules and tea1p in establishment and maintenance of fission yeast cell polarity. J Cell Sci *117*, 689-700.

Sawin, K.E., and Tran, P.T. (2006). Cytoplasmic microtubule organization in fission yeast. Yeast *23*, 1001-1014.

Schmidt, S., Sohrmann, M., Hofmann, K., Woollard, A., and Simanis, V. (1997). The Spg1p GTPase is an essential, dosage-dependent inducer of septum formation in Schizosaccharomyces pombe. Genes Dev *11*, 1519-1534.

Shirayama, M., Zachariae, W., Ciosk, R., and Nasmyth, K. (1998). The Polo-like kinase Cdc5p and the WD-repeat protein Cdc20p/fizzy are regulators and substrates of the anaphase promoting complex in Saccharomyces cerevisiae. EMBO J *17*, 1336-1349.

Simanis, V. (2003). Events at the end of mitosis in the budding and fission yeasts. J Cell Sci *116*, 4263-4275.

Simons, K., and Ikonen, E. (1997). Functional rafts in cell membranes. Nature *387*, 569-572.

Sipiczki, M. (2000). Where does fission yeast sit on the tree of life? Genome Biol *1*, REVIEWS1011.

Sohrmann, M., Fankhauser, C., Brodbeck, C., and Simanis, V. (1996). The dmf1/mid1 gene is essential for correct positioning of the division septum in fission yeast. Genes Dev *10*, 2707-2719.

Sohrmann, M., Schmidt, S., Hagan, I., and Simanis, V. (1998). Asymmetric segregation on spindle poles of the Schizosaccharomyces pombe septum-inducing protein kinase Cdc7p. Genes Dev *12*, 84-94.

Sparks, C.A., Morphew, M., and McCollum, D. (1999). Sid2p, a spindle pole body kinase that regulates the onset of cytokinesis. J Cell Biol *146*, 777-790.

Stearns, T., Evans, L., and Kirschner, M. (1991). Gamma-tubulin is a highly conserved component of the centrosome. Cell *65*, 825-836.

Stegmeier, F., Rape, M., Draviam, V.M., Nalepa, G., Sowa, M.E., Ang, X.L., McDonald, E.R., 3rd, Li, M.Z., Hannon, G.J., Sorger, P.K., Kirschner, M.W., Harper, J.W., and Elledge, S.J. (2007). Anaphase initiation is regulated by antagonistic ubiquitination and deubiquitination activities. Nature *446*, 876-881.

Sundberg, H.A., and Davis, T.N. (1997). A mutational analysis identifies three functional regions of the spindle pole component Spc110p in Saccharomyces cerevisiae. Mol Biol Cell *8*, 2575-2590.

Sundberg, H.A., Goetsch, L., Byers, B., and Davis, T.N. (1996). Role of calmodulin and Spc110p interaction in the proper assembly of spindle pole body compenents. J Cell Biol *133*, 111-124.

Tanaka, K., Petersen, J., MacIver, F., Mulvihill, D.P., Glover, D.M., and Hagan, I.M. (2001). The role of Plo1 kinase in mitotic commitment and septation in Schizosaccharomyces pombe. EMBO J *20*, 1259-1270.

Tange, Y., Fujita, A., Toda, T., and Niwa, O. (2004). Functional dissection of the gamma-tubulin complex by suppressor analysis of gtb1 and alp4 mutations in Schizosaccharomyces pombe. Genetics *167*, 1095-1107.

Tatebe, H., Shimada, K., Uzawa, S., Morigasaki, S., and Shiozaki, K. (2005). Wsh3/Tea4 is a novel cell-end factor essential for bipolar distribution of Tea1 and protects cell polarity under environmental stress in S. pombe. Curr Biol *15*, 1006-1015.

Tatebe, H., and Yanagida, M. (2000). Cut8, essential for anaphase, controls localization of 26S proteasome, facilitating destruction of cyclin and Cut2. Curr Biol *10*, 1329-1338.

Toda, T., Umesono, K., Hirata, A., and Yanagida, M. (1983). Cold-sensitive nuclear division arrest mutants of the fission yeast Schizosaccharomyces pombe. J Mol Biol *168*, 251-270.

Tolic-Norrelykke, I.M., Sacconi, L., Stringari, C., Raabe, I., and Pavone, F.S. (2005). Nuclear and division-plane positioning revealed by optical micromanipulation. Curr Biol *15*, 1212-1216.

Tolic-Norrelykke, I.M., Sacconi, L., Thon, G., and Pavone, F.S. (2004). Positioning and elongation of the fission yeast spindle by microtubule-based pushing. Curr Biol *14*, 1181-1186.

Tournier, S., Gachet, Y., Buck, V., Hyams, J.S., and Millar, J.B. (2004). Disruption of astral microtubule contact with the cell cortex activates a Bub1, Bub3, and Mad3-dependent checkpoint in fission yeast. Mol Biol Cell *15*, 3345-3356.

Toya, M., Iino, Y., and Yamamoto, M. (1999). Fission yeast Pob1p, which is homologous to budding yeast Boi proteins and exhibits subcellular localization close to actin patches, is essential for cell elongation and separation.
. Mol Biol Cell *10*, 2745-2757.

Tran, P.T., Marsh, L., Doye, V., Inoue, S., and Chang, F. (2001). A mechanism for nuclear positioning in fission yeast based on microtubule pushing. J Cell Biol *153*, 397-411.

Uehara, R., Nozawa, R.S., Tomioka, A., Petry, S., Vale, R.D., Obuse, C., and Goshima, G. (2009). The augmin complex plays a critical role in spindle microtubule generation for mitotic progression and cytokinesis in human cells. Proc Natl Acad Sci U S A *106*, 6998-7003.

Van Criekinge, W., and Beyaert, R. (1999). Yeast Two-Hybrid: State of the Art. Biol Proceedings Online *4*, 1-38.

van de Weerdt, B.C., van Vugt, M.A., Lindon, C., Kauw, J.J., Rozendaal, M.J., Klompmaker, R., Wolthuis, R.M., and Medema, R.H. (2005). Uncoupling anaphase-promoting complex/cyclosome activity from spindle assembly checkpoint control by deregulating polo-like kinase 1. Mol Cell Biol *25*, 2031-2044.

van Leuken, R., Clijsters, L., van Zon, W., Lim, D., Yao, X., Wolthuis, R.M., Yaffe, M.B., Medema, R.H., and van Vugt, M.A. (2009). Polo-like kinase-1 controls Aurora A destruction by activating APC/C-Cdh1. PLoS ONE *4*, e5282.

Vardy, L., and Toda, T. (2000). The fission yeast gamma-tubulin complex is required in G(1) phase and is a component of the spindle assembly checkpoint. EMBO J *19*, 6098-6111.

Vavylonis, D., Wu, J.Q., Hao, S., O'Shaughnessy, B., and Pollard, T.D. (2008). Assembly mechanism of the contractile ring for cytokinesis by fission yeast. Science *319*, 97-100.

Venkatram, S., Jennings, J.L., Link, A., and Gould, K.L. (2005). Mto2p, a novel fission yeast protein required for cytoplasmic microtubule organization and anchoring of the cytokinetic actin ring. Mol Biol Cell *16*, 3052-3063.

Venkatram, S., Tasto, J.J., Feoktistova, A., Jennings, J.L., Link, A.J., and Gould, K.L. (2004). Identification and characterization of two novel proteins affecting fission yeast gamma-tubulin complex function. Mol Biol Cell *15*, 2287-2301.

Verollet, C., Colombie, N., Daubon, T., Bourbon, H.M., Wright, M., and Raynaud-Messina, B. (2006). Drosophila melanogaster gamma-TuRC is dispensable for targeting gamma-tubulin to the centrosome and microtubule nucleation. J Cell Biol *172*, 517-528.

Vinh, D.B., Kern, J.W., Hancock, W.O., Howard, J., and Davis, T.N. (2002). Reconstitution and characterization of budding yeast gamma-tubulin complex. Mol Biol Cell *13*, 1144-1157.

Vjestica, A., Tang, X.Z., and Oliferenko, S. (2008). The actomyosin ring recruits early secretory compartments to the division site in fission yeast. Mol Biol Cell *19*, 1125-1138.

Wachtler, V., Rajagopalan, S., and Balasubramanian, M.K. (2003). Sterol-rich plasma membrane domains in the fission yeast Schizosaccharomyces pombe. J Cell Sci *116*, 867-874.

Waters, J.C., and Salmon, E. (1997). Pathways of spindle assembly. Curr Opin Cell Biol *9*, 37-43.

Wiese, C., and Zheng, Y. (2000). A new function for the gamma-tubulin ring complex as a microtubule minus-end cap. Nat Cell Biol *2*, 358-364.

Wiese, C., and Zheng, Y. (2006). Microtubule nucleation: gamma-tubulin and beyond. J Cell Sci *119*, 4143-4153.

Wolfe, B.A., and Gould, K.L. (2005). Split decisions: coordinating cytokinesis in yeast. Trends Cell Biol *15*, 10-18.

Wood, V., Gwilliam, R., Rajandream, M.A., Lyne, M., Lyne, R., Stewart, A., Sgouros, J., Peat, N., Hayles, J., Baker, S., Basham, D., Bowman, S., Brooks, K., Brown, D., Brown, S., Chillingworth, T., Churcher, C., Collins, M., Connor, R., Cronin, A., Davis, P., Feltwell, T., Fraser, A., Gentles, S., Goble, A., Hamlin, N., Harris, D., Hidalgo, J., Hodgson, G., Holroyd, S., Hornsby, T., Howarth, S., Huckle, E.J., Hunt, S., Jagels, K., James, K., Jones, L., Jones, M., Leather, S., McDonald, S., McLean, J., Mooney, P., Moule, S., Mungall, K., Murphy, L., Niblett, D., Odell, C., Oliver, K., O'Neil, S., Pearson, D., Quail, M.A., Rabbinowitsch, E., Rutherford, K., Rutter, S., Saunders, D., Seeger, K., Sharp, S., Skelton, J., Simmonds, M., Squares, R., Squares, S., Stevens, K., Taylor, K., Taylor, R.G., Tivey, A., Walsh, S., Warren, T., Whitehead, S., Woodward, J., Volckaert, G., Aert, R., Robben, J., Grymonprez, B., Weltjens, I., Vanstreels, E., Rieger, M., Schafer, M., Muller-Auer, S., Gabel, C., Fuchs, M., Dusterhoft, A., Fritzc, C., Holzer, E., Moestl, D., Hilbert, H., Borzym, K., Langer, I., Beck, A., Lehrach, H., Reinhardt, R., Pohl, T.M., Eger, P., Zimmermann, W., Wedler, H., Wambutt, R., Purnelle, B., Goffeau, A., Cadieu, E., Dreano, S., Gloux, S., Lelaure, V., Mottier, S., Galibert, F., Aves, S.J., Xiang, Z., Hunt, C., Moore, K., Hurst, S.M., Lucas, M., Rochet, M., Gaillardin, C., Tallada, V.A., Garzon, A., Thode, G., Daga, R.R., Cruzado, L., Jimenez, J., Sanchez, M., del Rey, F., Benito, J., Dominguez, A., Revuelta, J.L., Moreno, S., Armstrong, J., Forsburg, S.L., Cerutti, L., Lowe, T., McCombie, W.R., Paulsen, I., Potashkin, J., Shpakovski, G.V., Ussery, D., Barrell, B.G., and Nurse, P. (2002). The genome sequence of Schizosaccharomyces pombe. Nature *415*, 871-880.

Woods, A., Sherwin, T., Sasse, R., MacRae, T.H., Baines, A.J., and Gull, K. (1989). Definition of individual components within the cytoskeleton of Trypanosoma brucei by a library of monoclonal antibodies. J Cell Sci *93 (Pt 3)*, 491-500.

Wu, J.Q., Bahler, J., and Pringle, J.R. (2001). Roles of a fimbrin and an alpha-actinin-like protein in fission yeast cell polarization and cytokinesis. Mol Biol Cell *12*, 1061-1077.

Wu, J.Q., Kuhn, J.R., Kovar, D.R., and Pollard, T.D. (2003). Spatial and temporal pathway for assembly and constriction of the contractile ring in fission yeast cytokinesis. Dev Cell *5*, 723-734.

Wu, J.Q., and Pollard, T.D. (2005). Counting cytokinesis proteins globally and locally in fission yeast. Science *310*, 310-314.

Wu, J.Q., Sirotkin, V., Kovar, D.R., Lord, M., Beltzner, C.C., Kuhn, J.R., and Pollard, T.D. (2006). Assembly of the cytokinetic contractile ring from a broad band of nodes in fission yeast. J Cell Biol *174*, 391-402.

Yamada, H., Kumada, K., and Yanagida, M. (1997). Distinct subunit functions and cell cycle regulated phosphorylation of 20S APC/cyclosome required for anaphase in fission yeast. J Cell Sci *110 (Pt 15)*, 1793-1804.

Yamashita, A., Sato, M., Fujita, A., Yamamoto, M., and Toda, T. (2005). The roles of fission yeast ase1 in mitotic cell division, meiotic nuclear oscillation, and cytokinesis checkpoint signaling. Mol Biol Cell *16*, 1378-1395.

Yamashita, Y.M., Nakaseko, Y., Samejima, I., Kumada, K., Yamada, H., Michaelson, D., and Yanagida, M. (1996). 20S cyclosome complex formation and proteolytic activity inhibited by the cAMP/PKA pathway. Nature *384*, 276-279.

Yanagida, M. (1998). Fission yeast cut mutations revisited: control of anaphase. Trends Cell Biol *8*, 144-149.

Yoon, H.J., Feoktistova, A., Wolfe, B.A., Jennings, J.L., Link, A.J., and Gould, K.L. (2002). Proteomics analysis identifies new components of the fission and budding yeast anaphase-promoting complexes. Curr Biol *12*, 2048-2054.

Zachariae, W., and Nasmyth, K. (1999). Whose end is destruction: cell division and the anaphase-promoting complex. Genes Dev *13*, 2039-2058.

Zhang, J., and Megraw, T.L. (2007). Proper recruitment of gamma-tubulin and D-TACC/Msps to embryonic Drosophila centrosomes requires Centrosomin Motif 1. Mol Biol Cell *18*, 4037-4049.

Zhang, L., Keating, T.J., Wilde, A., Borisy, G.G., and Zheng, Y. (2000). The role of Xgrip210 in gamma-tubulin ring complex assembly and centrosome recruitment. J Cell Biol *151*, 1525-1536.

Zheng, Y., Wong, M.L., Alberts, B., and Mitchison, T. (1995). Nucleation of microtubule assembly by a gamma-tubulin-containing ring complex. Nature *378*, 578-583.

Zimmerman, S., and Chang, F. (2005). Effects of {gamma}-tubulin complex proteins on microtubule nucleation and catastrophe in fission yeast. Mol Biol Cell *16*, 2719-2733.

Zimmerman, S., Daga, R.R., and Chang, F. (2004a). Intra-nuclear microtubules and a mitotic spindle orientation checkpoint. Nat Cell Biol *6*, 1245-1246.

Zimmerman, S., Tran, P.T., Daga, R.R., Niwa, O., and Chang, F. (2004b). Rsp1p, a J domain protein required for disassembly and assembly of microtubule organizing centers during the fission yeast cell cycle. Dev Cell *6*, 497-509.